FS/RV SONNE

FAHRTBERICHT SO173/2
CRUISE REPORT SO173/2

SEDUCTION

SO173/2
CALDERA - CALDERA. AUGUST 8 - SEPTEMBER 2, 2003

116

GEOMAR REPORT

FS/RV SONNE

FAHRTBERICHT SO173/2
CRUISE REPORT SO173/2

SEDUCTION

PART A:
SEISMOGENESIS AND TECTONIC EROSION
DURING SUBDUCTION: MIDDLE AMERICA MARGIN

PART B:
SENSORY MECHANISM IN MESOPELAGIC FISH

SO173/2
CALDERA - CALDERA. AUGUST 8 - SEPTEMBER 2, 2003

Edited by
Wilhelm Weinrebe and Cesar R. Ranero (Part A)
and Jochen Wagner (Part B)
with contributions of cruise participants

Investigations in the frame of SFB 574
„Volatiles and Fluids in Subduction Zones:
Climate Feedback and Trigger Mechanisms for Natural Disasters“

Contribution 48 of SFB 574

GEOMAR
Forschungszentrum
für marine Geowissenschaften
der Christian-Albrechts-
Universität
zu Kiel

KIEL 2003

GEOMAR REPORT 116

GEOMAR
Research Center
for Marine Geosciences
Christian Albrechts University
in Kiel

Redaktion dieses Reports:
Wilhelm Weinrebe und Cesar R. Ranero (Part A)
Jochen Wagner (Part B – Kap. 2.3, 5.4, 6.5)
Umschlag und Titelei: Gerhard Haass

GEOMAR REPORT

GEOMAR
Forschungszentrum
für marine Geowissenschaften
Wischhofstr. 1-3
D - 24148 Kiel
Tel. (0431) 600-2555, 600-2505

Editors of this issue:
Wilhelm Weinrebe and Cesar R. Ranero (Part A)
Jochen Wagner (Part B – Chapter 2.3, 5.4, 6.5))
Cover and prelims: Gerhard Haass

GEOMAR REPORT

GEOMAR
Research Center
for Marine Geosciences
Wischhofstr. 1-3
D - 24148 Kiel
Tel. (49) 431 / 600-2555, 600-2505

Table of contents

1. Summary

During cruise SO-173/2 (8 August to 2 September 2003, Caldera to Caldera) a new multibeam bathymetry and magnetic survey has mapped the continental margin and incoming plate of NW Nicaragua, El Salvador and Guatemala, extending existing coverage from offshore Costa Rica and part of Nicaragua to a full coverage map of about 1200 km long by 100 km wide area along the plate boundary. The incoming plate along Nicaragua, El Salvador and Guatemala is of similar age and was formed at superfast spreading rates; however, its morphology changes drastically along strike. The seafloor-spreading inherited morphology is very smooth along Nicaragua, but with ridges up to 800 m high in Guatemala, with a transition across El Salvador. The development and dimensions of the dominant inherited fabric seems to be related to discontinuities at the paleospreading center. A series of troughs oblique to the main fabric may indicate the location of pseudofaults and correspond to areas where the seafloor fabric is most prominent. Bending of the oceanic plate into the trench reactivates the inherited fabric forming a well pervasive faulting system along the oceanic trench slope. The continental slope displays three morphotectonic units that roughly correspond to the upper, middle and lower slope, although the across slope width of each unit is fairly variable. Small canyons and gullies that form at the sudden dip change across the shelf break carve the upper slope. The canyons coalesce and become shallower as the dip decreases downslope. Locally some large canyons continue into the slope toe. The middle slope is a rough terrain variable in width and dip sculptured by pervasive normal faulting and locally by mass wasting processes. The lower slope is formed by en echelon terraces striking similar to the rough terrain of the incoming plate and mimicking the half graben morphology of the underthusting plate. The three morphotectonic slope domains represent differences in tectonic activity, with more stable upper slope, a middle slope dominated by tectonic extension and the thin, highly fractured upper plate of the lower slope riffling over the incoming plate topography. The trench axis is largely empty, with local turbidite ponds at the mouth of a few large canyons transecting the entire slope.

To study various aspects of the sensory systems in mesopelagic animals, predominantly fish, 18 trawls were taken in Guatemalan and Nicaraguan waters. The trawls in Guatemalan waters yielded only small catches both in terms of absolute number of specimens and the number of species obtained. Most noticeable was the total absence of some species considered to have a global distribution. The trawls in Nicaraguan waters brought up a greater number of species and specimens.

2.1 Geophysical objectives of the cruise

(Ranero, C. R., Weinrebe, W.)

The project SEDUCTION aims at collecting data offshore Guatemala and Costa Rica that will allow to understand the recent and long-term evolution of the Middle America Landbridge and in particular the mass flux into the subduction system. Offshore Costa Rica and Nicaragua numerous seismic profiles and a full multibeam bathymetric and magnetic coverage of the margin and adjacent ocean plate (Figure 2.1.1) have yielded a rapid change in the concepts of the margin formation and evolution. That area of Middle America is currently considered an erosional type of margin (Ranero and von Huene, 2000; Ranero et al., 2000; von Huene et al., 2000) whereas it was previously considered an accretionary margin. In contrast Guatemala has no high resolution bathymetric or magnetic coverage, although there exist numerous seismic profiles (Figure 2.1.2) and perhaps the best set of drilling information across the entire continental slope for the whole Middle America, (Figure 2.1.3; DSDP legs 67 and 84). On the other hand, Costa Rica and Nicaragua lack of drilling information across much of the slope that can be used to decipher the long term evolution. The data to be gathered in Guatemala will permit to reinterpret the existing seismic and drill core data and to better understand the evolution of Middle America.

a) Continental margin structure offshore Guatemala.

High resolution swath bathymetry will be used to study the neotectonics of the continental margin of Guatemala in the area of the legs 67 and 84 of the Deep Sea Drilling Program (DSDP) (Figure 2.1.1 and 2.1.2). Guatemala was the area where the theory of continental growth through long-term large-scale accretion (e.g. Seely et al., 1974) was first tested. It was shown that basically no accretion has occurred since early Tertiary times (von Huene et al., 1980). However, the importance of current active accretion is still disputed because folding at the toe of the continental slope has been observed in high resolution seismic data (e.g. Moore et al., 1986). A major shortcoming in understanding the recent tectonics of Guatemala is the lack of high resolution swath bathymetric coverage of the area. Swath bathymetry mapping was only carried out in a portion of the lower slope and suffers from incomplete coverage, poor navigation and the inability to clean the recorded soundings with interactive software. A similar controversy of accretion versus non-accretion has been under debate in Costa Rica for more than 20 years. Seismic data were interpreted as showing a large accretionary prism (Silver el at., 1985; Shipley et al., 1992, McIntosh et al., 1993). However, once enough modern high resolution swath bathymetry was collected along the margin it demonstrated that the initial interpretations based only of seismic data were wrong and that the margin is in fact largely being tectonically eroded (e.g. Ranero and von Huene, 2000; von Huene et al., 2000). A high resolution swath coverage of the Guatemala margin will permit to map the different morphotectonic units and show the existence of any recently accreted body at the toe of the slope. In additon it will show the style of tectonics in the middle upper slope. Normal faulting and important mass wasting structures (e.g. slumps scars, Figure 2.1.4) would indicate an overcritical slope dip and that processes associated to tectonic erosion may be active, rather than simply non-accretion as is currently envisioned by many scientists.

Furthermore, high resolution bathymetry will also help to understand the origin of the San José canyon (Figure 2.1.2) an unusually large structure that may be tectonically controlled. Is the canyon currently active or is it a fossil structure (flat bottom, v-shaped bottom). If the canyon is active, where is the sediment transported? Can it give rise to local accretion? Is all sediment subducted? And is the evolution of the canyon related to the vertical tectonics of the area? How can a deep canyon develop in a subsiding continental slope?

Another point of interest at the base of the slope are the serpentinites (altered peridotitic rock) found in DSDP drill cores from that area (von Huene et al; 1985). The drill cores have been recently re-examined and they show evidence that the serpentine is interlayed with mud flows (Paola Vannucchi, personnal comunication 2002), rising the question whether they represent serpertinite mud diapirs similar to those found in the forearc and at the toe of the slope of the Marinas subduction system (Park et al., 2002). Detailed swath

bathymetry mapping will exhibit such structures if they have dimensions > 100 meter wide and tens of meters high. Sediment-mud diapirs of such a size have been clearly identified offshore Costa Rica using the Simrad multibeam system from Sonne.

Mapping of the continental slope with magnetic data will permit to decipher if the igneous basement composed of gabbros, basalts and peridotites of oceanic origin drilled and dreged near San José canyon extends laterally and is similar to the basement in other areas of Middle America like Costa Rica and Nicaragua. This will help to understand in particular the process of formation of the Middle America landbridge (Hoernle et al., 2002) and in general continental growth through oceanic plateau accretion.

b) The outer rise and ocean trench slope

Mapping the incoming ocean plate from the trench axis to the outer rise with swath bathymetry and magnetics will help to understand the tectonic structure due to bending of the plate, its relation to the tectonic fabric formed at the spreading center and the age of the ocean lithosphere.

The ocean plate near the trench offhore Guatemala is surprisingly deeper than the plate offshore Nicaragua, in spite of its younger age off Guatemala (Figure 2.1.1). Does bending of the ocean plate as it approaches the trench and faulting due to the bending has a feedback and the plate bends more because it starts faulting farther away from the trench axis in Guatemala than in Nicaragua? The tectonic fabric formed at the spreading center may also play a role: if the inherited spreading fabric is ~ parallel to the trench the plate will break easier and more pervasively and bend-related faulting may lead to a control in the amount of flexure (von Huene et al., 2000). This in turn may control the amount of fluid that percolates into the ocean lithosphere at the trench (von Huene et al., 2000). The spreading-center fabric orientation can be found by mapping the seafloor spreading magnetic anomalies, as well as other structures that may have formed with orientations oblique to spreading direction like propagators (e.g. Barckhausen et al., 2001).

Normal faulting of ocean plates at trenches may give rise to half grabens or to full grabens and these different morphologies may facilitate the subduction of the sediment cover beneath the forearc. It has been proposed that half grabens facilitate the underthrusting of sediment to the depth of melt generation (Kelly et al., submitted) and produce a strong slab signal in the arc volcanoes of Nicaragua. By mapping the faulting off Guatemala (much smaller slab signal at the volcanic arc) we will be able to test this hypothesis.

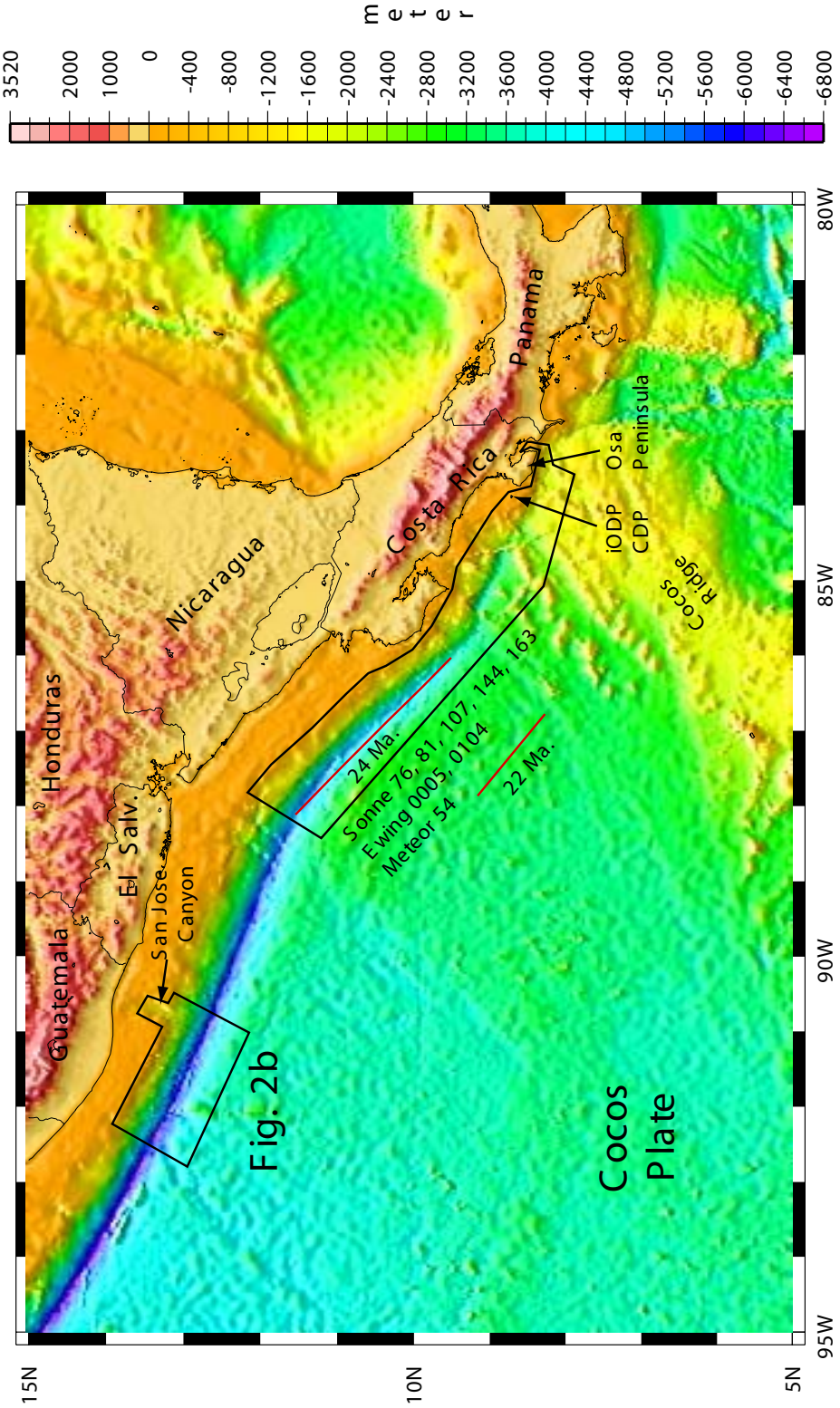

Figure 2.1.1: Colour coded, shaded relief map of Middle America and ocean Cocos plate. The black box offshore Costa Rica and Nicaragua delimits the area of investigation of SONNE cruises 76, 81, 107, 144 and 163, METEOR cruise 54, EWING cruises 0005 and 0104. The black box offshore Guatemala delimits the area proposed in this study. Red lines indicates the age of the incoming ocean plate (e.g. 24 Ma offshore Nicaragua). The projection of the age of the ocean plate offshore Nicaragua (Barckhausen et al., 2001) indicates that the plate offshore Guatemala is ~ 22 Ma, i.e. younger than offshore Nicaragua, however the ocean trench is deeper. Note the location off Osa Peninsula of the area of the proposed deep riser drilling. The Complex Drilling Proposal (CDP) for deep riser drilling has been recommended for submission of a final proposal by the International Ocean Drilling Program (iODP).

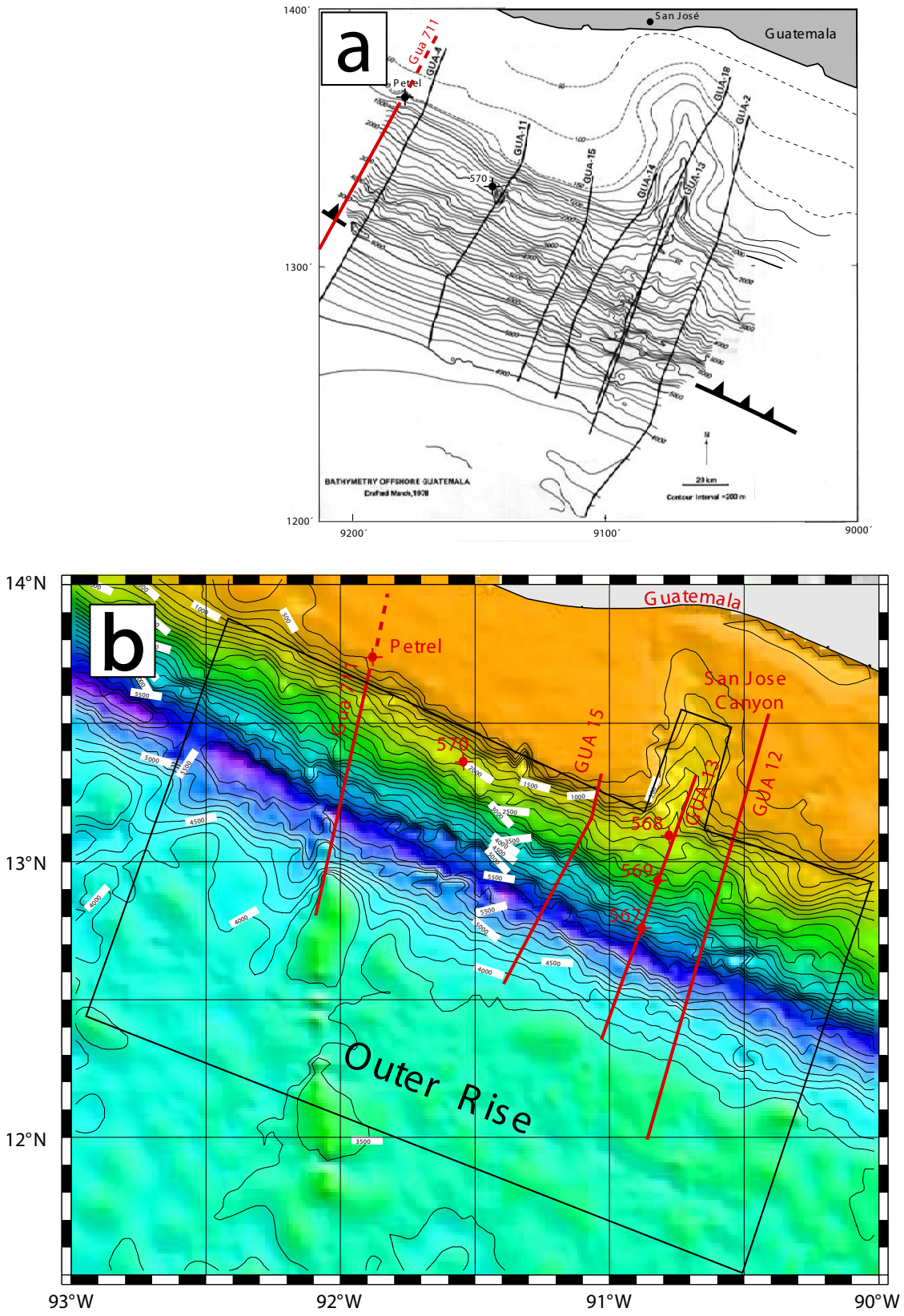

Figure 2.1.2: Bathymetry and multichannel seismic track lines offshore Guatemala. a) Low resolution contour bathymetry map compiled with seabeam mapping near the trench and single beam echosounders (Aubouin and von Huene 1982). b) Shaded relief bathymetry derived from satellite altimetry offshore Guatemala showing drill site locations (DSDP 84, von Huene et al., 1985). Black box indicates area proposed to be mapped with swath bathymetry and magnetic data. The area covers the continental slope and neighbor ocean plate including the outer rise. Multichannel seismic profiles are available at the University of Texas web site (raw shot gathers and processed profiles, www.itig.ut.edu).

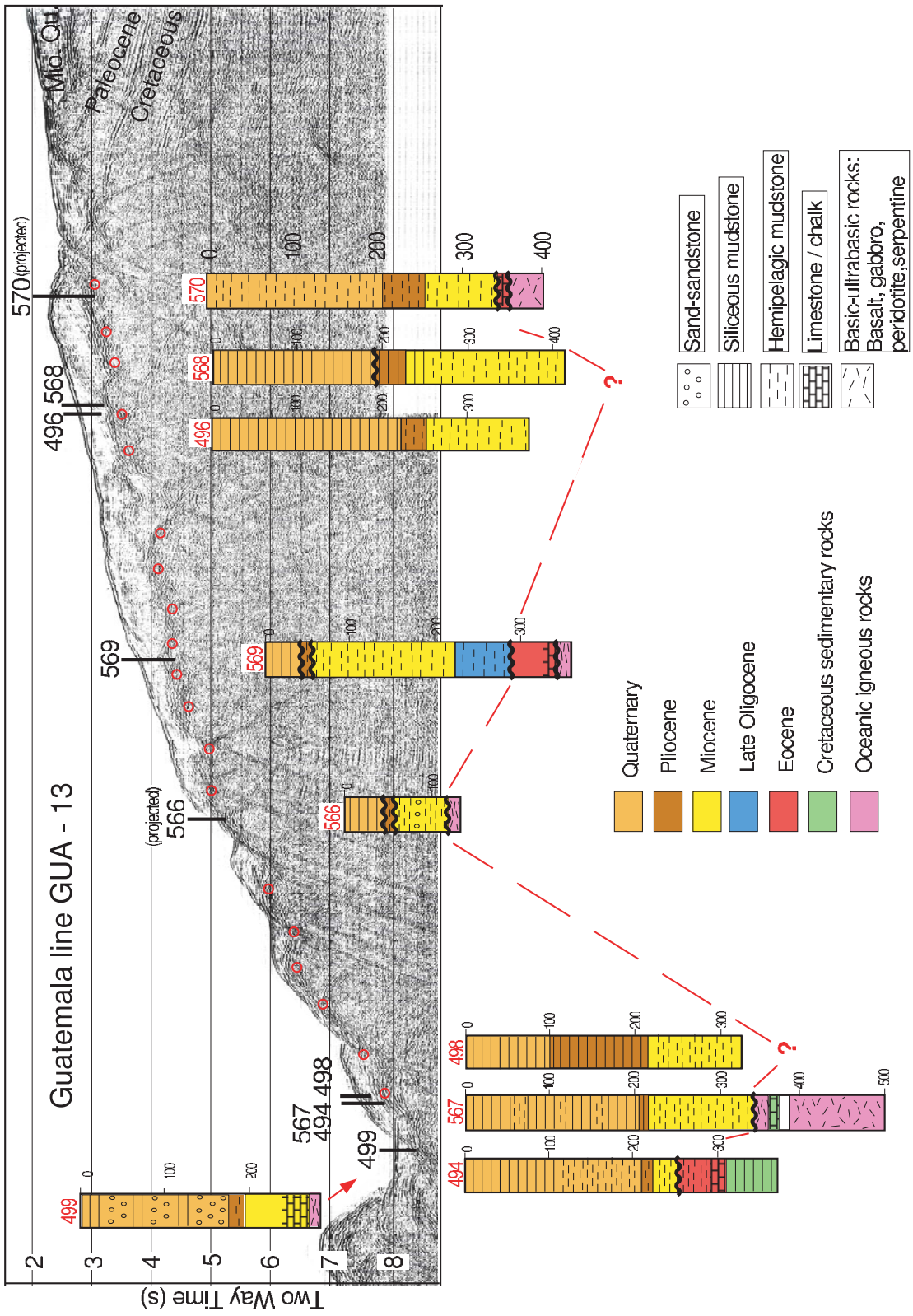

Figure 2.1.3: Compilation of drill sites (DSDP 67 and 84) offshore Guatemala and location of sites along multichannel seismic reflection profile GUA-13 (see location of GUA-13 in figue 2). The cores from DSDP leg 84 penetrated igneous basement underneath the continental slope at four sites (566, 567, 569, 570) and with the other sites of DSDP leg 67 have yielded a detailed stratigraphy of the slope sediment cover. Those sites represent the best drill data on the evolution of the continental margin available along Middle America. Serpentine drilled on site 567 is interlayered with mud flows and may represent serpentine diapirs (P. Vannucchi, personal communication 2002).

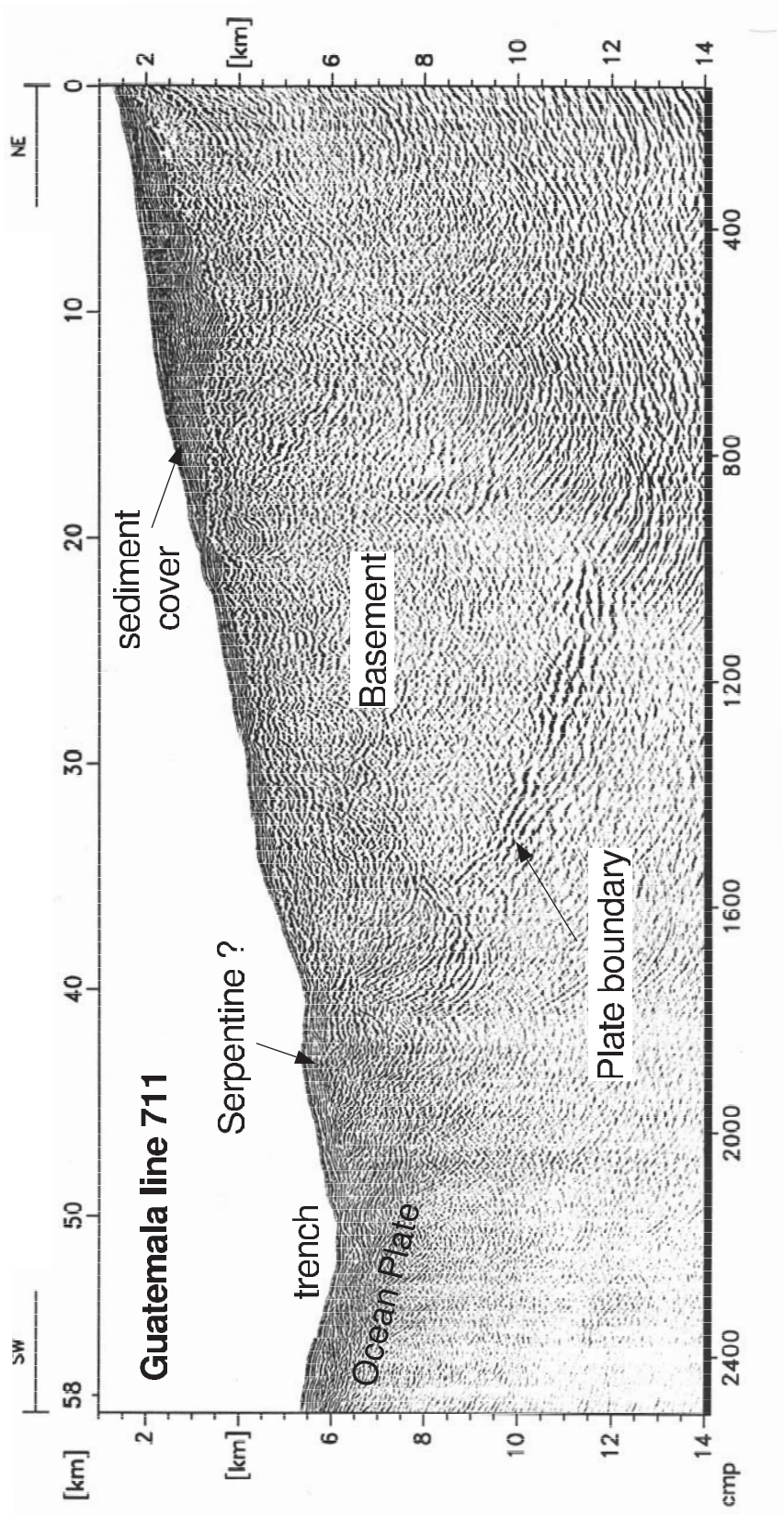

Figure 2.1.4: Reprocessed and prestack depth migrated Exxon line Guatemala 711 (Klaeschen and Bartsch, unpublished, location on figure 2). The basement is composed of igneous rocks. The tectonic structure shows evidence of extension probably related to subduction erosion at the base of the plate.

2.2 Tectonic settings of the area and previous studies

A summary of Central American tectonics from a recently accepted article is also a good introduction of SO 173/2. It is presented with some modification here to acquaint the reader with the tectonic setting of the area surveyed.

A Marine Perspective of Central American tectonics

César R. Ranero[1,2], Roland von Huene[1,3] and Wilhelm Weinrebe[1,2]

1) GEOMAR, Wischhofstrasse 1-3, 24148, Kiel, Germany
2) SFB 574, University of Kiel
3) University of Califonia, Davis

Abstract

We review the marine geological and geophysical studies carried out along the convergent margin of Middle America over the past 50 years. These studies have profoundly influenced the understanding of how convergent plate boundaries form and evolve. Interpretations of processes governing the development of the Middle America convergent margin have been markedly modified as techniques and quality of data improved. Proposed in early models was a steady growth of the continental plate by long-term accretionary processes through which material from the incoming oceanic plate was tectonically transferred to the overriding plate. Subsequently, as the accretionary hypothesis was tested, it was realized that the structure and rock bodies of the margin implied a non-accretionary character. In the last ~ 10 years a wealth of new, higher resolution data, have lead to the proposition that the continental margin has been tectonically eroded during the Neogene-Quaternary periods (~23 Ma) and that a large rock mass of the overriding plate has been removed and probably recycled to the mantle. Tectonic erosion seems to be the current dominant governing tectonic process. Modern data show the close correlation between the character of the incoming oceanic plate and the recent (~ 5 Ma) tectonic evolution of the arc-forearc system. Forearc tectonics, submarine sliding, arc magmatism and interplate seismicity differ in segments that parallel segmentation of the oceanic plate subducting along the Middle America Trench.

1. Introduction

The Central American convergent margin is a classic representative of the "Pacific Margin" in the nomenclature of Gutenberg and Richter (1954) and early Plate Tectonics. It extends from the Gulf of Tehuantepec to Panama (Figure 2.2.1). The dominant morphological feature is the Middle America Trench (MAT) that was named by Heacock and Worzel, (1955). This trench marks the convergent plate boundary between the Caribbean and Cocos Plates. Earthquakes clearly define a Wadati-Benioff Zone or a subduction zone where Cocos Plate subducts beneath the Caribbean Plate. Vening Meinesz, who found the negative gravity anomalies associated with trenches world–wide, first measured the MAT negative gravity anomalies in 1926. Concepts regarding the MAT parallel the evolution of concepts in the geosciences over the past 75 years.

The history of marine geoscience research along Central America and the Middle America Trench is intimately interwoven with the evolution of concepts regarding convergent plate boundaries. Geophysical data tested with scientific ocean drilling along the Central American margin (CAM) was significant in modifying ideas about convergent plate boundaries in the plate tectonic paradigm. We introduce this chapter with a narrative history of this evolution and then concentrate on the insights from modern bathymetry, improved seismic reflection information, and the current tectonic interpretation of CAM tectonics.

2 Accretion Versus Non-accretion

2.1 Early studies offshore Guatemala

Investigations offshore Central America by scientific institutions between 1950 and 1960 were numerous for the time. Bathymetric data compiled in the early 1960s (c.f. Fisher, 1957, Shor and Fisher, 1961) revealed the varied morphological character of the adjacent ocean basin. Soon afterwards, areas of the continental shelf were considered potentially petroliferous and were surveyed by industry explorationists who informally shared with academic colleagues that deformation on the slope indicated accretion. A concept of accretion was published by Dickinson (1971) suggesting that although ocean crust is carried down with the descending lithosphere, lighter sediment is probably scraped off against a more durable overriding plate. These off-scraped sediments and ophiolitic scraps were presumably equivalent to the materials exposed in the Sambagawa Formation of Japan and in the Fransciscan Formation in California, a vast tract of rock whose origin had long puzzled geologists. Dickinson proposed steady-state accretion and noted that the terrain between the arc and trench was proportional in width to the age of the arc-trench system. Dickinson (1971) summarized the model after his seminal workshop where the concept was debated between marine and land geoscientists. He proposed a steady-state process of continental growth that was commonly referred to as "the plate tectonic margin model". The origin of ophiolites of the Nicoya Peninsula thus became of significant interest to researchers.

Many proponents of plate tectonics were enthusiastic about the accretionary hypothesis, and when Exxon released a multichannel seismic reflection record across the MAT off Guatemala the model was convincingly backed by published data (Seely et al, 1974). The Exxon record showed many landward dipping reflections but at the time it was difficult to differentiate between real reflections and diffractions without today's more powerful processing software systems. The Guatemalan example elevated the accretionary hypothesis to broad acceptance and the Guatemalan seismic record was commonly cited as a type accretionary section. At this time, drilling in the Nankai Trough based mainly on industry records of JAPEX (Aoki et al, 1982) provided further evidence supporting accretion (Karig, 1975) and a tendency to equate convergent margins with accretion became common. With the Guatemalan record, Seely and his colleagues elevated the

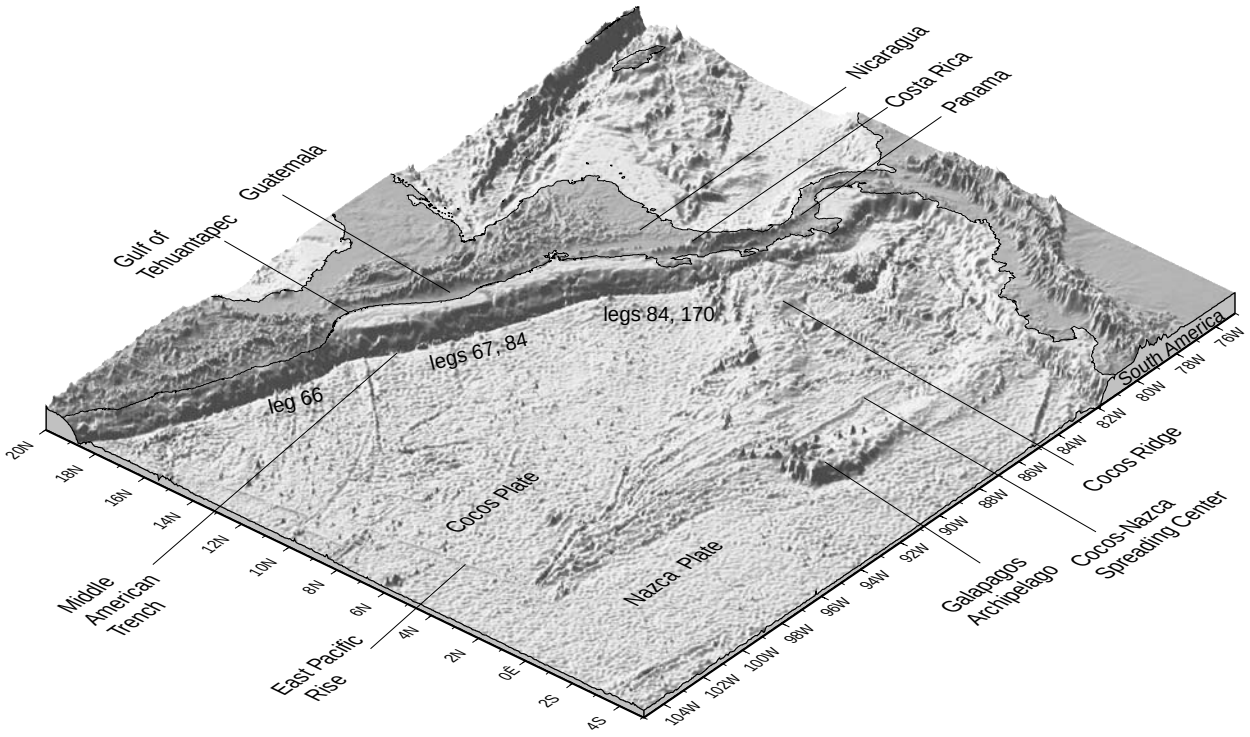

Figure 2.2.1: Shaded relief map of Cocos and Caribbean plates. Areas of Deep Sea Drilling Program

accretionary model from speculation to broad acceptance by geoscientists and other proprietary data were later integrated in an interpretation of the Oregon and Alaskan margins (Seely et al., 1979). Seely (1979) interpreted reflection data off Oregon and Alaska as he had interpreted the Guatemalan record inferring that slices were detached, then rotated upward by younger underthrusting slices, to progressively build continental crust. The actively accreting prism uplifted the shelf edge forming the seaward flank of forearc basins. Single-channel marine seismic reflection data of the academic community were grossly inadequate to reveal the complex structure along active convergent margins. In hindsight, even the early multichannel Exxon record processed with digital methods available only in industry was also over interpreted.

Notwithstanding the focus on accretion in the published literature, evidence was building that convergent margins were also subjected to tectonic erosion. As Miller (1970) and Rutland (1971) pointed out, some older arc-trench systems have narrow forearcs seaward of an exposed Mesozoic continental framework. This observation was not lost on Creighton Burk. At the time, Burk was Director of the University of Texas Marine Science Institute (UTMSI). In 1974, he formulated a program to investigate the tectonics of the MAT from the Cocos Ridge to the Riviera Fracture Zone. He and colleagues on the Deep Sea Drilling Project (DSDP) Active Margins Panel reasoned that investigating two adjacent areas one of which appeared accretionary and the other erosional would yield insights greater than those derived from studies of either margin type alone. In contrast to the accretionary Guatemalan margin, the southwestern Mexico margin appeared to have no older accreted mass because Mesozoic rock crops out along the coast as observed along the Chilean margin. Thus the volume of a possible accretionary prism cannot accommodate all incoming sediment on the lower plate and part of the prism must be missing. Site surveys by UTMSI produced the first multichannel seismic reflection data off Acapulco Mexico and off Guatemala, Nicaragua, and Costa Rica. These surveys formed a basis for selecting two transects that were drilled during DSDP Legs 66, 67, and 84 (Figure 2.2.1). Much to everyone's surprise, the Guatemalan margin proved non-accretionary (Aubouin et al, 1982, von Huene et al, 1985) and the Mexican margin was interpreted as accretionary (Watkins et al, 1982). The Guatemalan margin yielded Cretaceous limestone resting on igneous oceanic rocks of the upper plate within 4 km of the trench axis. Clearly, steady accretion had not affected the margin during Tertiary time (von Huene et al., 1980, Aubouin et al., 1982). Although many of the landward dipping reflections interpreted as accretionary thrusts were shown to be diffractions by later pre-stack depth processing, rare landward dipping reflections do occur in the margin wedge. The shortcomings of geophysics alone to assess basic convergent margin tectonic processes was also experienced along the Japan, Marianas, Tonga, Peru, and most recently the Costa Rica margins. Although the seismic reflection technique and the information content of the seismic reflection method has improved greatly in the past 40 years, the accretionary model that guided interpretations of geophysical data applied only to some margins. We return to this point after recounting the great advances made over the past 10 years with multibeam bathymetry (Figure 2.2.2) and seismic reflection investigations that include advanced pre-stack-depth processing.

2.2. Contribution of Bathymetric Mapping

Investigators at the Scripps Institution of Oceanography compiled bathymetric information along the CAM most of which are summarized in Fisher and Hess (1963). Geoscientists compiling conventional bathymetric data in the late 1950s (Fisher, 1967) were mindful of seafloor processes in constructing maps from widely spaced data. Fisher's maps showed numerous seamounts along the northern flank of the Cocos Ridge. The many transit legs of research vessels from ports in the area and through the Panama Canal became data of opportunity that Lonsdale and Klitgord (1978) later compiled, data included in the independent compilation of Case and Holcombe (1980). The latter compilation included continental geology and both compilations depicted the seamount covered ocean floor and the adjacent smooth ocean floor and less complicated slope off Nicoya Peninsula. This was termed the rough-smooth boundary by Hey (1977) who correlated it with the change in origin of ocean crust. The subducting Cocos Ridge was positioned opposite the uplifted Osa Peninsula and off both Costa Rican peninsulas the shelf is very narrow. At this time a first order morphology of the continental margin was known as well as could be expected from conventional bathymetry without GPS navigation.

A short multibeam bathymetric survey of the trench off Guatemala made with the French R/V *Jean Charcot* demonstrated the more coherent information acquired with multibeam bathymetry (Aubouin et al., 1981). Revealed were details of horst and graben as the plate bends into the trench. These horst and graben disappear under the base of the continental slope where the plate interface forms in a straight scarp parallel to the trench axis. Disruption of the lower slope by seafloor relief of ~300 m is minor but the slope morphology has a restless character that matches the poor coherence of reflectivity in seismic reflection records. Tectonism of the middle and lower slope is apparent from seismic data but without 100% coverage the tectonic significance of multibeam bathymetry is not obvious. Nonetheless, Aubouin correctly interpreted extensional tectonism and drilling established the non-accretionary nature of all but the slope toe.

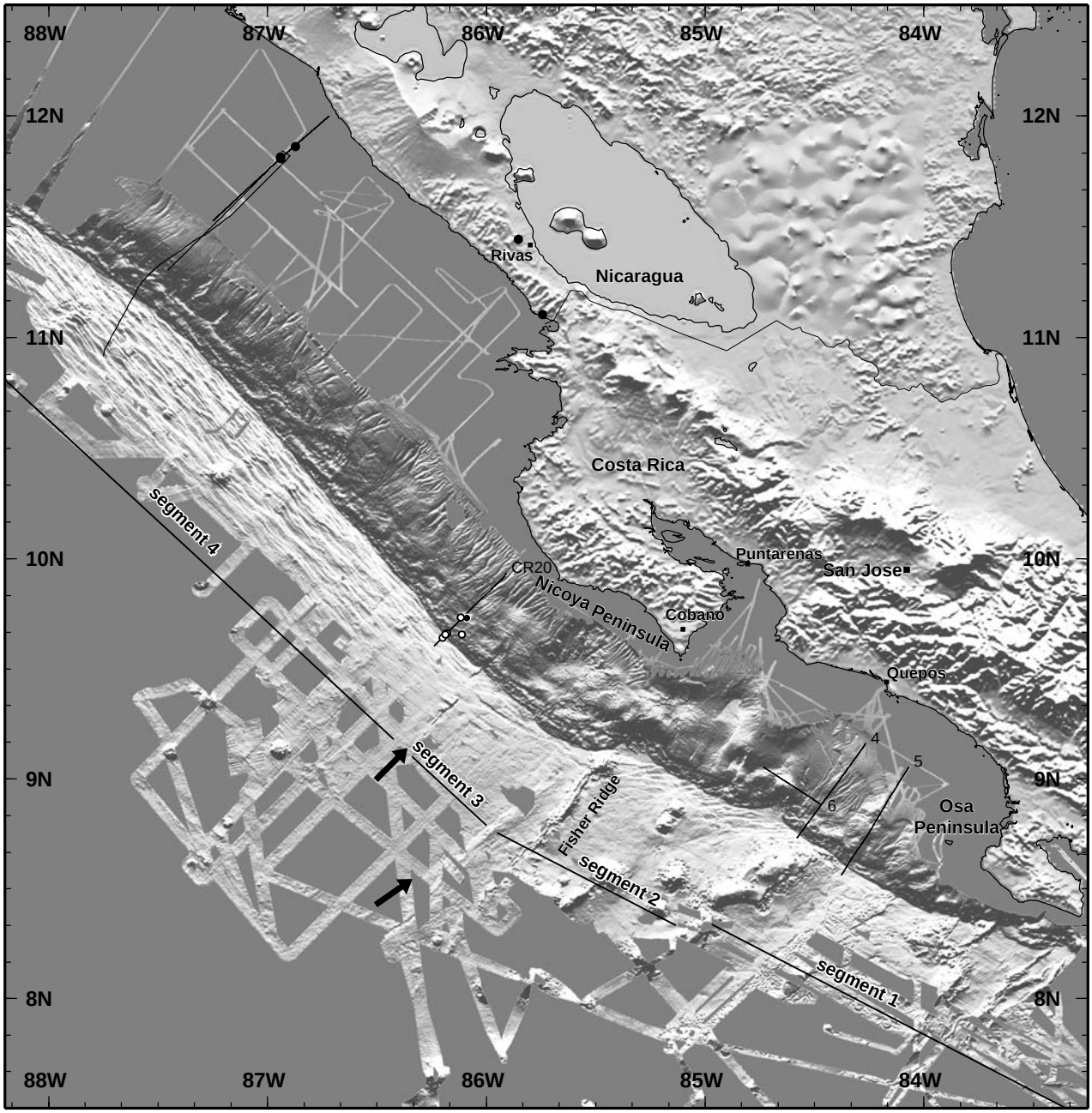

Figure 2.2.2: Shaded relief map of the bathymetry and topography of Costa Rica and Nicaragua. The oceanic plate has four segments with different morphological character. Segments 1-3 were formed at the Cocos-Nazca spreading center and segment 4 at the East Pacific Rise. Ocean Drilling Program (ODP) leg 170 sites are indidicated by black circles filled white. Deep Sea Drilling Program (DSDP) leg 84 site 565 is a white circle filled black. Oil exploration drills sites onshore and offshore Nicaragua are indicated by black filled circles. Black lines are tracks of seismic profiles.

A multibeam system was installed on the Scripps R/V *Thomas Washington* during a port stop in Puntarenas, Costa Rica in 1984. The instrument test data was preceeded by a survey off the Nicoya Peninsula where the continental slope morphology is least complicated (Shipley and Moore, 1986). It showed that even the simplest morphology was generously endowed with small scale gravity sliding as noted in DSDP drill cores (Baltuck et al., 1985). Off Guatemala the *Charcot* survey was expanded and the indications of accretion across the slope toe were emphasized (Moore et al., 1986). A small frontal prism was in evidence despite oceanic igneous rock covered by shallow water Cretaceous limestone close to the trench axis sampled during Legs 67 and 84.

The GEOMAR Geodynamics group selected Costa Rica for investigation because of the potential of subducting seamounts that had been raised inadvertently by the R/V Thomas Washington test survey. Scientific questions to investigate included the fate of large seamounts in a subduction zone, whether they remain on the lower plate or are sheared off, whether they form earthquake asperities, and whether they mechanically erode the continental margin. R/V *Sonne* mapped about 400 km of the CAM bathymetry with near 100% coverage (von Huene et al., 1995). These data were expanded during subsequent cruises and current maps include detailed morphology of the continental slope and incoming oceanic plate from northern Nicaragua to southern Costa Rica (Figure 2.2.2).

2.3 Accretion Versus Non-accretion Models

Seismic records acquired offshore Costa Rica by UTMSI in 1978 showed a thicker slope sediment section than offshore Nicaragua and Guatemala. Beneath that sediment section is a rough yet strong reflective top of the rock comprising the bulk of the continental margin, the so-called margin wedge. The base of the margin wedge is defined by strong reflections paralleling the plate interface (Figures 2.2.3 & 2.2.4). Within the margin wedge are landward dipping reflections clearly differentiated from diffractions (c.f. Shipley et. al.,1990). A hole drilled offshore Costa Rica during DSDP Leg 84 failed to reach basement for safety reasons and thus the accretionary model was not tested. The seismic records off Nicaragua and Costa Rica were interpreted in accord with the accretionary model (Shipley et al., 1986, 1990; Crowe and Buffler, 1985; Silver et al., 1985) although a non accretionary Costa Rican model was also proposed (Bourgois et al., 1984; von Huene et al., 1985). The UTMSI seismic data offshore the Nicoya Peninsula showed some of the strongest coherent plate interface reflections of any collected at the time and this area was chosen for the first academic 3-D reflection seismic experiment across a convergent margin. The 3-D survey was extended with lines shot from the continental shelf to the ocean plate (c.f. Shipley et al., 1990; 1992; McIntosh et al., 1993). Within the 3-D volume of rock, landward dipping reflections were traced from the within the margin wedge to the plate interface. They were interpreted as recently formed structures representing thrust faults,

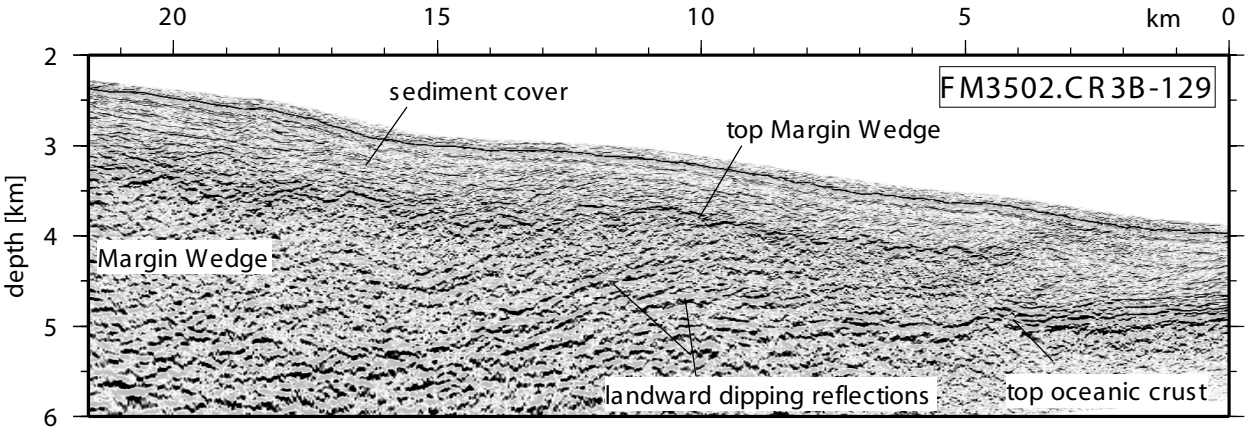

Figure 2.2.3: Seismic reflection section from a 3-D survey of the lower slope offshore Nicoya Peninsula, Costa Rica. After Shipley et al., 1992.

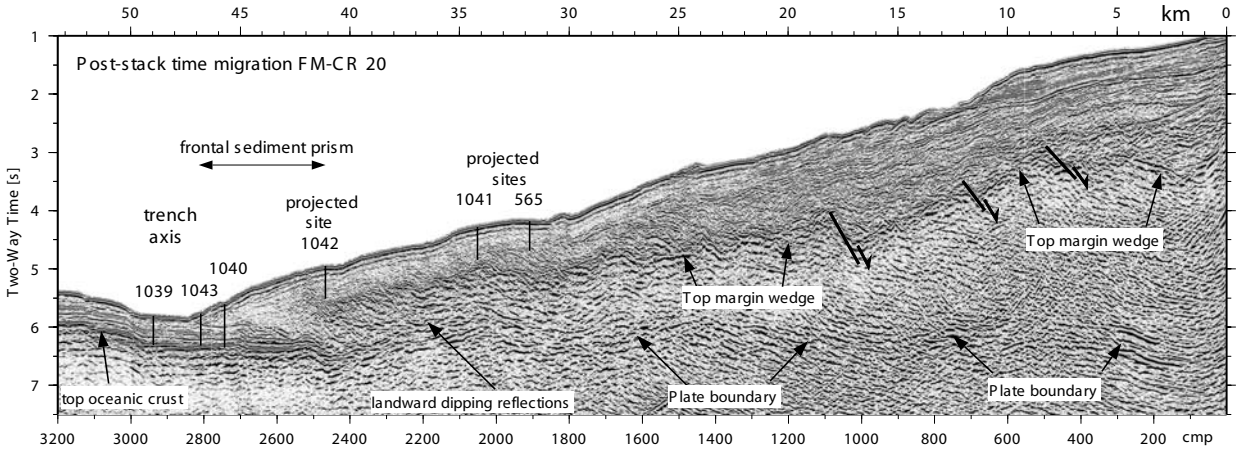

Figure 2.2.4: Seismic reflection profile FM-CR20. Stack produced at the Institute of Geophysics University of Texas at Austin (McIntosh et al., 1993). Post-stack deconvolution and time migration applied at GEOMAR. Ocean Drilling Program (ODP) leg 170 drill holes and Deep Sea Drilling Program (DSDP) leg 84 site 565 are shown. The margin wedge extends to ~ 7 km of the deformation front. The frontal sediment prism is composed of reworked slope sediment. All

duplex structures, and "out-of-sequence" faults. "Out-of-sequence" faults is a generic term derived from the constant accretionary model to explain landward dipping reflections that exceed the length of accretionary thrust faults. They are longer than the initially detached sections of accreted oceanic sediment and are proposed to cut the accretionary prism once the first thrust faults are rotated and become to steep to continue thickening the prism. Other structures were interpreted as underplated duplexes seaward of a post-Eocene accretionary prism forming the bulk of the continental margin (Figure 2.2.3 & 2.2.4). A major shortcoming of the interpretation was the lack of reliable velocity data and the difficulty to balance structure in the context of an accretionary model (von Huene and Flueh, 1994).

During the 1991 and 1992 R/V *Sonne* cruises 76 and 81, not only multibeam echosounding but also magnetic data (Barckhausen et al., 1998), seismic refraction data (Ye et al., 1996), and multichannel seismic reflection sections (Hinz et al., 1996) were acquired. The refraction data indicated higher velocity in margin wedge rock than that derived from time processing of the 3-D seismic reflection data. These velocities were similar to those in upper plate crustal rock of the Guatemalan margin (Ambos and Hussong, 1985) where the margin wedge had been shown to be igneous rock, and not indicative of young accreted sediment (von Huene and Flueh, 1994; Ye et al., 1996). In addition to the high velocities, the bathymetry offshore Central Costa Rica indicated only a small frontal prism. Also the subducting plate with seamounts and ridges appeared to erode the margin because opposite the seamounts the slope was indented (von Huene et al., 1995) (Figure 2.2.5). A non-accretionary origin explained most readily the structure imaged in reflection sections (Hinz et al., 1996). Modeling of magnetic anomalies was consistent with a margin wedge composed of igneous rather than sedimentary rock (Barckhausen et al., 1998). Drilling results from ODP Leg 170 confirmed that all sediment in the incoming plate is underthrust and no classical accretionary prism occurs, although the margin wedge rock was not unequivocally sampled (Kimura et al., 1997). In fact, the small "accretionary prism" at the lower slope was shown to consist only of tectonized slope sediment without transfer of oceanic sediment from the lower to the upper plate (Figure 2.2.4). Thus the former accretionary prism is now termed a frontal sediment prism. At this point the steady state accretionary model for Costa Rica was generally discarded.

3. Changes in the Paradigm

3.1. Long Term Subsidence and Subduction Erosion

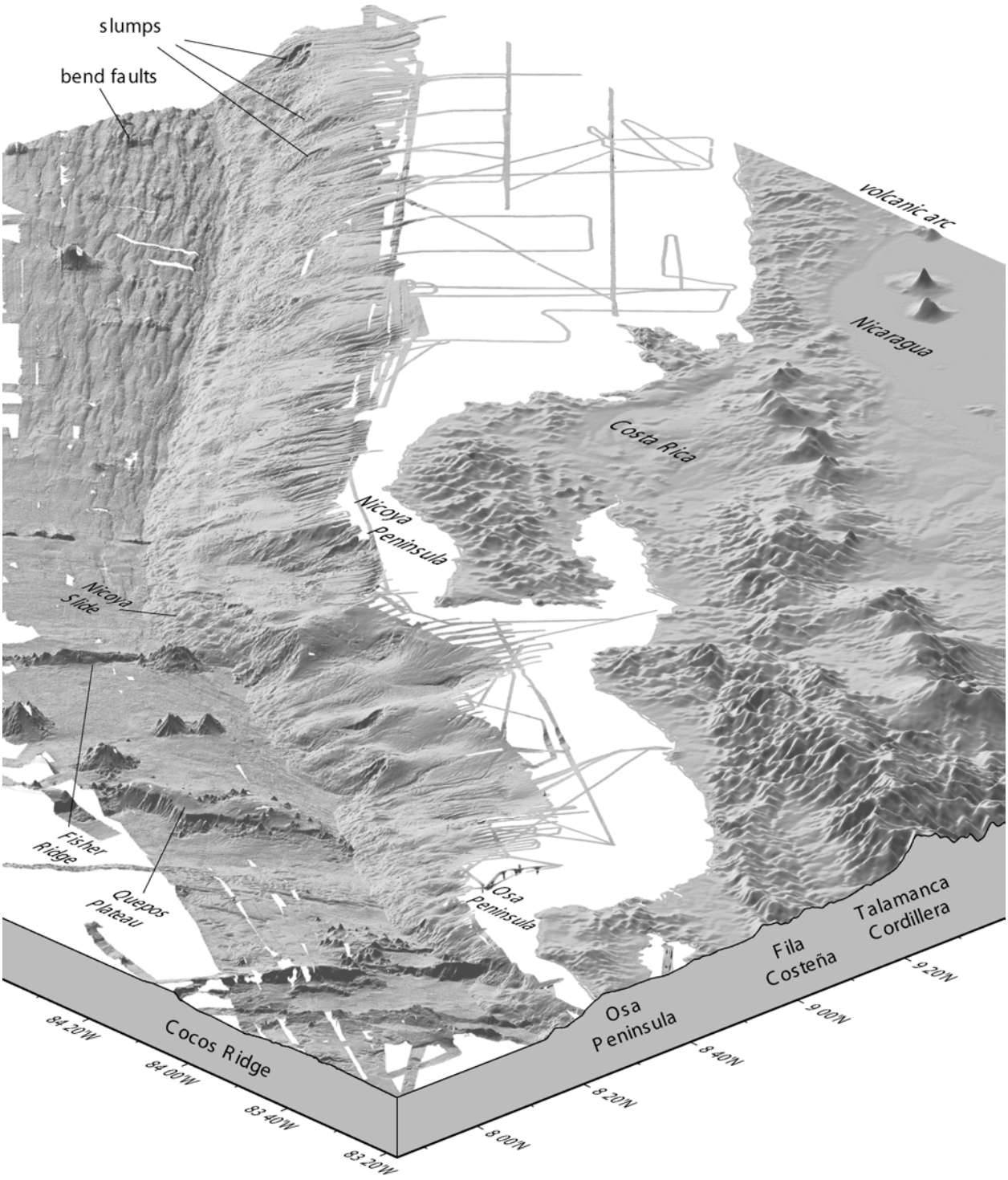

Figure 2.2.5: Perspective view of the shaded relief of bathymetry and topography of Costa Rica and Nicaragua. Main morphological features are labelled.

Tectonic processes controlling the past 5 Myr evolution of the CAM became much clearer once multibeam bathymetry was available and structure was imaged in true depth with multichannel seismic reflection sections (Figures 5 & 6). DSDP and ODP drill hole provided a lithostratigraphy of sedimentary units and benthic microfossil fauna documented paleo bathymetry to reveal a history of massive subsidence. These data indicated that a large mass of the CAM was missing and was presumed to be tectonically eroded during Neogene time.

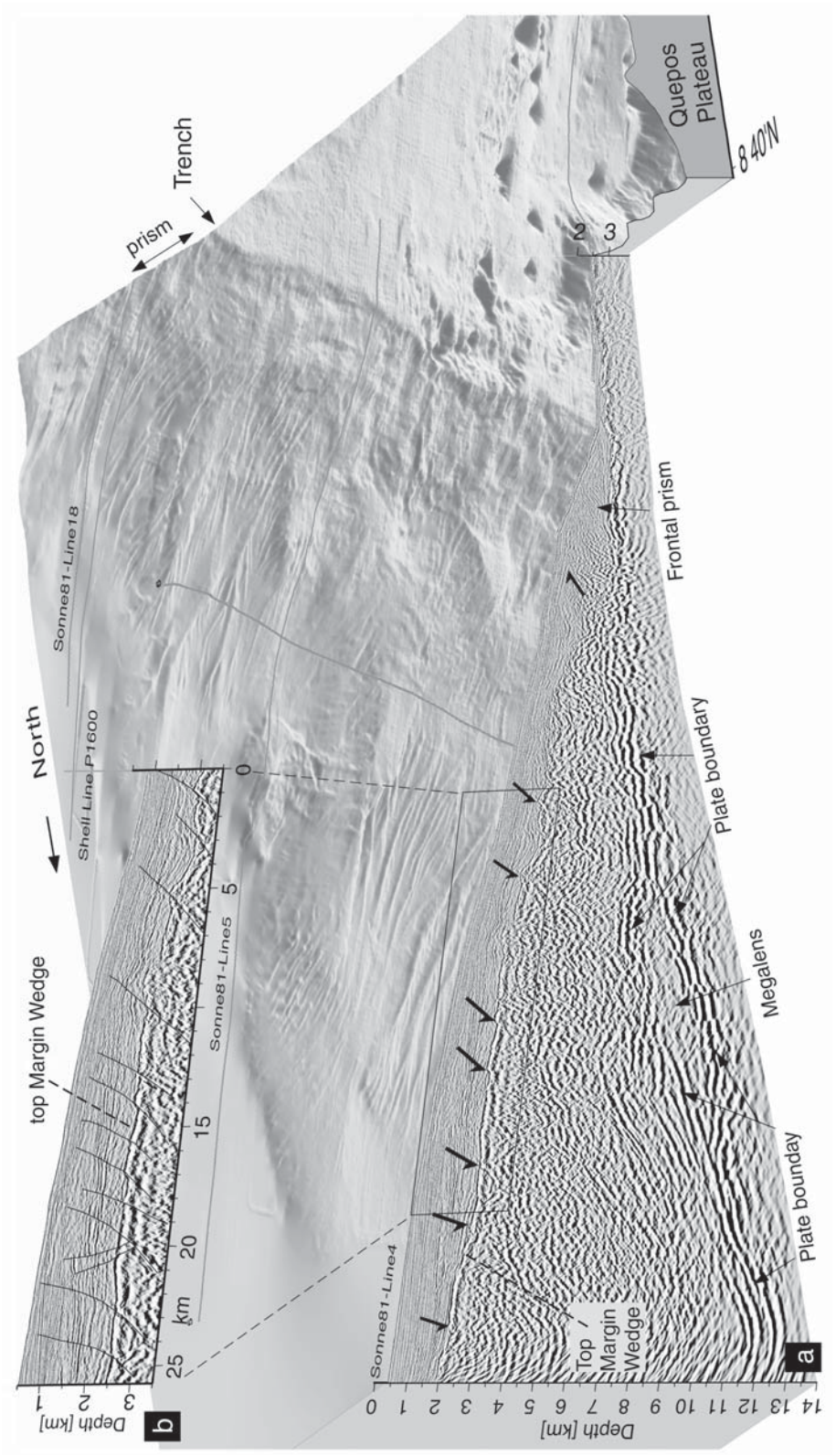

Figure 2.2.6: Pre-stack depth migration of SONNE-81 line 4 projected on bathymetic perspective. Resolution at ~10 km is ~0.5 km. Line 4 is 58 km long from the slope toe to the outer continental shelf. The top of the margin wedge is a smooth surface beneath the upper slope, cut by small offset normal faults (inset b). Fault offset increases and fault dip decreases downslope as the top of the margin wedge becomes rougher. The canyons in the upper and middle slope indicate a relatively stable environment where seamount have not recently underthrusted. Thrust faulting occurs only at the lower continental slope in the small frontal sediment prism. The frontal sediment prism is tectonically active as indicated by the disruption of the slope drainage system. Location on Figure 2.2.2. Modified from Ranero and von Huene (2000).

Paleontological evidence for Neogene margin subsidence offshore Costa Rica, and Guatemala supports the structural evidence for subsidence observed in the seismic data and this evidence is discussed below.
In Costa Rica, large-scale Neogene subsidence and upper plate extension has been interpreted from structure in seismic images and it is recorded in DSDP leg 84 and ODP leg 170 cores. The top of the margin wedge is a rough low-relief surface overlain by sedimentary strata that locally show onlap (Figure 2.2.6). Numerous normal faults offset these strata and some appear to continue as discrete reflections deep into the margin wedge. The upper plate landward of the frontal prism appears extended (Ranero and von Huene, 2000). Most likely, the rough surface at the top of the margin wedge is an erosional unconformity that subsided from the surf zone to its current depths beneath the outer shelf and the middle and lower slope (Figure 2.2.6).
The margin wedge lower boundary, the plate interface, is imaged as a reflective interface that retains a high amplitude signature for about 50 km from the trench and to about 12 km depth. Reflection and onshore-offshore refraction velocities constrain determinations upper plate thicknesses (± 300m) to the coast. If the margin wedge unconformity was formed by surf zone erosion near a former coast, the crust there may have been 14-16 km thick, similar to upper plate thicknesses beneath the current coast (Ye et al., 1996; Christeson et al., 1999; Sallares et al., 2001). The margin wedge in central Costa Rica is currently only 10 km thick beneath the outer shelf and about 3.5 km thick beneath the middle lower slope (e.g. km 35 on Figure 2.2.6). If the unconformity was formed near sea level, the upper plate must be thinned. Although faulting of the upper plate may account for some of the thinning, the small offsets along these faults is not sufficient to explain the much larger thinning observed and thus basal erosion and removal of material is a plausible explanation for subsidence. Upper plate extension is an apparent response to basal erosion and thinning rather than the cause of margin subsidence. The margin wedge unconformity and normal faulting has been mapped across the entire shelf and slope of Costa Rica (McIntosh et al., 1993; Ranero and von Huene, 2000; von Huene et al., 2000) and a similar unconformity separating igneous basement from overlying strata has been observed beneath the continental slopes of Nicaragua and Guatemala. Since onlap produces a time-transgressive unconformity, the age of the unconformity probably varies along the CAM.
Although the distinctive unconformity at the top of the margin wedge is seen regionally across the middle-upper slope, it becomes more irregular farther down slope and the upper plate is increasingly dismembered. Locally the unconformity is more disrupted where lower plate relief (seamounts and ridges) has subducted and stratigraphy is poorly imaged in seismic records because of the deformation (Ranero and von Huene, 2000). The margin wedge dismemberment beneath the lower slope is consistent with subduction erosion there.
Consistent with geophysical evidence for subsidence of the CAM in Costa Rica are results from studies of microfossil fauna in cores from site 565 of DSDP leg 84, and site 1041 of ODP leg 170. Additionally, the lithologies of rock from the margin wedge unconformity cored at site 1042, leg 170, have shallow-water affinities. Drilling at Sites 565 and 1041 penetrated much of the sediment overlying the margin wedge and good recovery provided a relatively continuous benthic foraminiferal stratigraphy. The depth at which the foraminiferal assemblages lived changes from shallow water at the base of the section, to abyssal fauna in the upper section consistent with the present depth of the sites (Vannucchi et al., 2000 and 2003 in press). The site 1042 cores just above the margin wedge unconformity recovered ~25 meter of carbonate cemented limestone breccia underlain by a ~10 meter of a breccia composed of clasts of red chert, doleritic basalt and mafic rock (Kimura, 1997). Deeper material from the high velocity body was not recovered because the site 1042 was located at the frontal tip of the margin wedge and a thrust truncated the stratigraphic section. The chert and igneous rock from the breccia are similar to rocks found in the Nicoya complex cropping out onshore (Kimura et al., 1997). Analysis of the carbonate cemented limestone breccia, currently at ~4 km beneath sea level, indicates a beach to near shore depositional environment (Vannucchi et al., 2000, Vannuchi et al., in press). These observations are explained by long-term margin subsidence as are faunal assemblages overlying the margin wedge that record progressive deepening. The beach to near shore carbonate cemented limestone breccia is ~16 Myr old and neritic fauna (water depth < 300 m) appears in sediment older than 5-6.5 Ma indicating slow average subsidence. However, the more detailed depth information from benthic foraminifera shows a sudden acceleration in subsidence offshore Nicoya Peninsula at ~5-6.5 Ma when that area of the margin subsided rapidly to upper-middle bathyal depth (< 800 m water depth). A renewed

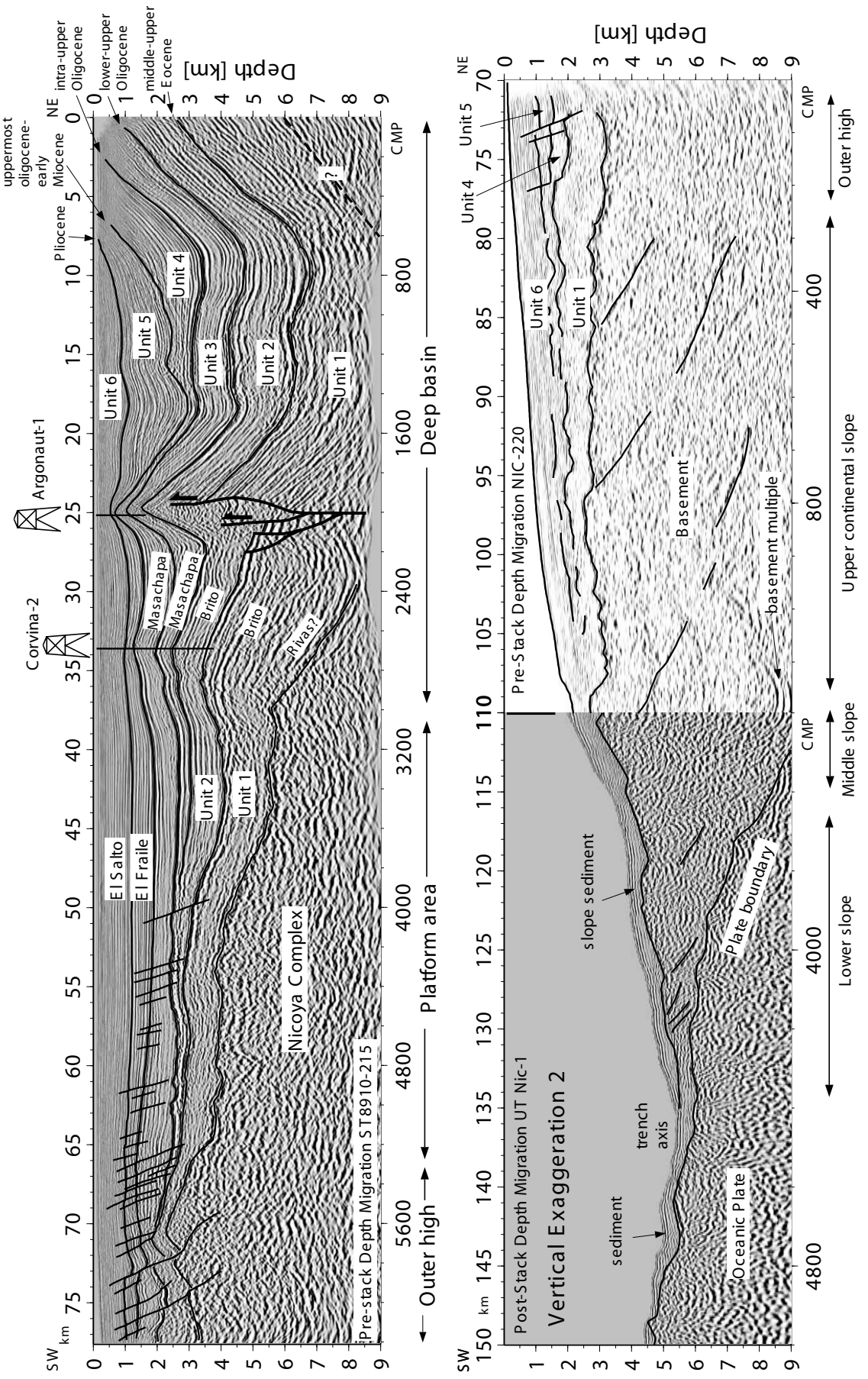

Figure 2.2.7: Pre-stack depth migration of a cross section composed of three multichannel seismic reflection profiles across the Nicaragua margin. Seismic stratigraphy have been calibrated with Corvina-

increase in subsidence rate occurred at ~1.8 Ma when the slope deepened to abyssal depths (> 2000 m) or the current core depth of ~3200 m. (Vannucchi et al., in press).
In Nicaragua, drill hole information along a seismic reflection/refraction transect across the Sandino Basin shows that the basin depocenter was located beneath the current continental shelf during Cretaceous to ~Middle Eocene time (Figure 2.2.7). The Cretaceous – early Tertiary sediment units rapidly pinch out up the basin seaward flank. Beneath the current upper continental slope, a thin Cretaceous – middle Eocene sediment sequence becomes indistinct down slope (Ranero et al., 2000) but probably extends to the middle slope where dredging recovered fragments of igneous basement rock and Cretaceous limestone (Silver et al., 2000). From about late Eocene to latest Oligocene or early Miocene time (~26-23 Ma) the outer shelf seafloor was sufficiently elevated to form a barrier to sediment transport and deposition was restricted to the inner shelf area where a stable depocenter accumulated sediment about 5 km thick. A major change in basin configuration and the beginning of long-term regional subsidence of the seaward part of the margin occurred in latest Oligocene or early Miocene time. When the outer shelf subsided, Neogene sediment covered the Cretaceous – early Tertiary units. Since early Miocene, a 70-km-wide swath of the Nicaraguan margin forming the current upper continental slope subsided about 2 km at the position of the current shelf break, and probably 3-4 km along the middle to-upper slope transition (Figure 2.2.7).
In Guatemala, paleo depths from benthic foraminifera of sites 568, 569 and 570 on the middle-upper slope yield a similar subsidence history as off Costa Rica (Vannucchi et al., submitted, 2003). Benthic foraminiferal assemblages indicate a progressive subsidence of the slope that might have started in latest Oligocene or early Miocene (~26-23 Ma) time. Subsidence began earlier (~26 Ma) in the middle slope (site 569 currently at 2799 m depth). Subsidence at site 568 (2030 m deep) started about 19 Ma and at site 570 (1720 m deep) about 11 Ma. The record of vertical tectonism shows a migration of margin subsidence toward the continent (Vannucchi et al., submitted, 2003).
The Neogene subsidence record in Guatemala and Nicaragua (~26-23 Ma), begins at approximately the same time but is somewhat later in Costa Rica offshore Nicoya Peninsula (~17 Ma). The rapid subsidence pulse at ~5-6.5 Ma in the latter area is not observed in Nicaragua or Guatemala. Widespread subsidence in the CAM might be related to a major kinematic reorganization of the plates in the eastern Pacific. Soon after the Farallon-Pacific spreading center collided with the North America Plate in the late Oligocene (Handschumacher, 1976) a latest Oligocene or Early Miocene (26-23 Ma) change in plate kinematics led to the opening of the Cocos-Nazca spreading center (Handschumacher, 1976, Barckhausen et al 2001). The plate kinematic reorganization produced a change from oblique to normal convergence along the MAT and was accompanied by an increased rate of crustal production along the East Pacific Rise (Wilson, 1996) adjacent to the newly formed Cocos Plate. Fast convergence rates and arrival of a younger and shallower slab at the trench may have induced subduction erosion along the plate boundary (Ranero et al., 2000; Vannuchhi et al., submitted, 2003). The rapid pulse of subsidence at 5-6.5 Ma recorded locally offshore Nicoya Peninsula is coeval with the arrival of the topographic swell associated with the Cocos Ridge (Vannuchhi et al., in press). Studies of the Talamanca Cordillera opposite the subducting Cocos Ridge, indicate that widespread calcalkaline volcanism ceased about 3.5-5 Ma (deBoer et al., 1995; Drummond et al., 1995). Adakitic rocks produced by partial melting of ocean crust were emplaced ~ 3.5 Ma (Abratis and Wörner, 2001) and fission track analysis date uplift of the cordillera (Graefe et al., 2002), These observations indicate a 5-7 Ma arrival time of Cocos Ridge at the trench. The arrival of Cocos Ridge further decreased the subduction angle of the incoming plate as far north as Nicoya Peninsula and after an initial uplift, a former shelf area subsided to its current abyssal depth (Vannucchi et al., in press).

3.2 Quaternary Tectonics

A compilation of multibeam bathymetry ~600-km-long and 100-150 km-wide offshore Costa Rica and Nicaragua provides an unprecedented map of the active tectonics exhibited as seafloor relief (Figures 2.2.2 & 2.2.5). Data were acquired with the hydrosweep system during *R/V Sonne* cruises 76, 81, 107, 144 and 150, R/V *M. Ewing* cruises 0005 (McIntosh et al., 2000) and 0104 (Fisher et al., 2003), and with a Simrad system during *R/V Sonne* cruise 163. Editing with MB system software (Caress and Chase, 1996) eliminated spurious soundings and accepted soundings were converted to depth with water velocities measured during

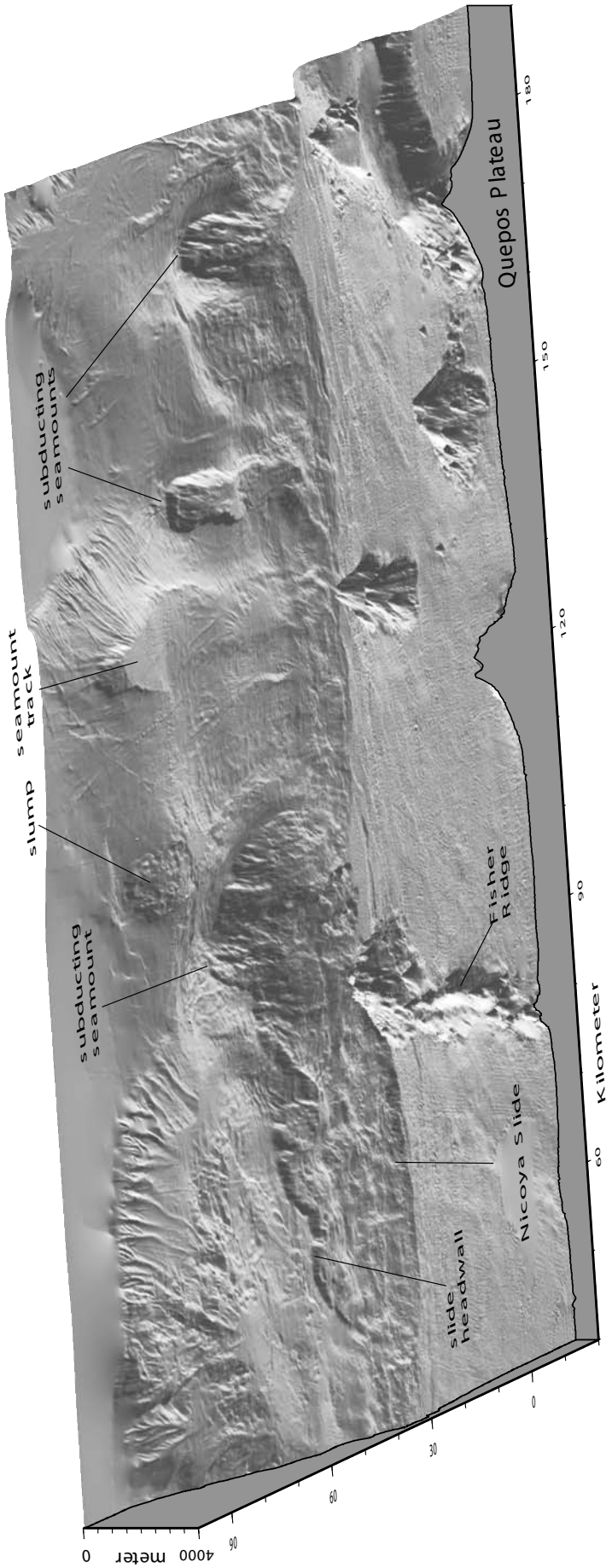

Figure 2.2.8: Perspective view of the shaded relief of the bathymetry from central Costa Rica showing seamount subduction and Nicoya slide.

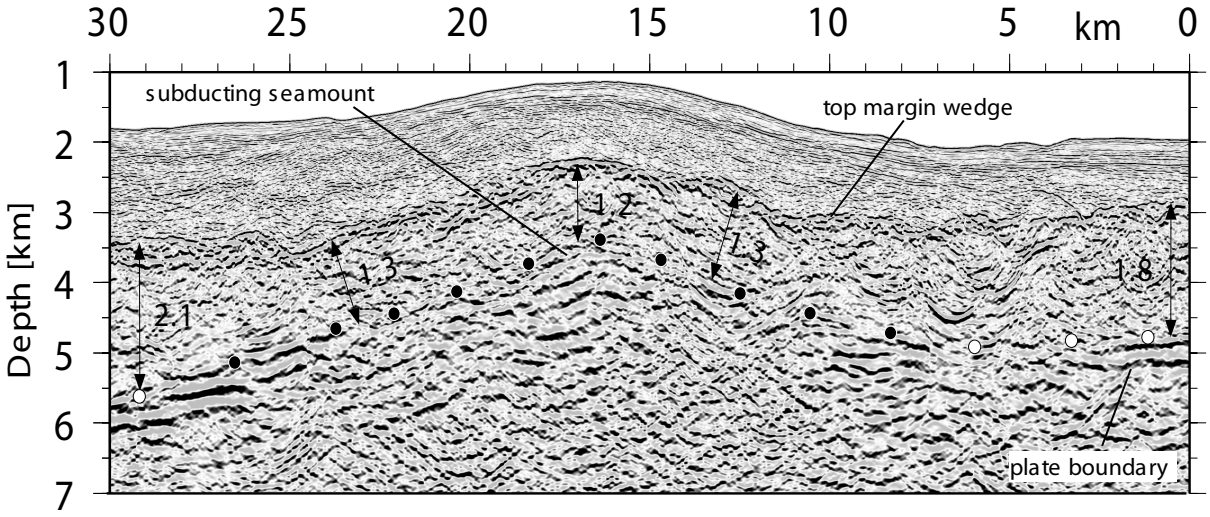

Figure 2.2.9: Prestack depth migration of SONNE-81 line 6 indicating active tectonic erosion above a subducting seamount as it tunnels underneath the continental plate. Dots mark the plate boundary, with black dots delineating the seamount flanks. This segment of line 6 is parallel to the continental margin and shows the lateral variations in margin wedge thickness. The margin wedge is 0.5-0.7 km thinner above the subducting seamount than on either side. The extension of the overriding plate caused by the uplift above the seamount is too small to explain the thinning. The thinning is probably due to ongoing tectonic erosion by the seamount. Location on Figure 2.2.2. Modified from Ranero and von Huene (2000).

different cruises. There data allowed gridding at ~100 m node spacing. This bathymetry resolves tectonic structure less than 0.5 km wide from which sedimentary and tectonic processes can be interpreted.

The emphasis of previous Costa Rica margin studies was on segmentation of the ocean plate which correlates with large-scale tectonic segmentation of the upper plate (von Huene et al., 2000; Ranero and von Huene, 2000). The current bathymetric compilation sharpens the correlation between lower ocean plate morphology and upper plate tectonics. Expanded coverage offshore Costa Rica and Nicaragua shows this upper/lower plate similarity that we interpret as a cause-and-effect relation between lower plate character and upper plate tectonism.

The along strike variability in ocean plate relief and water depth result from a combination of magmatic and tectonic processes. Magmatic processes at the Cocos-Nazca spreading center and the Galapagos hot spot govern crustal thickness from the 20 kms beneath the crest of Cocos Ridge to ~6 km offshore central Costa Rica (Ye et al., 1996; Stavenhagen et al., 1998; Walther, 2003). The higher than normal heatflow on and adjacent to Cocos Ridge and the much lower than normal heatflow offshore Nicoya Peninsula (Fisher et al., 2003) are probably also related to magmatic history and fluid circulation in ocean crust but causes for strong lateral changes have not yet been determined. Magmatism also constructed large volcanic edifices adjacent to Cocos Ridge. The tectonic process of bending-related normal faulting seems greatly influenced by crustal thickness and the orientation of tectonic fabric created at the spreading center with respect to the axis of bending. Seafloor relief in the study area defines 4 distinct oceanic plate segments (Figures 2.2.2 & 2.2.5). The lithosphere of segments 1-3 was formed at the Cocos-Nazca spreading center whereas segment 4 crust was formed at the East Pacific Rise. Segment 1 consists of the broad Cocos Ridge whose crest is the shallowest area (water depth 2.5-1.5 km) of the MAT. The shallow seafloor corresponds to the anomalously thick ocean crust of Cocos Ridge produced ~14 Myr ago by the interaction of the Galapagos hot spot with the Cocos-Nazca spreading center (Werner et al., 1999). Paralleling Cocos Ridge are large tilted normal fault blocks indicating extension perpendicular to the Ridge axis along Segment 1. Steep normal fault scarps dip toward the Cocos Ridge axis and bound a large graben over the thickest crust (Figures 2.2.2 & 2.2.5). Ridges, conical seamounts, and the Quepos Plateau characterize segment 2. The conical seamounts and Quepos Plateau are 13-15 Myr old (Werner et al., 1999) and are emplaced on 21-18 Myr old lithosphere (Barckhausen et al., 2001). The age and geochemistry of the seamounts is essentially the same as Cocos Ridge indicating emplacement during the hot spot activity in the adjacent Segment 1 lithosphere (Werner et

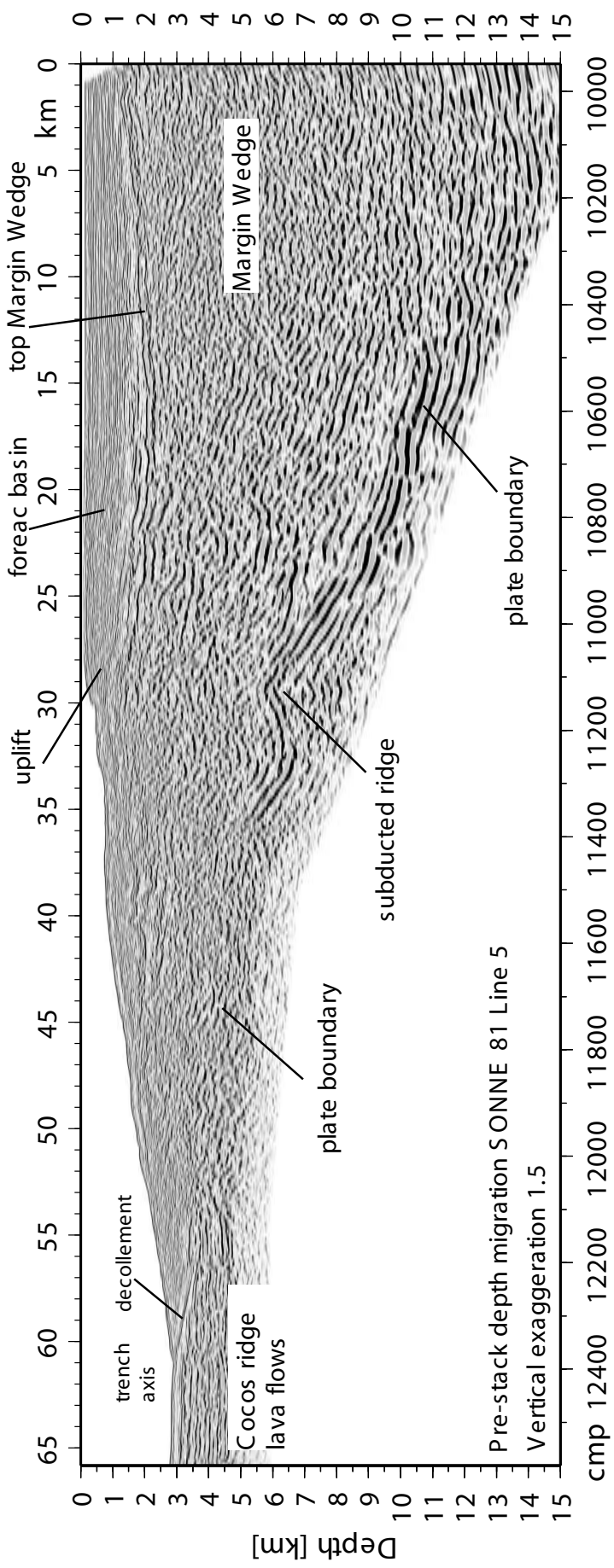

Figure 2.2.10: Prestack depth migration of SONNE-81 line 5 showing the subducted extension of the Quepos Plateau underneath the continental shelf. Note the uplift of the shelf strata above the subducting

al., 1999). The ocean crust of Segment 2 is 7-8 km thick (Ye et al., 1996, Walther 2003) and it is flexed into the trench more than the contiguous Segment 1. Bending at segment 2 is partially relieved by normal faulting near the trench axis, that strikes obliquely to the trench axis and to the seafloor spreading magnetic anomalies (Figures 2.2.2 & 2.2.5). Segment 3 has a 6 km thick crust (Ye et al., 1996) and has the smoothest morphology displaying a few bend faults with relatively small vertical displacement. Bending-related faults strike roughly parallel to the trench and are perpendicular to the magnetic anomalies, implying that bending, rather than reactivating the inherited tectonic fabric, formed new faults. The boundary between Segment 3 and Segment 4 is a low ridge that strikes perpendicular to the trench and marks the juncture between the lithosphere formed at the Cocos-Nazca spreading center and at the East Pacific Rise. The crust in Segment 4 is ~5-6 km thick (Ye et al., 1996; Walther et al., 2000) and is pervasively faulted as it bends into the trench. Faulting is roughly parallel to the trench axis and to magnetic lineations and thus parallel to the fabric formed at the East Pacific Rise (Figures 2.2.2 & 2.2.5). In this segment, trench depth and the width of the faulted area increase to the NW to ~5500 m depth.

In summary, the morphology of the subducting oceanic plate, the amount of bending and the associated increase in trench depth, change greatly in the segments of the CAM studied. Controlling parameters appear to be the changes in crustal thickness, its age and heatflow, and the angle between seafloor spreading fabric and the axis of bending. Remarkable is the parallelism between morphotectonics of the continental slope, the shelf, and land, and the morphological segmentation of the ocean plate. Active forearc structure is also greatly influenced by local uplift from subducting seafloor relief and the subsidence related to subduction erosion at the front and along the base of the upper plate. Thus, significant changes in the character of the subducting oceanic plate appear to influence differences in the Quaternary tectonic evolution of the continental margin. The influence of the character of the subducting oceanic plate is additionally correlated to the distinct styles of seismic activity occurring along the four segments of the margin.

Segment 1 of the incoming plate subducts offshore the Osa Peninsula of southeastern Costa Rica. It contains the thick and buoyant Cocos Ridge and correlates with singular morphotectonic features landward from the continental slope to the arc. Retreat of the margin is greatest opposite the colliding Cocos Ridge which implies accelerated Quaternary erosion (Figures 2.2.2 & 2.2.5). Opposite the subducting ridge, uplift of a broad area of the continental shelf culminates in the Osa Peninsula. The peninsula displays margin perpendicular topography parallel to the large tilted fault blocks on the ridge (von Huene et al., 2000). Landward of Osa Peninsula, the Fila Costeña thrust and fold belt is the only area along the margin where active contraction is significant. Further landward, arc volcanism is extinguished and the Talamanca Cordillera has been uplifted (Corrigan et al., 1990; Gardner et al., 1992) exposing mid crustal granodioritic plutons (de Boer et al., 1995). Rough relief from river incision characterizes the region where arc volcanism ceased and a drainage system developed (Figure 2.2.5). Large earthquakes of Mw 7-7.5 have nucleated in this area but during the past 20 years small earthquakes in this segment have been relatively few compared to those in the adjacent segments (Protti et al., 1995).

Segment 2 of the incoming plate subducts offshore central Costa Rica. The subducting ridges and chains of seamounts that are 2km to 3km high breach the margin front and leave seafloor grooves up the slope indicating material removal at the plate interface. Subducting seamounts breach the lower slope during initial collision with the margin (Figure 2.2.8) and as they tunnel beneath it they apparently erode the underside of the upper plate (Figure 2.2.9). The continental slope is uplifted above the subducting seamount relief causing mass wasting at the seafloor. Mass wasting produces slumps and slides locally extending several tens of km. The largest slide is the Nicoya slide with a headwall detachment running more than 50 km across the middle slope (Figure 2.2.8). The slide toe runs about 5 km up the ocean trench slope and it could have created a tsunami wave about 30 m high (von Huene et al., in press). Seamounts and ridges remain attached to the subducting plate beneath the continental shelf where they produce uplift (Figure 2.2.10). Subducted seafloor relief beneath the shelf induces a local increase of the stress on the megathrust interface and are areas of earthquake nucleation (Scholz and Small, 1997; Ranero and von Huene, 2000; Husen et al., 2001; Bilek et al., 2003). The chains of subducting seamounts are associated with clusters of earthquakes (Ranero and von Huene, 2000) but the largest events are Mw < 7. On land, some seamounts are associated with local uplift that may separate the Panama Block from northern Costa Rica along margin perpendicular faults (Fisher et

al., 1998; Marshall et al., 2000). In this segment the volcanic output is greater than along other segments of the arc.

Where large seamounts on the ocean plate are sparse, roughness of seafloor is confined to bending-related normal faulting. Segment 3 and the contiguous portion of segment 4 exhibit a relatively smooth subducting oceanic plate morphology (Figures 2.2.2 & 2.2.5) mainly opposite the Nicoya Peninsula. There the continental slope displays a relatively stable morphology with gentle dips and well-developed canyon systems in the upper-middle slope (Figure 2.2.5). Heatflow across the slope is exceptionally low (Langseth and Silver, 1996). Some of the largest historic earthquakes have nucleated in this segment (Protti et al., 1995). DSDP leg 84 and ODP leg 170 drilling sampled the lower continental slope and the adjacent oceanic sediment, and sills of a Galapagos composition above the East Pacific Rise crust of this segment.

Segment 4 displays a notable increase in bend faulting and morphological roughness that increases towards the NW (Figures 2.2.2 & 2.2.5). The vertical displacement of individual faults increases progressively from a few tens of m to a ~500 m average height. A parallel change in continental slope morphology occurs along the margin and the slope dip increases causing slumps whose scars become abundant in the NW (Figures 2.2.2 & 2.2.5). This is the area where the damaging 1992 tsunami earthquake occurred (Ihmlé, 1996).

Summary

The CAM was recognized as a Pacific type margin with a trench and Wadati-Benioff zone early in the exploration of the Pacific Basin and was identified as a subduction zone when the plate tectonic paradigm first developed. It was significant in developing the knowledge to correctly differentiate between accretionary and erosional convergent margin end-members. When only seismic data are available the constant accretionary end-member rooted in a steady-state accretionary model must be applied with greater care than it was invoked in the past. Landward dipping reflections in seismic records are not only derived from accretionary processes and in erosional margins may represented extensional structures or inherited fabric and their origin requires further investigation.

The CAM displays the effects of lower plate character on tectonics in the upper plate. The effects of relief, crustal thickness and heatflow, and the orientation of original oceanic crust fabric also shape continental slope structure, induce a pattern of earthquake seismicity, influence the potential for tsunamigenic submarine sliding, and correlate with changes in the volcanic arc. Oceanic crustal thickness and temperature correlate with trench depth and bending of the incoming plate. Orientation of oceanic crustal fabrics subdue or

accentuate bend faulting which imparts subducting plate roughness and correlates with rates of erosion. The interactive geological processes are not yet fully understood and are the topics of ongoing research. The differences in the character of the subducting plate are sharply segmented along the CAM and segment boundaries in the lower plate are features in the upper plate. This segmentation is also recognized in the separation of earthquake magnitude and pattern and to some extent the development of large submarine slides. Thus, the forefront research along the CAM contributes significantly to a basic understanding of natural hazards and towards the mitigating of their damaging effects.

References

Abratis, M., and Wörner, G., Ridge collision, slab-window formation, and the flux of Pacific asthenosphere into the Caribbean realm, *Geology, 29,* 127-130, 2001.

Ambos, E.L., and D.M. Hussong, Structure at the toe of the subduction complex: Middle America Trench offshore Guatemala, Deep Sea Drilling Project Leg 84, in R. von Huene, J. Auboin, et al., *Init. Rept. DSDP*, 84: Washington (U.S. Govt. Printing Office), 861-878, 1985.

Aoki, Y.; Tamano, T; Kato, S. Detail structure of the Nankai Trough from migrated seismic sections. Studies in Continental Margin Geology. Ed. J. S. Watkins and C. L. Drake, Am. Assoc. Pet. Geol. Mem. 34, 309-322, 1982.

Auboin, J., Stephan, J. F., Renard, V., Roump, J., Lonsdale, P. Subduction of the Cocos plate in the Middle America trench. Nature 94, 146-150 (1981).

Aubouin, J., von Huene, R.,Baltuk, M., Arnott, R., Bourgois, J., Leg 84 of the Deep Sea Drilling Project, subduction without accretion: Middle America Trench off Guatemala, *Nature, 247*, 458-460, 1982.

Aubouin, J. and von Huene, R., Summary: Leg 84, Middle America Trench transect off Guatemala and Costa Rica: *in* Von Huene R. and Aubouin, J., Eds.: Initial Reports, DSDP, 84: Washington, D.C., U.S. Government Printing Office, p. 939-956. 1985.

Baltuck, M., Taylor, E., and McDougall K., Mass movement along the inner wall of the Middle America Trench, Costa Rica, in *Initial Report DSDP Leg 84*, edited by R. Von Huene and J. Aubouin, pp. 551-570, U.S. Goverment Printing Office, Washington, 1985.

Barckhausen, U., H.A. Roeser, and R. von Huene, Magnetic signature of upper plate structures and subducting seamounts at the convergent margin off Costa Rica, *J. Geophys. Res*., *103*, 7079-7093, 1998.

Barckhausen, U., Ranero, C.R., von Huene, R., Cande, S.C., and Roeser, H.A., Revised tectonic boundaries in the Cocos Plate off Costa Rica: implications for the segmentation of the convergent margin and for plate tectonic models, *Journal of Geophysical Research, 106*, 19207-19220, 2001.

Bourgois, J., J. Azéma, P.O. Baumgartner, J. Tournon, A. Desmet, and J. Aubouin, The geologic history of the Caribbean-Cocos plate boundary with special reference to the Nicoya ophiolite complex (Costa Rica) and D.S.D.P. results (legs 67 and 84 off Guatemala): A syntesis, *Tectonophysics, 108*, 1-32, 1984.

Caress, D.W., and D.N. Chase, Improved processing of Hydrosweep DS multibeam data on the RV Maurice Ewing, *Mar. Geophys. Res*., *18*, 631-650, 1996.

Case, J.E., and Holcombe, T.L., 1980, Geologic-tectonic map of the Caribbean region: U.S. Geological Survey Miscellaneous Investigations Map I-11000, scale 1:250,000

Christeson, G.L., K.D. McIntosh, T.H. Shipley, E.R. Flueh, and H. Goedde, Structure of the Costa Rica convergent margin, offshore Nicoya Peninsula, *J. Geophys. Res*., *104*, 25, 443-25, 468, 1999.

Corrigan, J., P. Mann, and J.C. Ingle, Forearc response to subduction of the Cocos Ridge, Panama-Costa Rica, *Geol. Soc. Am. Bull., 102*, 628-652, 1990.

Crowe, J.C., and R.T. Buffler, Multichannel seismic records across the Middle America Trench and Costa Rica-Nicaragua convergent margin, NCY-7 and NCI-1, in Middle America Trench off western Central America, Ocean Drilling Program, Regional Data Synthesis Series, edited by J.W. Ladd and R.T. Buffler, Atlas 7, 11 p, Marine Science International, Woodshole, Massachusetts, 1985.

deBoer, J.Z., M.S. Drummond, M.J. Bordelon, H. Bellon, and R.C. Maury, Cenozoic magmatic phases of the Costa Rican island arc (Cordillera de Talamanca)*, Spec. Pap., Geol. Soc. Am., 295*, 35-55, 1995.

Dickinson, W. R. Clastic sedimentary sequences deposited in shelf, slope and trough between magmatic arcs and associated trenches. Pacific Geology, 3, 15-30, 1971.

Drummond, M.S., Bordelon, M., de Boer, J.Z., Defant, M.J., Bellon, H., Feigenson, M.D., Igneous petrogenesis and tectonic setting of plutonic and volcanic rocks of the Cordillera de Talamanca, Costa Rica-Panama, Central American Arc, *American Journal of Science, 295,* 875-919, 1995.

Fisher, A. T., Stein, C. A., Harris, R. N., Wang, K.; Silver, E., A.; Pfender, M.; Hutnak, M.; Cherkaoui, A.; Bodzin, R.; Villinger, H. Abrupt thermal transition reveals hydrothermal boundary and role of seamounts within the Cocos Plate. Geophys. Res. Let., 30, 10.1029/2002GL016766. 2003.

Fisher, D.M.; Gardner, T.W.; Marshall, J.S.; Sak, P.B.; and Protti, M. Effect of subducting sea-floor roughness on fore-arc kinematics, Pacific coast, Costa Rica, *Geology, 26*(5), 467-470, 1998.

Fisher, R. L. Geomorphic and seismic refraction studies of the Middle America Trench, 1952-1956, PhD Thesis, Los Angeles, Univ. of California. 1957.

Fisher, R.L., Middle America Trench: Topography and structure, *Geol. Soc. Am. Bull*., *72*, 703-720, 1961.

Fisher, R.L., Hess, H. H., in Hill, M. N. ed. The Sea, vol 3, New York Wiley. 1963.

Gardner, T.W., D. Verdonck, N. Pinter, R. Slingerland, K. Furlong, T.F. Bullard, and S.G. Wells, Quaternary uplift astride the aseismic Cocos Ridge, Pacific coast of Costa Rica*, Geol. Soc. Am. Bull*., *104*, 219-232, 1992.

Graefe, K., Frisch, W., Villa, I.M., and Meschede, M., Geodynamic evolution of southern Costa Rica related to low-angle subduction of the Cocos Ridge: constraints from thermochronology, *Tectonophysics, 348*, 187-204, 2002.

Gutenber, B., Richter, C. F. Seismicity if the Earth, N.J. Princeton Univ. Press. 1954.

Handschumacher, D. W., Post-Eocene Plate Tectonics of the Eastern Pacific. The Geophysics of the Pacific Ocean Basin and its margin, ed. G.H. Sutton, M.H. Manghnani and R Moberly, Geophysical Monograph, 19, 177-202, 1976.

Hey, R., Tectonic evolution of the Cocos-Nazca spreading center; Geol. Soc. Am. Bull. 88, 1414-1420, 1977

Hinz, K., R. von Huene, C. R. Ranero, and the PACOMAR Working Group, Tectonic structure of the convergent Pacific margin offshore Costa Rica from multichannel seismic reflection data, *Tectonics, 15*, 54-66, 1996.

Heacock, J. G., Worzel, J. L. Submarine topography west of Mexico and Central America. Bull. Geol. Soc. Am., 83, 1671-1692, 1955.

Ihmlé, P. F. Monte carlo slip inversion in the frequency domain: Application to the 1992 Nicaragua slow earthquake. *Geophys. Res. Lett*., vol. 23, 913-916, 1996.

Karig, D. E. Origin of the Philippine Sea basin complex, in Ingle, J. C., Karig, D. E. et al., Init. Rep. DSDP, vol 31, Washington, D. C., U.S. Govt. Printing Office, 1975.

Kimura, G., et al., *Proceedings of the Ocean Drilling Program Initial Reports,* vol. 170, Ocean Drill. Program, College Station, Tex., 1997.

Langseth, M.G., and E.A. Silver, The Nicoya convergent margin: A region of exceptionally low heat flow, *Geophys. Res. Lett., 23*, 891-894, 1996.

Lonsdale, P. and Klitgord, K. D. Structure and tectonic history of the eastern Panama Basin. Geol. Soc. Am. Bull., 89, 981-999, 1978.

McIntosh, K., E. Silver, and T. Shipley, Evidence and mechanisms for forearc extension at the accretionary Costa Rica convergent margin, *Tectonics, 12*, 1380-1392, 1993.

McIntosh, K., Silver, E., Ranero, C.R., Preliminary results of a Nicaragua-Costa Rica MCS/OBH seismic survey, Eos, 81, American Geophysical Union Fall Meeting (San Francisco). 2000.

Miller, H., Das Problem des hypothetischen „Pazifischen Kontinentes“ gesehen von der chilenischen Pazifikkuste, *Geol. Rundsch., 59*, 927-938, 1970.

Moore, G. F., Shipley, T. H., and Lonsdale, P. F., Subduction erosion versus dediment offscraping at the toe of the Middle America Trench off Guatemala: *Tectonics*, v. 5, no. 4, p. 513-523, 1986.

Protti, M., F. Gundel, and K. McNally, Correlation between the age of the subducting Cocos plate and the geometry of the Wadati-Benioff zone under Nicaragua and Costa Rica, *Spec. Pap. Geol. Soc. Am.,295*, 309-326, 1995.

Ranero, C. R.; von Huene, R.; Flueh, E., Duarte, M. and Baca, D. A cross section of the forearc Sandino Basin, Pacific Margin of Nicaragua. *Tectonics*, *19*, 335-357 2000.

Ranero, C.R. and Von Huene R., Subduction erosion along the Middle America convergent margin, *Nature, 404*, 748-752, 2000.

Rutland, R. W. R., Andean orogeny and ocean floor spreading. *Nature* 233, 252-255 (1971).

Scholz, C. H. & Small, C., The effect of seamount subduction on seismic coupling, *Geology*, 25, 487-490 (1997).

Seely, D. R., Geophysical investigations of continental slopes and rises, *in* Watkins, J. S., and Montadert, L., eds., Geological and Geophysical Investigation of Continental Margins: *American Association of etroleum ecologists Memoir* 51, p. 245-260, 1979.

Seely, D.R., P.R. Vail, and G.G. Walton, Trench slope model, in Geology of Continental Margins, edited by C.A. Burk, and C.L. Drake, pp. 261-283, Springer-Verlag, New York, 1974.

Shipley, T.H., and G.F. Moore, Sediment accretion, subduction, and dewatering at the base of the trench slope off Costa Rica: A seismic reflection view of the décollement, *J. Geophys. Res., 91*, 2019-2028, 1986.

Shipley, T.H., P.L. Stoffa, and D.F. Dean, Underthrust sediments, fluid migration paths, and mud volcanoes associated with the accretionary wedge off Costa Rica: Middle America Trench, *J. Geophys. Res., 95*, 8743-8752, 1990.

Shipley, T.H., K.D. McIntosh, E.A. Silver, and P.L. Stoffa, Three-dimensional seismic imaging of the Costa Rica accretionary prism: Structural diversity in a small volume of the lower slope, *J. Geophys. Res., 97*, 4439-4459, 1992.

Shor, G. G., Fisher, R. L., Middle America Trench, Bull. Geol. Soc. Am., 72, 721-730, 1961.

Silver, E.A., Ellis, M. J., Breen, N. A., Shipley, T. H., Comments on the growth of accretionary wedges. *Geology, 13*, 6-9, 1985.

Silver, E., et al., Influence of lower plate structure on the overriding slope offshore Nicaragua: New geophysical observations and the first dredge samples of basement rocks, Eos, 81, American Geophysical Union Fall Meeting (San Francisco). 2000.

Stavenhagen, A.. U., E.R. Flueh, C. Ranero, K. D. McIntosh, T. Shipley, G. Leandro, A. Schulze, and J.J. Dañobeitia, Seismic wide-angle investigations in Costa Rica: A crustal velocity model from the Pacific to the Caribbean Coast, *ZBL. Geol. Palaontol., Part I,* 393-408, 1998.

Vannucchi, P., Scholl, D.W., Meschede, M., and McDougall-Reid, K. Tectonic erosion and consequent collapse of the Pacific margin of Costa Rica: combined implications from ODP Leg 170, seismic offshore data and regional geology of the Nicoya Peninsula, *Tectonics, 20,* 649-668, 2001.

Vannucchi, P., Ranero, C.R., Galeotti, S., Straub, S.M., Scholl, D.W., McDougall-Ried, K., Fast rates of subduction erosion along the Costa Rica Pacific margin: implications for non-steady rates of crustal recycling at subduction zones, Journal of Geophysical Research (in press.).

Vannucchi, P., Galeotti, S.; Clift, P. D.; Ranero, C.R.; von Huene, R. Long term subduction erosion along the Middle America Trench offshore Guatemala. Geology (submitted).

von Huene et al. Leg 67: The Deep Sea Drilling Project Mid-America Trench transect off Guatemala. *Geol. Soc. Am. Bulletin*, 91, 421-432, 1980.

von Huene R., J. Aubouin, et al., Site 565, in *Initial Report DSDP Leg 84*, edited by R. Von Huene and J. Aubouin, pp. 21-78, U.S. Goverment Printing Office, Washington, 1985.

von Huene, R., et al., Morphotectonics of the Pacific convergent margin of Costa Rica, in *Geologic and Tectonic Development of the Caribbean Plate Boundary in Southern Central America*, edited by P. Mann, *Spec. Pap. Geol. Soc. Am*., *295*, 291-308, 1995.

von Huene, R., and Flueh, E.R. A review of marine geophysical studies along the Middle American Trench off Costa Rica and the problematic seaward terminus of continental crust, *Profil 7*, Stuttgart, 143-159, 1994.

von Huene, R., Ranero C.R., Weinrebe W., and Hinz K., Quaternary convergent margin tectonics of Costa Rica, segmentation of the Cocos plate, and Central American Volcanism, *Tectonics, 19*, 314-334, 2000.

von Huene, R., Ranero, C. R. and Watts, P. Tsunamigenic slope failure along the Middle America Trench in two tectonic settings. Marine Geology (in press).

Walther, C. The crustal structure of the Cocos ridge off Costa Rica. J. *Geophys. Res., 108*, doi:10.1029/2001JB000888, 2003.

Walther, C.H.E., E.R. Flueh, C.R. Ranero, and R. von Huene, Seismic investigations at the Pacific Margin of Nicaragua, *Geophys. J. Int*., 141, 759-777, 2000.

Watkins, J. S, et al., Init. Repts. DSDP, 66, Washington, D. C., U.S. Govt. Printing Office, 1982

Werner, R., K. Hoernle, P. van den Bogaard, C.R. Ranero, R. von Huene, and D. Korich, Drowned 14 m.y. old Galapagos archipelago off the coast of Costa Rica: Implications for tectonic and evolutionary models, *Geology, 27*, 499-502, 1999.

Wilson, D., 1996, fastest known spreading on the Miocene Cocos-Pacific plate boundary: Geophysical Research letters, v. 23, p. 3003-3006.

Ye, S., J. Bialas, E.R. Flueh, A. Stavenhagen, R. von Huene, G. Leandro, and K. Hinz, Crustal structure of the Middle American Trench off Costa Rica from wide-angle seismic data, *Tectonics, 15*, 1006-1021, 1996.

2.3. Biological objectives of the cruise

(Wagner, J.)

The sensory systems of cephalopods, crustaaceans and teleosts living in the mesopelagic zone have to work in an environment in which the diversity of stimuli they are exposed to is poorer than in any other (aquatic) habitat on earth. At the limit of the penetration range of sunlight, vision based on image forming processes is (probably) much reduced, whilst chemical cues mediated by the gustatory and olfactory system are present, as is information encoded in pressure changes of various frequencies and perceived by the lateral line organs and, possibly, audition. In spite of this situation of relative deprivation, a remarkably speciose fauna has evolved showing various, highly specific specialisations of their sensory systems. This is particularly true for vision, which gained a new role due to the evolution of bioluminescence.

Most of our knowledge of the sensory systems of mesopelagic fauna is derived form indirect conclusions and speculations from morphological, biophysical or biochemical studies of individual organs. The reliability of such observations is often limited by the unsatisfactory preservation of the specimens. Phsysiological or biological mesurements on living fish, organs,or isolated cells are rare. Likewise, direct observations of the mesopelagic fauna in their natural environment are limited due to the high cost associated with the deployment of submersibels, remotely operated vehicles (ROVs) and lander systems.

The aim of the present Sonne cruise is to use trawl gear which minimises damage to the animals during capture, and to attempt physiological, biophysical and biochemical experiments in addition to morphological techniques to study the hair cell system of mesopelagic fish (lateral line organs and hearing), as well as the bioluminescence and the visual system of cephalopods, crustaceans and teleosts. Furthermore, and in an integrative approach, the relative importance of the various sensory systems will be analysed by morphometric studies of the brains.

The key component of the trawling equipment is a closing cod end, a rigid cylinder which isolates the animals from the high temperatures of the surface waters and protects them against the mechanical stress during hauling of the net, and therefore brings many specimes on deck alive. Furthermore, animals remain dark adapted even during daylight trawls,- an essential prerequisite for physiological work on the visual system. The subsequent experimental instruments include an electrophysiological set-up for recording electroretinograms to determine the sensitivity of fish and crustacean eyes, a spectrophotometer for the analysis of the absorption spectra of visual pigments, and a range of biochemical instruments for the study of the acitvity of coelenterazine, a key enzyme in the reaction cascade of bioluminescence. While these experiments can be carried out on board, the moprhological work includes delicate dissection work at sea (preparaiton of the lateral line components and the inner ear, incl. Innervation, or the craninal nerves an dapplication of tracer substances) with a subsequent chemical fixation, storage at –80°C and fine-structural analysis using confocal, or electron microscopes in the various land-based laboratories.

The major specific topics to be studied on this cruise include:

- a possible depth denpendency of the activity of coelenterazine
- the distribution and frequency of occurrence of chlorophyll as a photosensitiser in fish eyes
- the search for animals that have developed a defense strategy against the red stealth light ofstomiid dragonfish, by acquiring red senstivity without, however emitting bioluminescence in the long wavelength range
- the mechanisms of regeneraiton of bleached rhodopsin in deep sea fish eyes?

- a possible correlation of visual sensitivity and depth in fish and crustacean eyes.

- a search for novel differentiations of the lateral line system based on living, and minimally harmed specimens, which may have been missed peviously due to skin abrasions in non-closing cod ends

- an analysis of the inner ear with the search for specialisations of the sacculus, utriculucs, lagena and otoliths in order to identify fish with hearing capabilities?

- a comaprative study of brain areas to find out which sensory systems play a dominant role in central processing?

- An investigation of the pineal organ including morphology, the melatonin content at various stages in the 24h cycle and the search for possible cyclic patterns in the mealtonin release.

Details about the various projects are presented in the context of the description of the respective instruments and methods used and/or the results obtained.

3. Participants

3.1 Scientists

Wilhelm Weinrebe	GEOMAR, SFB574, chief scientist
Xiaohong Deng	University of Maryland
Ronald Douglas	City University
Noemi Fekete	SFB574
Tamara Frank	Harbor Branch
Claudio Gonzalez Solis	Universidad de Costa Rica
Ingo Grevemeyer	GEOMAR
Kylie Jennings	University of Queensland
Cecile Marchand	UCL
Fabienne Paasch	UCL
Julian Partridge	Bristol University
Jason Phipps Morgan	GEOMAR, SFB574
Cesar R. Ranero	GEOMAR, SFB574
Gerardo J. Soto	ICE
Alison Sweeney	Duke University
Paola Vannucchi	Universita di Firenze
Roland von Huene	UC Davies
Hans-Joachim Wagner	Universität Tübingen
Elizabeth White	City University

3.2 Crew

Hartmut Andresen	Master
Carsten Simon	Chief Mate
Matthias Linnenbecker	1st Mate
Ronald Stern	1st Mate
Holger Dietz	Surgeon
Volker Hartig	Chief Engineer
Ralf-Michael Krösche	2nd Engineer
Matthias Häckel	2nd Engineer
Rainer Papendieck	Electrician
Rudi Angermann	Chief Electronic Engineer
Michael Dorer	Electronic Engineer
Peter Holler	System Operator
Jörg Leppin	System Operator
Rainer Rosemeyer	Fitter
Uwe Szych	Motorman
Stefan Werner	Motorman
Hermann Rademacher	Motorman
Klaus Hermann	Chief Cook
Volkhard Falk	2nd Cook
Jan Hoppe	Chief Steward
Anette Nickel	2nd Steward
Bernd Gerischewski	2nd Steward
Peter Mucke	Boatswain
Hans-Jürgen Vor	A. B.
Jürgen Kraft	A. B.
Detlef Etzdorf	A. B.
Götz vom Berg	A. B.
Andreas Schrapel	A. B.
Christian Milhahn	Trainee
Manfred Walderstein	Trainee

3.3 Addresses of Participating Institutions

City University:
City University
Applied Vision Research Centre
Northampton Square
London EC1V OHB
Tel.: +44-20-7040-5060
Fax.: +44-20-7040-8355
e-mail: r.h.douglas@city.ac.uk
Internet: www.city.ac.uk

Duke University:
Duke University
Johnsen Laboratory
Box 90338
Durkham NC 27708
Tel.: 919-660-7274
e-mail: ams27@duke.edu

GEOMAR:
GEOMAR
Forschungszentrum für marine Geowissenschaften der
Christian-Albrechts-Universität zu Kiel
Wischhofstr. 1-3
24148 Kiel, Germany
Tel.: +49-431-600-2281
Fax: +49-431-600-2922
eMail: Iname@geomar.de
Internet: www.geomar.de

Harbor Branch:
Division of Marine Science
Harbor Branch Oceanographic Institution
5600 U.S. 1 North, Fort Pierce,
Florida, 34946, U.S.A.
Tel.: 772-465-2400 ext. 311
Fax.: 772-468-0747
e-mail: frank@hboi.edu

ICE:
Insituto Costaricense de Electricidad
C.S. Exploratió Subterránea, Sabana Norte
Apartado 10032 San José, Costa Rica
Tel.: 00506-220-6394
00506-695-6522
Fax.: 00506-220-8212
e-mail: GSotoBo@ice.go.cr

SFB 574:
Sonderforschungsbereich 574
Christian-Albrechts-Universität zu Kiel
c/o GEOMAR Forschungszentrum
Wischhofstr. 1-3
24148 Kiel, Germany
Tel.: +49-431-600-1413
Fax.: +49-431-600-2922
e-mail: Iname@geomar.de
Internet: www.geomar.de

UC Davis:
University of California, Davis
2910 North Canyon Rd. Camino
CA., 95709 U.S.A.
Tel.: 001-530-644-6078
e-mail: rhuene@mindspring.com

UCL:
UCL, Louvain
J.-F. Rees, Institut science de la vie,
Carnoy, place croix du sud 5
1348 LLN
Tel.: 32-10-478751
Fax.: 32-10-473515
e-mail: fabpaasch@hotmail.com

Universidad deCosta Rica:
Universidad de Costa Rica
San Josè, Costa Rica
Tel.: 506-229-4224
Fax.: 506-229-4224
e-mail: claudiogeo@hotmail.com

Universita di Firenze:
Universita` di Firenze
Via La Pira, 4
50121 Firenze
Tel.: +39-055-2757494
Fax.: +39-055-218628
e-mail: paolav@geo.unifi.it

Universität Tübingen:
Universität Tübingen
Anatomisches Institut
Österbergstrasse 3
72074 Tübingen, Germany
Tel.: +49-7071-297-3019
Fax.: +49-7071-29-4014
e-mail: hjwagner@anatu.uni-tuebingen.de

University of Bristol:
School of Biological Sciences
University of Bristol
Woodland Road, Bristol BS8 1UG, U.K.
Tel.: 0117-9287591
Fax.: 0117-9257374
e-mail: j.c.partridge@bristol.ac.uk
Internet: www.bio.bris.ac.uk/people/partridge.htm

University of Maryland:
University of Maryland
1210 Biology-Psychology Building
College park, MD 20742, U.S.A.
Tel.: 301-405-6903
Fax.: 301-314-9358
e-mail: xiaohongdeng@hotmail.com

University of Queensland:

The University of Queensland
Level2, Ritchie Laboratourues
St Lucia Queensland,
4072 Australia
Tel.: +61-7-33654484
Fax.: +61-7-33654522
e-mail: k.jennings@uq.edu.au

Figure 3.1.1: Cruise participants of SO-173/2

4 Agenda of the cruise

(Weinrebe, W.)

Cruise SO-173/2 „SEDUCTION“ started on August 8, 2003 in Caldera, Costa Rica. SONNE left the pier at 11:30 a.m. after 19 scientists had embarked, but had to wait at anchorage until 23:00 when the last delayed luggage arrived. Two groups of scientists working in two different projects in different fields with different methods comprised the scientific crew. This combination was chosen because neither group would have used the ship-time and laboratory facilities efficiently, and their programmes could scheduled perfectly together. The group of marine geoscientists – geophysicists, geologists and petrologists – were studying “Seismogenesis and tectonic erosion during subduction: Middle America margin off Guatemala and Osa peninsula”, giving the whole project the acronym: SEDUCTION. 9 scientists from Germany, Spain, Italy, Hungary, USA, and Costa Rica formed this group. The group of 10 marine biologists from Germany, Belgium, UK, USA, Australia, and China (PRC) studied “Sensory mechanisms in mesopelagic fish”. The planned experiments of both groups fit very well in a work plan so that available ship time was used without any wasted time. The mutual information on their respective work during many discussions and the information was given in 10 science meetings with these presentations a stimulating working athmosphere was created, both groups benefitted from this interaction.

After leaving the anchorage of Caldera SONNE steamed northwestwards towards the research area offshore Guatemala. The transit track was carefully planned to survey areas off Costa Rica and Nicaragua with the Simrad EM-120 multibeam system which were not covered by former cruises, or which had bad data. The transit was interrupted for a first haul with the mesopelagic RMT 8 trawl off Nicaragua on August 9 in the evening which resulted in a very good catch of big eels; few hatchetfish; big melamphaeids;1 mesopelagic grenadier; some unknowns; 1 Malacosteus; lots of transparent things on deck. Trawl 2 using a tucker trawl with CCE (closed cod end) was hauled on Sunday August 10 in the morning, still in Nicaraguan waters shortly before entering the exclusive economic zone of El Salvador. It brought many live fish on deck. Following a long track parallel to the coast we passed El Salvador and entered Guatemalan waters on Monday August 11. The research permission required that an observer of the Guatemalan Navy had to stay onboard as long as SONNE worked in Guatemalan territory. So RV SONNE headed towards a meeting point with a Navy boat about 10 miles off the coast near Puerto Quetzal. On Tuesday August 12, Guatemalan Navy Lt. Munoz Duarte boarded SONNE to join the expedition.

The survey area offshore Guatemala covered the subduction zone from the upper slope across the deep sea trench to the ocean plate including the outer rise, an area the size of approxiamtely 170 nm by 100 nm. This area was mapped with the Simrad EM-120 multibeam system and the magnetometer along a pattern of a parallel profiles trending perpendicular to the coast. The PARASOUND system was run continuously at the same time, however, due to the steep seafloor only an occasional profile of sufficient in length could be recorded without multiple steps. As prevailing currents forced us to do the trawling heading towards southeast or northwest, the trawls were generally scheduled to take place on the connections between two adjacent bathmetry profiles, in order to make optimal use of shiptime. Trawl 3 and 4 were hauled on Wednesday August 13, Trawl 6 on August 14, Trawl 7 on August 15, Trawl 8 on August 16, Trawl 9 on August 18, Trawl 10 on August 20, Trawl 11 on August 22 and Trawl 12 on August 23. Generally, all the trawls in Guatemalan waters did not show the quantity of fish and the variety of species as were hauled further southeast in the first two trawls off Nicaragua.

In addition to the 50 bathymetry profiles perpendicular to the coast, mm profiles parallel to the coast were run to fill areas with sparse coverage. The map of the surveyed area showed a prominent mound-like structure of about 800 m height and about 3.500 m in diameter on the upper slope in a water depth of around 2000 m. This structure at 13°17.1’ N, 91°25.3’ W was named “Mound Quetzal” after the important port of Puerto Quetzal nearby. Rock samples of this mound were taken on Saturday August 23 in two dredge hauls. The first dredge recovered variously altered boulders of mudstone, fine grained sandstone and volcanic rocks. A first comparison with the rocks recovered close by during DSDP Leg 84 gives them an approximate Eocene

age. The second dredge recovered fresher, mainly dentritic rocks characterised by widespread deformation due to brecciation and veining. The age is still referable to pre-Eocene.

The work offshore Guatemala was finished with detailed mapping of the San Jose Canyon, a steeply incised and probably still active canyon cutting the continental margin from the upper slope down to the trench. Towards the end of this survey on Sunday August 24 SONNE steamed to the meeting point with Guatemalan Navy. After 12 days Lt. Munoz Duarte left us and went ashore on a small Guatemalan Navy boat.

The following days were used to map the adjacent continental margin of El Salvador. Here a profile layout parallel to the shore were chosen. Along one of these profiles in the early morning of August 27 SONNE was escorted by a gunbboat of El Salvadorian Navy, checking our research permit for El Salvador. Only at the southeastern end of these lines in Nicaraguan waters trawls were hauled, as the research permit for El Salvador did not include any biological work. So Trawl 13 was hauled on Monday August 25, Trawl 14 on August 26, Trawl 15 on August 28 and Trawl 16, 17, and 18 on August 29. Generally these trawls brought more fish and a greater variety of species, in particular the last three hauls at the most southeasterly position.

A small network of 4 Ocean Bottom Hydrophones (OBH) which had been deployed during cruise SO-173 leg 1 for studying microseismicity on the ocean plate, had to be recovered latest on August 29. The 4 OBHs were recovered in the night of August 28 to August 29 from 20:00 to 03:30 without any problems. All 4 instruments had worked continuously. A quick investigation of the recorded data showed recordings of several earthquakes in the area in good quality.

On Saturday August 30 and Sunday August 31 the bathymetric survey was completed with two long profiles parallel to the coast of El Salvador across the ocean plate seaward of the Middle America Trench.

In the morning of September 1 at 08:00 RV SONNE moored at the pier in port of Caldera, Costa Rica. Thus, the Cruise SO173/2 ended after 23 days at sea.

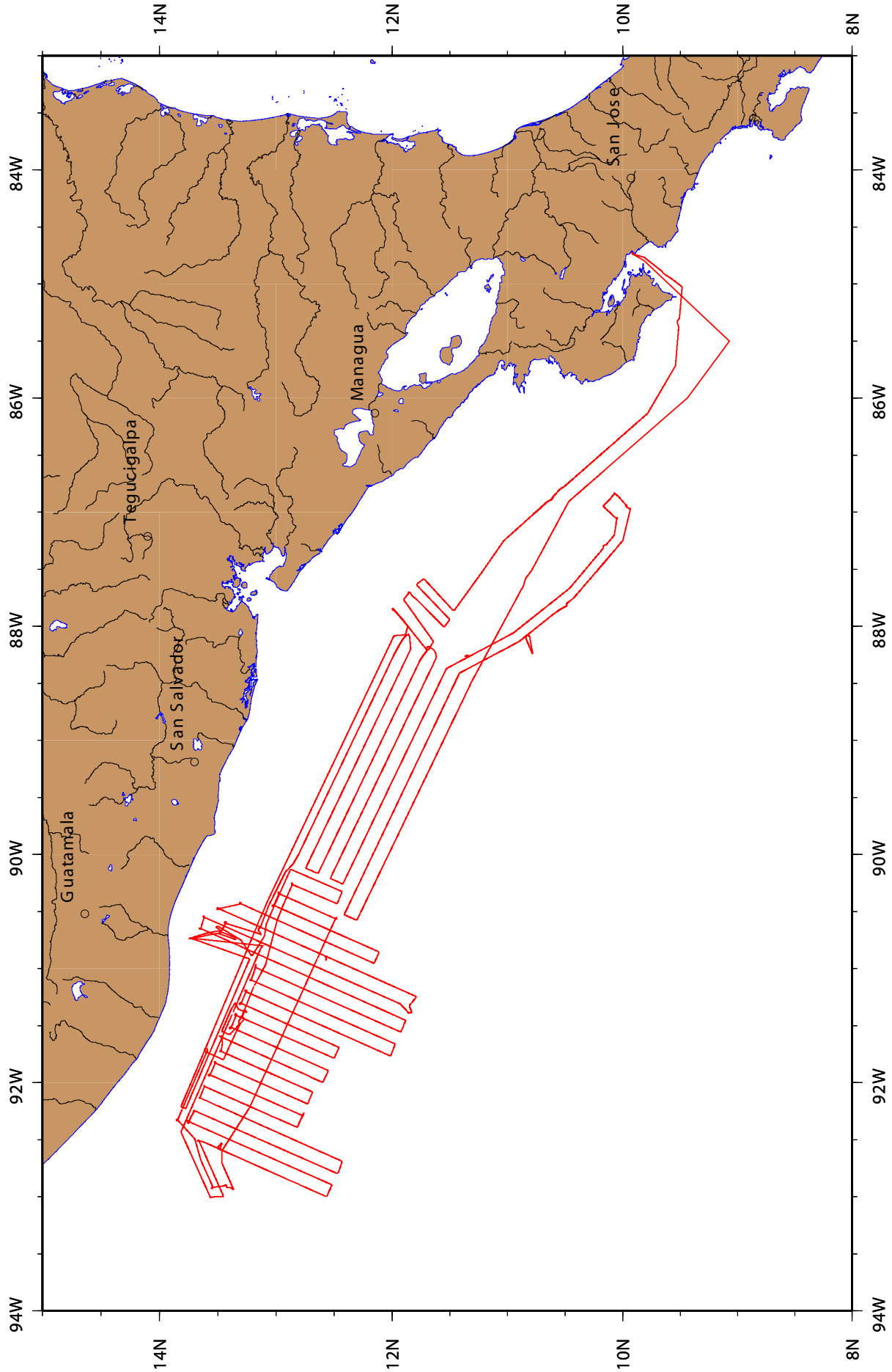

Figure 4.1: Cruise track of SO-173/2

5.1 Computer facilities for bathymetry, magnetic, and seismic data processing

(W. Weinrebe)

The experiments and investigations during SO173/2 required special computing facilities in addition to the existing shipboard systems. For programming of ocean bottom stations, processing and interpretation of seismic data and analysis of magnetics several workstations and a dedicated PC-laptop were installed by the wide angle and seismology groups of GEOMAR. Due to the large amount of data transfer GEOMAR installed a workstation cluster onboard comprising the following systems:

1	“moho”	SUN Sparc20 2 CPU	256 MB memory	20 GB disks DAT	Sun Solaris 5.8
2	”devonia”	SUN Ultra 60 2 CPU	2 GB memory	1.500 GB - RAID-array 1x DLT8000	Sun Solaris 5.6
3	”hotblack”	SUN Ultra 1 1 CPU	394 MB memory	1.500 GB - RAID-array 1x DLT8000	Sun Solaris 5.8
4	”galicia”	SUN Sparc 10 1 CPU	128 MB memory	12 GB disks DAT	Sun Solaris 5.8
5	”crimea”	AMD DURON 700 MHz	128 MB memory	68 GB disks 6x PCMCIA	Windows2000
6	„pinta“	AMD DURON 700 MHz	128 MB memory	68 GB disks 6x PCMCIA	Windows2000

In addition to these computers, several laptops were used. For plotting and printing two HP Postscript Laserprinters (papersize A3 and A4) as well as the shipboard color plotters were available.

The workstation cluster was placed in the Magnetiklabor and the Reinlabor where it was set up according to a ”client-server” model, with ”moho” being the server. All important file systems from the main server at GEOMAR were duplicated onto the ”moho”-disks. Using NFS-, NIS-, and automounter services the computing environment was nearly identical to that at GEOMAR, so every user found his/her familiar user interface. The convenience of network mounted file systems has to be paid for with a heavy network load, particularly during playback of OBH-data (c.f. SO123 cruise report, Flueh et al., 1997). This required a high-performance network, which was accomplished by a switched twisted-pair ethernet. A 12-port ethernet switching-hub (3COM-SuperstackII 1000) with an uplink connection of 100 Mbps to the server ”moho” and dedicated 10 Mbps ports for the client workstations maintained the necessary network performance. In order to keep the shipboard network undisturbed by the workstation cluster, but to allow for communication between them, the server ”moho” was equipped with two network interfaces and served as a router. This provided the additional benefit of a simplified network configuration. Considerable setup work was dedicated to ”moho”, while the other workstations used the same IP-addresses and network configuration as at GEOMAR. In addition, „hotblack“ was set up as an redundant server, so in case „moho“ would have failed, „hotblack“ could easily switched to replace „moho“ as a server.

This network setup showed a reliable and stable performance, and no breakdowns were observed.

5.2 The Magnetometer

(I. Grevemeyer)

Over the incoming oceanic plate and the adjacent margin wedge the local magnetic field generated by crustal rocks and perhaps alterated uppermost mantle may yield important constraints on the age of the down-going oceanic lithosphere, mantle serpentinization, and the structure and composition of the fore-arc crust. During the cruise SO173-2 we used a GeoMetrics G801/3 Marine Proton Magnetometer. The instrument itself – a gasoline-filled sensor – was towed astern the vessel. A 250-m-long marine cable connects the sensor with the control unit aboard RV SONNE. To obtain the Earth's total magnetic field strength an electric current (called the polarization cycle) generates a strong magnetic field in the coil of the sensor and forces the magnetic moments of the protons in the gasoline to be aligned for a short time parallel to the artificial field. During the following measuring cycle, i.e., when the electric current is turned off, the previously excited field is removed and the protons "try" to realign themselves with the Earth's magnetic field. According to the fundamental physical law of moment preservation, this happens by precession of the protons with a certain frequency, which is directly proportional to the intensity of the Earth's magnetic field. Basically, this frequency is measured as AC electric current created by magnetic induction in the coil, amplified, counted and transformed to magnetic field intensity values (measuring unit: 10^{-9} Tesla = 1 nT), which are recorded.

In order to minimize the contamination of the measurements by artificial magnetic fields caused by the vessel (i.e., the field induced in the ship's hull, the ship's engine, and other sources on the vessel), the sensor of the Magnetometer is towed ~180 m behind the ship. A record generally avoid of spikes and high frequency noise suggests that this distance was long enough; the achieved resolution was about 5 nT.

On board of RV SONNE, the magnetometer winch was placed on the port back deck and the sensor was towed to the port side of the vessel. A boom leads the cable about 7 m to the side of the ship in order to prevent it from being tangled with the ship during turns and during times of strong wind facing the port side.

The measured values of the total intensity magnetic field are provided as digital time series coded in BCD values. The system was set to deliver one data point every 3 seconds via digital multi-port interface to a PC, where the data were stored along with time in ASCII tables.

After data backup the files were transferred to a SUN workstation. Here the measured magnetic field records were supplemented with geographical (GPS) coordinates, using UTC time as common factor. The magnetic data and the navigation data were smoothed with a Gauss filter and re-sampled at an interval of 10 s. In a final step the appropriate International Geomagnetic Reference Field (IGRF) was removed to yield the magnetic field caused by the magnetization of crustal rocks.

5.3 Seismic Instrumentation

The Ocean Bottom Hydrophone

The first GEOMAR Ocean Bottom Hydrophone was built in 1991 and tested at sea in January 1992. This type of instrument has proved to have a high reliability; in fact during this cruise we celebrated the 2000 successful deployment. A total of 20 OBH and 9 OBS instruments were available for SO163. Altogether 212 sites were occupied during the SO163 cruise.

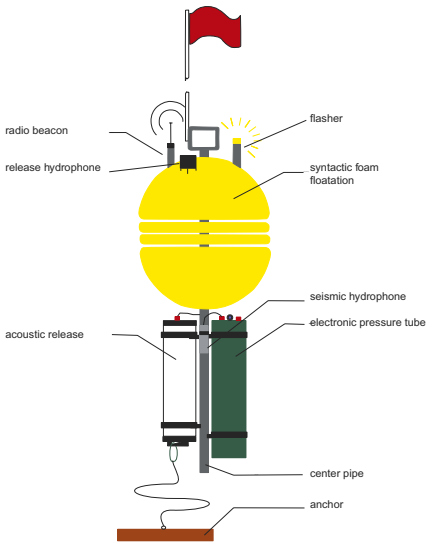

Figure 5.3.1: Principle design of the GEOMAR OBH (after Flueh and Bialas, 1996)

Figure 5.3.1 Principle design of the GEOMAR OBH (after Flueh and Bialas, 1996).

The principle design of the instrument is shown in Figure 5.3.1, and a photograph showing the instrument upon deployment can be seen in Figure 5.3.2. The design is described in detail by Flueh and Bialas (1996).
The system components are mounted on a steel pipe which holds the buoyancy body on its top. The buoyancy is made of syntactic foam and is rated, as are all other components of the system, for a water depth of 6000 m, except for the pressure cylinders holding the recording electronics. Here, various models are available for variable depths (2500 m, 3000 m, and 6000 m). Attached to the buoyant body are a radio beacon, a flash light, a flag and a swimming line for retrieving from aboard the vessel. The hydrophone for the acoustic release is also mounted here. The release transponder is a model *RT661CE* made by *MORS Technology*. Communication with the instrument is possible through the ship's transducer system, and even at maximum speed and ranges of 4 to 5 miles release and range commands are successful. For anchors, we use pieces of railway tracks weighing about 40 kg each. The anchors are suspended 2 to 3 m below the instrument. The sensor is an *E-2PD* hydrophone from *OAS Inc.*, or the HTI-01-PCA hydrophone from *HIGH TECH INC.* and the recording device is a *MBS* recorder of *SEND GmbH*, which is contained in its own pressure tube and mounted below the buoyant body opposite the release transponder (see Figures 5.3.1 and 5.3.2).

Marine Broadband Seismic Recorder (MBS)

The so-called *Marine Broadband Seismic recorder (MBS;* Bialas and Flueh, 1999*)*, manufactured by *SEND GmbH*, was developed based upon experience with the DAT based recording unit Methusalem (Flueh and Bialas, 1996) over the last few years. This new recorder avoids a mechanically driven recording media, and the PCMCIA technology enables static flash memory cards to be used as unpowered storage media. Read/ write errors due to failure in tape handling operations should not occur with this system. In addition, a data compression algorithm is implemented to increase data capacity. Redesign of the electronic layout enables a decreased power consumption (1.5 W) of about 25% compared to the *Methusalem* system. Depending on the sampling rate, data output could be in 16 to 18 bit signed data. Based on digital decimation filtering, the system was developed to serve a variety of seismic recording requirements. Therefore, the bandwidth reaches from 0.1 Hz for seismological observations to the 50 Hz range for refraction seismic experiments and up to 10 kHz for high resolution seismic surveys. The basic system is adapted to the required frequency range by setting up the appropriate analog front module. Alternatively, 1, 2, 3 or 4 analogue input channels may be processed. Operational handling of the recording unit is similar to the *Methusalem* system or by loading a file via command or automatically after power-on. The time base is based on a DTCXO with a 0.05 ppm accuracy over temperature. Setting and synchronizing the time as well as monitoring the drift is

carried out automatically by synchronization signals (DCF77 format) from a GPS-based coded time signal generator. Clock synchronization and drift are checked after recovery and compared with the original GPS units. After software preamplification the signals are low-pass filtered using a 5-pole Bessel filter with a -3 dB corner frequency of 10 kHz. Then each channel is digitised using a sigma-delta A/D converter at a resolution of 22 bits producing 32-bit signed digital data. After delta modulation and Huffman coding the samples are saved on PCMCIA storage cards together with timing information. Up to 4 storage cards may be used. Currently, up to 640 MB per card are available. Data compression allows allows to increase this capacity. Recently technical specifications of flashdisks (disk drives of PCMCIA technology) have been modified to operate below 10 °C, therefore 2 GB drives are now available for data storage. After recording the flashcards need to be copied to a PC workstation. During this transcription the data are decompressed and data files from a maximum of four flash memory are combined into one data set and formatted according to the PASSCAL data scheme used by the *Methusalem* system. This enables full compatibility with the established processing system. While the *Methusalem* system did provide 16 bit integer data, the 18 bit data resolution of the *MBS* can be fully utilized using a 32 bit data format.

Figure 5.3.2: The GEOMAR OBH ready for deployment.
Background left: GEOMAR OBS
Bachground right: OBH container

The Marine Longtime Seismograph

For the purpose of low frequent recordings such as seismological observations of earthquakes during long term deployments of about one year time a new data logger, the Marine Longtime Seismograph (MLS) was developped by *SEND GmbH* with support from GEOMAR.
The MLS is again a four channel data logger whose input channels have been optimized for 3-component seismometers and one hydrophone channel. The modular design of the analogue front end allows to adopt for different seismometers and hydrophones or pressure sensors. Currently front ends for the Spahr Webb, PMD and Guralp seismometers as well as for a differential pressure gauge (DPG) and the OAS hydrophone are available. With these sensors we are able to record events between 50 Hz and 120 s. The very low power consumption of 250 mW during recording together with a high precision internal clock (0.05 ppm drift) allows data acquisition for one year. Data storage is done on up to 12 PCMCIA type II flashcards. The instrument can be parameterized and programmed via a RS232 interface. After low pass filtering the signals of the input channels are digitized using Sigma-Delta A/D converters. A final decimating sharp digital low-pass filter is realized in software by a Digital Signal Processor. The effective signal resolution depends on the sample rate and varies between 18.5 bit at 20 ms and 22 bits at 1 s. Playback of the data is done under the same scheme as described for the MBS above. After playback and decompression the data is provided in PASSCAL format from where it could be easily transformed into standard seismological data formats.

5.4 Biological equipment and methods of investigation

5.4.1 Nets

Two types of net were used for trawling: A rectangular midwater net with an opening area of 8m² (RMT 8) fitted with a non-closing cod end (obtained from the British Anatarctic Survey), and a Tucker trawl net with an opening area of 3m² equipped with a timer.controlled closing cod end brought by T. Fank from HBOI. The original plan to fish with the SOC RMT 8 and its cod end including a depth sensor and a timer control had to be abandoned due to the changes in funding policy by the BMBF.
Since both nets used had no depth sensor the depth values given for the individual trawls are rough estimates.

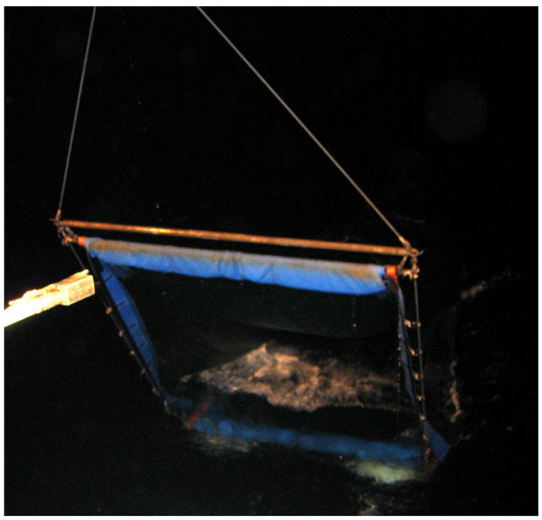

The HBOI net (Tucker trawl) with closing cod end The BAS net with open cod end

As explained in the cruise objectives (2.3.), the use of a closing cod end is an essential prerequisite for most of the physiological and morphological work planned for this cruise. The closing cod end brought animals on board ship which were isolated against the high temperatures in the upper water layers, protected from mechanical damage during hauling, and shielded against the sunlight, i.e. dark adapted. Due to the smaller size of the Tucker trawl net we were forced to make choices between getting fewer specimens in optimal conditions, and a higher yield of animals in less good a shape.

This was all the more unfortunate, since it turned out that in Guatemalan waters both nets produced only small catches both in terms of the absolute number of specimens and the number of species obtained.

5.4.2 The visual systems of mesopelagic fish with special emphasis on the visual pigments of lanternfish (Myctophidae) and their role in the detection of bioluminescence.

R.H. Douglas
Dept. Optometry & Visual Science, City University, Northampton Sq, London EC1V 7DD, UK
J.C. Partridge, E.M. White
School of Biological Sciences, University of Bristol, Woodland Rd, Bristol BS8 1UG, UK

I.

II. *Background*

Animals living in the deep-ocean are exposed to two sources of illumination: weak downwelling sunlight and the bioluminescence that is produced by most mesopelagic animals (Denton, 1990). Irradiance due to sunlight decreases exponentially with depth and below 1000m bioluminescence is the only source of visible radiation. Since the intensity of both the residual sunlight and most bioluminescent emissions are maximal at around 460-490nm, the vast majority of deep-sea fish have retinae containing a single visual pigment maximally sensitive at these wavelengths (Douglas et al., 1995, 1998a; Douglas & Partridge, 1997).

Three genera of deep-sea dragon fish (*Malacosteus, Aristostomias* and *Pachystomias*), however, whose suborbital photophores have emission maxima beyond 700nm, form a striking exception to this general trend. To enable them to see their own far-red bioluminescence these animals have been shown, using retinal extracts and microspectrophotometry, to posses two long-wave shifted visual pigments. Using a retinal wholemount technique we also demonstrated the existence of an additional, more long-wave absorbing, pigment in the retinae of *Aristostomias tittmanni* (Partridge & Douglas, 1995) and *Pachystomias microdon* (Douglas et al., 1988a) . We were unable to find a similar third pigment in *Malacosteus niger*. This species instead employs a chlorophyll-derived photosensitiser to enhance its long-wave sensitivity (Douglas et al., 1998b, 1999).

Since stomiids are sensitive to their own far red bioluminescence, which other animals in the deep-sea with 'conventional' visual pigments cannot see, they have what could be regarded as a 'private' waveband. This could be used for intraspecific signalling immune from detection by potential predators or for the covert illumination of prey (Partridge & Douglas, 1995). However, "*It would ... not be altogether surprising if other, non-red light producing, organisms had also evolved similar longwave sensitivity to counteract the advantage enjoyed by the stomiids*." (Douglas, 2001).

Myctophid visual pigments

The lanternfish are a very abundant component of the mesopelagic fish fauna. Surprisingly, their visual pigments have been investigated to a lesser degree than other, often more 'spectacular', species. Most are assumed, like the majority of deep-sea fish, to contain a single visual pigment maximally sensitive in the blue/green part of the spectrum

During a previous cruise aboard the *FS Sonne* (SO142), however, we found evidence that at least two species of myctophid depart from this general trend. Retinal extracts of *Bolinichthys longipes* revealed that, in addition to a 'conventional' deep-sea visual pigment absorbing maximally (λ_{max}) around 480 nm, the retinae of these animals also contain a substance with an absorption spectrum similar to that of chlorophyll. Subsequent (preliminary) fluorescence studies were consistent with this substance being a chlorophyll-derivative. A single microspectrophotmetric record showed that this chlorophyll-like pigment may be linked to a visual pigment absorbing maximally at 540 nm, which occurs in addition to another visual pigment with λ_{max} 492nm that is not co-localised with the putative

photosensitizer. This species may therefore employ the same mechanism displayed by *Malacosteus niger* for detecting long-wave bioluminescence.

To date these data were generated from the deep-frozen retinae of only three individuals and are incomplete. There is, for instance, no proof that the chlorophyll-like pigment actually functions as a photosensitizer in *Bolinichthys longipes,* and we only have a single microspectrophotometric record suggesting it co-occurs with a visual pigment within a photoreceptor outer segment.

In this cruise we therefore planned to do the following on any *Bolinichthys longipes* captured;

1. Preserve retinae by light fixation specifically for microspectrophotometry. This would enable us to confirm the presence of a longwave visual pigment and co-localised photosensitizer.
2. Spectrophotometrically measure fresh retinal wholemounts for evidence of extreme long-wave sensitive visual pigments
3. Perform photosensitivity experiments using retinal wholemounts and visual pigment extracts to demonstrate whether the chlorophyll-like pigment acts as a photosensitizer

Another species of myctophid collected during *Sonne* cruise142, *Ceratoscopelus warmingii*, was shown by careful partial bleaching of retinal extracts, to contain two visual pigments within its retinae, with maximum absorption at *ca.* 480 and 525 nm. The most red-sensitive of these pigments is the most long-wave sensitive visual pigment described in a deep-sea fish that does not produce far-red bioluminescence. During the present cruise we therefore planned to;

4. Examine *Ceratoscopelus warmingii* retinae using wholemount spectrophotometry to (possibly) reveal even more long-wave sensitive visual pigments.

The stomiids use two methods for detecting the long-wave bioluminescence they produce; extremely red-sensitive visual pigments (*Aristostomias* & *Pachystomias*), or a chlorophyll-derived photosensitizer (*Malacosteus*). As outlined above, preliminary data obtained from two species of myctophid, a family preyed upon by the stomiids, but not known to produce far red bioluminescence themselves, indicate they may use the same two strategies to detect stomiid bioluminescence. They might, therefore, be involved in a sensory arms race with the stomiids, having evolved a method of sensing their predator's 'private wavelength' and thus protecting themselves from dragon fish predation.

Clearly the myctophids are a more interesting group, in terms of their visual pigments, than previously supposed. Therefore, apart from investigating the two myctophids named above, we planned to;

5. Examine the visual pigments of as many species of myctophid as possible to determine how extensive long-wave sensitivity is in this family.

Short-wave sensitivity among deep-sea fish

Although most deep-sea fish are maximally sensitive to a relatively narrow part of the spectrum around 480 nm, and there are, as described above, some examples of far-red sensitivity, there have not yet been any descriptions of enhanced short-wave sensitivity. Extreme short-wave sensitivity is common among terrestrial and shallow water animals. However, the electrophysiological (Frank & Case, 1988) and behavioural (Frank & Widder 1994, 1996) demonstration of UV/violet sensitivity in some deep-sea oplophorid shrimps such as *Systellaspis debilis*, and the characterisation of a short-wave sensitive visual pigment in this species (λ_{max} 410nm; Cronin & Frank, 1996), was surprising, since these wavelengths were traditionally assumed not to penetrate the deep-ocean. However, measurements in the Caribbean have shown that enough UV reaches depths of up to 600m during the daytime to be perceived by these animals (Frank & Widder, 1996). Such short-wave sensitivity has not yet been demonstrated in deep-sea fish, although it would not be surprising if it were to be found, and

spectrophotometry of retinal pigments of fish caught on *FS Sonne* was directed specifically towards the identification of such pigments.

Regeneration of visual pigments

Once a visual pigment molecule has been bleached it rapidly regenerates in the presence of un-isomerised chromophore. For several reasons it would be interesting to know the extent and speed of such regeneration in deep-sea fish. Firstly, due to the often high density of deep-sea visual pigments and the relatively low number of photons they are exposed to, it might be argued that the pigments of some deep-sea fish may have no need to regenerate, although calculations show pigment bleaching is probably appreciable even in the deep-ocean (Denton & Locket, 1989). Furthermore, since regeneration involves the retinal pigment epithelium (RPE), it is difficult to see how significant regeneration could occur in those species with several banks of photoreceptors, most of whose photoreceptors are not in contact with the RPE. In fact it has been suggested that only the most vitread bank of photoreceptors in a multibank retina is functional, the visual pigments in the more sclerad layers having been bleached and not regenerated (Denton & Locket, 1989). Electrophysiological (Shapley & Gordon, 1990) and morphological (Fröhlich & Wagner, 1996) evidence supports the view that only the most vitread layer of rods is fully functional. Limited *in vitro* experiments (Crescitelli *et al.*, 1985; Crescitelli, 1991) have shown the degree of visual pigment regeneration to vary widely between different deep-sea fish. We are interested in how such variation is related to species' habitat depth and retinal structure or whether it is affected by ambient pressure (see below). The rate of regeneration of visual pigments, in the presence of exogenous chromophore, will be measured with tissue collected on *Sonne* cruise 173/2.

Affect of pressure on visual pigment absorbance

Since the spectral characteristics of a visual pigment depend heavily on the tertiary structure of a protein (opsin), it is possible that the pressure experienced in the deep-sea will affect the configuration of the protein and hence the absorption characteristics of the pigment. However, all measurements made on visual pigments to date have been performed at atmospheric pressure. We have now built a device for measuring the absorption characteristics of visual pigments at up to 400 atmospheres pressure, and we plan to use samples collected during the current trip for later spectrophotometry under pressure.

Methods

Animals

Animals (fish and cephalopods) were caught in one of two nets: an $8m^2$ RMT or a $4m^2$ Tucker trawl fitted with a closing cod end (as described elsewhere in this report). In order to protect photolabile retinal pigments from exposure to light the entire catch was quickly transferred from the cod end into a light-tight plastic container on the after deck of the ship before being transferred to a darkroom where the catch was sorted under dim red light. Selected animals were placed in light-tight containers in cold sea water before further processing. After removal of tissue, bodies were preserved in 10% formaldehyde solution in sea water and preliminary identifications were made using keys: Whitehead *et al*. (1986a,b, 1989), and Wisner (1974).

Visual pigment extracts

For the extraction of visual pigments, eyes were removed under dim red illumination (head-torches fitted with red acetate filters passing wavelengths greater than 670 nm) after which they were subjected to procedures detailed by Douglas *et al.*, (1995). Briefly, eyes were dissected and retinae from a single animal placed in a 1.5ml Eppendorf tube and physically homogenized in 300 microlitres of PIPES buffered saline (pH 6.9, 400 mOsm/kg) with 30 microlitres of the detergent beta-D-maltoside (200mM in PIPES buffered saline). The tubes were wrapped in aluminium foil to exclude

all extraneous light and placed on a rotator at room temperarure (24-26°) for 1 hour before being placed in a cooled (4°C) centrifuge and spun at 15k rpm (= 23000 g) for 10 mins.

Spectrometry of visual pigment extracts

200 microlitres of supernatant was removed from the visual pigment extract and placed in a quartz glass cuvette (Helma black-sided low volume: 105.201-QS) with 15 microlitres of 1 molar hydroxylamine in PIPES buffered saline. The cuvette was placed in a holder in the spectrophotometer and left for 15 minutes to allow time for the hydroxylamine to convert all free retinal to the retinaloxime before absorption spectra were recorded.

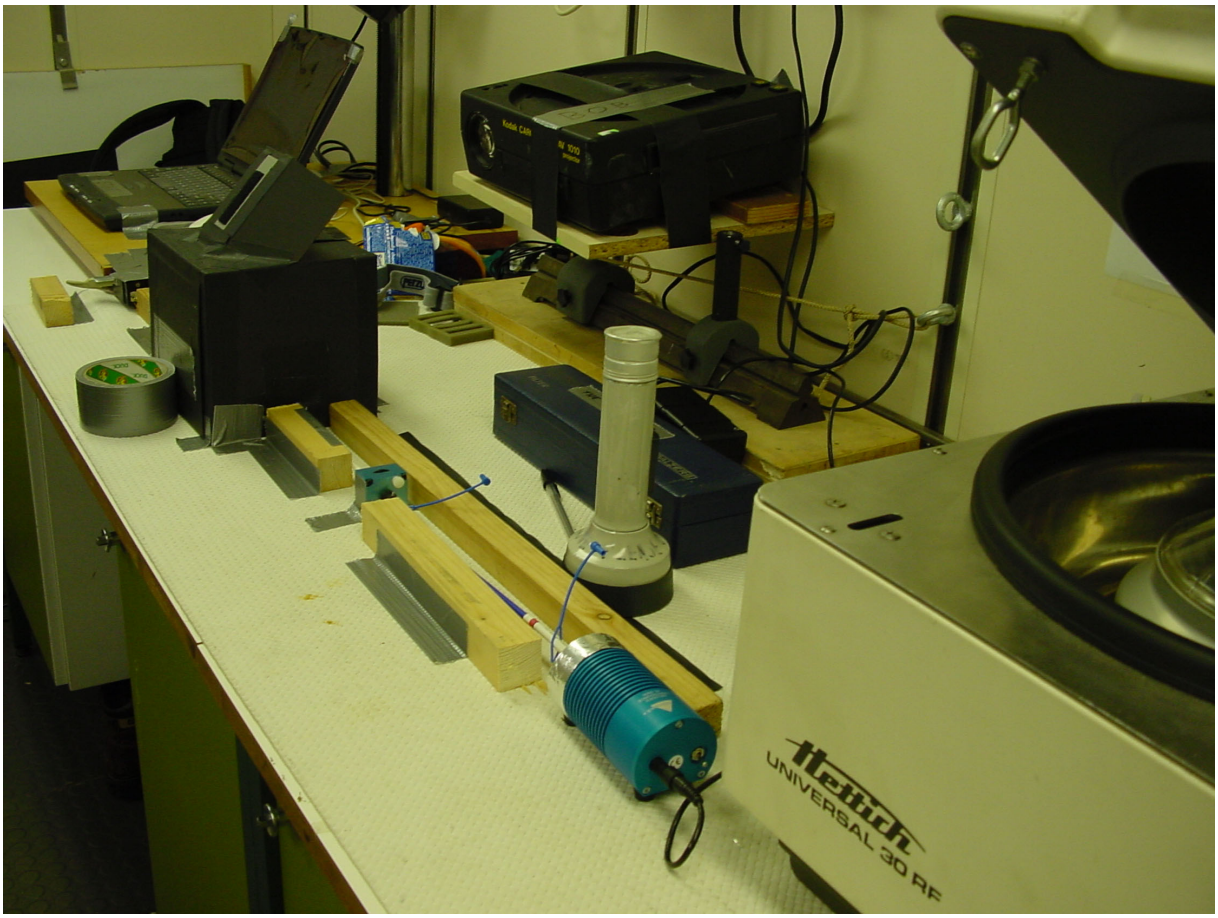

Darkroom with centrifuge, spectrophotometer, and bleaching light source

Spectra (189 - 854 nm) were recorded with a field-portable miniature spectrophotometer constructed from a solid state (CCD array) spectrometer and stabilised tungsten light source, coupled via fibre optics. Specifically, this consisted of an Ocean Optics USB2000 spectrometer connected via a USB interface to a Toshiba Satellite Pentium notebook PC and controlled via Ocean Optics OOIBase32 software running under Windows 2000. Light from an Ocean Optics HL2000 stabilised tungsten source (powered from the ship's stabilised 230V AC supply and a 12V DC transformer) was fed to an ocean optics light attenuator by a 250 mm, 400 micron diameter solarisation resistant quartz fibre optic (Ocean Optics QP400-025-SR). The output from the attenuator, which was used to control the light flux through the system, was coupled via another 250mm, 400 micron diameter fibre optic (P400-025-AL-SR) to an Ocean Optics cuvette holder and thence via a QP400-025-SR fibre to the input port of the USB2000. It was found that the performance of the system was considerably enhanced (i.e. stability, and hence signal to noise, increased) by aligning all fibres as straight as possible and ensuring that movement, including that induced by the ship's vibrations, was minimised. Alternative configurations, including a dual beam set-up, were tried but abandoned in preference for this arrangements of components.

Before recording absorbance spectra, a 'dark' spectrum was recorded, with the light blocked at the cuvette holder, followed by a 'reference' spectrum recorded with only PIPES buffered saline with hydroxylamine in the cuvette. Typically, the light flux was adjusted with the attenuator until a 10ms integration time resulted in peak recorded counts of ca. 3500 from the spectrometer. Recordings were averaged from 100 scans and were made with electrical dark current adjustment ON and the correction for detector non-linearity selected. The wavelength calibration of the spectrometer was checked by recording the output from a miniature mercury-argon discharge lamp (Ocean Optics HG1). Calibration accuracy averaged –0.37 nm (N=18) within the range 297 to 811 nm (s.d. = 0.57 nm; N = 18) and a regression of the data showed no significant difference from zero for either gradient or intercept.

The cuvette holder was screened from all extraneous sources of light by a box of black card above which was mounted a 45 degree planar mirror. The mirror directed light from a slide projector directly downwards into the top aperture of the cuvette. In order to deliver 'monochromatic' light, horizontally mounted narrow band interference filters (Balzer B40 25x25mm 10nm FWHM bandwidth) were placed in the light path below the mirror. The projector light flux, with and without filters, was measured on board with the USB2000 spectrometer and 2m 600 micron diameter fibre optic fitted with a cosine collector, but post-hoc calibration will be required to determine irradiance at the cuvette. This irradiance setup was used to bleach the visual pigment (without moving the cuvette from the measuring system) with a series of controlled exposures to light of decreasing wavelength in order to determine whether the visual pigment extract was homogeneous or consisted of a mixture of pigments (see Results, Figs 1&2), or to deliver quantifiable photon doses for photosensitivity experiments.

Attempts were made to measure absorbance spectra both from suspensions of rod outer segments purified on a 20%:40% sucrose gradient in PIPES buffered saline, and from retinal wholemounts (see Douglas et al. 1995, 1999 for methods). However, the low signal to noise ratios in the data made these approaches unsatisfactory.

Visual pigment absorbance spectra were analysed first by creating sequential difference spectra and determining the wavelength of peak absorbance (λ_{max}) with a VisualBASIC macro running in MS Excel. Data from the USB2000 were interpolated from the *ca*. 0.3 nm intervals recorded by the spectrometer to 1 nm intervals and a rhodopsin template best-fitted to the longwave limb of the data as described by Douglas *et al.* 1995. If the λ_{max} remained stable from bleach to bleach, indicative of a homogenous visual pigment extract, an overall difference spectrum was calculated between first (i.e. 15 minutes after addition of hydroxylamine to the extract) and last measured absorbance spectra and the λ_{max} determined from these data. Where mixed visual pigments were indicated by a shift in λ_{max} of the sequential difference spectra, the first difference spectrum which showed significant bleaching and the last difference spectrum were used to determine the λ_{max} values of the two visual pigments.

The same protocol was followed for visual pigment extracts from cephalopod retinae with the following differences: Firstly, animals were always held in darkness for at least 24 hours before preparation of visual pigment extracts to ensure maximum conversion of metarhodopsin to rhodopsin; all dissection was conducted with the absolute minimum exposure to even dim red light; no hydroxylamine was added to the extracts; no series of bleaches with successively more shortwave light was delivered but, instead, the visual pigment extract was irradiated with red or blue light to promote metarhodopsin build-up, before being scanned, bleached with actinic white light, and re-measured.

Reflexion spectrophotometry

Reflexion measurements were made to obtain objective measurements of the dermal colours of representative myctophids. Light from the HL2000 light source was directed via the multi-fibre bundle of an Ocean Optics R-400-7-UV/VIS reflexion probe and reflected light returned to the USB2000 via the single central fibre of the probe. The reflexion probe was held horizontally in a clamp and reflexion measurements were made from different areas (ca. 1.5mm diameter) on the surface of fish which were held at a fixed distance from the end of the reflexion probe and

perpendicular to the axis of the probe. Measurements (189 – 854 nm) were recorded relative to the flattenned matt surface of aluminium foil and interpolated to 1 nm intervals for display (see Results, Fig 3). Data will be re-calibrated into absolute units (% reflexion) on return in the UK by reference to calibrated specular and Lambertian reflexion standards.

Cephalopod pupilometry

The kinetics of the pupiliary reaction to light was investigated in a number of species of cephalopod by video recording. Animals were held in darkness, in a cold room (4°C) for several hours after capture before being removed and, under dim red light, placed before a video camera (Sony DCR-TRV330E). Video records were obtained under IR illumination, provided by the camera's in-built 'night shot' capability, before the eye was irradiated with bright light from a slide projector mounted 180 mm from the animal. Video records will be analysed using 'ImageJ' software to quantify the rate of pupil closure. *In situ* measurements of the light flux from the projector will allow post hoc calibration of the spectral irradiance stimulating the eye during the experiments.

Tissue Collection

Tissue was collected and preserved by freezing, fixation or other methods for a variety of purposes. These include: freezing of retinae and visual pigment extracts for spectrophotometry (including under pressure to 400 bar, and studies of rates of visual pigment regeneration *in vitro*); fixation for LM and EM studies of retinal and iris histology; preservation in 70% ethanol or 'RNAlater' for molecular biological study (opsin sequencing from somatic DNA, or cDNA from retinal and liver mRNA); preservation in 4% paraformaldehyde followed by cryopreservation in 40% sucrose in PIPES buffered saline and freezing for *in situ* hybridization studies to locate visual pigments in the retinae of multi-pigment fishes (e.g. *Scopelarchus analis*).

References

Crescitelli, F. (1991) Adaptations of visual pigments to the photic environment of the deep-sea. *J. Exp. Zool. (Suppl.)* **5:** 66-75.

Crescitelli, F., McFall-Ngai, M. and Horwitz, J. (1985) The visual pigment sensitivity hypothesis: further evidence from fishes of varying habitats. *J. Comp. Phys. A* **157:** 323-333.

Cronin, T.W. and Frank, T. (1996) A short-wavelength photoreceptor class in a deep-sea shrimp. *Proc. Roy. Soc. Lond. B* **263:** 861-865.

Denton, E.J. (1990). Light and vision at depths greater than 200 metres. In: *Light and life in the sea.* (P.J. Herring, A.K. Campbell, M. Whitfield and L. Maddock, eds), pp127-148. Cambridge University Press, Cambridge, New York.

Denton, E.J. and Locket, N.A. (1989) Possible wavelength discrimination by multibank retinae in deep-sea fishes. *J. Mar. Biol. Ass. U. K.* **69:** 409-435.

Douglas, R.H. (2001) The ecology of teleost fish visual pigments: a good example of sensory adaptation to the environment? In *Ecology of Sensing*. (Barth FG, Schmid A.eds) Springer Verlag.

Douglas, R.H and Partridge, J.C. (1997) On the visual pigments of deep-sea fish. *J. Fish Biol*. **50**,68-85.

Douglas, R.H., Partridge, J.C. & Hope, A.J. (1995) Visual and lenticular pigments in the eyes of demersal deep-sea fishes. *Journal of Comparative Physiology A* **177**, 111-122.

Douglas, R.H., Partridge, J.C. & Marshall, N.J. (1998a) The Eyes of deep-sea fish I: Lens pigmentation, tapeta and visual pigments. *Prog. Ret. Eye Res*. 17(4), 597-636.

Douglas, R.H., Partridge, J.C., Dulai, K., Hunt, D., Mullineaux, C.W., Tauber, A. & Hynninen, P.H.(1998b) Dragon fish see using chlorophyll. *Nature* 393, 423-424.

Douglas, R.H., Partridge, J.C., Dulai, K.S., Hunt, D.M., Mullineaux, C.W., & Hynninen, P.H. (1999) Enhanced retinal longwave sensitivity using a chlorophyll-derived photosensitizer in *Malacosteus niger*, a deep-sea dragon fish with far red bioluminescence. *Vision Res.* , 39, 2817-2832.

Frank, T.M. and Case, J.F. (1988) Visual spectral sensitivities of bioluminescent deep-sea crustacea. *Biol. Bull.* **175:** 261-273.

Frank, T.M. and Widder, E.A. (1994) Evidence for behavioural sensitivity to near-UV light in the deep-sea crustacean *Systellaspis sebilis*. *Mar. Biol.* **118:** 279-284.

Frank, T.M. and Widder, E.A. (1996) UV light in the deep-sea: *in situ* measurements of downwelling irradiance in relation to the visual threshold sensitivity of UV- sensitive crustaceans. *Mar. Fresh. Behav. Physiol.* **27(2-3):** 189-197.
Fröhlich, E. and Wagner, H.-J. (1996) Rod outer segment renewal in the retinae of deep-sea fish. *Vision Res.* **36(19):** 3183-3194.
Partridge, J.C. and Douglas, R.H. (1995) Far-red sensitivity of dragon fish. *Nature* **375**, 21-22.
Shapley, R. and Gordon, J. (1980) The visual sensitivity of the conger eel. *Proc. Roy. Soc. Lond. B* **209:** 317-330.
Somiya, H. (1982) 'Yellow lens' eyes of a stomiatoid deep-sea fish, *Malacosteus niger. Proceedings of the Royal Society of London B*, 215, 481-489.
Whitehead, P.J.P., Bauchot, M.-L., Hureau, J.-C., Nielsen, J. and Tortonese, E. (1986a, 1986b, 1989) Fishes of the North-eastern Atlantic and Mediterranean Volumes II, III, & I. Unesco, Paris.
Wisner, R.L. (1974) *The taxonomy and distribution of lantern fishes (Family Myctophidae) of the Eastern Pacific Ocean.* Navy Ocean Research and Development Activity, Bay St. Louis.

5.4.3 Electrophysiological recordings from fish and crustacean eyes (T. Frank, HBOI, USA)

The purpose of this research was to determine the physiological adaptations in the visual systems of midwater organisms. This is part of an ongoing study funded by the Ocean Sciences Division of the National Science Foundation, to determine how the visual ecology of midwater organisms, particularly those that vertically migrate, is correlated with their distribution in the water column. Vertical migrators (organisms that live in deep water during the day and migrate up at night to feed in surface waters) are of particular interest because they are at the base of many oceanic food webs, including those of many commercially important fish species. Previous *in situ* studies have demonstrated that these migrators are staggered with respect to their depth distributions during the day, and my recent studies on crustaceans indicates that their photosensitivity is related to their depth distribution. In addition, their temporal resolution, or how well they are able to track moving objects, is inversely correlated to their photosensitivity. The photosensitivity and temporal resolution of midwater fish from mesopelagic depths (200-900 m), of which many species are vertical migrators, have never been studied, due to the difficulty in 1) bringing up live deep-water species and 2) keeping them alive long enough for transport to shore-based laboratories should live specimens be obtained. This cruise represents a unique opportunity to attempt to study the visual systems of mesopelagic fish, with slight modifications to the shipboard based apparatus I used for studying crustacean eyes. In addition, having never trawled in this region before, new species of crustaceans may come up in the trawl, allowing me to continue my studies on their adaptations to low light environments as well.

Specimen preparation: All fish used for these experiments were collected in the Tucker Trawl with a closing cod-end, while the stomatopod crustaceans were caught in the RMT-8 without a closing cod-end. Sorting and specimen preparation were conducted under dim red light. Crustaceans were maintained in the dark in light tight containers until used for experiments.

Fish

All experiments on fish were conducted in collaboration with Dr. Ron Douglas, who was also on the cruise. Putting his experience with isolated eye preps together with my experience in recording from intact eyes, we felt we had the best chance for success with this very difficult set-up. If a live fish was retrieved from a trawl with the closing cod-end, the fish was placed in bath containing MS222 until the loss of righting reflex occurred. Recordings utilizing, at various times, a metal microelectrode, a silver chloride wire electrode, and a silver chloride pellet electrode, were attempted on:

1) Intact eye in various orientations
   a) slit made in eye and electrode inserted into slit, both in differential mode, with a reference electrode on the body, and single-ended mode without the reference electrode

b) electrode inserted into eye without making slit first, both differential and single-ended modes
c) electrode laid on surface of eye, both differential and single-ended modes.

In all cases, the animal was laid on a sponge pad in a chilled seawater bath, sloped in such a manner that the body was covered with water to just below the eyes, ensuring that the gills were covered with water but the eyes were not.

2) Isolated eye in single-ended mode and differential mode, on both sponge and moist paper towel

3) Isolated eye cup in single-ended and differential mode, on both sponge and moist paper towel

4) Eye cup in animal

Crustaceans

Crustaceans are anesthetized with magnesium chloride, and mounted on a plastic holder in a refrigerated water bath such that the pleopods were free to generate respiratory currents. They were mounted in the water bath such that the dorsal surface of the left eye remained above the water on a small plastic post. A 15 μ tip metal microelectrode was placed subcorneally, with the reference electrode on the body, and a ground electrode in the water bath.

Equipment

The microscope, water bath and microelectrodes were fastened to an aluminum plate to prevent movement during heavy seas. The aluminum plate was placed on air feet to dampen vibrations generated by the ship's engines, which are otherwise picked up by the microelectrodes, and attached to the top of the bench. A Faraday cage covered with a black cloth prevented introduction of stray light and electrical noise during the course of an experiment.

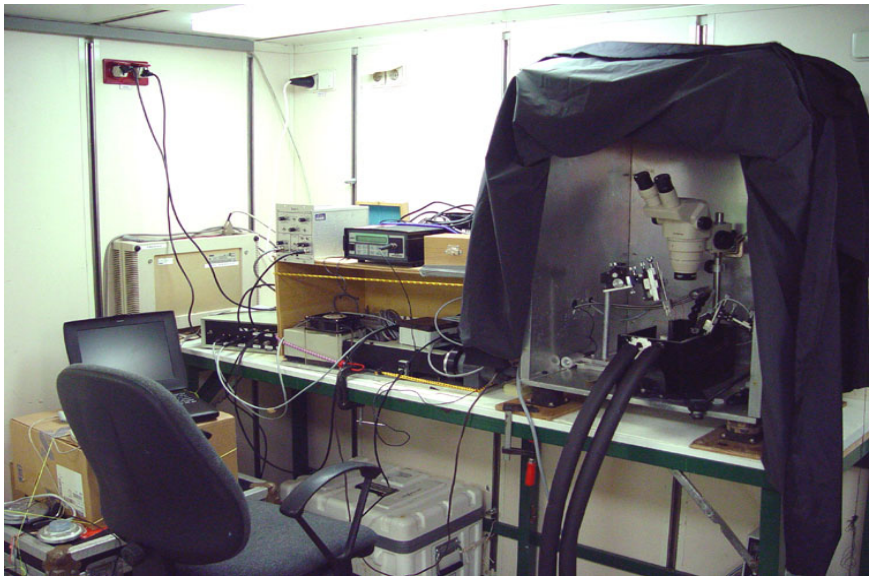

The gravimeter laboratory was used for electrophysiological recordings

Electrophysiological Recordings:

The eye was stimulated with a monochromatic flashes of light from an Instruments SA monochromator. The light was transmitted to the eye through a bifurcated light guide composed of randomized silica fibers. Flash irradiance was controlled with neutral density filters, and flash

duration was controlled with a Uniblitz Shutter. Irradiance was measured with a UDT optometer calibrated in 10 nm intervals. The extracellular response recorded from the eye, the electroretinogram, is the summed mass response from a large number of receptor cells. The signal was amplified by a Haer XCELL 3 microelectrode amplifier, digitized by a National Instrumentents DAQ board, analyzed with a program written in Labview, and stored to disk for further analysis. The electroretinogram can be used to determine spectral sensitivity, photosensitivity and temporal resolution.

a) Spectral sensitivity: the irradiance of light at each wavelength required to generate a50 μV response from the eye was determined. To ensure that the sensitivity of the eye is not changing during the course of the experiment, a test flash of set wavelength and irradiance was presented every five flashes. If the response to the test flashes changed by more the 5%, the experiment was abandoned. The reciprocal of irradiance graphed against wavelength generates a spectral sensitivity curve. Once the spectral sensitivity was been determined in the dark-adapted eye, in the animal was still viable, then a chromatic adaptation experiment was conducted. An adapting light (violet, blue, green, yellow or orange) was transmitted to the eye through the other end of the bifurcated (or forked) light guide. Another spectral sensitivity curve is generated in this chromatically-adapted eye, and the peaks of the two curves were compared to determine if more than one spectral sensitivity peak is present, which would be indicative of the presence of more than one visual pigment.

b) Temporal Resolution: the response speed of the eye can be determined by looking at the latency of the response to a flash of light, in addition to determining the critical flicker fusion frequency (FFF). The FFF is the frequency of flashing light at which individual flashes fuse into one, such that the eye now sees a continuous glow rather than individual flashes of light. In the human eye, the FFF in a moderately light adapted eye is 60 Hz. Because the FFF is dependent on the intensity of the flashing light, maximum flicker fusion frequency, which is the highest flicker frequency the eye is able to track accurately at any light intensity, was used as the comparator in these experiments. FFF was determined in the dark-adapted eye, as well as the light-adapted eye, as previous experiments have determined that in some species, light adaptation significantly increases FFF.

Photosensitivity: Response-irradiance functions, or V-log I curves, were generated by plotting data obtained by measuring the response of the eye to increasingly brighter flashes of 490 nm light, until further increases in light intensity produced no further increases in response amplitude. The stimulus irradiance eliciting a half -maximal response ($0.5V_{max}$) can be used as an indicator of sensitivity in the various species tested.

5.4.4 Antioxidative defence mechanisms and bioluminescence in deep sea fish

Cécile Marchand and Fabienne Paasch
Life science Institute, Laboratoire de Biologie cellulaire, Université Catholique de Louvain
Croix du Sud 5
1348 Louvain-la-Neuve
Belgium
Tel:32-10-473517/3509

Introduction

Bioluminescence is a very widespread phenomenon among deep-sea organisms, encompassing several phyla from protists to fishes. Besides organisms relying on symbiotic luminous bacteria harboured in specialised culture pouches, most pelagic organisms rely on coelenterazine, an imidazolopyrazinone compound belonging to the family of luciferins. These are the luminescent substrate for luciferases, the enzymes which catalyse the reaction in presence of oxygen.
Coelenterazine is also abundant in non-luminescent tissues and in non-luminescent organisms. It has therefore been suggested that this compound has some other role besides its chemiluminescent properties. In fact, coelenterazine is endowed with strong antioxidant properties as it is highly reactive with reactive oxygen species (Rees et al.,1998; Dubuisson et al., 2000).

Our team has developed an evolutionary model for coelenterazine based luminescence. It postulates that the first physiological role of coelenterazine was not that of a luciferin, but that of an antioxidant participating in the antioxidative arsenal of cells and tissues. The functional shift from its antioxidative to its light emitting function might have occurred when the strength of selection for antioxidative defence mechanisms decreased. This might have occurred when marine organisms began colonising deeper regions of the oceans, where exposure to oxidative stress is considerably reduced because of reduced light irradiance and lower oxygen levels. A reduction in metabolic activity with increasing depth would also have decreased the endogenous production of reactive oxygen species. Therefore, in these organisms, mechanisms for harnessing the chemiluminescence of coelenterazine in specialised organs could have developed, while the beneficial antioxidative properties were maintained in other tissues (Rees et al., 1998). The antioxidative properties of coelenterazine could still have significant physiological importance in non-luminescent tissues.

Objective of the project

This project aims at: (1) investigating further the antioxidative defences of cells from mesopelagic fishes living at different depth; and (2) investigating the protection conferred by coelenterazine to cells from deep sea fishes.
In addition to this research on oxidative stress we attempt to develop methods for deep sea fish cell lines in culture.

Materials and method

(1) <u>Antioxidative defences of cells from fishes living at increasing depth</u>

This work focusses on the blood plasma and red blood cells, as these can be tested for their resistance to oxidative stress. Blood was collected from the caudal vein and from the heart with a syringe previously rinsed with EDTA. 10µl of EDTA was added to the blood to avoid coagulation. After centrifugation (at 11000g for 5min) the plasma was removed and replaced by the same volume of saline buffer (NaCl 176mM, KCl 5.4mM, $MgSO_4$ 0.81mM, KH_2PO_4 0.44mM, $NaHCO_3$ 5mM, $CaCl_2$ 1.5mM, HEPES-Na 10mM, pH 7.6). The osmolarity of this saline was established after measurements of the osmolarity of the plasma from mesopelagic fish. The red blood cells were washed three times using the same procedure.

A. <u>PLASMA: Total antioxidative capacity</u>.
   The total antioxidative capacity of the plasma was studied by luminometry with luminol and an azo free-radical initiator, AAPH. The reaction of luminol and AAPH emits light. If there are antioxidants in the plasma, they will capture the AAPH and the luminous reaction will start later.
   For luminometry we simultaneously injected 50µl of luminol (in H_3BO_3 buffer 50mM, pH 9.5) and 50µl of AAPH (in PO_4 buffer 0.1mM, pH 7.4) to the plasma diluted in PO_4 buffer (in each well: 50µl of PO_4 and 50µl of the plasma dilution). The luminescent reaction was measured for 30 minutes. To compare the results, we also measured the luminescence of different concentrations of a standard antioxidant, Trolox.

B. <u>RED BLOOD CELLS: Susceptibility to oxidative stress</u>.
   Before measuring the resistance of the red blood cells to oxidative stress the cell suspension in the saline solution was diluted to a final RBC optical density (at 540nm) of 0.25. The stress compound was t-BHP prepared in the RBC buffer. This compound attacks the membrane of the cell and the resulting haemolysis of the red blood cells was followed by spectrophotometric assay. The extent of RBC haemolysis was monitored continuously by the decrease in the absorbance at 540nm and 575nm, recorded every 90 s during 2h. In each well, 100µl of the RBC stock solution were

incubated with 50µl t-BHP and 50µl saline. All tests were carried out at 25°C. The time of half-haemolysis (THH), representing the time at which 50% of the RBC are haemolysed, was calculated.

(2) Protection conferred by coelenterazine to cells from deep sea fishes

Coelenterazine was measured in the plasma and in the red blood cells by renilla-luciferase. 50µl of renilla-luciferase (1/500 dilution in buffer) was injected into the luminometer with 55µl of buffer containing 5µl of the plasma or the red blood cell solution. The luminescence level was measured 10s after the injection. To compare the results a range of different concentrations with coelenterazine was tested. After the establishment of the coelenterazine concentration the same experiments as before was carried out with different concentrations of coelenterazine allowing us to determine whether coelenterazine participates in the antioxidative defence.

(3) Deep sea fish cell line cultures

Working on a sterile workbench in a laminar flow hood fish received different washes at room temperature: 2 minutes in Javel water (0.5%) then rapidly in 70% ethanol, in PBS saline solution and finally 30 minutes in PBS containing streptomycin, penicillin and Fungizone (amphotericin). The tissues (skin, muscles and liver) to be used were removed with sterile instruments and trypsinated for several minutes (8, 15, 20, 25 30 or 40 minutes). Small fragments of tissue were cultured in 1ml growth medium in 24 well microplates. The wells were pre coated with collagen for 4h. The growth medium was a modified MEM containing Fetal Calf Serum, antibiotics, glutamine, essential amino acids and Fungizone (amphotericin). Two different conditions were studied: 4°C and 15°C. The growth and development of the cells was studied under an inverted compound microscope.

The dry chemistry lab with the equipment for analysing plasma and red blood cells of fish

C. RED BLOOD CELLS: Susceptibility to oxidative stress.
Before measuring the resistance of the red blood cells to oxidative stress the cell suspension in the saline solution was diluted to a final RBC optical density (540nm) of 0.25. The stress compound was t-BHP prepared in the RBC buffer. This compound attacks the membrane of the cell and the resultig hemolysis of the red blood cells was followed by spectrophotometric assay.
The extent of RBC hemolysis was monitored continuously by the decrease in the absorbance at 540nm and 575nm, recorded every 90 s during 2h. In each well, 100µl of the RBC stock solution were incubated with 50µl t-BHP and 50µl saline. All tests were carried out at 25°C. The time of half hemolysis (THH), representing the time at which 50% of the RBC are haemolysed, was calculated.

(2) Protection conferred by coelenterazine to cells from deep sea fishes

Coelenterazine was measured in the plasma and in the red blood cells by renilla-luciferase. 50µl of renilla-luciferase (1/500 dilution in buffer) was injected by the luminometry to 55µl of buffer containing 5µl of the plasma or the red blood cell solution. The luminescent level was measured 10s after the injection. To compare the results a range of different concentrations with coelenterazine was tested. After the establishment of the coelenterazine concentration the same experiments as before was carried out with different concentrations of coelenterazine allowing us to determine whether coelenterazine participates in the antioxidative defence.

(3) Deep sea fish cell line cultures

Under a sterile workbench the fish received different washes at room temperature: 2minutes in Javel water (0.5%) then rapidly in 70% ethanol, in PBS saline solution and finally 30 minutes in PBS containing streptomycin, penicillin and fongizone. The tissues (skin, muscles and liver) to be used were removed with sterile instruments and trypsinated for several minutes (8, 15, 20, 25 30 or 40 minutes). Small fragments of tissue were cultured in 1ml growth medium in 24 well microplates. The wells were precoated with collagen for 4h. The growth medium was a modified MEM containing Fetal Calf Serum, antibiotics, glutamine, essential amino acids and fungizone. Two different conditions were studied: 4°C and 15°C. The growth and development of the cells was studied under an inverted microscope.

References

Dubuisson M., De Wergifosse B., Trouet A., Baguet F., Marchand-Brynaert J., Rees J.-F. (2OOO) Antioxidative properties of natural coelenterazine and synthetic methyl-coelenterazine in rat hepatocytes submitted to tert-butl hydroperoxide-induced oxidative stress. Biochem.Parmacol., 60, 471-478.

Janssens B., Childress J-J., Baguet F., Rees J.-F. (2000) Reduced enzymatic antioxidative defense in deep- sea fish. J. exp. Biol. 206, 3717-3725.

Rees J.-F., De Wergifosse B., Noiset O., Dubuisson M., Janssens B.,Thompson E. (1998) The origins of marine bioluminscence : turning oxygen defence mechanisms into deep-sea communication tools. J. exp. Biol. 201, 1211-1221.

5.4.5 – 5.4.9 Microscopic equipment

(Wagner, Deng, Jennings)

The equipment brought on board Sonne consisted of two stereomicroscopes with epi-illumination, one of which was fitted with a digital camera. These were put at the disposal of all members of the team requiring difficult identification tasks or delicate dissection procedures. Dissection was particularly difficult for exposing and mapping the lateral line organs, the inner ears, and the brains and pineal organs of fish.

The wet chemistry lab with stereomicroscopes for dissection and preservation of tissues and organs; furthermore with a photometer for the analysis of transparency in mesopelagic animals

5.4.5 Study of the world's most frequently used sensory system: lateral lines in the deep-sea.

Kylie Jennings & Justin Marshall
The University of Queensland, Australia
K.Jennings@uq.edu.au

The deep-sea is the largest living space on the planet and probably the most important sensory structure for life here is the lateral line. As light from the surface is lost, eyes may become reduced or highly specialised for detection of bioluminescent sources and as a result other senses begin to 'take over'. One of these is the lateral line vibrational detection system, or distance-touch-sense. Despite the relative importance of this sensory system, it is poorly understood in the deep-sea with only a handful of studies devoted to its elucidation.

Lateral lines are essentially ears that extend over the body of fish in order to detect relatively low frequency vibrations. They are constructed from the same building-blocks as ears - that is cells that

project sensory hairs from their surface and monitor the way in which these hairs bend in response to movements in the environment. Lateral line organs come in 2 varieties, some are found basically naked on the surface of the fish (free standing, FS, organs) while others are housed in canals (canal organs). There are suggestions as to the differential functions of these 2 types of organs and deep-sea fish provide an excellent chance to study this question as some have only canal or FS organs while others have both. In any of these 3 cases, the organs often seem specialized for existence in the relatively still waters of the deep. The central aim of this project is to describe these sensory structures in detail and place their function within an ecological context where possible.

Previous work on lateral line systems in deep-sea fish is essentially confined to gross anatomical description and guesses on ultrastructure. This work aims to look at ultrastructural aspects of the lateral line systems in deep-sea fish in more detail using both scanning electron microscopy (SEM) and transmission electron microscopy (TEM). This is only now becoming possible with careful capture techniques such as closing cod-end nets. This cruise aboard Sonne included such net techniques and very excitingly sampled areas of the oceans which have been largely ignored from the lateral line perspective.

Aims:

a) To describe the structure, ultrastructure and distribution of FS organs in deep-sea fish and relate this to lifestyle.
b) To describe the ultrastructure of canal organs in deep-sea fish and relate this to lifestyle.
c) Specifically to target deep-sea eels and other species with very elongated papillae for a full description of structure related to function.
d) To compare the following lateral line strategies in deep-sea fish and attempt a functional / ecological / phylogenetic explanation of this: canals and stud-like FS organs, canals and stitch-like FS organs, canals only, stitch-like FS organs only (none found yet), stitch-like FS organs only and those FS organs with highly elongate papillae.
e) With J. Wagner and S. Collin, describe the various aspects of innervation of lateral line organs and their central projections.
f) To map sensitivity distributions of the lateral line organs based on hair morphology (Marshall 1986).

Materials and Methods
Normal net trawls inflict severe abrasions to the skin of deep-sea fishes. The majority of the fish collected come aboard with no skin left on their bodies and heads. The skin of deep-sea fishes is delicate and often jelly-like. The lateral line is a fragile set of sensory organs distributed all over the fish's head and body. In order to study this sensory system, fish need to be collected in the best possible condition to ensure that the lateral line is not damaged. Trawling with a net equipped with a closing cod end ensures that fish are not subject to the associated drag and abrasion bought about by conventional nets. It is essential that a closing cod end be used in collecting deep-sea fishes in order to study the lateral line system. On the Sonne 2003 fish were collected using a closing cod end provided by Dr T. Frank.

Once collected and on board the vessel, photographs and detailed drawings of the specific locations of the lateral line organs were made. I have used an Olympus compound microscope and light source and an Olympus C-4040zoom digital camera and microscope attachment for photography (see fig. 1). The tissue was then preserved in high-grade fixative consisting of 3% glutaraldehyde in 0.1M phosphate buffer with 35% sucrose at a pH of 7.4. Tissue was fixed for the duration of 5 to 15 days and placed in non-toxic phosphate buffer and 35% sucrose for transportation.

Once back at The University of Queensland, Brisbane, Australia, the tissue will be prepared for scanning electron microscopy. This involves post fixation in osmium tetroxide and subsequent dehydration, mounting and gold or platinum coating. The lateral line organs or neuromasts will be examined under a JOEL 6400 Scanning Electron Microscope and the ultrastructure of the organs described. Details such as type and location of neuromasts has been describe during the cruise. Further ultrastructure details such as orientation and sensitivity of neuromasts, number of hair cells and length of hairs per neuromast will be described at The University of Queensland. This sensory information can give us invaluable information about the animals little know life style and evolution of this sense in the deep-sea environment.

5.4.6 Melatonin as a mediator of biological rhythms in mesopelagic fish

(H.-J. Wagner, Anatomisches Institut, Universität Tübingen)

Many mesopelagic fish undertake vertical migrations during a 24h cycle, staying at depths around or below 500m during the day and coming closer to the surface at night. It is as yet unclear what triggers these migrations, the two rival hypotheses being (i) a response to the changing light intensities, or, (ii) alternatively an endogenous circadian rhythm. The most important signal molecule mediating circadian rhythms is melatonin, secreted by the pineal gland. In other fish (e.g. goldfish) with a strong circadian rhythm, melatonin content and release is high during the dark phase and low during the light phase. Therefore pineal organs were isolated from fish caught during various phases of the 24h cycle, shock frozen and stored until the melatonin content will be determined using the ELISA technique in Tübingen. In order to ascertain that possible differences in melatonin content are not due to exogenous cues (e.g. light), pineals were also isolated from fish that were caught alive, and kept in a culture medium for up to 56h. All procedures were carried out in the dark under red torch light. Melatonin release in these preparations is determined by changing the culture medium every 4 h and assaying it for its melatonin content.
As “model” species for mesopelagic fish we chose *Bathylagus longirostris*, a migratory species , and *Scopeloberyx robustus*., a melamphaeid that does not migrate. Unfortunately, the pineal gland of *Scopeloberyx* is so deeply embedded in the cranial cartilage that it is not possible to isolate it for organ culture. This latter experiment was therefore only carried out in *Bathylagus*. Contrary to pineal melatonin, retinal melatonin is released in a more tonic way. It can therefore serve as a control to the experiments with pineal organs. Therefore we also cultured isolated retinae and will assay their release pattern.

In order to localise the cellular basis of the pineal and retinal oscillator histological sections will be cut in Tübingen and the expression of melatonin receptors (Mel Ib) and PER-gene mapped by in-situ hybidisation.

Furthermore, since, in these two species, the morphology of the retina and the pineal gland has not yet been studied, tissue was fixed for light and electron microsopic analysis.

For previous work on deep sea fish pineals see: Wagner, H.-J. and U. Mattheus (2002) Pineal organs in deep demersal fish. Cell Tissue Res. 307, 115-127

5.4.7 Comparative Studies of Inner Ear Morphology and Ultrastructure in Mesopelagic Deep-Sea Fishes

Xiaohong Deng[1], H-J Wagner[2], Arthur N. Popper[1]
[1]Dept. of Biology, University of Maryland, College Park, MD 20742, USA
[2]Anatomisches Institut, Universität Tübingen, Tübingen, D-72074 Germany

Introduction:

Fishes are one of the most successful groups of organisms on the earth. They dominate all the aquatic habitats with enormous numbers of individuals and species. They have developed various specializations to enable them to live in all kinds of extreme environments, including the deep sea. In the dim or lightless deep water, most fishes evolved highly adaptive and sensitive sensory systems for survival, which include vision, olfactory, machenosensory systems, and hearing. On the other hand, sensory organs may regress if they become more or less useless under certain environment conditions. Previous studies have provided documentation of adaptations and specifications of deep-sea fish's sensory systems in both sensitization and regression (Marshall, 1979). However, we still know very little about any functional specification in the auditory system of any deep-sea fish. Thus the investigations of the characteristics and specializations in deep-sea fish hearing will not only provide information of deep-sea fish's life history, but also provide insight of the evolution and adaptation of the inner ear in fishes.

Although very little is known about the life of deep-sea fishes, some aspects of their sensory systems are of special interests and have been the subject to extensive study. So we are able to know some interesting phenomena of sensory system adaptations in deep-sea fishes. For example, the visual system of most mesopelagic fishes is adapted to the low light environment by an increase in the sensitivity of their eyes by means of having a pure-rod retina, tubular lenses, and wide-open eyes. However, although large eyes are still found in many species living below 1000 meter, regressed eyes become more common at greater depths (Munk, 1964, 1966). In bottom dwellers such as benthopelagic and benthic fishes, the olfactory, gustatory, and acoustic-lateral lines organ may take over the function of vision (Marshall, 1971).

The structure and function of the inner ear in deep-sea fishes is yet to be explored. The earliest data might be the drawing of three ears from two mesopelagic species and one rat-tail fish by Bierbaum in 1914 (Marshall, 1971). During the 1960s and 1970s, N. B. Marshall described some of the gross morphological features in deep-sea fish inner ear (Marshall 1979). On the ultrastructure of deep-sea fish inner ear, the only data we have so far are Popper's (1979, 1980) SEM studies of saccules and lagena in ten species of deep-sea fishes. These ten species covered some of the major groups from mesopelagic to bathypelagic fishes: Myctophidae, Stomiiformes, Osmeriformes, Lophiiformes, Scorparniformes, and a pelagic Gadiformes codlet. Although the data on deep-sea fish hearing and inner ear structure are still scarce, we have started comparative studies on inner ear structure of some benthopelagic deep-sea fish familes systematically, which includes eight species from the family Macrouridae, one species from Moridae, and two species from Synaphobranchidae, (Deng, 2002, 2003, Buran 2003). We have found considerable complexities in the morphology and ultrastructure of the inner ears in these species, which support our hypothesis that these deep-sea fishes may have evolved auditory specializations to enhance their hearing ability, which help them to gain information from the acoustic environment in the deep water, or to detect possibly communication sounds.

5.4.8 Retinal ganglion cells in deep sea fish retinae

(H.-J. Wagner, Anatomisches Institut, Universität Tübingen)

Retinal ganglion cells provide the llink between the eyes and the visual projection areas of the brain. Depending on the intraretinal connectivity and the target region in the brain, at least 20 different types are distinguished in teleost and mammalian retinae. In addition to their functional differentiation the distribution of the various types within the retina has been used to derive interesting cues as to the visual capabilities and specialisations of a given species (Wagner, H.-J., Fröhlich, E., Negishi, K. and Collin, S.P. (1998) The eyes of deep-sea fish: II. Functional morphology of the retina. Progress in Retinal and Eye Research, Vol. 17, pp 637-685). Novel tracing techniques using retrograde axonal transport of fluorescent-labelled dextranes allow the simultaneous study of the cellular differentiation of ganglion cells and the topography of the various cell types. Apart from the relevance for understanding vision in deep-sea fishes, this approach is potentially of major interest for understanding the basic role of ganglion cells in general. Since the retinae of deep-sea fish are mainly specialised for optimising visual sensitivity and have only reduced intraretinal processing (ref. see above) these retinae may present a model system to identify primitve types of ganglion cells in the sense that the adaptive pressure for functional specialisation may have been less strong than in surface dwelling fish.

For the proposed study of ganglion cells, surviving fish are killed by cervical transection and the eyes isolated. Crystals of rhodamine-coupled dextranes (Molecular Probes, Eugene, Oregon) are applied to the stump of the optic nerve. After 10-15 min, the eyes are transferred to a culture medium (modified L-15) and cultured at 4°C for 36-48h depending on the size of the eye. Subsequently, the retinae are isolated, fixed for 6h in 4% paraformaldeyde (in PBS) , rinsed in PBS, transferred to 30% sucrose and stored at –80°C. In the home lab, retinal wholemounts are prepared and studied with a confocal microscope.

5.4.9 Sensory brain areas in mesopelagic fish

(H.-J. Wagner, Anatomisches Institut, Universität Tübingen)

Previous studies have shown that a comparative volumetric analysis of the sesnory areas in fish brains may be a good predictor for the sensory modalities with a preferential use in individual species (Wagner, H.-J. (2002) Sensory brain areas in three families of deep sea fish (slickheads, eels, and grenadiers): comparison of mesopelagic and demersal species. Marine Biology 141, 807-817; Wagner, H.-J. (2003) Volumetric analysis of brain areas indicates a shift in sensory orientation during development in the deep sea grenadier *Coryphaenoide armatus.* Marine Biology 142, 791-797). Some of the conclusions derived from these findings have been corroborated in observations with landers with baited cameras. In the present cruise, it was mostly planned to increase the number of species analysed in previous cruises (Sonne 142, Discovery 143) which comprised 76 species of mesopelagic fish.

5.5.1 Navigation

(Weinrebe, W.)

A crucial prerequisite for all kinds of marine surveys is the precise knowledge of position information (latitude, longitude, altitude above/below a reference level). Since 1993 the global positioning system (GPS) is commercially available and widely used for marine surveys. It operates 24 satellites in synchronous orbits, thus at least 3 satellites are visible anywhere at any moment (Seeber, 1996). The full precision of this originally military service yields positioning accuracies of a few meters. In the past this was restricted to military forces and unaccessible to commercial users (Blondel and Murton, 1997). Since about two years the full resolution is generally available.

The resolution of GPS can be enhanced with the Differential GPS (D-GPS) scheme (Blondel and Murton, 1997, Knickmeyer, 1996). Using several reference stations the determination of the ship's position can be corrected in real time and enhanced to a 1 m to 5 m accuracy. Since the cruise SO-109 (1996) D-GPS service is available onboard R/V SONNE. The ships ASHTEC system provides a validated accuracy better than 5 - 10 m in the area off Costa Rica.

D-GPS-values as well as most other cruise parameters are continuously stored in the navigation database, and are distributed via the DVS- („data distribution system") on the ship's network.

Unfortunately, the precision of the position information does not correspond to the accuracy of the time base in the navigation database, as the navigation processing unit Atlas ANP 2000 does not copy the precise GPS-time values, but adds time stamps of its internal unsynchronized clock.

5.5.2 Simrad EM120 Multibeam System

(Weinrebe, W.)

The EM120 system is a deep-water multibeam echosounder providing accurate bathymetric mapping up to full ocean depth. A system overview is presented in fig. 5.5.2.1. Basic components of the system are two linear transducer arrays in a Mills cross configuration with separate units for transmit and receive. The nominal sonar frequency is 12 kHz with an angular coverage sector of up to 150° and 191 beams per ping.. The emission beam is 150° wide across track, and 2° along track direction The reception is obtained from 191 beams, with widths of 2° across track and 20° along track (fig. 5.5.2.2). Thus the actual footprint of a single beam has a dimension of 2° by 2°. Achievable swath width on a flat bottom will normally be up to six times the water depth dependent on the character of the seafloor (fig. 5.5.2.3). The angular coverage sector and beam pointing angles may be set to vary automatically with depth according to achievable coverage. This maximizes the number of usable beams. The beam spacing is normally equidistant with equiangle available.

For depth measurements, 191 isolated depth values are obtained perpendicular to the track for each ping. Using the 2-way-travel-time and the beam angle known for each beam, and taking into account the ray bending due to refraction in the water column by sound speed variations, depth is estimated for each beam. A combination of amplitude (for the central beams) and phase (slant beams) is used to provide a measurement accuracy practically independant of the beam pointing angle.

Postprocessing of the EM120 data comprises the merging of navigation data, the calculation of water depth and positions of the footprints of the beams taking into account the water sound velocity profile, removing artifacts and erroneous data points, and calculation of a digital terrain model (DTM).

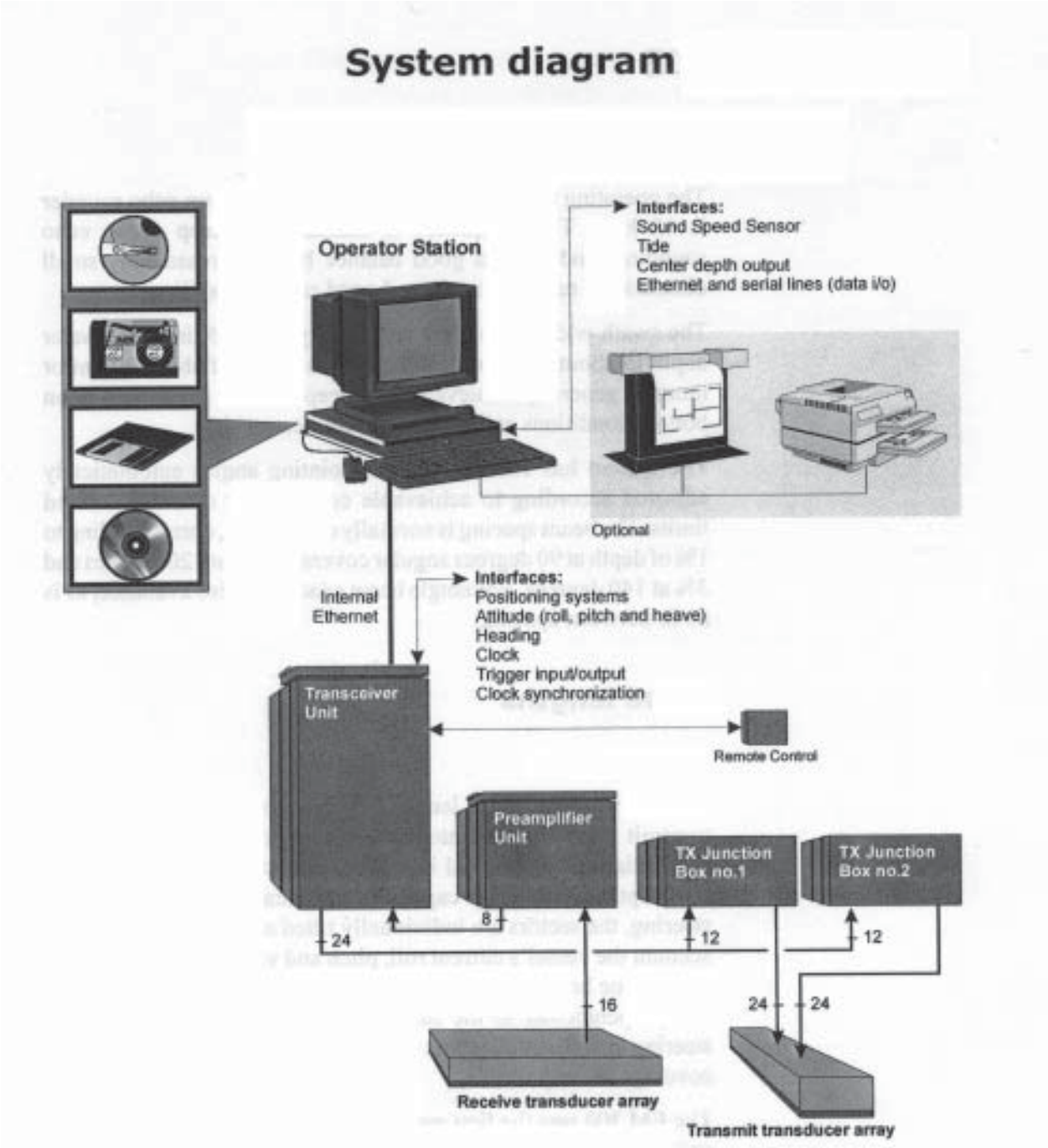

Figure 5.5.2.1: System diagram

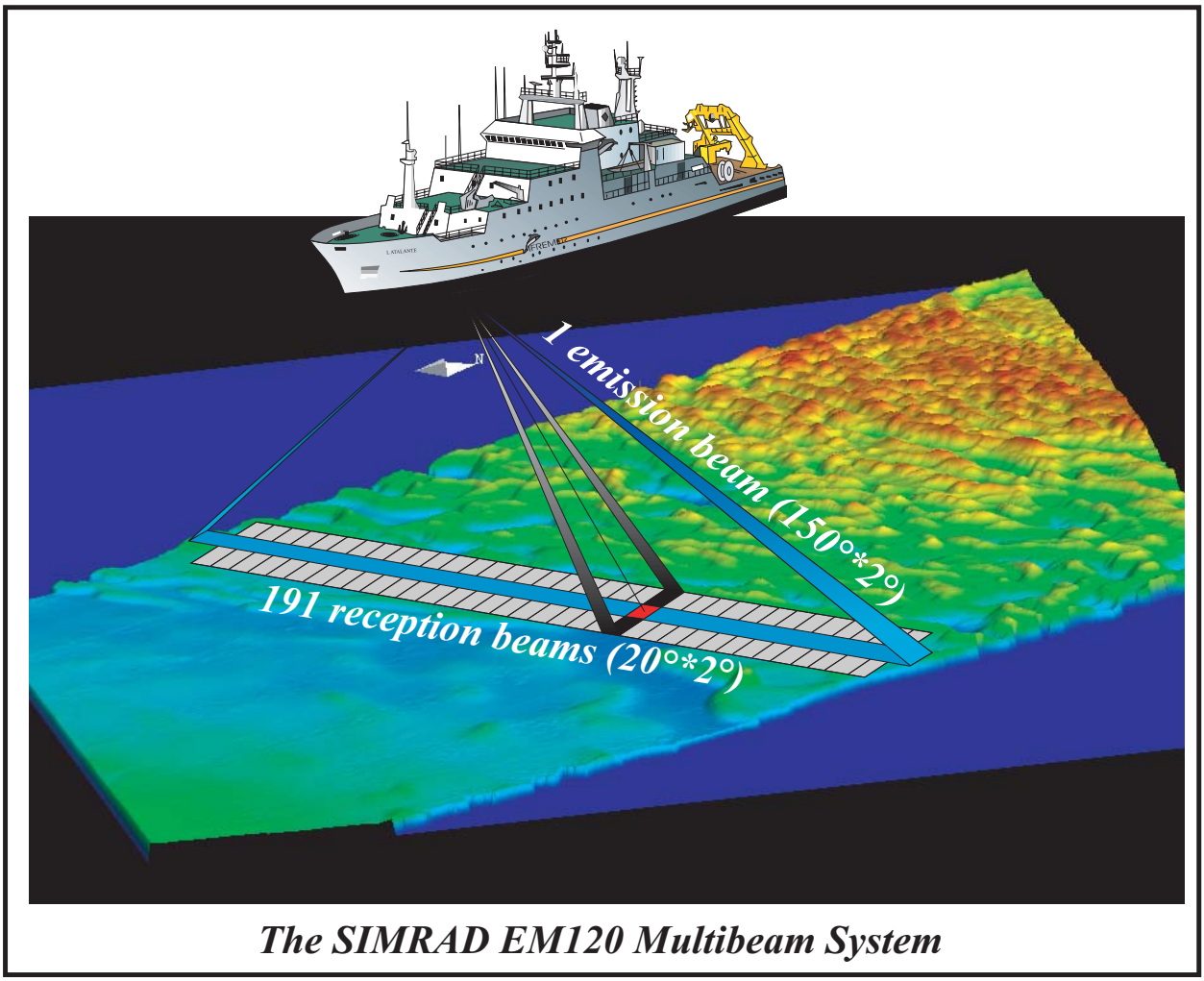

*Figure 5.5.2.2: Acquisition method for bathymetric and backscatter data from the Simrad EM120 system (crossed beams technique). (Figure by **C. Hugue**)*

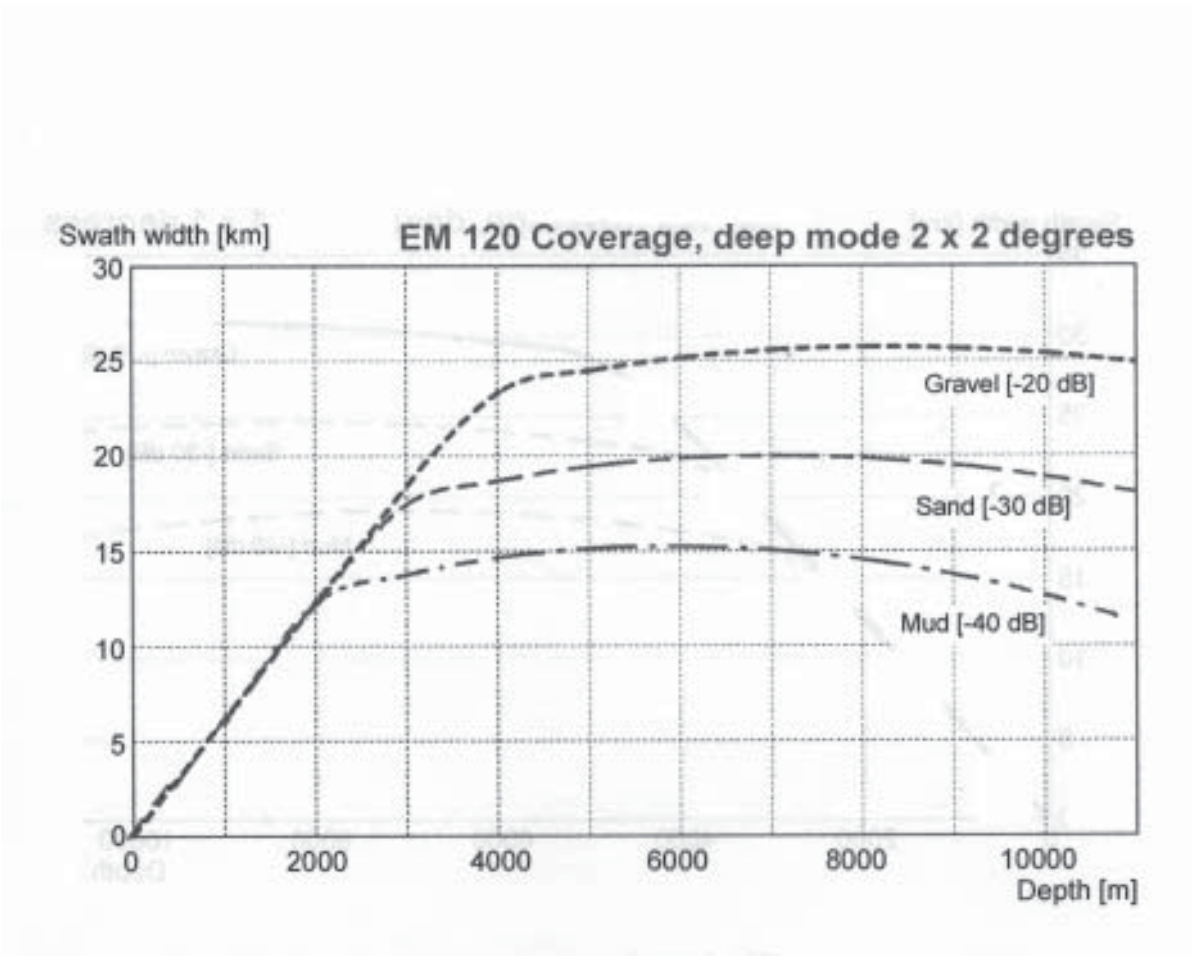

Figure 5.5.2.3: EM 120 Coverage diagram

5.5.3 Parasound

The PARASOUND system works both as a low-frequency sediment echosounder and as a high-frequency narrow beam sounder to determine the water depth. It utilizes the parametric effect, which produces additional frequencies through nonlinear acoustic interaction of finite amplitude waves. If two sound waves of similar frequencies (here 18 kHz and e.g. 22 kHz) are emitted simultaneously, a signal of the difference frequency (e.g. 4 kHz) is generated for sufficiently high primary amplitudes. The new component travels within the emission cone of the original high frequency waves, which are limited to an angle of only 4° for the equipment used. Therefore, the footprint size of 7% of the water depth is much smaller than for conventional systems and both vertical and lateral resolution are significantly improved.
The PARASOUND system is permanently installed on the ship. The hull-mounted transducer array has 128 elements within an area of 1 m2. It requires up to 70 kW of electric power due to the low degree of efficiency of the parametric effect. In 2 electronic cabinets, beam formation, signal generation and the separation of the primary (18, 22 kHz) and secondary frequencies (4 kHz) is carried out. Using the third electronic cabinet located in the echosounder control room, the system is operated on a 24 hour watch schedule.

Since the two-way travel time in the deep sea is long compared to the length of the reception window of up to 266 ms, the PARASOUND System sends out a burst of pulses at 400 ms intervals, until the first echo returns. The coverage in this discontinuous mode is dependent on the water depth and also produces non-equidistant shot distances between bursts.

The main tasks of the operators are system and quality control and to adjust the start of the reception window. Because of the limited penetration of the echosounding signal into the sediment, only a short time window close to the sea floor is recorded.

In addition to the analog recording features with the b/w DESO 25 device, the PARASOUND System is equipped with the digital data acquisition system ParaDigMA, developed at the University of Bremen. The data is stored on removable hard disks using the standard, industry-compatible SEGY-format. The 486-processor based PC allows for buffering, transfer and storage of the digital seismograms at very high repetition rates. Of the emitted series of pulses, usually only every second pulse can be digitized and stored, resulting in recording intervals of 800 ms for a given pulse sequence. The seismograms were sampled at a frequency of 40 kHz, with a typical registration length of 266 ms for a depth window of ~200 m. The source signal was a band limited, 2-6 kHz sinusoidal wavelet with a dominant frequency of 4 kHz and duration of 1 period (250 µs total length). Data was stored on DAT-tapes using Windows NT backup software.

6.1 Multibeam Bathymetric Mapping

(Ranero, C. R.; von Huene, R.; Fekete, N.; Gonzalez, C.; Grevemeyer, I.; Phipps Morgan, J.; Soto, G., Vannucchi, P.; Weinrebe, W.)

A full coverage multibeam bathymetric map was obtained along the El Salvador and Guatemala continental slope including a 50-100 km wide swath of the incoming Cocos plate. Tracks were also collected along the continental slope and oceanic plate of Nicaragua to fill gaps left during previous mapping. The results of swath mapping on this cruise are a full coverage data set extending the existing maps of Costa Rica and much of Nicaragua across the El Salvidorian margin to the northern Guatemalan border.

6.1.1 Continental plate

Along the Guatemalan margin, the continental slope has been mapped from about the shelf break to the trench axis. Previous bathymetry was inadequate to show the location of the shelf break along the entire margin and the first tracks of the survey positioned on those data ran over some shelf areas. Mapping the location of the shelf break permitted design of a survey with lines perpendicular to the margin and oceanic plates so that some lines could be extended well into the oceanic plate beyond the outer rise and others were run shorter to optimize survey acquisition time (Figures 6.1.1, 6.1.2, 6.1.3). The gaps between tracks in the upper slope were minimized by running a line parallel to the shelf edge through blank areas on the map. A dedicated survey was run into the continental shelf to map the upper reaches of the San Jose Canyon that extend close to the coast.
Along the El Salvadorian continental slope lines were run parallel to the slope to conserve time giving a lower priority to mapping the oceanic plate. Lines were designed to overlap with the data collected in Guatemala and data in Nicaragua (Figures 6.1.4, 6.1.5). Time did not allow mapping of the uppermost slope and shelf break of El Salvador and coverage stops at about 1000 – 1500 m depth.
Three morphotectonic domains trending roughly parallel to the strike of the slope correspond roughly with the upper, middle and lower slope. The change from one domain to the next may be controlled by the intensity of tectonic processes that increase downslope.

6.1.1.1 Upper slope

The upper slope is characterized by numerous gullies and small canyons. Where coverage reaches the shelf break, maps show that canyons start at the shelf break and rapidly incise the continental slope. Canyons tend to coalesce towards the middle slope, where slope dip is shallower, becoming generally shallower. A few large canyons cut across the entire slope and are described below in section 6.1.1.4.
The upper slope of Guatemala displays a unique large mound of roughly circular shape and large dimensions. This feature was sampled with two dredges and the results are described in the corresponding section 6.4.
The lower portion of the morphotectonic unit of the upper slope is marked by a gradual decrease in dip and a disappearance of the canyon systems.
The relatively well developed canyon system of the upper slope indicates that this is the most stable tectonic unit of the continental slope.
The Salvadorian continental slope is very similar to the Guatemalan slope but without a large active canyon similar to San Jose Canyon The general similarity would be expected since both the Salvadorian and Guatemalan segments are on the same southeast trend of the Central American coast and the Middle American Trench.
The Salvadorian upper slope is heavily rilled and its relation to a source area at the edge of the shelf was not included in our survey. However its similarity would suggest that a breached shelf-edge high as off Guatemala borders El Salvador also. Small turbidity currents that originated during periods (Pliocene?) when the shelf-edge high stood at surf zone depths probably caused the erosion of these rills. The rills are prominent to 3000m depth and disappear by 3500 m depths.

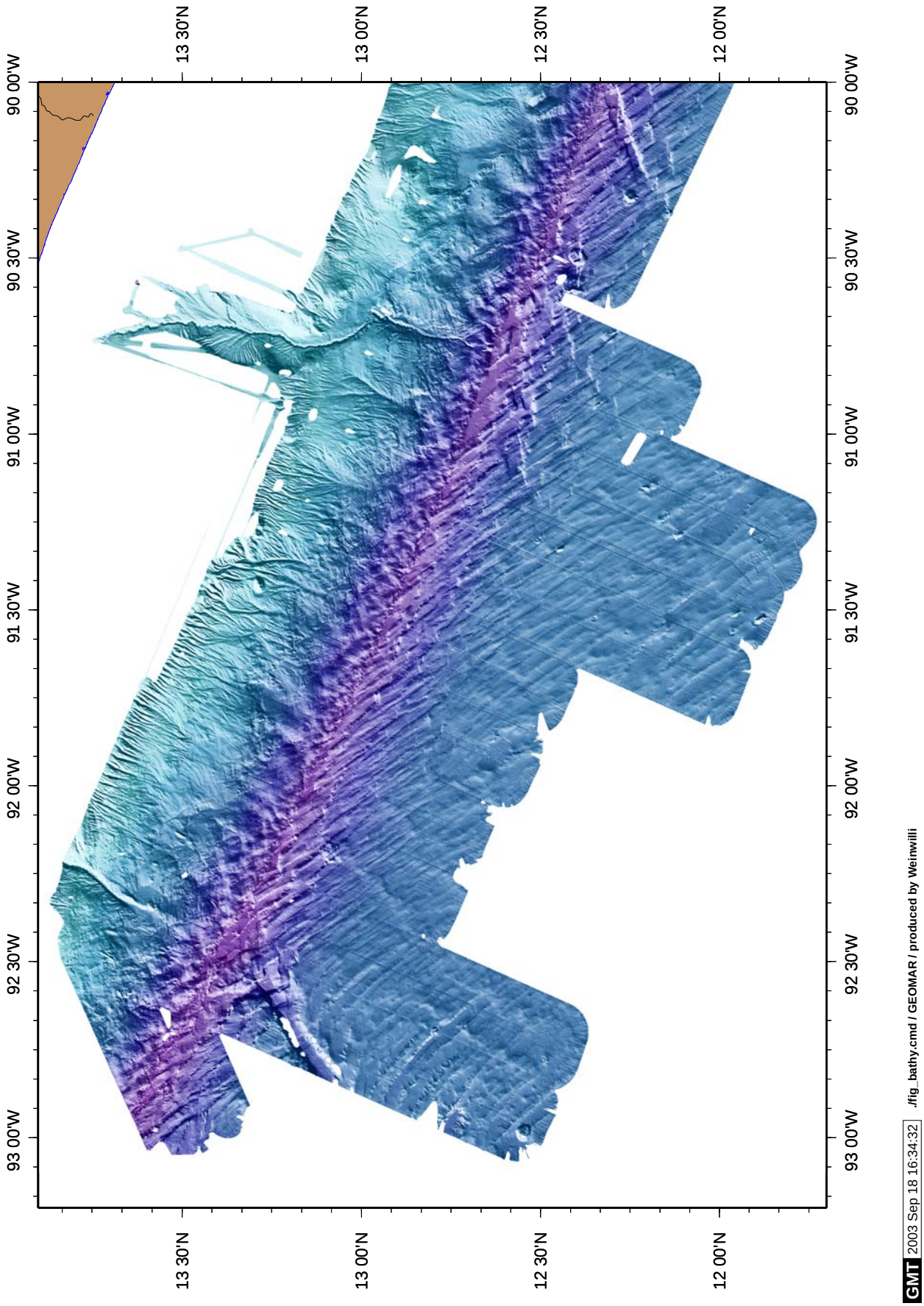

Figure 6.1.1: Shaded relief map of the bathymetry of the continental margin and incoming Cocos Plate offshore Guatemala.

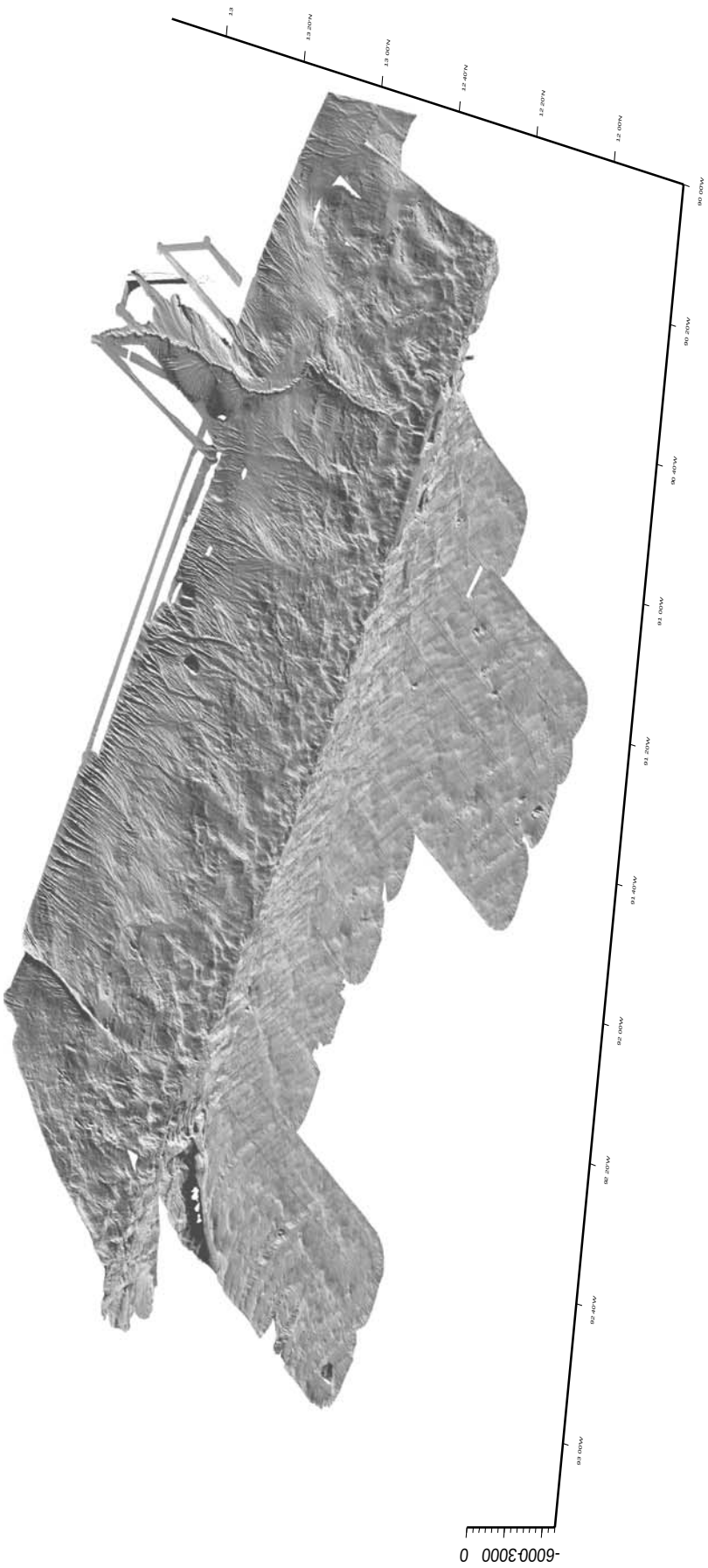

Figure 6.1.2: Perspective view of shaded relief bathymetry of the continental margin and incoming Cocos Plate offshore Guatemala. View is from the SW and illumination from the north.

6.1.1.2 Middle slope

The middle slope is characterized by in general by a slight increase in slope dip and also by a disrupted seafloor morphology with numerous small seafloor scarps cutting the seafloor. The seafloor scarps mark normal faults that contribute to the formation of the small-scale roughness of an irregular terrain.
Faulting indicates that the upper plate is disintegrating due to tectonic processes and that the upper plate is in extension. The most likely possibility is that tectonic erosion and basal removal of upper plate material is active in El Salvador and Guatemala as has also been proposed for Costa Rica and Nicaragua (Ranero and von Huene, 2000; von Huene et al., 2000; Ranero et al., 2000; Vannucchi et al. 2001; Vannucchi et al. in press.). Similar structures related to the collapse of the upper plate have also been described in other continental margins where tectonic erosion is currently active (von Huene and Ranero, 2003).
Numerous small mounds spot the middle slope and seem to occur coeval with the faulting. Similar mounds sampled in Nicaragua and Costa Rica are mud diapirs that are related to the fluid flow of deeply sourced fluids through the upper plate.
In El Salvador, the narrower than usual middle slope is without many canyons and has the typical restless microtopography characterized by slope failure and extensional tectonism. . Its topography merges gradually with the lower slope morphology.

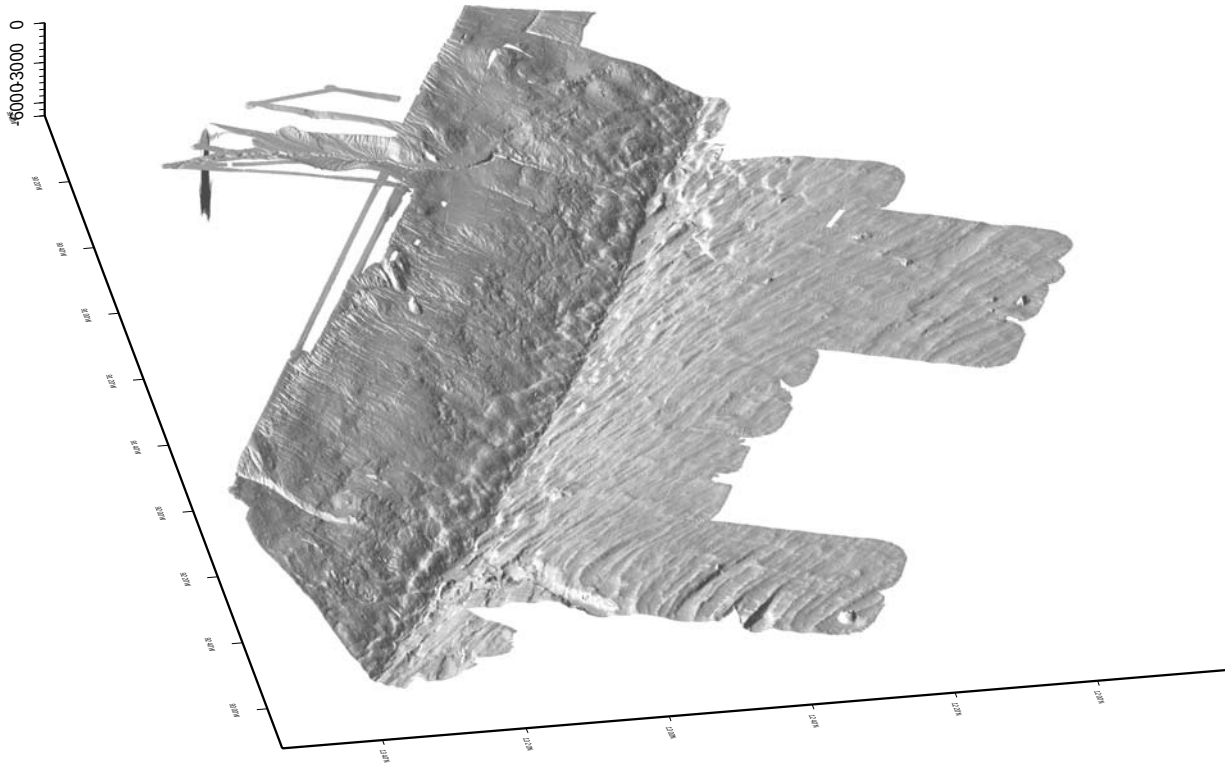

Figure 6.1.3: Perspective view of shaded relief bathymetry of the continental margin and incoming Cocos Plate offshore Guatemala. View is from the NW and illumination from the north.

6.1.1.3 Lower slope

The morphology of the lower slope is characterized by elongated ridges that have strikes similar to the ridges in the incoming oceanic plate. The lower slope ridges probably represent the rifling of the thin apex of the upper plate over the rough topography of the underthrusting oceanic plate. The close resemblance of the lower slope ridges with the ocean plate morphology indicates that the upper plate has been highly fractured and has probably lost its coherence. The lower slope is the most tectonically active area of the entire slope.
. In El Salvador too the lower slope topography mimics the many subducted horst and grabens of the oceanic plate. The trench axis is essentially empty of ponded turbidite with a very sharply defined deformation front.

6.1.1.4 Large canyons

Exceptions to the general morphology are several large canyons that cut across much of the slope. In the NW of Guatemala a large deep canyon cuts the upper and much of the middle slope. The canyon is an amazingly straight feature with a marked v-shaped cross-profile, which indicates that it is an active structure and possibly tectonically controlled. The continuation across the lower slope is less pronounced, possibly because it is a shallower angle dip morphology and perhaps because it is modified by the most tectonically active morphological domain. The trench axis opposite the canyon mouth is locally smoothed by trench fill that seems to locally overwhelm the oceanic plate topography.
The most prominent erosional structure is the San José canyon in the SE portion if the Guatemalan slope. The geometry is fairly complex and possibly indicates a lengthly evolution. Erosion has carved a broad 20 km wide gap into the topographic high at the edge of the continental shelf, narrowing landward across the shelf. Numerous gullies scupture the flanks of the shelf basin and converge towards a central relatively narrow v-shaped channel that seems to extend close to the coast. The central channel V-shape indicates an erosional structure that seems to be currently actively transporting turbidites. The central channel cuts across the entire continental slope as a deep incision, although it is less well defined in the lowermost slope. No evidence for a tectonic control of the canyon has been observed. The trench axis in the vicinity of the canyon mouth shows a smoother topography than in the surrounding areas, indicating turbidites that smooth ocean plate morphology. It is interesting to note that the turbidite filled half grabens are the location of the DSDP Leg 67 drilling of the trench (von Huene et al. 1980) and that some of the drill site information has been commonly used as a reference column throughout the literature. The bathymetric map shows that the trench turbiditic fill in this area is actually atypical for the Middle America Trench.
A third example of a large canyon occurs near the border of El Salvador and Nicaragua (Figure 6.1.4). There, a prominent embayment of the slope topography marks the location of a canyon that produces a re-entrant in the continental shelf break and is coincident with the Gulf of Fonseca between El Salvador and Nicaragua, This shallower portion of the structure was not mapped with swath bathymetry due to time constraints. Although the canyon is a broad depression in the slope, no v-shaped channel is observable and thus the structure may currently be inactive.

6.1.2 Structure of the Incoming Cocos Plate

6.1.2.1 Cocos Plate offshore Guatemala

The morphological fabric of the ~20Ma incoming plate appears to be largely the byproduct of processes during plate accretion at the East Pacific Rise superimposed by the tectonics associated with bend-faulting approaching the Middle American Trench. Figure 6.1.1 shows a shaded-relief map of the region. In the west, the incoming plate has a strong abyssal hill fabric that appears to have been created in the wake of a northward-moving ridge propagation event. Traces of the pseudofault are visible as an NNE-striking oblique trough at 13°10'N, 92°50'W. At (13°15'N, 92°35'W) the trough changes strike to a N10W orientation,

either because it terminates into a prior southward propagation event, or because it terminates, and its terminus was then used as the nucleation site of a strongly developed bending-related graben. Near the pseudofault, the abyssal hill fabric orientation progressively rotates up to ~20° counterclockwise in the typical J-curvature associated with propagating ridge segments, and the relief of individual hills reaches up to ~500m. Seafloor created more than 50km away from the pseudofault trace of the propagating ridge tip have a typical orientation of N30°W, and characteristic abyssal hill relief of up to several hundred meters.

Seamounts are relatively sparse in this region of seafloor, with no obvious small chains of seamounts, unlike seafloor subducting beneath Nicaragua (Ranero et al., in press). The seafloor offshore Costa Rica has unussually tall seamounts because they were formed off-axis by the Galapagaos hotspot (von Huene et al., 2000). The few seamounts offshore Guatemala evident in the map all have maximum relief of a few hundred meters or less, suggesting that all were created on young lithosphere near the spreading center.

In summary, it appears that the seafloor fabric created at the mid-ocean ridge was fairly typical for that of a fast-spreading ridge axis, with perhaps slightly larger abyssal hill relief than anticipated for this fast spreading rate, and the obvious disturbance of the wake of a fairly large propagating ridge axis offset.

The plate bending associated with subduction affects the incoming plate in several striking ways. Roughly 40km from the trench axis, abyssal hill faults appear to become reactived as their relief increases approaching the trench axis. In addition to fault reactivation, a new set of faults also develops oriented 70° with respect to the abyssal hill fabric (this is especially well developed near 12°30'N, 90°50'W), so that the reactivated faults and new faults strike in a conjugate pattern with the strike of the trench, the reactivated faults striking ~35° clockwise from the trench axis while the new faults strike ~35° counterclockwise. Maximum fault-relief is observed around the site where the pseudofault trace intersects the trench-axis; whether this relief is original or bend-faulting related in origin is unclear. The observed bend-faulting pattern is quite different from that seen offshore Nicaragua where the abyssal hill fabric of the (similar age) incoming plate, also formed at the East Pacific Rise, strikes almost exactly parallel to the trench axis.

Another interesting morphologic feature that appears to form as a byproduct of bend-faulting are 'pinnacles'; mound-shaped structures typically associated with normal faults. Many of these structures are visible near the trench axis (for example at least 6 are visible near 12°52'N, 91°33'W). Since pinnacles are only seen near the trench axis, we infer they form as a consequence of bend-faulting. Our preferred hypothesis is that they are likely to be linked to fluid-flow within the bending plate, perhaps they are large hydrothermal outflow structures.

6.1.2.2 Cocos Plate offshore El Salvador

Mapping of the ocean plate offshore El Salvador was restricted to the ~ 40 km near the trench axis due to time limitations (Figure 6.1.4 and 6.1.5). The ocean plate is fairly similar to Guatemala with a well developed bending-related faulting fabric altough fault patterns seem more complex that at Nicaragua (Ranero et al., in press). Also, the seafloor spreading topographic fabric does not seem as prominent as in Guatemala, but the bathymetric coverage towards the outer rise is very limited. The seafloor spreading-related topography seems to gradlly change from Nicaragua, where it is completely muted by the sediment cover and it looks very smooth in seismic reflection data (Ranero et al., in press) to Guatemala, where seafloor spreading related ridges are up to several hundred meters high.

Several structures striking roughly SW-NE occur at high angles to the spreading fabric and they may be traces of pseudofaults, similar to the structure in Guatemala, although they are less prominent.

Bending-related faulting seems to not only reactivate the seafloor spreading fabric, but new faults striking ~ WSW-ENE develop near the trench. Interestingly, these structures are at relatively large angles (~15-25°) to the trench axis strike. Simialrly to Guatemala no large seamounts have been observed in the surveyed area.

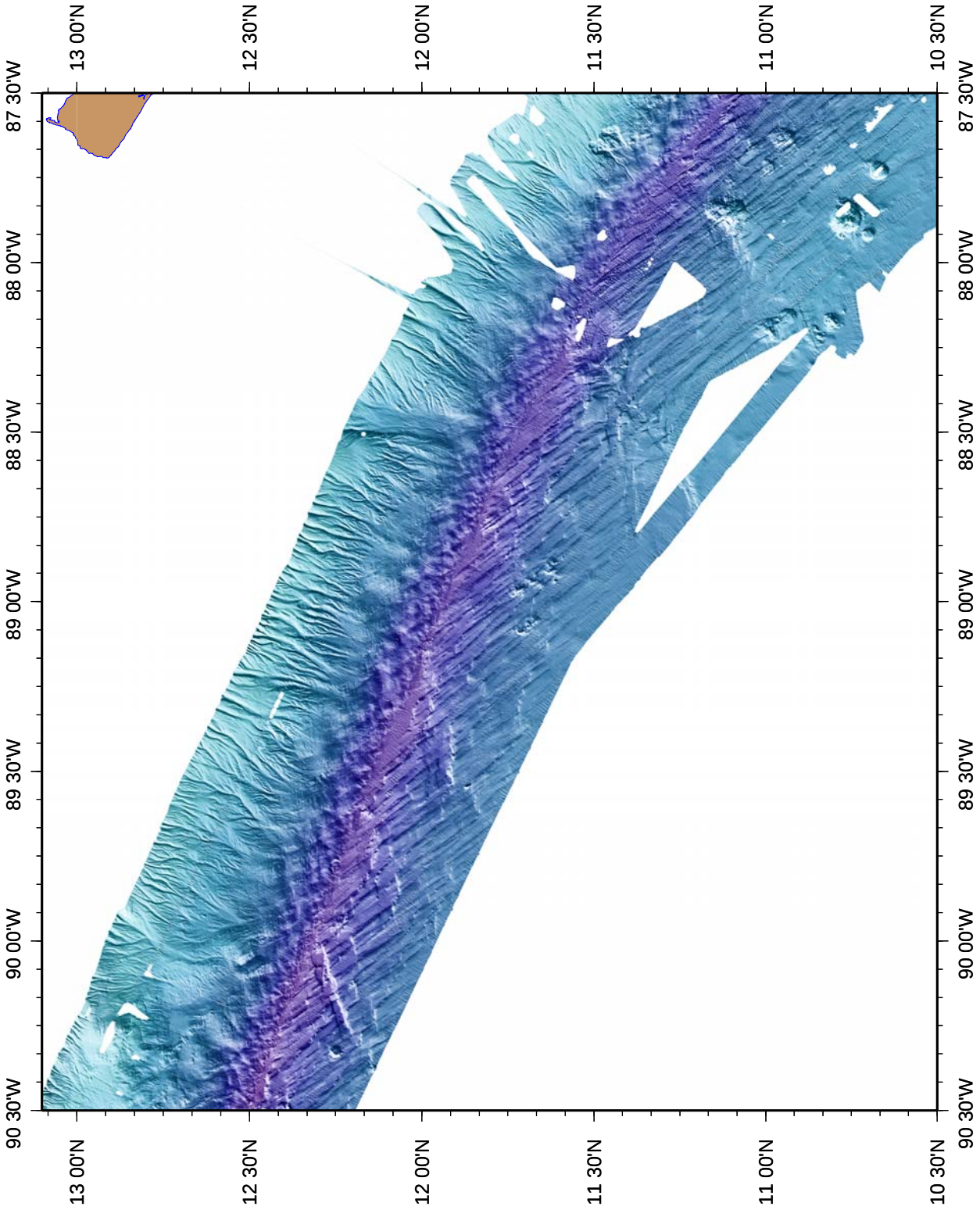

Figure 6.1.4: Shaded relief map of the bathymetry of the continental margin and incoming Cocos Plate offshore El Salvador.

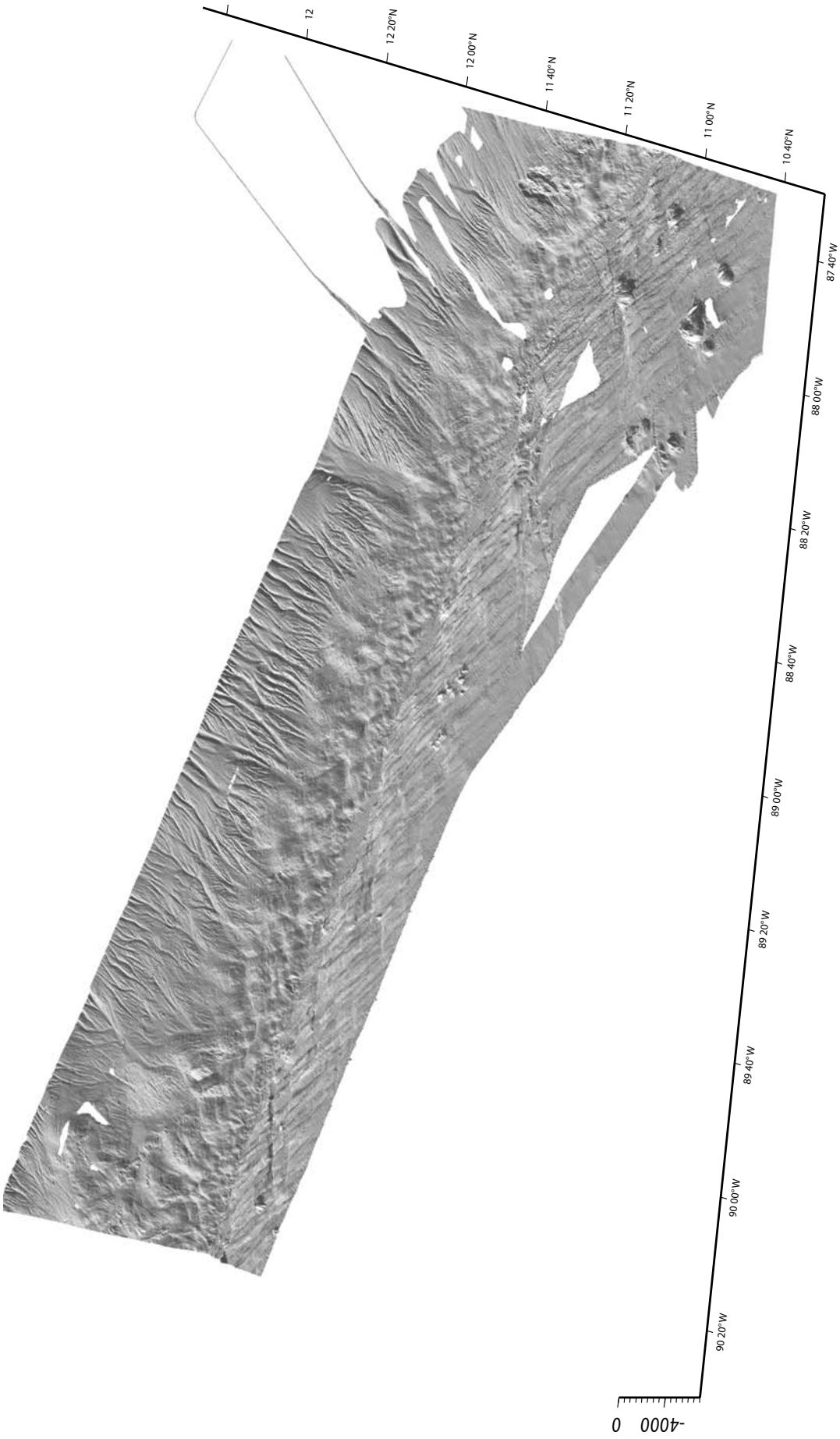

Figure 6.1.5: Perspective view of shaded relief bathymetry of the continental margin and incoming Cocos

6.2 Magnetic survey off Middle America, 88°W to 93°W

(I. Grevemeyer)

The magnetic survey during the cruise SO173-2 began after entering the territorial waters of Guatemala. Magnetic data were obtained along most bathymetric survey lines. The continental slope and incoming oceanic plate off Guatemala were surveyed with 22 lines normal to the strike of the margin. The lines were between ~200 km and ~60 km long. In addition, a few tie lines were run parallel to the trench axis (Fig. 6.2.1). In general, the magnetometer provided data of good quality. However, during August 15, 2003 the instrument failed to record data useful for geophysical data analysis; data along two lines are lost.

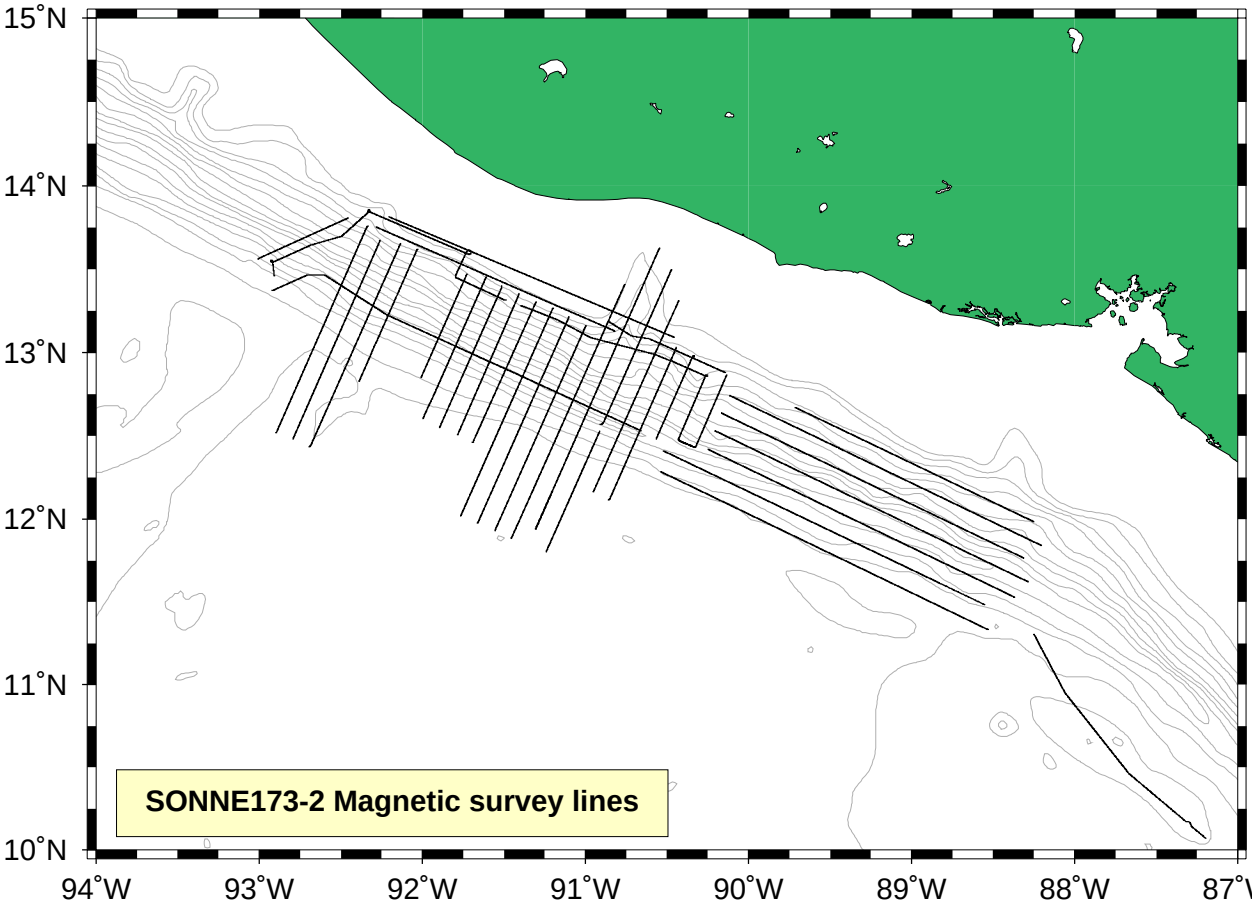

Figure 6.2.1: Track chart of magnetic survey lines obtained during SO173-2.

The most striking feature of the magnetic data is that the margin wedge is characterised by a prominent magnetic anomaly (Fig. 6.2.2), which indicates that the wedge consists of highly magnetised rocks, perhaps related to ophiolitic basement. Mesozoic ophiolitic rocks were recovered during Deep Sea Drilling Project Leg 84 in San Jose Canyon and elsewhere off Guatemala (von Huene et al., 1985). In addition, magnetic and seismic surveys off Nicaragua and Costa Rica revealed similar properties for the margin wedge, i.e., a prominent magnetic anomaly over the slope and high-velocity continental basement (Barkhausen et al., 1998; Walter et al., 2000). In Costa Rica and Nicaragua these features are interpreted as an offshore extension of the igneous complex exposed on the Nicoya Peninsula.

The most prominent anomaly occurs at the self edge. Seismic studies on the slope and shelf (Ladd and Schroeder, 1985) indicates a post Miocene uplift that brought basement to shallow levels. The strength of

the magnetic field over continental crust is generally controlled by the depth to the igneous basement and the magnetic highs correlate with areas of uplifted basement. From the edge of the shelf landward the magnetic anomaly decreases over 30-40 km to increase again ~60 km off the coast line. This pattern mimics the forearc basin that developed in Early Tertiary time when uplift of the shelf-edge began.

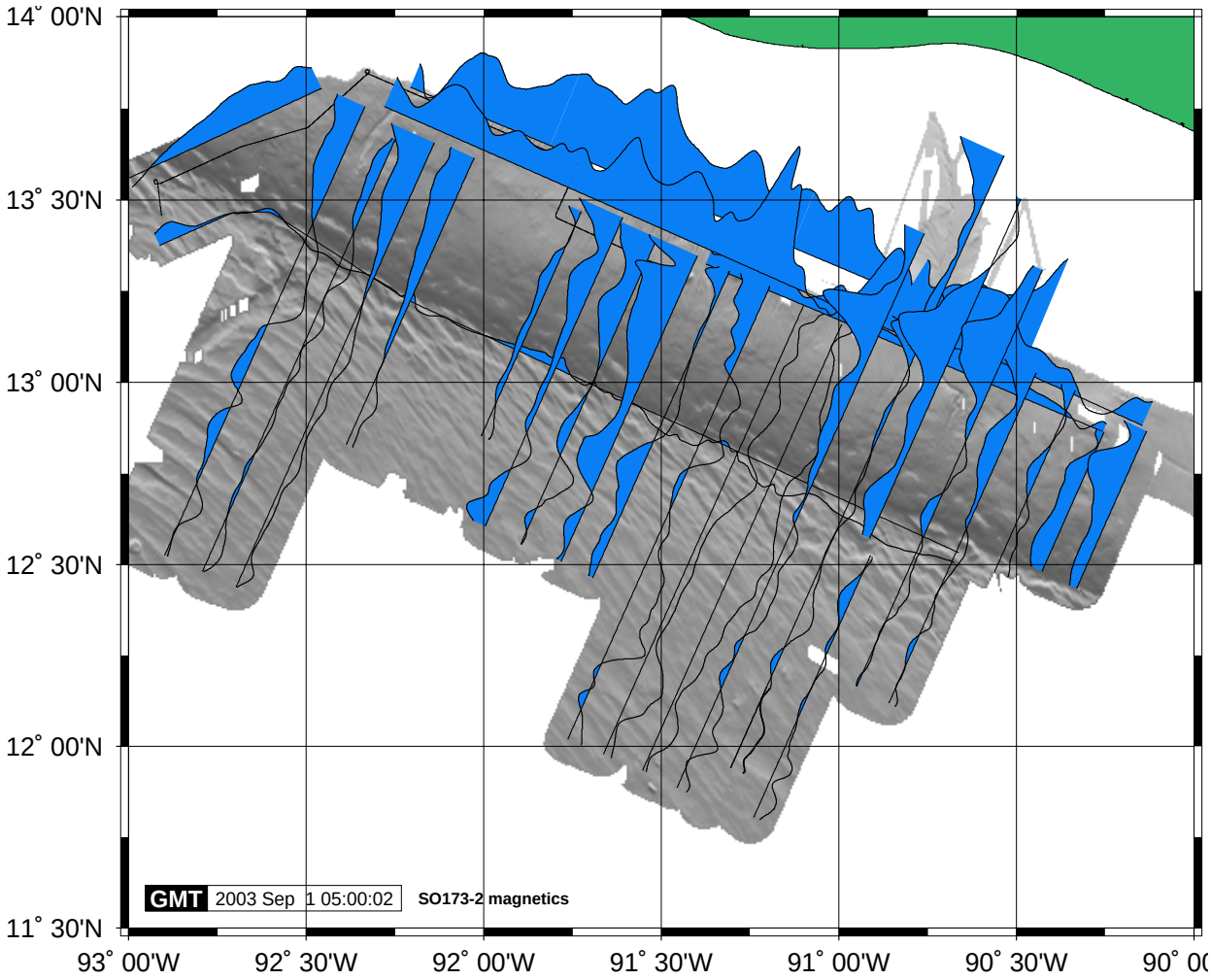

Figure 6.2.2: Wiggle plot of magnetic anomalies acquired offshore Guatemala superimposed on swath mapping bathymetry.

The abyssal hill fabric of the incoming plate off Guatemala strikes obliquely to the margin. Characteristic magnetic stripes related to seafloor spreading generally mimic this trend. Thus there is a profound contrast between the strike of anomalies on the ocean crust and margin parallel anomalies over the margin wedge. This fact was already noticed during geophysical pre-site surveying preceding the DSDP drilling off central Guatemala (Ladd and Scroeder, 1985). However, the oblique trend of seafloor spreading anomalies seems to be contaminated in places. It might be reasonable to hypothesize that bending of the plate into the trench axis may result in fault generation and re-activation in the outer rise area. Water may use such faults to reach the mantle and generate serpentine which is often characterised by a high magnetisation. Thus, assuming that bending starts at a constant distant from the trench, the formation of serpentine may superimpose other magnetic anomalies on that of ocean ridge spreading.

During the bathymetric survey of the continental slope and trench area off El Salvador 7 additional lines of magnetic anomalies were acquired. This survey was designed to optimise the trade off between the coverage of swath-mapping bathymetry and time. Consequently, tracks were run parallel to the margin. Unfortunately, at the given strike of the magnetic spreading anomalies on the incoming plate this pattern of tracks was less suitable to reveal seafloor spreading anomalies on the incoming plate. However, the survey provides useful information with respect to the magnetisation of the basement of the margin wedge. Like in Guatemala, the

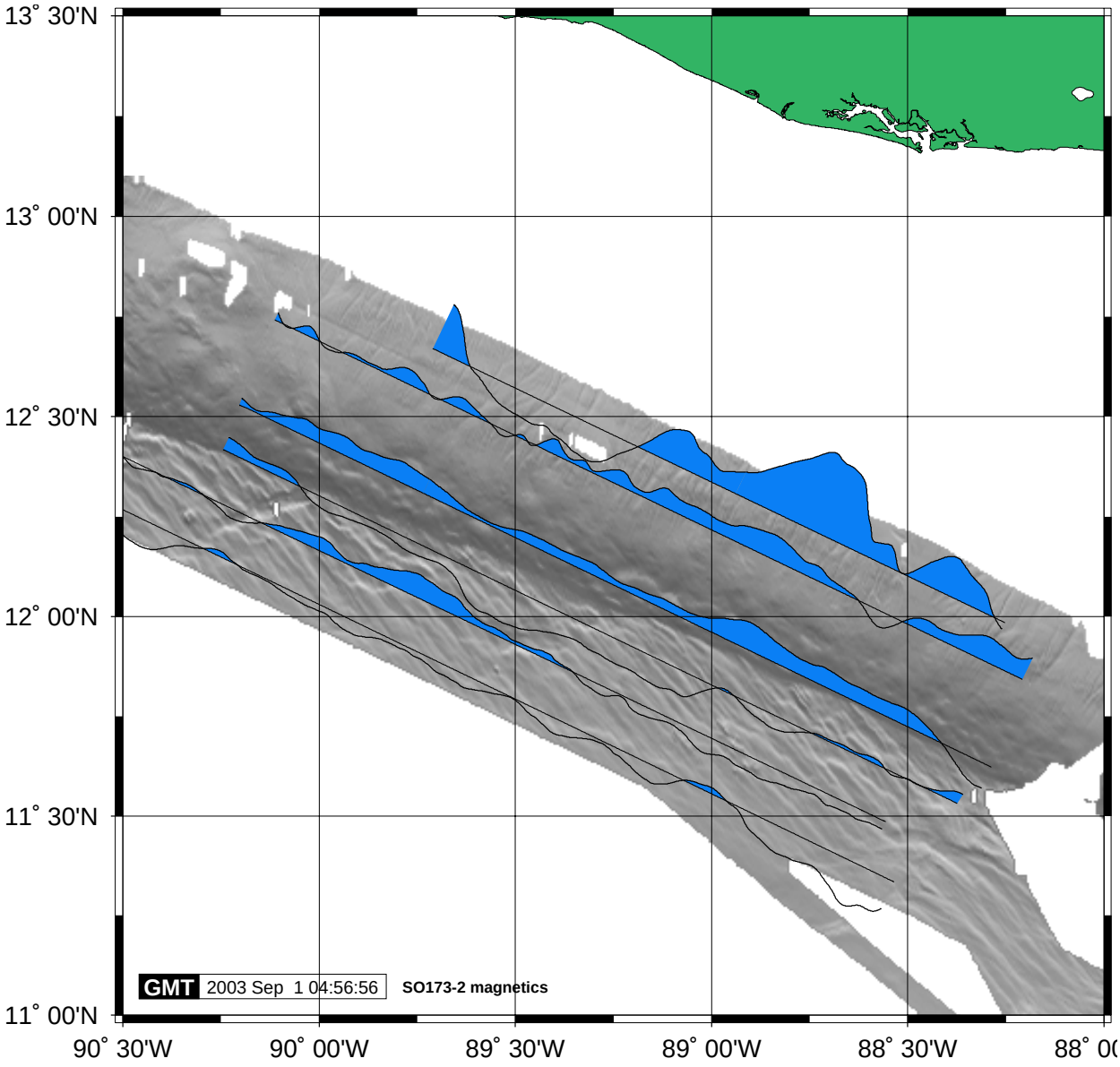

Figure 6.2.3: Wiggle plot of magnetic anomalies recorded along the slope off El Salvador. Data are superimposed on swath-mapping bathymetry.

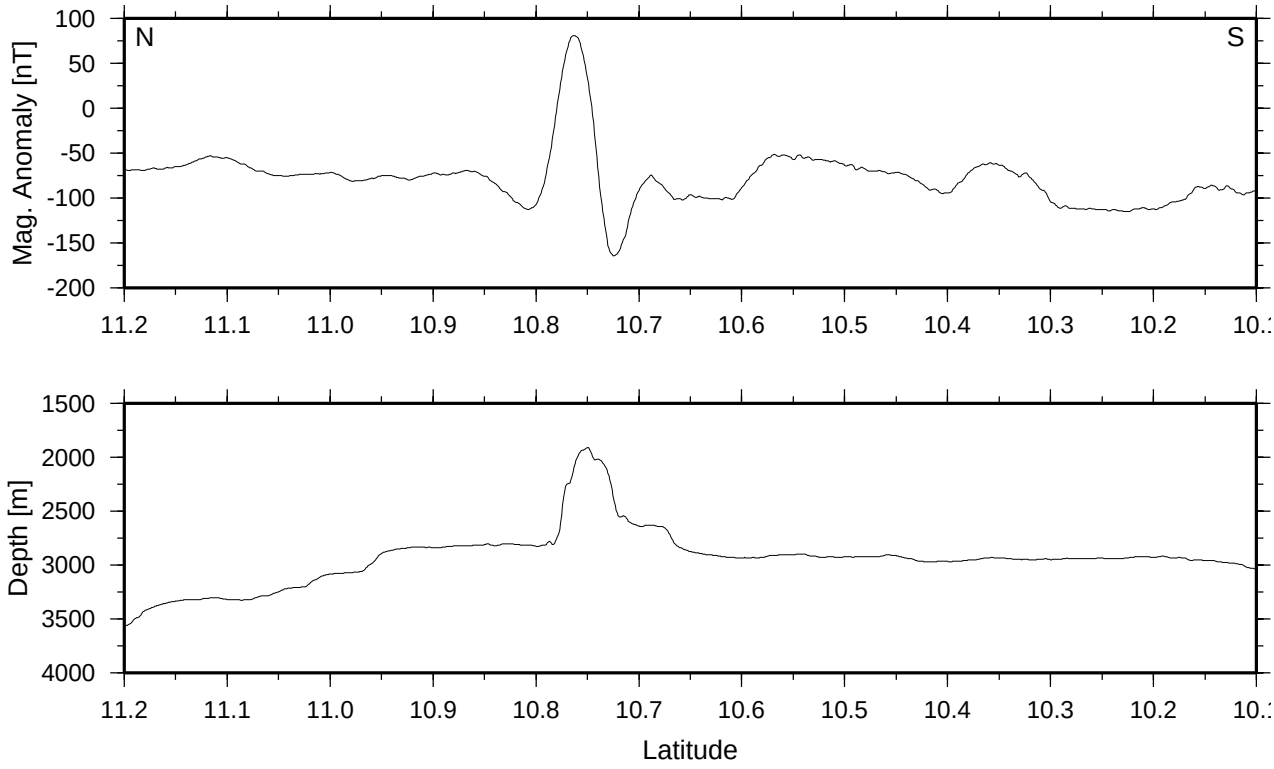

Figure 6.2.4: Magnetic field anomaly along the outer rise offshore Nicaragua. Note the dipole like anomaly over the seamount.

6.3 Dredges of the Mound Quetzal

(P. Vannucchi, Gerardo Soto)

The Mound Quetzal is located on the Guatemalan upper slope on the northwest side of the san José Canyon (~13°18'N-91°26'W). The new bathymetry collected during SO 173-2 showed a number of small mounds on the slope, but the Mound Quetzal is a unique feature on the Guatemalan slope both because of the shape, well rounded, and the dimensions of about 3.5km x 5.5km and 800m high. The dredges approached the mound from the south and from the north, and the exact locations of the hauls are shown in Fig. 6.3.1.

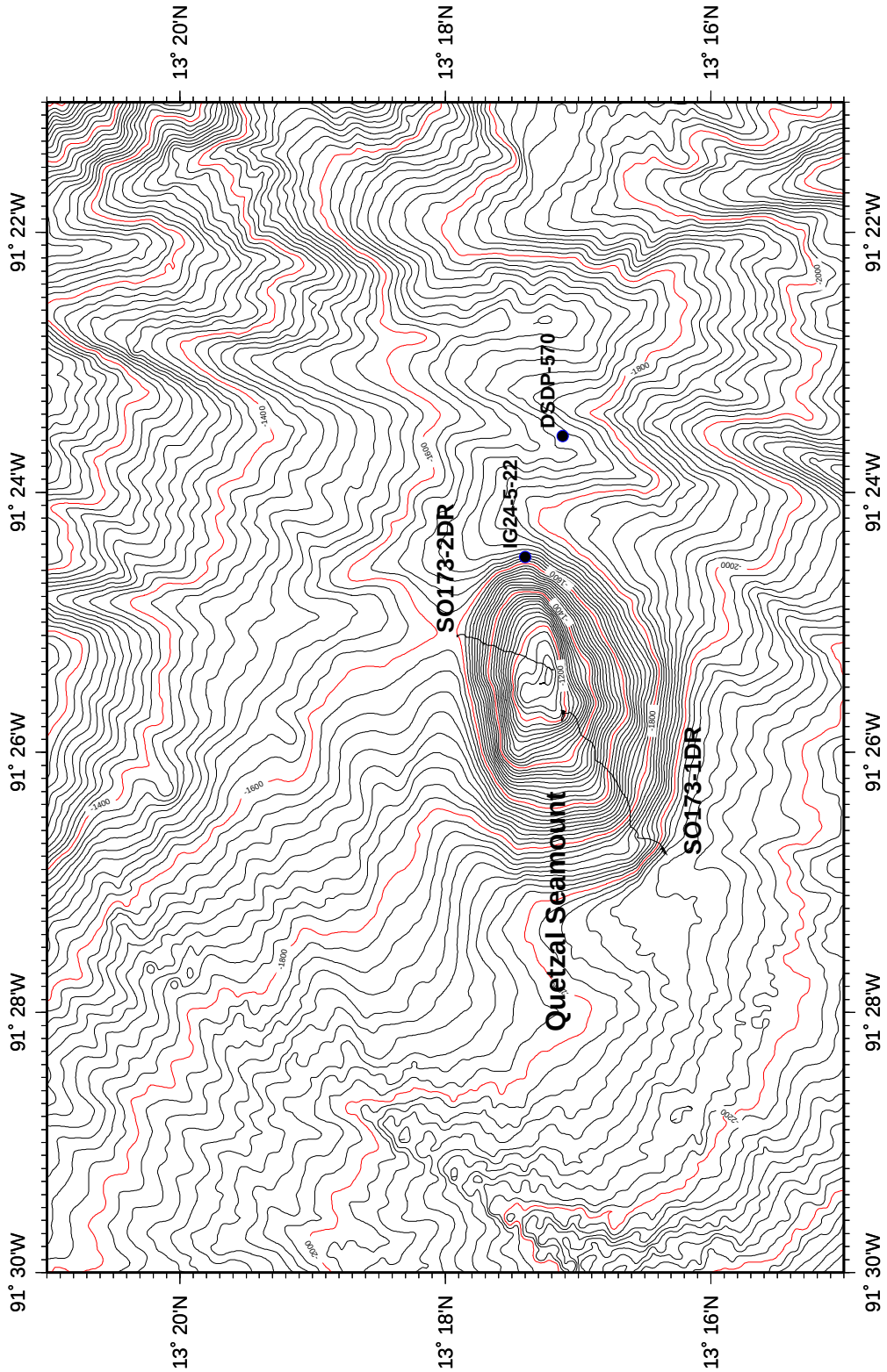

Figure 6.3.1: Location map and tracks of dredge haulse.

Both dredges were successful in recovering rock samples. Once on board the rocks were cleaned, labelled, mesoscopically described through a reflection light microscope and sealed for transportation to GEOMAR, Kiel. Further study will involve petrographic examination of thin sections, dating and analysis on the mineral precipitation phases due to hydraulic deformation. The key objective of that work will be to detect the geological characteristics of the mound, why it appears as a unique feature on the Guatemalan upper slope, and what kind of mechanisms contributed to its elevation and shape.

SO 173-1DR. The first dredge haul was taken from a steep southwest slope of the mound with about 900 m relief going from 2075 m to 1168 m. It started at 15.20 UTC at 13°16.33' N-91°26.79'W and ended at 19.05 at 13°17.14'N-91°25.67'W. The dredge was full and 60 samples have been collected and labelled from SO 173-1DR. The rocks consisted essentially of well lithified volcanoclastic conglomerate (Fig. 6.3.2), fine to coarse sandstones (Fig. 6.3.3), and minor amount of mudstones (Fig. 6.3.4), marls (Fig. 6.3.5), and tuffs (Fig. 6.3.6).
The volcanoclastic rocks are:
- Gray to green, carbonate cemented, volcanoclastic conglomerates (Fig. 6.3.2). Well sorted, contain well rounded grains of: basalt, pumice, cherts.
- White to light green, fine-grained, variously-sorted volcanoclastic sandstones (Fig. 6.3.3). They are mainly composed of: feldspars, glass shards and pumice, mafic minerals (Hbl and px), micas, organic matter. Density and packing varies according to weathering degree. Some of them shows some grading. Some have laminae of organic material.
The rocks appeared as boulders, some of then well-rounded, coated with MnOx and generally with alteration rims from few mm to 5 cm thick.

Figure 6.3.2: Volcanoclastic conglomerate

Figure 6.3.3: Volcanoclastic sandstone

Figure 6.3.4: Red Mudstone

Figure 6.3.5: Pebble of red marlstone

Figure 6.3.6: Tuff

SO173-2DR. The second dredge haul went from 1598 m depth to 1126 m along the northern slope of the mound and clear indication of wire tension indicated that the material was taken just from the top of it. The dredge started at 20.17 UTC at 13°17.91'N-91°25.09'W and ended at 21.31 at 13°17.19'N-91°25.36'W. The dredge was full and recovered broken pieces from an outcrop as far as the shape and the alteration is concerned. 61 samples have been collected and labelled. The rocks were for the majority gray mudstone and siltstone (Fig. 6.3.7), only one tuff sample and few pieces of fine cherts were recovered (Fig. 6.3.8). Almost all the recovered rock pieces are brecciated and veined suggestive of hydrofracturation and the occurrence of light-greenish impregnation in the fine grained wall rock would recall hydrothermal alteration (Fig. 6.3.9). The rocks are abundantly altered and coated with FeOx and MnOx crust giving them a bright orange-yellow colour (Fig. 6.3.10).

Figure 6.3.7: Mudstone

Figure 6.3.8: Chert

Figure 6.3.9: Veined mudstone

Figure 6.3.10: siltstone coated with FeOx

Previous dredging, gravity coring and DSDP Site 570

The Mound Quetzal was the target of dredging and gravity coring in 1977 during the DSDP Leg 84 site surveys.

The RV Ida Green took the Gravity Core IG24-5-22 at 13°17.4'N and 91°24.5'W on the eastern side and at the very base of the mound (von Huene et al., 1984). The Gravity Core IG24-5-22 was 94cm long and recovered two units: an upper (0-25cm) very coarse muddy gravel with angular clasts of basalt, whose texture was indicative of pillowed flows, and a lower unit (25-94cm) with medium coarse to very fine grained foraminiferal sandy mud.
The dredge was also taken during the RV Ida Green site survey in 1978 and recovered about 15 kg of rocks from the flank of the mound. Unfortunately an error of about 2km does not give the exact location. The dredge recovered red-brown nannofossil limestone, and volcanogenic sandstones and tuff. The sandstones are finely bedded to massive, rarely thinly graded. Sand grains are angular and include red pumice, biotite, amphibole, feldspar and glass.

DSDP Site 570 was located about 5-6 km from the mound crest at 13°17.12'N and 91°23.57'W and it was drilled on the edge of a small bench positioned in a canyon. It penetrated into 374 m of sediments before encountering the basement where it went until 401.9 m below the sea floor. The sediments at DSDP Site 570 where subdivided in four units:
Unit 1: 0-208 m Pleistocene green mud with sand layers
Unit 2: 208-255 m Pliocene green mud with sand layers
Unit 3: 255-330 m late Miocene green mud
Unit 4: 330-374 m early Eocene sequence of siliceous limestone, green volcanoclastic sandstones, blackish red mudstone with limestone, pumice, and cemented sandstone pebbles at the base.
The basement (374-401.9 m) consisted of black serpentinized peridotites with horizons of pale blue green serpentinitic mud in the upper 10 cm.

The Early Eocene sequence has some similarities with the rocks dredged during SO 173-2. In particular the volcanoclastic sand/sandstones recovered in cores 84-570-37 and 38 (Fig. 6.3.11 and 12) and the red mudstones. Also RV Ida Green dredge in 1978 describes volcanogenic sandstones and tuffs similar to those recovered during the first dredge of SO173-2.
Other ODP Sites on the Guatemalan slope recovered Early Tertiary and even Cretaceous rocks. DSDP Site 569, for example, recovered 90 m of late Oligocene mudstone, and 30 m of late-early Eocene radiolarian-rich mudstone. DSDP Site 567 in the lower slope recovered also mudstones, siltstones and limestones of late Cretaceous to Eocene age. The common character of all these sequences is to be few tens of meters thin in each site. Unconformities are common in the record of DSDP drilling on the Guatemalan trench.

As a preliminary result and based on previous studies in the area, the rocks dredged in the first haul of SO 173-2 would be assigned to the early Tertiary and belonging to a distal to hemipelagic environment well in agreement with

Figure 6.3.11: DSDP Site 570 early Eocene volcanoclastic sand and sandstone

Figure 6.3.12: DSDP Site 570 early Eocene volcanoclastic turbiditic sandstone pebble with alteration rim.

6.4 Seismology

(I. Grevemeyer)

During the cruise a seismological network of four ocean bottom differential pressure gauges (DGP) was recovered. The deployment of the ocean bottom seismological stations was a pilot experiment to detect the local and regional earthquake activity off southern Central America. The results will be used to design a future SFB574 "outer rise seismological experiment" proposed to yield the depth of faulting in the incoming plate. Faults are re-activated or created while the brittle lithosphere is bend during subduction (Ranero et al., 2003). The centroid depth of these earthquakes can be used as proxy to assess the depth down to which fluids may migrate and hence alteration and perhaps serpentinzation occurs. In addition, waveforms of deep earthquakes may provide important information about the properties of the lithosphere at greater depth (e.g., Abers et al., 2003). The instruments have been on the seafloor four a period of 34 days and were deployed during leg SO173-1 of RV SONNE.

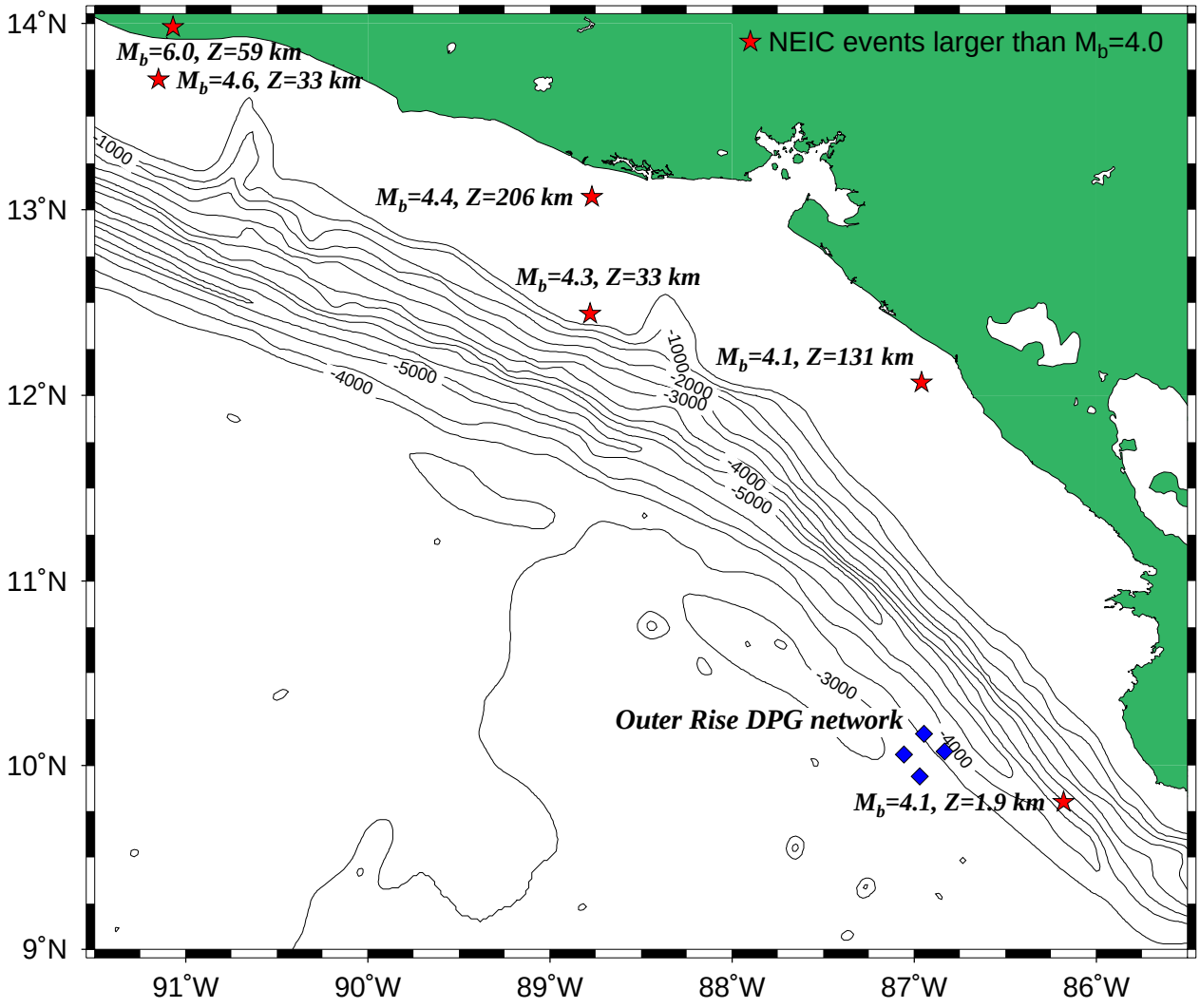

Figure 6.4.1: Location of the network of ocean bottom stations (diamonds) deployed for a pilot „outer rise seismological experiment. Earthquake locations with magnitude m_b> 4 are shown by stars. Six events have been reported by the National Earthquake Information Center (NEIC) for the 34 days of network operation.

A first assessment of the quality of data recorded during this time interval was accomplished by cutting out earthquakes with a magnitude of $m_b > 4$. Event origin times and geographical locations were obtained from the National Earthquake Information Center (NEIC) in Boulder, Colorado. Six events were reported by NEIC for the period of deployment. The earthquakes had magnitudes of 4.1 to 6.0 and occurred between July, 30 and August 26, 2003 (Fig. 6.4.1). Examples of the recorded events are shown in Figs 6.4.2 to 6.4.5. The regional earthquakes occurred at epicentral distances of ~90 to ~620 km. The nearest event was located off Nicoya Peninsula near the trench axis and was perhaps related to bend faulting in the down-going lithosphere. The event furthest away occurred at 60 km depth under the coast line of Guatemala.

In general, high quality waveforms were obtained form all large events and clear *P*-onset times and polarity of first motion can be reported for all events, even for magnitude $m_b=4$ earthquakes at Dð=400-600 km. However, the $m_b=6.0$ earthquake at Dð=605 km from the centre of the network overloaded the recording systems. The *P*-onset and polarity of the first wave train is well recorded, though. A common feature of all events is a prominent second arrival, which is in good agreement with the multiple in the water column at the site of deployment. A more refined analysis of the $m_b > 4$ events and a search for local earthquakes below the teleseismic detection level will be done in the post cruise phase.

Event times and locations for the $m_b > 4$ events were provided by R. Herber form the Geophysical Observatory of the University of Hamburg.

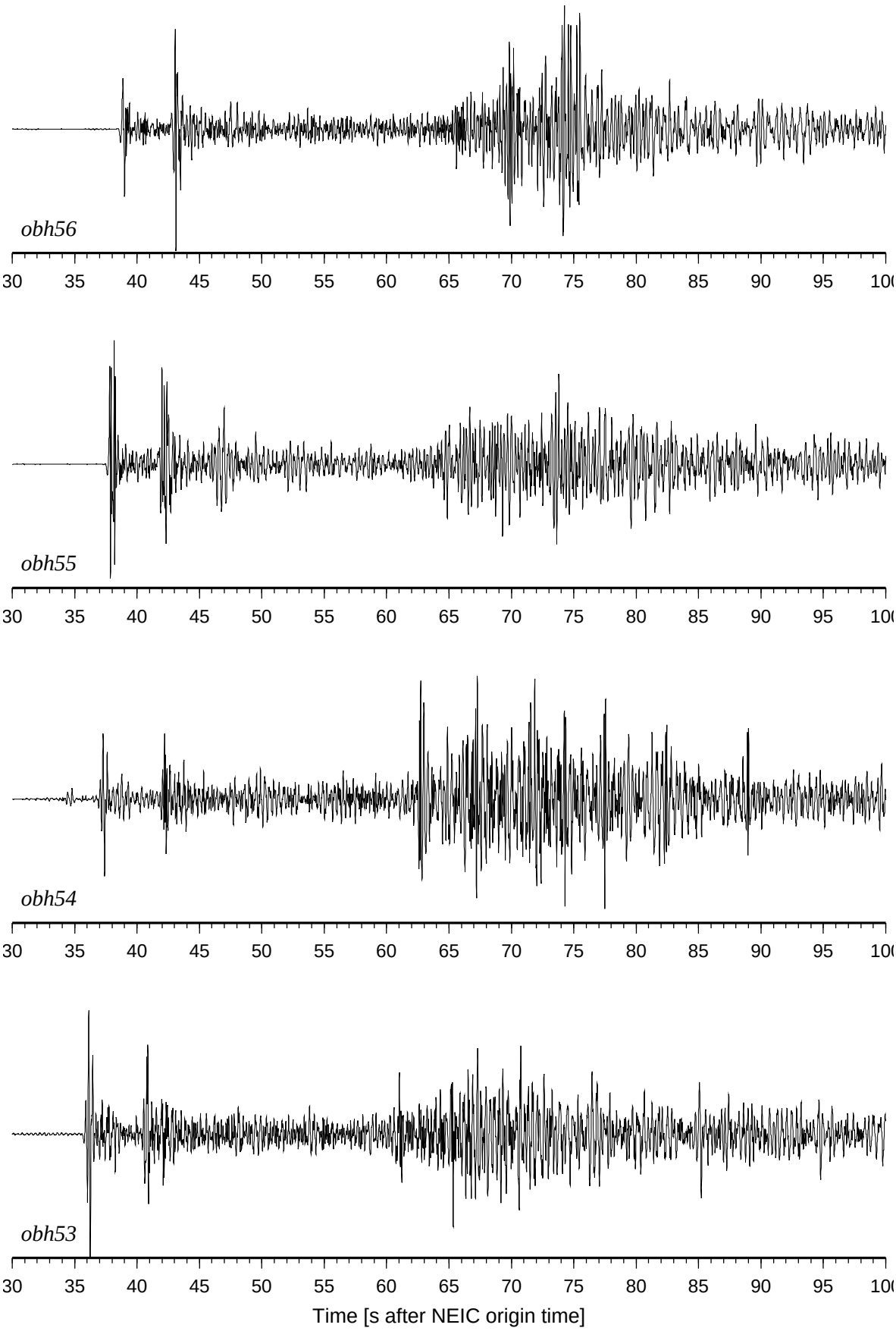

Figure 6.4.2: Waveforms from all four instruments for an event near the trench axis offshore Nicoya Peninsula (D ~ 90 km, depth ~ 2 km).

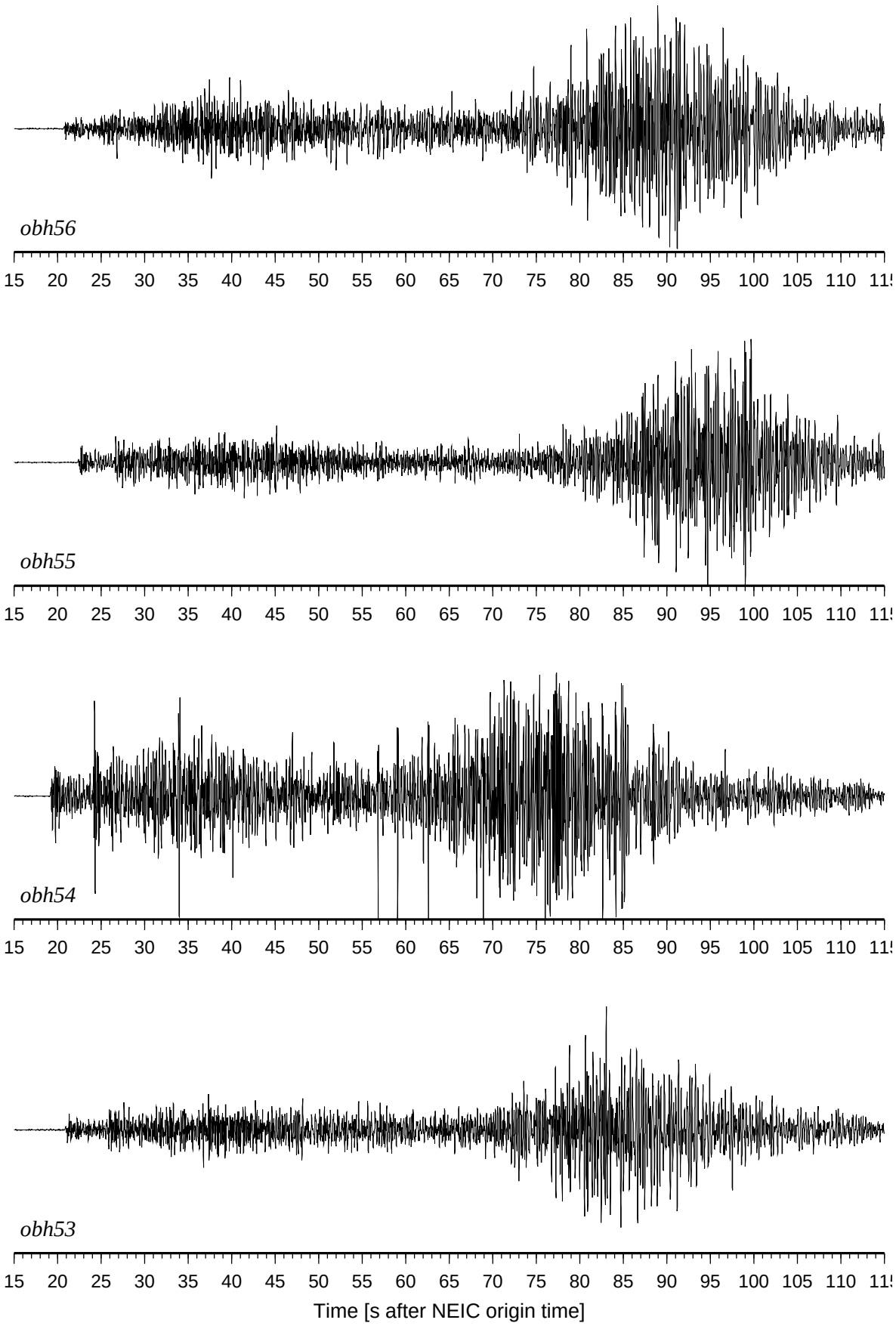

Figure 6.4.3: Waveforms from all four instruments for an event at 130 km depth off Nicaragua.

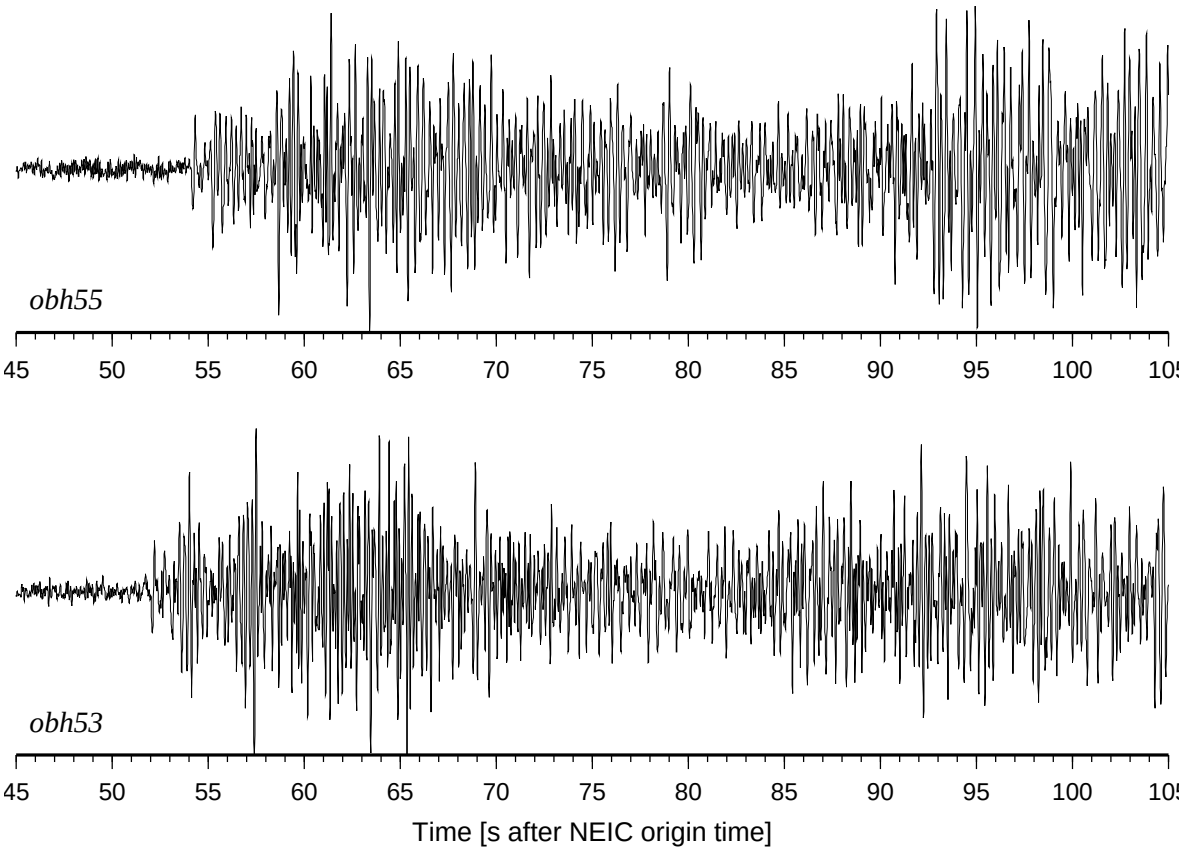

Magnitude 4.4 at 206 km depth, El Salvador, August 16, 2003

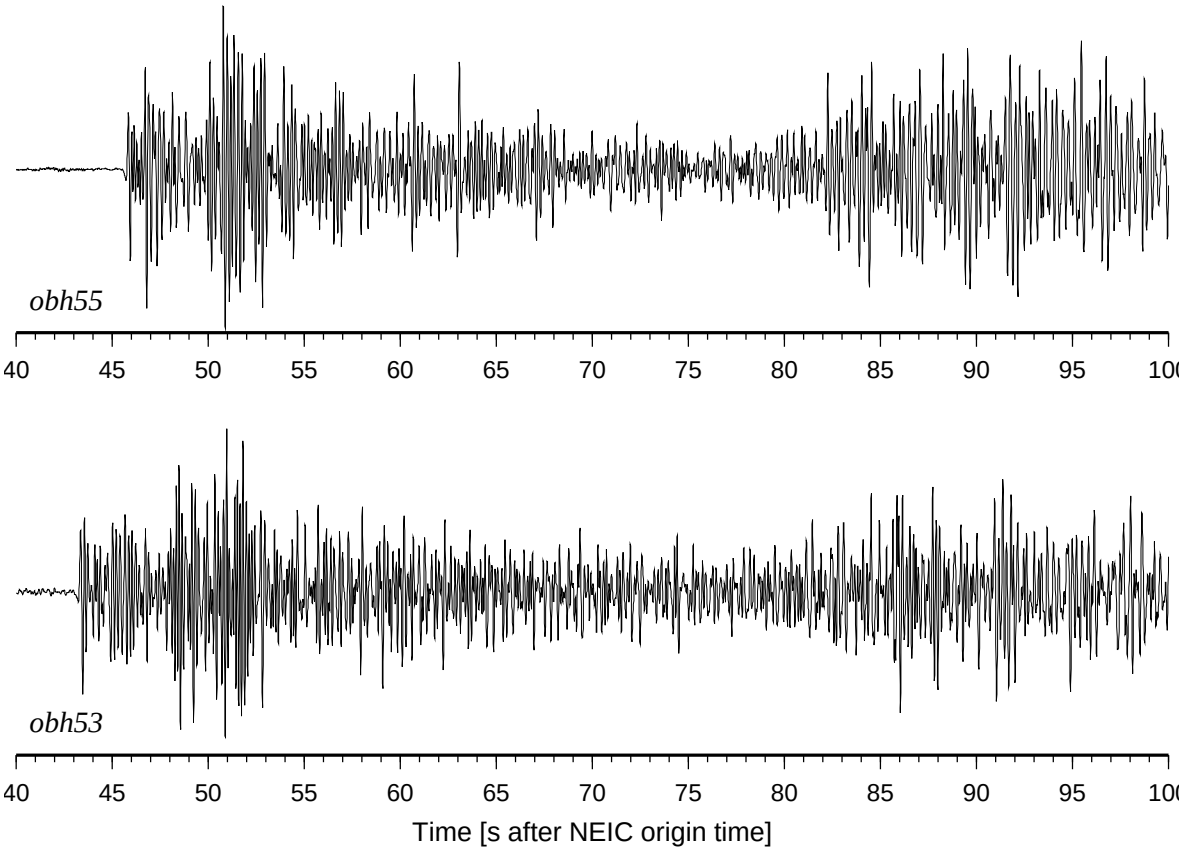

Figure 6.4.4: Waveforms from two events off El Salvador recorded on OBH53 and OBH55.

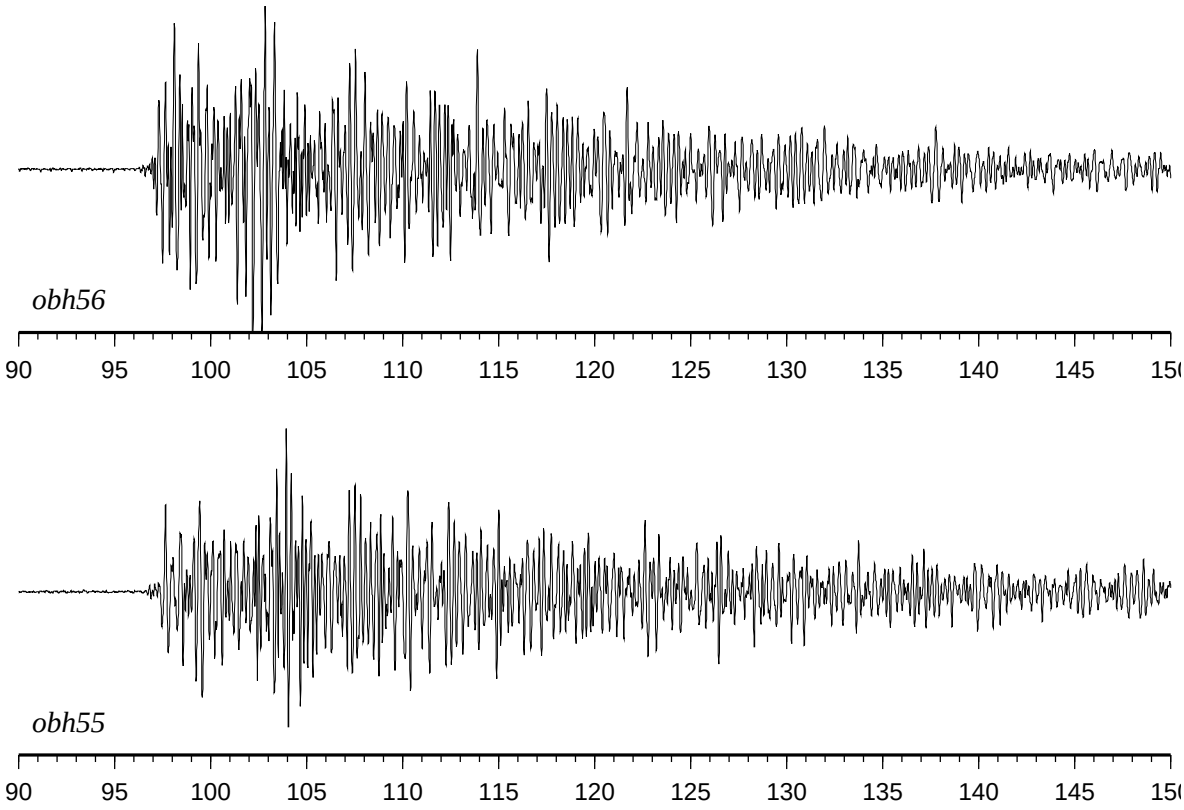

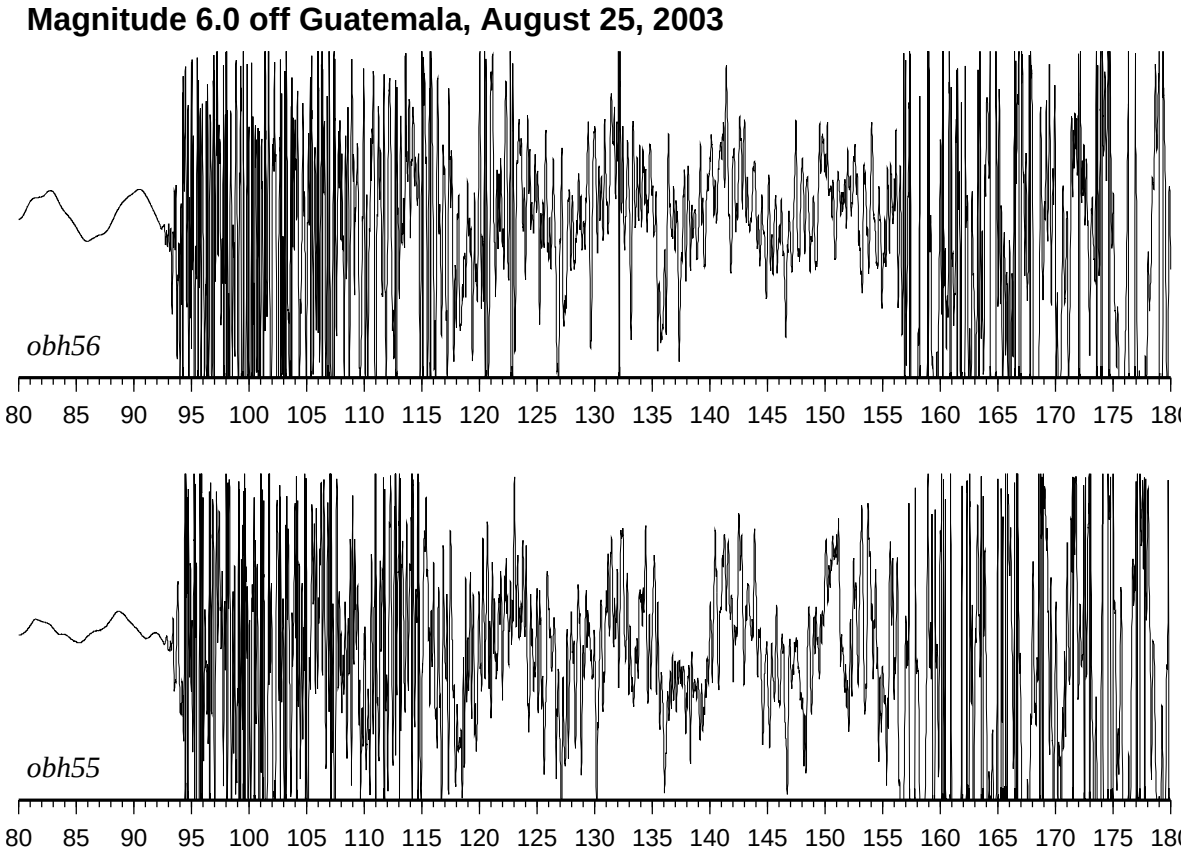

Figure 6.4.5: Waveforms from two events off Guatemala recorded on OBH55 and OBH56. The m_b=4.6 event (top) is well recorded while the m_b=6.0 event (bottom) overloaded the recording system.

6.5 Deep sea fish trawls

6.5.1 Results of the trawls

A detailed list of all trawls including times, estimated depths, coordinates, and comments on the resultig catches is given in the Appendices (9.4)

6.5.1.1 Trawls in Guatemalan waters:

The yield of both nets produced only small catches both in terms of the absolute number of specimens and the number of species obtained. Apart from consistently high numbers of Cyclothone sp. three families of fish were regularly caught: myctophids, melamphaeids, and Bathylagids. In addition, some anglerfish, scopelarchids and deep sea eels, and, rarely a stomiid came up in the net. Most noticeable was the total absence of hatchetfish (*Sternoptyx, Hemigymnus*), gonostomids, *Chauliodus* (except for a single, tiny specimen), *Anoplogaster*, *Eurypharynx* and other species considered to have a circumglobal distribution.

The reasons for this finding are unclear. It may be of interest, however, to note two more episodical observations made in Guatemalan but not in Costa-Rican waters. The first concerns sightings of flying fish from the bow of the ship. .Again, these were quite rare in the former but frequent and abundant in the latter. This also applies to the encounter of fishing boats. Taken together, they may indicate that the fish fauna of the surface waters may also be less abundant in Guatemala. The second point that appears worth mentioning concerns frequent sightings of all kinds of plastic objects and other waste material of human origin far off the coast of Guatemala.

6.5.1.2 Trawls in Nicaraguan/Costa Rican waters

The very first and the three last trawls brought up a number of species in addition to the ones mentioned above: Among these were Malacosteus, a red light sensitive dragonfish, several stomiids, numerous hatchetfish (both Sternoptyx and Hemigymnus) and a wider variety of myctophids. Interestingly, Chauliodus and Gonostoma were also absent from these catches.

While it is always possible, that the “missing” species were present but did not get caught in the nets used, or were staying in those depths not targeted in the respective trawls, it is still unusual that even in waters of poor productivity species which are generally considered as typical circumglobal have not been found.

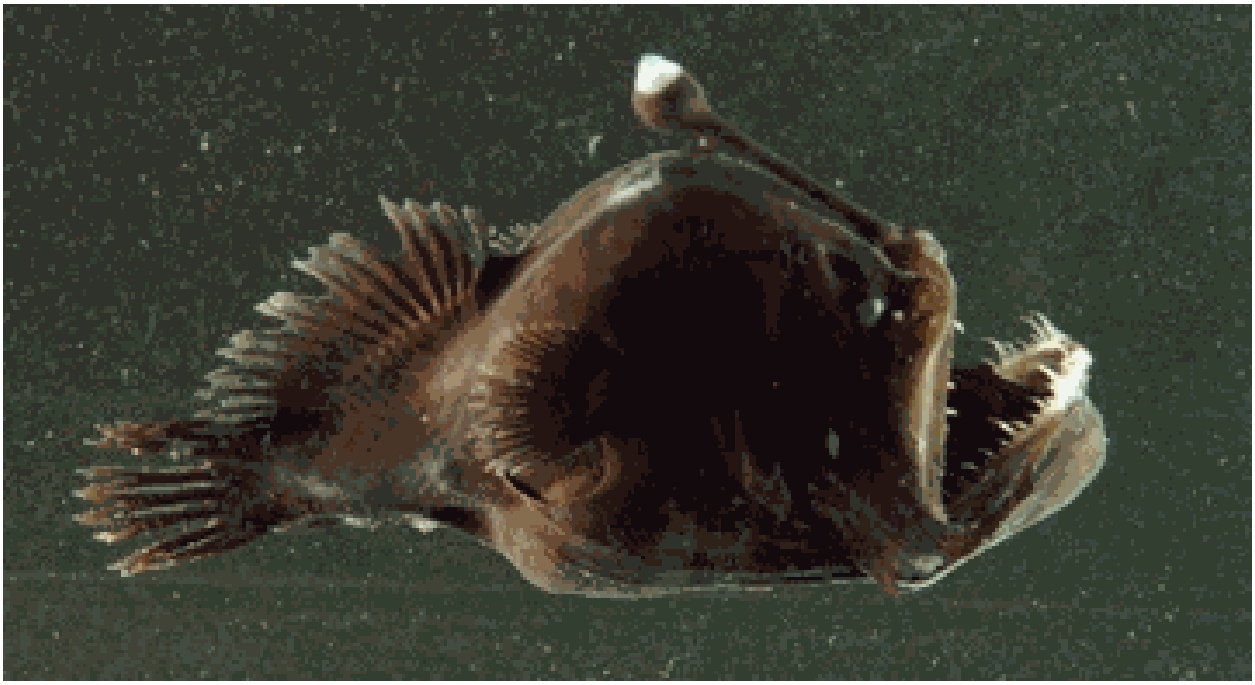

Figure 6.5.1.2.1: Melanocetes johnsonii (Photograph: T. Frank)

Figure 6.5.1.2.2: *Scopeloberyx opisthopterus* (Photograph: K. Jennings)

The biology group wishes to specially mention the expertise and helpfulness of the bosun, and thank Peter Mucke for supervising and handling the nets.

6.5.2 The visual systems of mesopelagic fish with special emphasis on the visual pigments of lanternfish (Myctophidae) and their role in the detection of bioluminescence.

(R.H. Douglas[1], J.C. Partridge, E.M. White[2])

Results

We collected a total of 107 teleost fish representing 26 species, as well as eight individual cephalopods. These were used for a variety of purposes.

Visual pigment spectroscopy

The primary aim of this cruise was to examine the retinae of myctophid fish for the presence of either red shifted visual pigments, or signs of chlorophyll-derived photosensitizers that might allow the detection of longwave bioluminescence. In particular we were hoping to catch specimens of *Bolinichthys longipes*. Unfortunately, no individuals of this species were caught, neither did any of the other myctophids contain signs of enhanced longwave sensitivity. Nonetheless, material was gathered from 71 individuals representing 23 species for visual pigment spectroscopy. The scotopic pigments of 31 individuals from 21 species were examined by partial bleaching of extracts on board ship. 17 of these had never had their visual pigments examined before. Where possible at least two individuals from each species were examined. Specimens not measured on board ship will be transported to the UK on dry ice and subjected to further analysis to verify the results obtained at sea. Representative spectra of single and two pigment species are shown in Figs 1 and 2 respectively, and the l_{max} values for all pigments are given in Table 1.

Table 6.5.2.1: Summary of all visual pigments examined during *FS Sonne* cruise 173/2

species	n caught	n examined	ave λ_{max}	published λ_{max}
Mesopelagic (19)				
Bathophilus vaillanti	1	1	487.4	
Bathylagus longirostris	2	1	478.6, 496.9	474, 502
Bathytroctes apus	1	1	475.9	
Benthosema panamense	4	2	489.6	
Benthosema suborbitale	3	2	488.7	487
Diaphus pacificus	9	3	487.0	
Diogenichthys laternatus	2	1	487.9	
Diretmidae (species unknown)	1	1	497.0, 517.5	(500, 484)
Lampanyctus idostigma	10	2	485.3	
Lampanyctus omostigma	2	1	485.9	
Lampanyctus parvicauda	15	3	485.1	
Lampanyctus ritteri	1	1	485.1	491
Melanocetus johnsoni	2	1	482.4	
Melanphais suborbitalis	1	1	482.3	
Myctophum aurolaternatum	1	1	484.5,495.0	
Scopeloberyx robustus	1	1	484.3	
Vincinguerria nimbaria	**3**	**2**	**477.4**	**477**
Unknown species 1	3	2	482.0	
Unknown species 2	1	1	?	
Epipelagic (4)				
Muglidae (species unknown)	3	1	485.5	
Scomber sp. (juvenile)	1	1	490.7	
Psenes sp (juvenile)	1	1	482.4 (488.3)	
Callionymus sp. (juvenile)	3	0	?	
TOTAL (19)	**71**	**31**		

[1]Dept. Optometry & Visual Science, City University, Northampton Sq, London EC1V 7DD, UK
[2]School of Biological Sciences, University of Bristol, Woodland Rd, Bristol BS8 1UG, UK

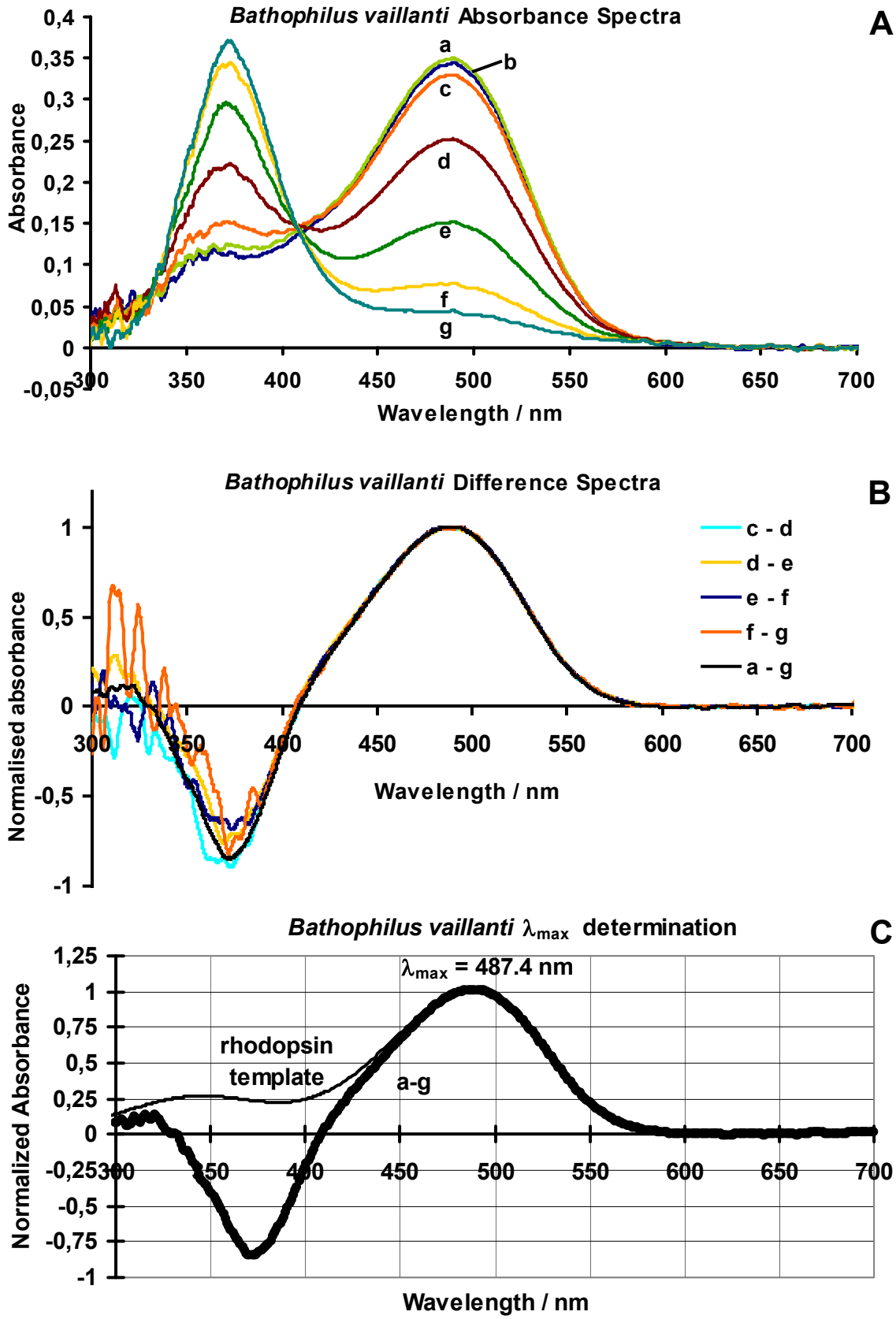

Figure 6.5.2.1: A) Absorbance spectra of a retinal visual pigment extract from Bathophilus vaillanti *following bleaches of decreasing wavelengths. B) Difference spectra constructed using the curves shown in A. As there is no shift in the l_{max} of sucessive difference spectra, the retina contains only a single visual pigment that is described by fitting a rhodopsin template to the overall difference spectrum (C).*

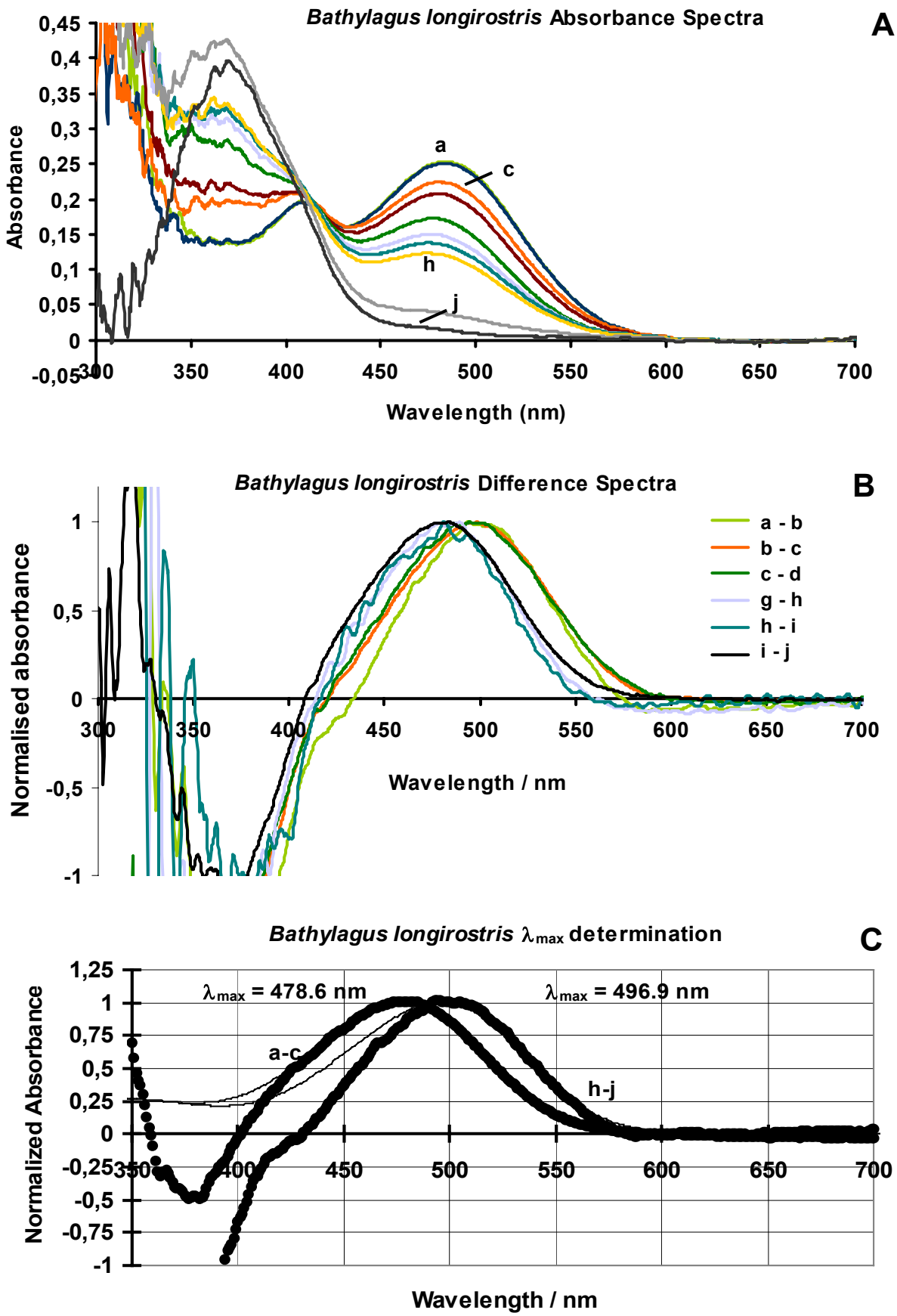

Figure 6.5.2.2: *A) Absorbance spectra of a retinal visual pigment extract from* Bathylagus longirostris *following bleaches of decreasing wavelengths. B) Difference spectra constructed using the curves shown in A. As there is a consistent shift in the l_{max} of sucessive difference spectra, the retina contains multiple visual pigments that are described by fitting 2 rhodopsin templates to the difference spectra indicted (C).*

Although the data await further detailed analysis, several things appear immediately noteworthy:

1. The two relatively longwave shifted pigments of an unidentified Diretmidae. Although *Diretmus argenteus* has previously been shown to posses two visual pigments by wholemount spectroscopy (Denton & Locket, 1989), these are at considerably shorter wavelengths (l_{max} 480, 500nm)

2. The retinae of four female and four male *Diaphus pacificus* were grouped and extracted separately. Both sexes were shown to contain identical visual pigments despite sexually dimorphic light organs

3. Surprisingly, the scotopic visual pigments of the three epipelagic species examined had visual pigments similar to those of most deep-sea fish, suggesting that the perhaps visual pigments of all oceanic teleosts are similar and are an adaptation to a 'blue water' environment.

   One of these shallow water fish belongs to a family, the Muglidae, that are considered coastal animals that only enter the open ocean to spawn. It is possible that this species changes its visual pigments in different stages of its life:

Effect of pressure on visual pigment absorption
Retinal extracts from 21 species were frozen and will be transported to the UK and some of these will be subjected to spectrophotometry under pressure to determine any effect of pressure on absorption.

Photophores of Malacosteus niger
The sub- and post-orbital photophores of a single *Malacosteus niger*, the first animal caught on the cruise, were preserved in 'RNAlater', for the molecular identification of their bioluminescent proteins by Professor P.J. Herring. Liver and muscle tissue was similarly preserved

Molecular biology and in situ hybridisation of animals with multiple visual pigments
Tissue samples from six *Scopelarchus analis* and one *Bathylagus longirostris* were preserved as described in the methods for for molecular biological study of visual pigments and *in situ* hybridization to locate visual pigments in the retinae.

Myctophid body reflectance
One of the ultimate aims of research on the visual system of animals is to describe what they see. However, this not only requires information about their visual pigments, and, in the case of deep-sea fish, bioluminescent emission spectra, it also needs details of the spectral reflectance of animals within the deep-sea. To this end we generated reflectance spectra from various body parts of a variety of myctophid fish. These will be used in future modelling of mesopelagic fish visual performance (Fig. 6.5.2.3).

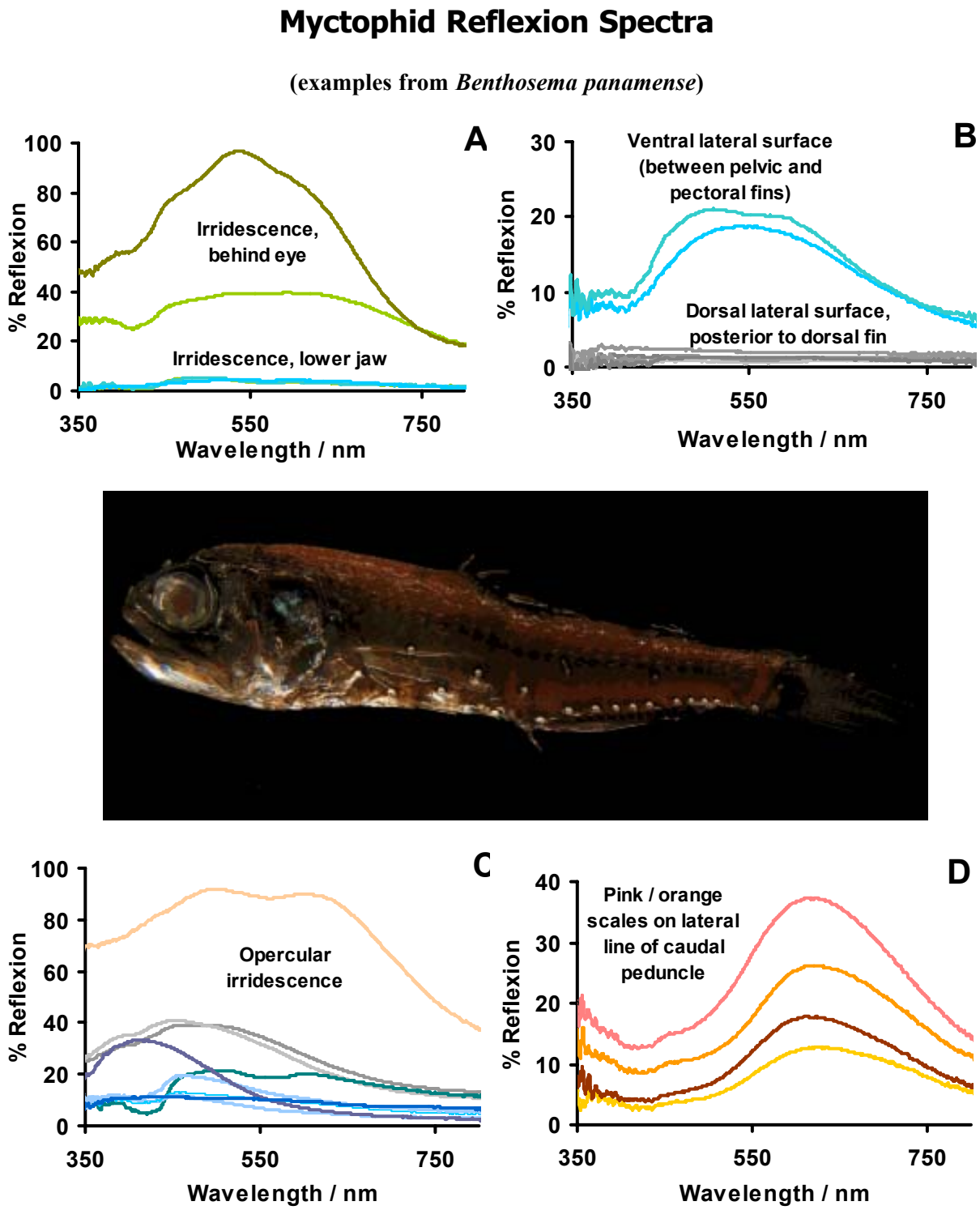

Figure 6.5.2.3: *Reflexion spectra from various parts of the body of Benthosema panamense.*

The pupil response of cephalopods

Five live cephalopods were dark adapted in a cold room and their eyes were filmed in darkness under infrared illumination. The pupil was seen to be oval. On illumination the pupil constricted to a thin strip with a small pinhole at either end. This process took about 10 seconds and the kinetics of pupil closure will be analysed in greater detail in the UK. To our knowledge this is the first time the pupils of mesopelagic squid have been examined. The response is very much slower than in coastal cephalopods (e.g. *Sepia officinalis*), but does indicate that these animals are occasionally exposed to significant illumination and can adapt to different light levels. Interestingly, sometimes, just as in shallower water species, the pupil constricted even in the absence of light, perhaps indicative of 'emotional' influences.

Cephalopod visual pigments

The visual pigments from the retinae of five cephalopods were either extracted or simply immersed in PIPES saline and frozen for later detailed analysis in the UK. One sample was analysed on board, which suggested a rhodopsin with l_{max} around 450nm and a metarhodopsin with peak absorbance at 550nm. However, experiments on board ship were hampered by the unavailability of a light source with sufficiently high radiance to completely bleach the cephalopod visual pigments.

Teleost iris morphology

Seven *Vincinguerria nimbaria*, one *Benthosema panamense*, two *Psenes sp.,* five *Lampanyctos omostigma* and eight *Callionymus sp.* were fixed in 5% gluteraldehyde for later light microscopy of their irises. These will form part of an ongoing investigation into the comparative morphology of teleost irises. To the best of our knowledge there are no descriptions of the irideal structure of oceanic teleosts.

6.5.3 Electrophysiological recordings from fish and crustacean eyes

(T. Frank, HBOI, USA)

15 preparations were attempted with various species of fish – 2 species of Melamphaeid, *Bathylagus* sp., a surface fish of unknown identification, and several species of myctophid. Unfortunately, the largest response we were able to record from a fish was 30 uV, as shown in Fig. 6.5.3.1 A. This was considerably smaller than the >1 mV response that should be possible in this type of recording.

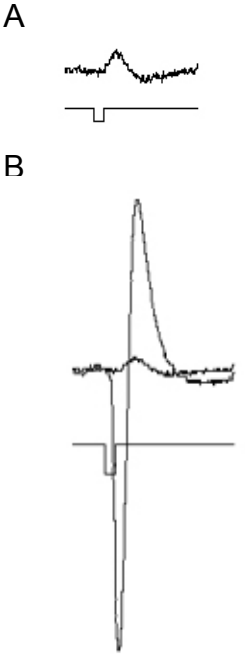

Figure 6.5.3.1: ERGs recorded from fish and stomatopod photoreceptors. A) 30 uV was the largest response from a fish. Upper trace is ERG; lower trace is light stimulus. B) ERG of a stomatopod superimposed over the fish ERG, demonstrating the half maximal response is routinely recorded in crustaceans using the identical electrodes used to recorded the response in A.

A significantly larger response was recorded from a stomatopod crustaceans, with considerably smaller eyes, using the identical electrodes, 15 minutes later. Due to the demonstrated viability of the recording technique in crustaceans, we can only surmise that somehow, the signal was being grounded out in the fish preparations. In at least 5 of the preparation, the fish was clearly alive after we gave up, indicating that the condition of the fish was not responsible for the lack of success.

Knowing that fish preparations would be difficult, I also brought out the chambers to continue my work on crustaceans. Unfortunately, we encountered a distinct lack of crustaceans once we left Costa Rica waters, which was on the second day of the cruise. The only large crustaceans that were seen consistently were *Acanthephyra (Fig.6.5.3.2)*, which I have already worked on, and several species of *Sergia,* which I have also already worked on.

Figure 6.5.3.2: Acanthephyra sp

However, we did get several specimens of a small stomatopod (Fig. 6.5.3.3), which was quite unusual, as stomatopods are generally considered benthic animals, so this may have been a pelagic juvenile stage.

Figure 6.5.3.3: Stomatopod

Using the identical electrodes, which failed so miserably with the fish preparations, I obtained data from 4 stomatopods. As their sensitivity is quite low, it was difficult to do chromatic adaptation with sufficient intensity to see a distinct shift in spectral sensitivity, but these preliminary data indicate that such a shift does occur. The spectral sensitivity was recorded in three specimens, and a mean peak of 510 nm was obtained. Figure 6.5.3.4.4 shows the results of a chromatic adaptation on an individual using an orange bandpass filter.

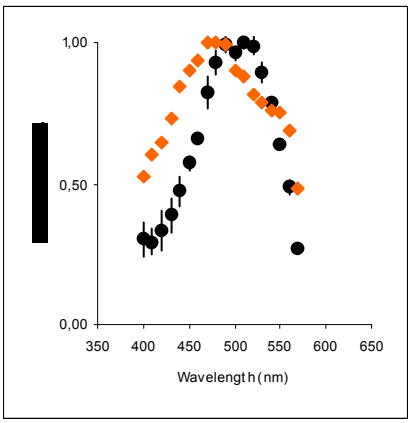

Figure 6.5.3.4: Spectral sensitivity of stomatopod crustacean. Black circles represent the mean-dark adapted spectral sensitivity of three individuals, with a peak at 510 nm. The error bars represent standard errors. The orange triangles represent the spectral in one individual after chromatic adaptation with an orange light.

As can been seen from the figure, there is a shift in spectral sensitivity to higher sensitivity at the shorter wavelengths. Similarly, chromatic adaptation on an individual using a blue bandpass filter shifted sensitivity slightly towards longer wavelengths (Figure 6.5.3.5).

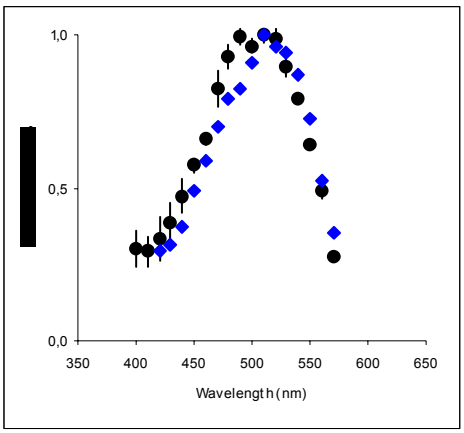

Figure 6.5.3.5: Spectral sensitivity of stomatopod crustacean. Black circles represent the mean-dark adapted spectral sensitivity of three individuals, with a peak at 510 nm. The error bars represent standard errors. The blue triangles represent the spectral sensitivity in one individual after chromatic adaptation with a blue light.

Maximum critical flicker fusion frequency (CFF)

Flicker fusion frequency was dependent on both temperature and state of light adaptation. As these specimens were captured with a trawl net fishing primarily at deep depths, the initial experiments were conducted at 6° C, the temperature at the primary fishing depth of the trawl net. However, observations on the increase in activity in individuals left in the trawl bucket and gradually allowed to come to room temperature indicated that these specimens may have been trapped in warmer surface water as the open trawl net came to the surface. The CFF of a specimen tested at 6° C was 16 Hz, while the CFF of the same individual at 16° C was 24 Hz. The average CFF of the dark-adapted eyes of three individuals tested at 16° C was 24 Hz (±1.0), while the average CFF of the same three individuals under chromatic adapting lights was 35 Hz (± 2.0 Hz). This increase in CFF under chromatic adaptation, in addition to the lack of sensitivity, suggests that these species are shallow water inhabitants.

6.5.4 Antioxidative defence mechanisms and bioluminescence in deep sea fish

(Cécile Marchand and Fabienne Paasch[1])

(1) Antioxidative defences of cells from fishes thriving at increasing depth

Three methodological problems were encountered:
Firstly there were some problems with the EDTA. On the one hand too little EDTA did not prevent the coagulation, and on the other hand too much EDTA (or not enough blood) caused haemolysis. In fact, the EDTA changed the osmolarity of the solution.
Secondly, the blood was often impure, being mixed with tissue solutions or mucus.
Thirdly, the amount of blood collected was sometimes too low (about 100µl) to measure the osmolarity (we need 150µl of plasma) necessitating the use by a standard RBC buffer of 385mOsm/kg. If this osmolarity was incorrect for the species concerned sometimes the red blood cells haemolysed after adding the buffer.

PLASMA: Total antioxidative capacity.

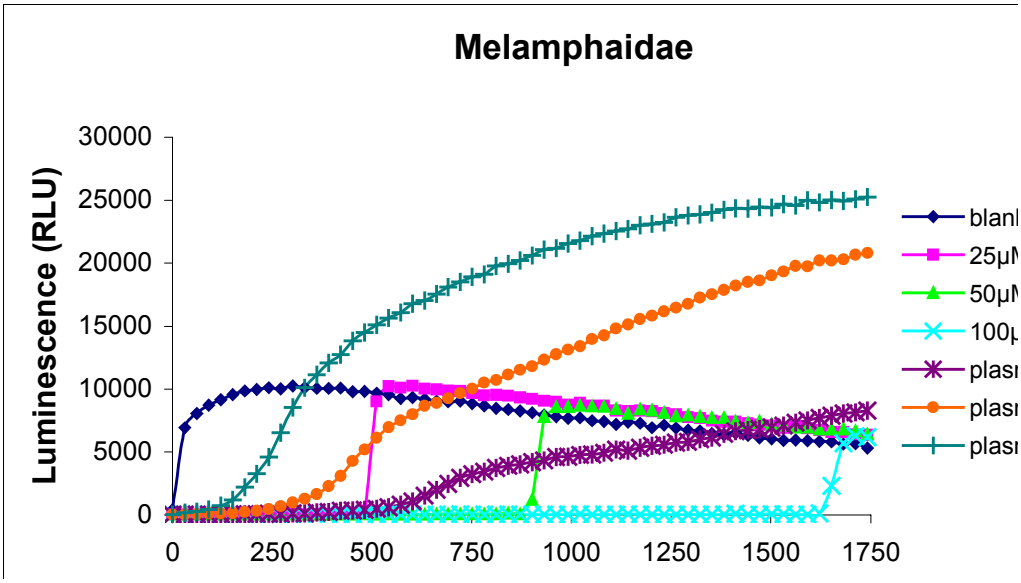

In this experiment the antioxidative capability of fish plasma was compared with that of standard antioxidant, trolox, at concentrations from 25 to 100µM.
Plasma was diluted 2 to 8 times to avoid the influence of the plasma pH on the measurements. Results were compared with those obtained with buffer solution alone (blank, above).

From this first graph the relationship between trolox concentration and the time of luminescence onset was calculated. Previously work was shown that this is a linear relationship.

[1]Life science Institute
Laboratoire de Biologie cellulaire
Université Catholique de Louvain

The concentration of antioxidant in this plasma is expressed in trolox equivalent: in the above case approximately 61µM.

Another observation was that the slopes of the curves of the standard antioxidant and of the plasma antioxidant are different. This could be explained by the presence of a lot of different antioxidants which were consumed sequentially.

The quantity of antioxidants of the plasma of other species (*Nemichthys scolopaceus*, *Scopelengys tristis*) was measured.

(2) Protection conferred by coelenterazine to cells from deep sea fishes

Unfortunately we were not always able to collect enough blood to do this experiment. Nevertheless, blood from *Melamphaes longivelis* was analysed.

A. Coelenterazine concentration in the plasma:

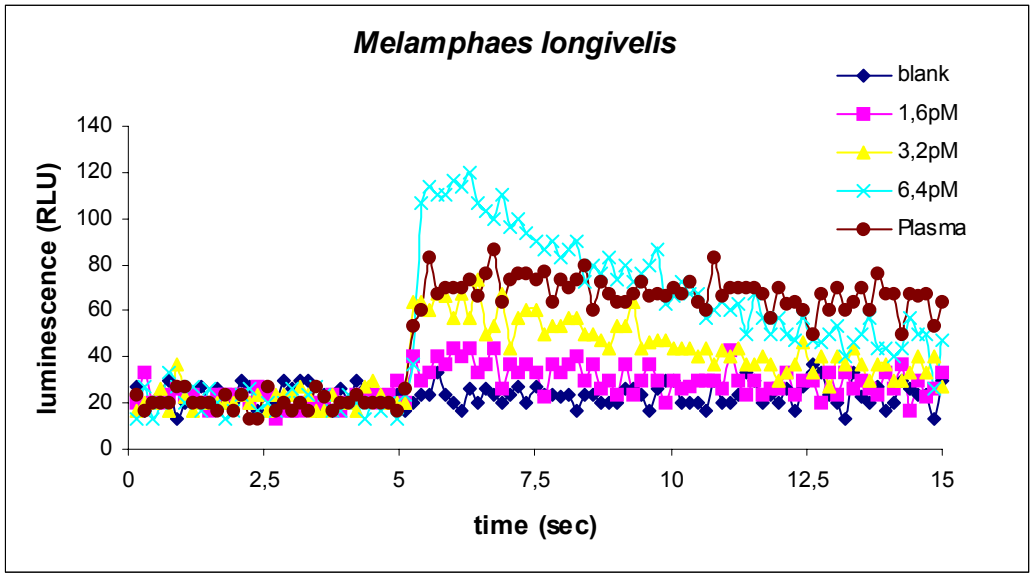

In this experiment the antioxidative properties of plasma were compared with that of the standard antioxidant, coelenterazine (1,6pM to 6,4pM). The plasma was not diluted. The blank is only buffer solution.

From this first graph the relationship between coelenterazine concentration and the time to peak luminescence was calculated.

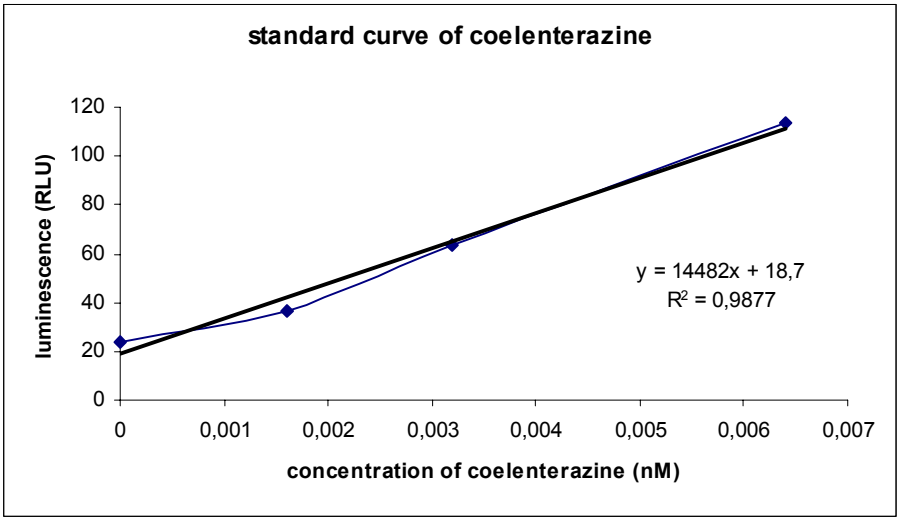

In the plasma there was 4,5pM of coelenterazine.

B. Coelenterazine concentration in the red blood cells:

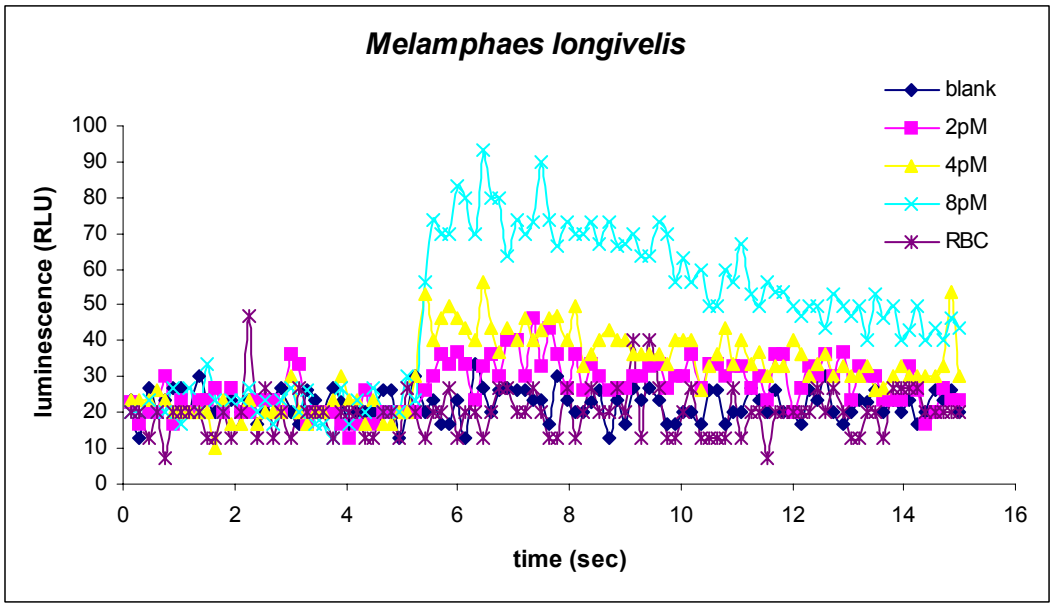

In this experiment the antioxidative properties of red blood cells were compared with that of the standard antioxidant, coelenterazine (0,2pM to 0,8pM). The plasma was not diluted. The blank is only buffer solution.

From this first graph the relationship between coelenterazine concentration and the time to peak luminescence was calculated.

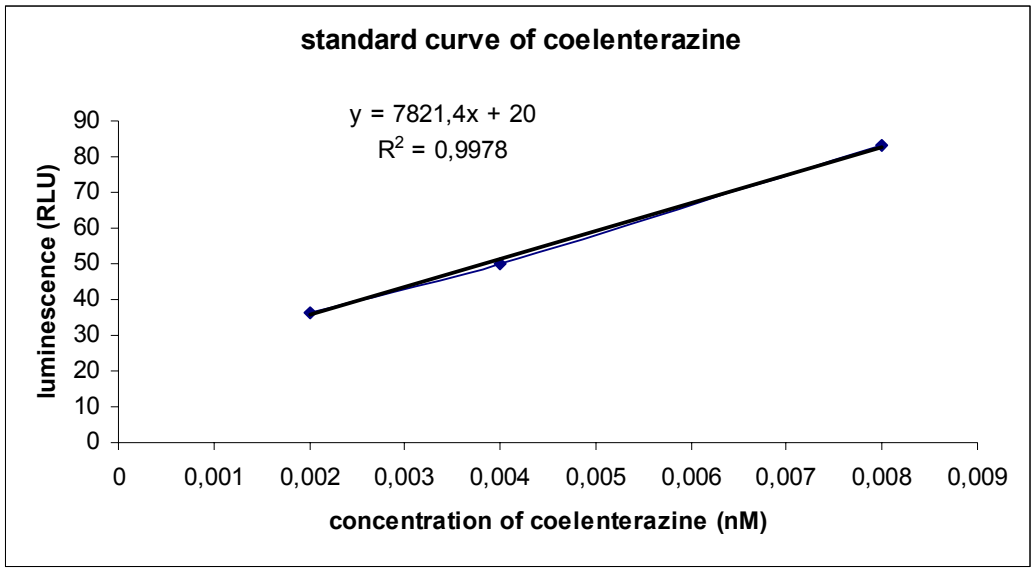

As the graph already indicates there is no coelenterazine detected in this sample.

To determine whether coelenterazine has any physiological role in the antioxidative defence mechanism, we carried out the same experiments as in the first part of the report with different concentrations of this antioxidant.

C. PLASMA: Total antioxidative capacity.

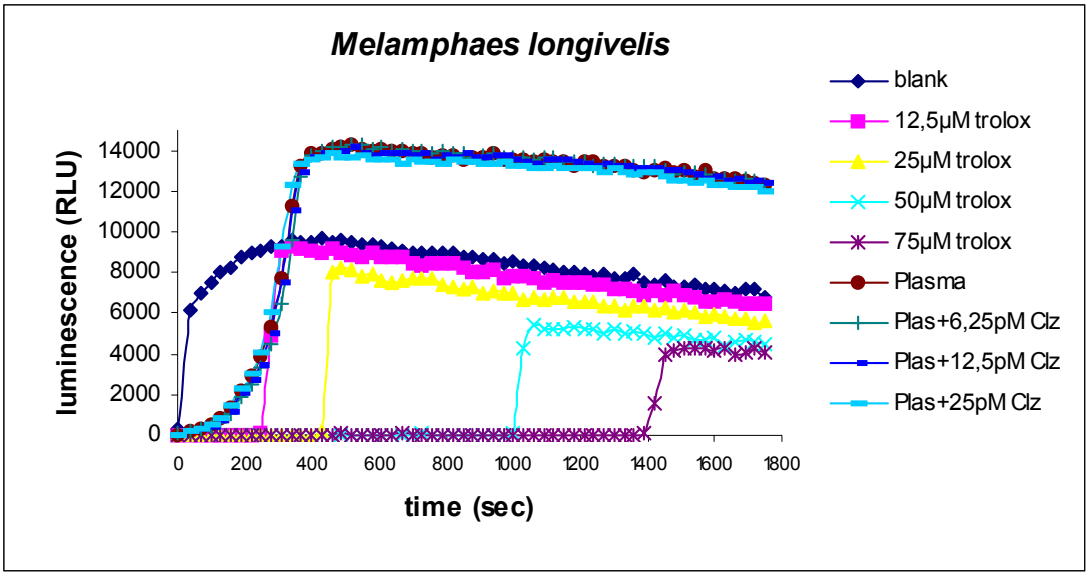

From this first graph the relationship between trolox concentration and the time of luminescence onset was calculated.
The concentration of antioxidant in this plasma is expressed in trolox equivalent: in the above case approximately 24µM.
By adding coelenterazine to the plasma the curve did not change, there seems to be no effect of coelenterazine to antioxidative mechanism. However, the sensitivity of this method is relatively low, therefore this conclusion should be considered only tentatively.

D. RED BLOOD CELLS: Susceptibility to oxidative stress.
As we there is no coelenterazine in the red blood cells and the volume of RBC is limited, the resistance of the cells to T-BHP was measured without adding coelenterazine.

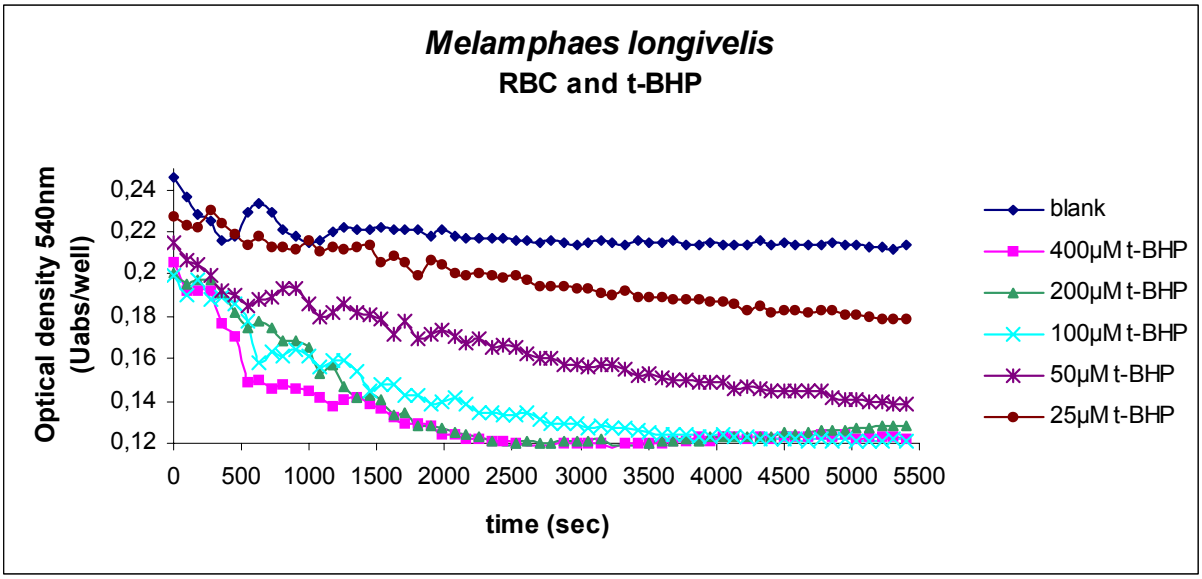

Most of the trawls during the cruise were very poor in fish species. However, the last trawls south near Costa Rica were successful and we replicated a lot of experiments. The analyses of the data has not yet finished.

(3) Deep sea fish cell line culture

Several problems were encountered with this protocol.

Firstly, even in the wells with collagen the cells hardly attached to the substrate and after one day we changed the medium and the cells detached, prematurely ending the experiment.

We therefore prolonged the time before changing the medium, the cells had a much better shape at 4°C then at 16°C, but even at 4 °C they detached easily after 3 days.

Secondly, we could not do cell culture in suspension because we have not the sterile conditions necessary to prevent contamination.

In consequence, we started a new culture at the end of the cruise to transport it directly to our laboratory in Belgium to continue the culture under sterile conditions.

6.5.5 Melatonin as a mediator of biological rhythms in mesopelagic fish

(H.-J. Wagner, Anatomisches Institut, Universität Tübingen)

For the evaluation of the role of melatonin two types of experiments were performed.
Firstly, the content of melatonin of pineal glands and isolated retinae has to be determined, and value from the scotophase compared to those of the photophase.
In the migratory species *Bathylagus longirostris*, 32 pineals were collected during day-time trawls and 18 during catches at night. In the non-migratory *Scoplobeyx robustus*, 24 pineals were isolated during night trawls, 25 pineals glands were taken from day catches. In addition, 10 day-time retinae and 10 night-time retinae werd frozen and stored in *B. longirostris*, as well as 22 scotophase retinae and 12 photophase retinae in *S. robustus*. These tissues were quick frozen, stored, and will be assayed for melatonin content in Tübingen.
Secondly, the release of melatonin of *Bathylagus longirostris* under constant dark conditions was tested. For this pupose, 10 pinelas were isolated under dim red light, pooled and put into organ culture. The culture medium (900µl) was changed every 4 h during a 56h period and will be tested for the amount of melatonin relased. This type of experiment could be be done twice. As a control, 10 isolated retinae were also cultured and the culture medium containing the melatonin liberated collected.f

The results of these measurements will be compared to similar work performed on two species of deep demersal fish (*Coryphaenoideus armatus* and *Synaphobranchus kaupi*).

6.5.6 Comparative Studies of Inner Ear Morphology and Ultrastructure in Mesopelagic Deep-Sea Fishes

(Xiaohong Deng[1], H-J Wagner[2], Arthur N. Popper[1])

Results

We have collected 66 speciemens for inner ear study during this cruise. Most of the speciemens are from the family Melamphaidae, in which we have four species from the genus *Melamphaes*, two species from the genus *Poromitra* and three species from the genus *Scopeloberyx*. Some of the identification is only in tentatively; the complete identification will be done on land. We had two reasons for focusing on these species for our inner ear study. One was because there fishes are most common catch in the trawls, the supply of different species and even different genera were abundant, which provides us comparisons between species and genera. The second reason was that, during dissections of different fishes on board, we have found very intriguing inner ear saccular otoliths in this family, and there are significant diversities thought out the family. The saccule structures in some species also indicate that they may have very good hearing ability. This fish family are also interesting for their very elaborate lateral line organs, intensive studies of the lateral line system are also carried on by another team of scientists on this cruise. All these features make us believe that study of this mesopelagic deep-sea fish family very valuable.

Six speciemens of one species are from the family Macrouridae in genus *Nezumia.* It added a very good mesopelagic member into our on going comparative studies of benthopelagic macrourids fishes, which broadened the ecological coverage of this study.

Most of the specimens were EM fixed in cold 4% paraformaldehyde and 2% gluteraldehyde in 0.1 M cacodylate buffer with 0.05% $CaCl_2$ and 0.1 M sucrose.
Investigations of the morphology and ultrastruture of the inner ears will be done in Aquatic Acoustic Popper Lab in the University of Maryland with light microscopy and scanning electromicroscopy.

Six specimens from two species of *Melamphaes* and two species of *Scopeloberyx* were also fixed in 4% formaldehyde in PBS. The fishes were dissected after 24 hours to expose the ramus saccularis of one side of the eighth nerve. Tracers were put on the transverse section of the nerves to reveal the projection of the saccule and/or lagena.

Figure 6.5.6.1 shows the comparison of the saccular otoliths from five species of the family Melamphaes, which is the first result we obtained thought dissections of fresh, non-fixed specimens on board. Such step is essential and valuable for the studies of these fishes, this is because deep-sea fish samples are hard to get so they are usually preserved in fixatives or buffers for a long time before researches working on them. Although the soft structure of the ears can be preserved reasonably well, part of the otoliths may dissolve in the chemical solution, which makes interpretation of the function of the otolith difficult.

All species studied have a very large saccular otolith, a small utriclar otolith and a tiny lagenar otolith. This is opposing to what N. B. Marshall had described in the 1970s. After compared inner ears of fishes from different depths, he found that mesopelagic and bathypelagic fishes have large utricles and small saccules, whereas most benthopelagic fishes (macrourids, deep-sea cods, and brotulids) tend to have very large saccules and saccular otoliths (Marshall 1979).

The most interesting finding is the long, thin stalk protruding ventral-posterior from the saccular otoliths of the *Melamphase* and *Poromitra.* This is extremely obvious in *Melamphaes suborbitalis* and *Poromitra sp*. In *Melamphaes suborbitalis,* the stalk touches on the ventral wall of the skull, which is the bottom of the bony labyrinth. Instead of the usual rigid bony wall that is found in most fishes, the *Melamphaes suborbitalis*'s bottom part of the bony labyrinth is soft and elastics. This kind of contact has never been described by any researchers. The stalk may give some kind of support to the large otolith or provide a connection between the otolith and some other structures out side of the ear chamber. The detail of this structure and its relation with the sensory epithelium is yet to be explore by further light and electronmicroscopy investigations,

however, it may provide a door way to solve a long existing puzzle: What is the functional significance of the size and shape of the various otoliths? on the function of the sculpture. While some researchers believe that the shape of otolith may affect its pattern of movement, some researcher speculate that certain degree of variation in otolith structure may not have any functional significance at all. Here we have a collection of saccular otoliths that have such extreme asymmetry structure and such prominent variations within the same family, a functional significance of the long otolithic stalk can not be denied and will be intensively studied!

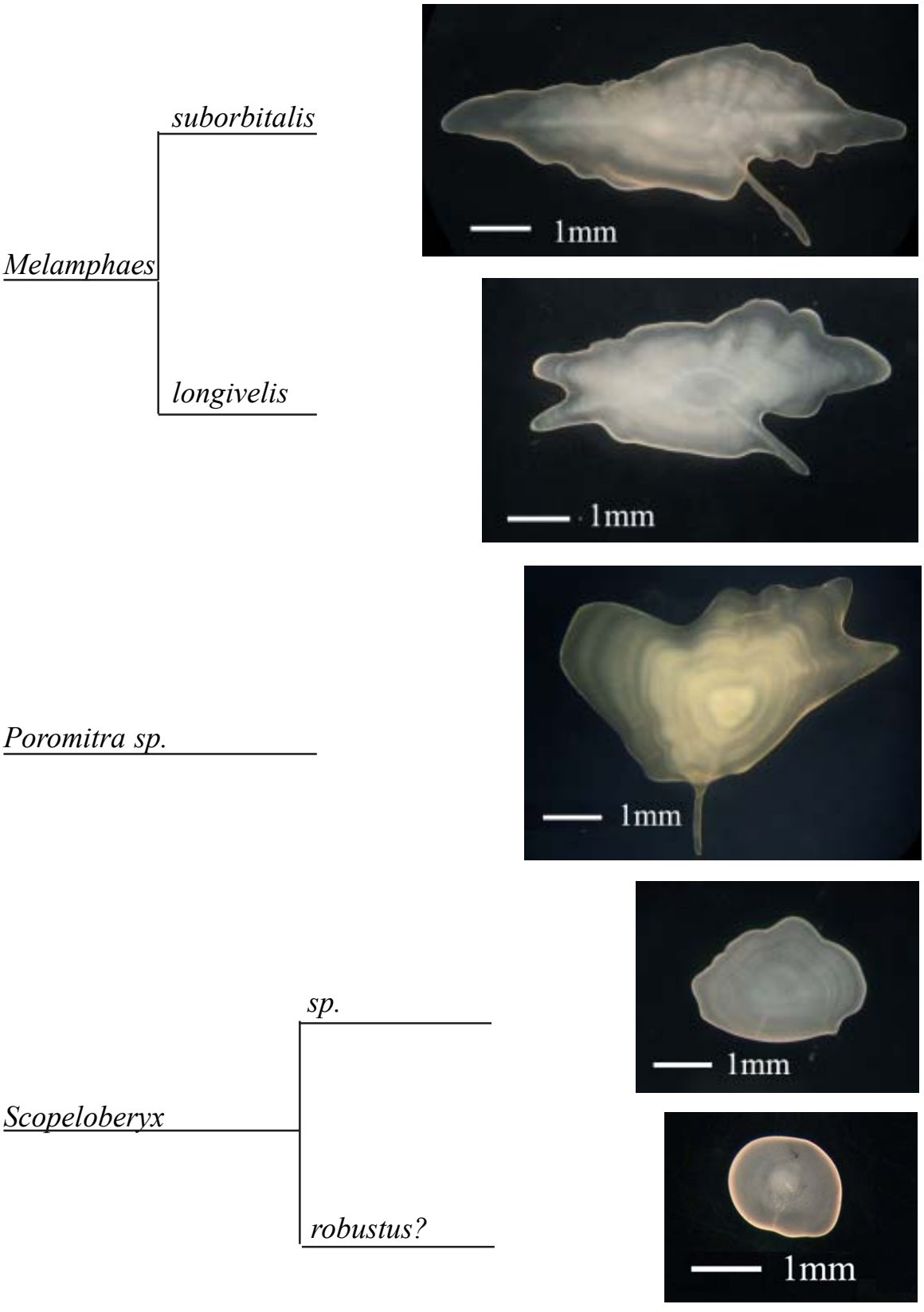

Figure 6.5.6.1: Saccule Otolith from five species of the family Melamphaidae

References

Deng, X., Wagner, H-J, Popper, A.N. (2003) *Ears of macrourid deep-sea fishes*. First International Conference on Acoustic Communication by Animals, July 27-30, 2003. College Park, Maryland. pp. 63-64

Marshall, N. B. (1971) *Explorations in the life of fishes.* Harvard University Press. Cambridge, MA.

Marshall, N. B. (1979) *Deep-sea biology Developments and perspectives.* Garland STPM Press, New York and London.

Marshall, N. B. (1966) Sound-producing mechanisms and the biology of deep-sea fishes. In *Marine Bio-acoustics, volume 2.* pp. 123-133, (William N. Tovolga eds), Pergamon Press, Oxford

Munk, O. (1964) Ocular degeneration in deep-sea fishes. *Galathea Rep*. 8:21. (From Marshal 1971)
Popper A. N. (1980) Scanning electron microscopic study of the sacculus and lagena in several deep-sea fishes. Am. J. Anat., 157:115-136.

[1]Dept. of Biology, University of Maryland, College Park, MD 20742, USA
[2]Anatomisches Institut, Universität Tübingen, Tübingen, D-72074 Germany

6.5.7 Study of the world's most frequently used sensory system: lateral lines in the deep sea

(Kylie Jennings & Justin Marshall[1])

Findings

Table one is a complete list of all specimens collected during the cruise (see Appendix). Sixty-two specimens spanning 15 species across 10 families were collected on Sonne. This is a diverse array of species ranging from eels to rat-tails, big scales to anglerfish. All variations and combinations of neuromast types have been found across these species.

[1]The University of Queensland, Australia
K.Jennings@uq.edu.au

Scopeloberyx opisthopterus

— Stitch

• Papillate FS organs

Canal organs

a)

Stitches

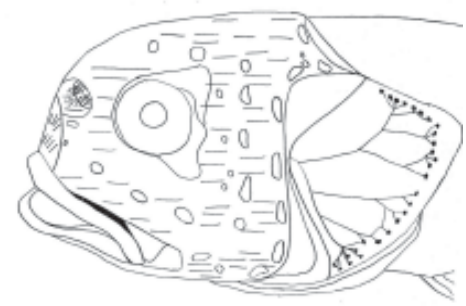

b) Stitches in lateral view

c) Stitches in ventral view and dorsal view

Canal Organs

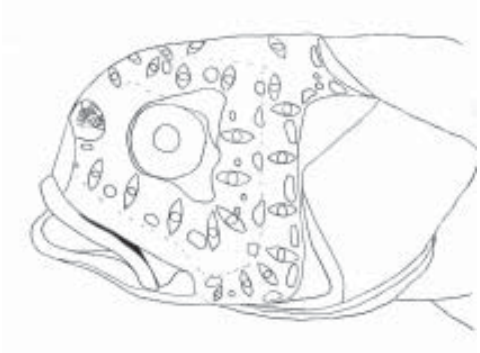

d) Canal organs in lateral view

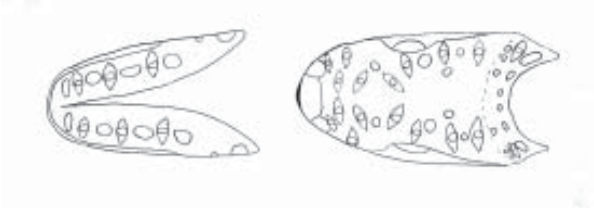

e) Canal organs in ventral view and dorsal view

Direction of sensitivity indicated along the axis of the arrows

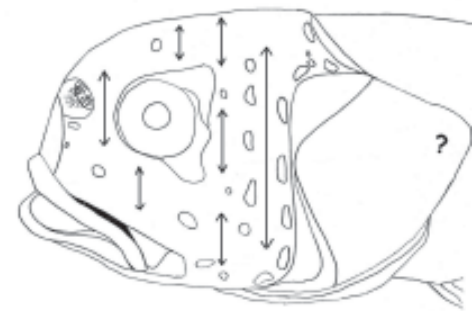

f) Direction of stitch sensitivity in lateral view

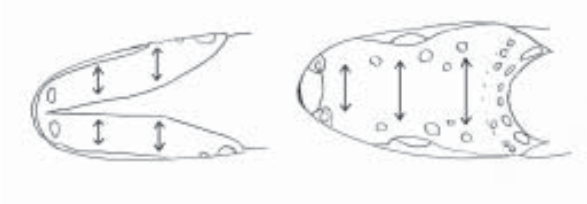

g) Direction of stitch sensitivity in ventral view and dorsal view

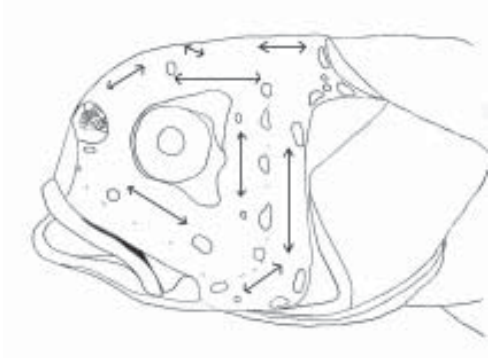

h) Direction of canal organ sensitivity in lateral view

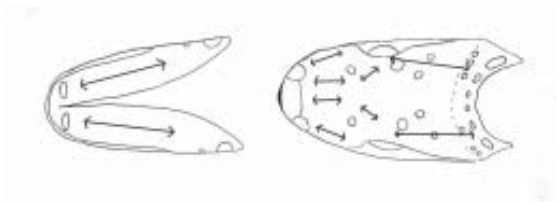

i) Direction of canal organs in ventral view and dorsal view

Figure 6.5.7.1:

Figure 6.5.7.1a is a photo of the head of *Scopeloberyx opisthopterus* . The transparent, delicate, jelly-like skin is intact due its gentle collection with a closing cod end net. The skin is covered with parallel lines running anterior-posterior along the head. These organs are free-standing neuromasts or stitches and contain thousands of hair cells. The underlying innervation of the stitches can clearly be seen over the whole head. Figure 6.5.2.1b&c are diagrammatic representation of the distribution of the stitches on the head of *S. opisthopterus*. The inferred direction of sensitivity of these organs based on previous work by Marshall is perpendicular to the axis of the stitch (see Fig. 6.5.7.1f&g). The orientation of the stitches gives the animal a dorso-ventral sensitivity over the whole head. Under the thick layer of epidermis is a network of large canals containing extremely large neuromasts or canal organs. Figure 6.5.7.1d&e are diagrammatic representation of this canal organ system. The direction of sensitivity of the diamond shaped canal organs based on previous work by Jennings and Marshall is perpendicular to the axis on the diamond. Therefore in figure two you can see that the dorsal and ventral portions of the head are sensitive in the anterior-posterior axis but behind the eye the sensitivity is perpendicular to that, running dorso-ventrally. Another type of neuromast was identified and mapped on this specimen. Twenty-seven papillate free standing organs were located lining the posterior margin of the operculum. The associated innervations were clearly visible radiating from the anterior region of the operculum. The orientation and direction of sensitivity cannot be induced from previous work and careful analysis of their ultrastructure is required to obtain this information. This is the first time that all three varieties of neuromasts have been located on the same species.

Melanocetes johnsonii

a)

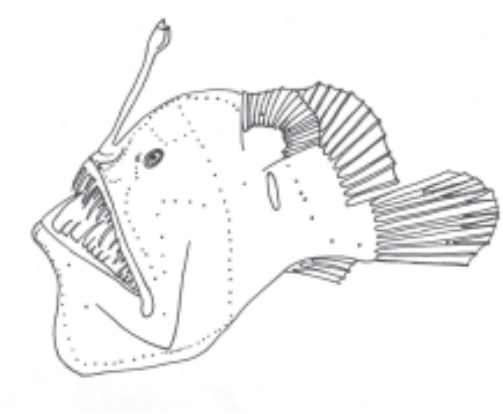

Drawing of papillate FS organs

b)

Photograph of live specimen

Figure 6.5.7.2:

The ‘studs’ over the surface of this anglerfish, *Melanocetes johnsonii*, (Fig. 6.5.7.2a&b) are papillate, FS lateral line organs. This fish was caught alive as a result of gentle capture techniques. This species has no canal system or stitches and these have been replaced with papillate FS organs situated where the canal organs are normally located.

Due to the low light levels in the deep sea, fish have evolved a well developed lateral line system. The neuromasts have developed 3 different varieties that appear to be structurally specialised for life in the deep sea. Canal organs are often enlarged and the number of hair cells increased to several thousand per organ in order to increase sensitivity and possibly to tune frequency response. Papillate FS organs have developed at the end of a long and are extended in the environment. This adaptation may be for enhanced detection of low frequencies. The large numbers of surface FS organs or stitches on the head also indicates enhanced vibrational detection. Little is known about the ultrastructure of these organs and after careful analysis under a scanning electron microscope, the answers to these questions may be discovered.

It is also worth asking why some species have elaborate both FS and canal systems and why other 'chose' one system or the other. All neuromast variations have been displayed in this species collection. The anglerfish and idiacathids have papillate FS organs only, the nemichthyids have both canal organs and stitches and the amazing melamphaids have all three variations including the canal organs, papillate FS organs and stitches. *Scopeloberyx opisthopterus* has papillate free standing neuromasts on the operculum only where it does not have canal organs or stitches. This is interesting because these different organs may have different functions and may detect different frequencies. The ultrastructural detail that will be obtained by SEM will provide more clues to the puzzle. It seems that the presence of all neuromast variations on the single animal indicates that these different types did not evolve separately. Further investigation at The University of Queensland, Australia, will give us more information of the morphology, development and function of the lateral lines of deep sea fishes. This information will be used to infer details of the lifestyles of these poorly understood animals.

A summary table of results is given in the Appendix section:

Marshall, N. J. (1986). Structure and general distribution of free neuromasts in the black goby, *Gobius niger*. *J. Mar. Biol. Ass. U.K.* 66**,** 323-333.

6.5.8 Retinal ganglion cells in mesopelagic fish

(H.-J. Wagner, Anatomisches Institut, Universität Tübingen)

Eyes of 5 different species of mesopelagic fish were labelled with rhodamine-coupled dextranes, fixed, croyprptected and frozen until microscopic evaluation in Tübingen.
(*Serrivomer, Poromitra, Scopelarchus, Idiacanthus, Bathylagus*)

6.5.9 Sensory brain areas in mesopelagic fish

(H.-J. Wagner, Anatomisches Institut, Universität Tübingen)

In view of the low diversity of species encountered in most of our trawls, we focussed on one family for continuing our comparative study of deep-sea fish brains. Preliminary observations of melamphaeids indicate a very special and highly complex development of the octavolateral area. For this purpose, the brains of five different species were collected and fixed in situ. Together with the differentiation of the auditory area (Xiaohong Deng), these will be studied in detail. In one specimen, we tried to label the saccular nerve with DiI in order to determine its exact projection area in the brain.
But we now know that all three end organs can be involved in hearing. Thus, it is possible that the enlarged utricle is also for sound detection. Again, this is a case where you need to know much more about hearing and other topics and then integrate these new data with the purely descriptive work from Marshall and others. We need to talk about a regular reading schedule for you I suspect.

7 Acknowledgements

Cruises SO-173 was funded by the German Ministery of Education and Research (BMBF) under project No. 03G0173B to GEOMAR within the continued and generous most commendable support for marine sciences with an outstanding research vessel such as SONNE.
This cruise is part of SFB574 at Christian Albrechts University in Kiel, the SFB is supported by the Deutsche Forschungsgemeinschaft.
We warmly thank master H. Andresen and his crew for their excellent support in all work done and for the splendid working atmosphere throughout the entire and the ambitious working program.

8 References

Abratis, M., and Wörner, G., Ridge collision, slab-window formation, and the flux of Pacific asthenosphere into the Caribbean realm, *Geology, 29,* 127-130, 2001.

Ambos, E.L., and D.M. Hussong, Structure at the toe of the subduction complex: Middle America Trench offshore Guatemala, Deep Sea Drilling Project Leg 84, in R. von Huene, J. Auboin, et al., *Init. Rept. DSDP*, 84: Washington (U.S. Govt. Printing Office), 861-878, 1985.

Aoki, Y.; Tamano, T; Kato, S. Detail structure of the Nankai Trough from migrated seismic sections. Studies in Continental Margin Geology. Ed. J. S. Watkins and C. L. Drake, *Am. Assoc. Pet. Geol. Mem.* 34, 309-322, 1982.

Auboin, J., Stephan, J. F., Renard, V., Roump, J., Lonsdale, P. Subduction of the Cocos plate in the Middle America trench. *Nature* 94, 146-150 (1981).

Aubouin, J., von Huene, R.,Baltuk, M., Arnott, R., Bourgois, J., Leg 84 of the Deep Sea Drilling Project, subduction without accretion: Middle America Trench off Guatemala, *Nature, 247*, 458-460, 1982.

Aubouin, J. and von Huene, R., Summary: Leg 84, Middle America Trench transect off Guatemala and Costa Rica: *in* Von Huene R. and Aubouin, J., Eds.: *Initial Reports*, *DSDP, 84*: Washington, D.C., U.S. Government Printing Office, p. 939-956. 1985.

Baltuck, M., Taylor, E., and McDougall K., Mass movement along the inner wall of the Middle America Trench, Costa Rica, in *Initial Report DSDP Leg 84*, edited by R. Von Huene and J. Aubouin, pp. 551-570, U.S. Goverment Printing Office, Washington, 1985.

Barckhausen, U., H.A. Roeser, and R. von Huene, Magnetic signature of upper plate structures and subducting seamounts at the convergent margin off Costa Rica, *J. Geophys. Res.*, *103*, 7079-7093, 1998.

Barckhausen, U., Ranero, C.R., von Huene, R., Cande, S.C., and Roeser, H.A., Revised tectonic boundaries in the Cocos Plate off Costa Rica: implications for the segmentation of the convergent margin and for plate tectonic models, *Journal of Geophysical Research, 106*, 19207-19220, 2001.

Bourgois, J., J. Azéma, P.O. Baumgartner, J. Tournon, A. Desmet, and J. Aubouin, The geologic history of the Caribbean-Cocos plate boundary with special reference to the Nicoya ophiolite complex (Costa Rica) and D.S.D.P. results (legs 67 and 84 off Guatemala): A syntesis, *Tectonophysics, 108*, 1-32, 1984.

Caress, D.W., and D.N. Chase, Improved processing of Hydrosweep DS multibeam data on the RV Maurice Ewing, *Mar. Geophys. Res.*, *18*, 631-650, 1996.

Case, J.E., and Holcombe, T.L., 1980, Geologic-tectonic map of the Caribbean region: U.S. Geological Survey Miscellaneous Investigations Map I-11000, scale 1:250,000

Christeson, G.L., K.D. McIntosh, T.H. Shipley, E.R. Flueh, and H. Goedde, Structure of the Costa Rica convergent margin, offshore Nicoya Peninsula, *J. Geophys. Res.*, *104*, 25, 443-25, 468, 1999.

Corrigan, J., P. Mann, and J.C. Ingle, Forearc response to subduction of the Cocos Ridge, Panama-Costa Rica, *Geol. Soc. Am. Bull., 102*, 628-652, 1990.

Crowe, J.C., and R.T. Buffler, Multichannel seismic records across the Middle America Trench and Costa Rica-Nicaragua convergent margin, NCY-7 and NCI-1, in *Middle America Trench off western Central America, Ocean Drilling Program, Regional Data Synthesis Series*, edited by J.W. Ladd and R.T. Buffler, Atlas 7, 11 p, Marine Science International, Woodshole, Massachusetts, 1985.

deBoer, J.Z., M.S. Drummond, M.J. Bordelon, H. Bellon, and R.C. Maury, Cenozoic magmatic phases of the Costa Rican island arc (Cordillera de Talamanca)*, Spec. Pap., Geol. Soc. Am., 295*, 35-55, 1995.

Dickinson, W. R. Clastic sedimentary sequences deposited in shelf, slope and trough between magmatic arcs and associated trenches. *Pacific Geology*, 3, 15-30, 1971.

Drummond, M.S., Bordelon, M., de Boer, J.Z., Defant, M.J., Bellon, H., Feigenson, M.D., Igneous petrogenesis and tectonic setting of plutonic and volcanic rocks of the Cordillera de Talamanca, Costa Rica-Panama, Central American Arc, *American Journal of Science, 295,* 875-919, 1995.

Fisher, A. T., Stein, C. A., Harris, R. N., Wang, K.; Silver, E., A.; Pfender, M.; Hutnak, M.; Cherkaoui, A.; Bodzin, R.; Villinger, H. Abrupt thermal transition reveals hydrothermal boundary and role of seamounts within the Cocos Plate. *Geophys. Res. Let.*, 30, 10.1029/2002GL016766. 2003.

Fisher, D.M.; Gardner, T.W.; Marshall, J.S.; Sak, P.B.; and Protti, M. Effect of subducting sea-floor roughness on fore-arc kinematics, Pacific coast, Costa Rica, *Geology, 26*(5), 467-470, 1998.

Fisher, R. L. Geomorphic and seismic refraction studies of the Middle America Trench, 1952-1956, *PhD Thesis*, Los Angeles, Univ. of California. 1957.

Fisher, R.L., Middle America Trench: Topography and structure, *Geol. Soc. Am. Bull.*, *72*, 703-720, 1961.

Fisher, R.L., Hess, H. H., in Hill, M. N. ed. *The Sea*, vol 3, New York Wiley. 1963.

Gardner, T.W., D. Verdonck, N. Pinter, R. Slingerland, K. Furlong, T.F. Bullard, and S.G. Wells, Quaternary uplift astride the aseismic Cocos Ridge, Pacific coast of Costa Rica*, Geol. Soc. Am. Bull.*, *104*, 219-232, 1992.

Graefe, K., Frisch, W., Villa, I.M., and Meschede, M., Geodynamic evolution of southern Costa Rica related to low-angle subduction of the Cocos Ridge: constraints from thermochronology, *Tectonophysics, 348*, 187-204, 2002.

Gutenber, B., Richter, C. F. Seismicity if the Earth, N.J. Princeton Univ. Press. 1954.

Handschumacher, D. W., Post-Eocene Plate Tectonics of the Eastern Pacific. The Geophysics of the Pacific Ocean Basin and its margin, ed. G.H. Sutton, M.H. Manghnani and R Moberly, *Geophysical Monograph*, 19, 177-202, 1976.

Hey, R., Tectonic evolution of the Cocos-Nazca spreading center; *Geol. Soc. Am. Bull.* 88, 1414-1420, 1977

Hinz, K., R. von Huene, C. R. Ranero, and the PACOMAR Working Group, Tectonic structure of the convergent Pacific margin offshore Costa Rica from multichannel seismic reflection data, *Tectonics, 15*, 54-66, 1996.

Heacock, J. G., Worzel, J. L. Submarine topography west of Mexico and Central America. *Bull. Geol. Soc. Am.*, 83, 1671-1692, 1955.

Hoernle, K., van der Bogaard, P., Werner, R., Lissinna, B., Hauff, F., Alvarado, G., Garbe-Schönberg, D. *Geology*, 30, 795-798 (2002).

Ihmlé, P. F. Monte carlo slip inversion in the frequency domain: Application to the 1992 Nicaragua slow earthquake. *Geophys. Res. Lett*., vol. 23, 913-916, 1996.

Karig, D. E. Origin of the Philippine Sea basin complex, in Ingle, J. C., Karig, D. E. et al., *Init. Rep. DSDP,* vol 31, Washington, D. C., U.S. Govt. Printing Office, 1975.

Kelly, R. and 9 others, New Be-10 and bathymetric constraints on sediment recycling in Central America, *Science* (submitted).

Kimura, G., et al., *Proceedings of the Ocean Drilling Program Initial Reports,* vol. 170, Ocean Drill. Program, College Station, Tex., 1997.

Langseth, M.G., and E.A. Silver, The Nicoya convergent margin: A region of exceptionally low heat flow, *Geophys. Res. Lett., 23*, 891-894, 1996.

Lonsdale, P. and Klitgord, K. D. Structure and tectonic history of the eastern Panama Basin. *Geol. Soc. Am. Bull.,* 89, 981-999, 1978.

McIntosh, K., E. Silver, and T. Shipley, Evidence and mechanisms for forearc extension at the accretionary Costa Rica convergent margin, *Tectonics, 12*, 1380-1392, 1993.

McIntosh, K., Silver, E., Ranero, C.R., Preliminary results of a Nicaragua-Costa Rica MCS/OBH seismic survey, Eos, 81, *American Geophysical Union Fall Meeting* (San Francisco). 2000.

Miller, H., Das Problem des hypothetischen „Pazifischen Kontinentes“ gesehen von der chilenischen Pazifikkuste, *Geol. Rundsch., 59*, 927-938, 1970.

Moore, G. F., Shipley, T. H., and Lonsdale, P. F., Subduction erosion versus dediment offscraping at the toe of the Middle America Trench off Guatemala: *Tectonics*, v. 5, no. 4, p. 513-523, 1986.

Park, J., Tsuru, T., Takahashi, N., Kodaira, S., Kaneda, Y., Seismic reflection images across the Izu-Bonin Island Arc System. *Eos trans. AGU,* 83 (47) Fall. Meet. Suppl., Abstract T72A-1224, F1318 (2002).

Protti, M., F. Gundel, and K. McNally, Correlation between the age of the subducting Cocos plate and the geometry of the Wadati-Benioff zone under Nicaragua and Costa Rica, *Spec. Pap. Geol. Soc. Am., 295*, 309-326, 1995.

Ranero, C. R.; von Huene, R.; Flueh, E., Duarte, M. and Baca, D. A cross section of the forearc Sandino Basin, Pacific Margin of Nicaragua. *Tectonics*, *19*, 335-357 2000.

Ranero, C.R. and Von Huene R., Subduction erosion along the Middle America convergent margin, *Nature, 404*, 748-752, 2000.

Ranero, C. R., Phipps Morgan, J., McIntosh, K., Reichert, C., Bending, faulting and mantle serpentinization at the Middle America Trench. *Nature*, 425, 367-373 (2003).

Rutland, R. W. R., Andean orogeny and ocean floor spreading. *Nature* 233, 252-255 (1971).

Scholz, C. H. & Small, C., The effect of seamount subduction on seismic coupling, *Geology*, 25, 487-490 (1997).

Seely, D. R., Geophysical investigations of continental slopes and rises, *in* Watkins, J. S., and Montadert, L., eds., Geological and Geophysical Investigation of Continental Margins: *American Association of Petroleum Geologists Memoir* 51, p. 245-260, 1979.

Seely, D.R., P.R. Vail, and G.G. Walton, Trench slope model, in *Geology of Continental Margins,* edited by C.A. Burk, and C.L. Drake, pp. 261-283, Springer-Verlag, New York, 1974.

Shipley, T.H., and G.F. Moore, Sediment accretion, subduction, and dewatering at the base of the trench slope off Costa Rica: A seismic reflection view of the décollement, *J. Geophys. Res., 91*, 2019-2028, 1986.

Shipley, T.H., P.L. Stoffa, and D.F. Dean, Underthrust sediments, fluid migration paths, and mud volcanoes associated with the accretionary wedge off Costa Rica: Middle America Trench, *J. Geophys. Res., 95*, 8743-8752, 1990.

Shipley, T.H., K.D. McIntosh, E.A. Silver, and P.L. Stoffa, Three-dimensional seismic imaging of the Costa Rica accretionary prism: Structural diversity in a small volume of the lower slope, *J. Geophys. Res., 97*, 4439-4459, 1992.

Shor, G. G., Fisher, R. L., Middle America Trench, *Bull. Geol. Soc. Am.,* 72, 721-730, 1961.

Silver, E.A., Ellis, M. J., Breen, N. A., Shipley, T. H., Comments on the growth of accretionary wedges. *Geology, 13*, 6-9, 1985.

Silver, E., et al., Influence of lower plate structure on the overriding slope offshore Nicaragua: New geophysical observations and the first dredge samples of basement rocks, Eos, 81, *American Geophysical Union Fall Meeting* (San Francisco). 2000.

Stavenhagen, A.. U., E.R. Flueh, C. Ranero, K. D. McIntosh, T. Shipley, G. Leandro, A. Schulze, and J.J. Dañobeitia, Seismic wide-angle investigations in Costa Rica: A crustal velocity model from the Pacific to the Caribbean Coast, *ZBL. Geol. Palaontol., Part I,* 393-408, 1998.

Vannucchi, P., Scholl, D.W., Meschede, M., and McDougall-Reid, K. Tectonic erosion and consequent collapse of the Pacific margin of Costa Rica: combined implications from ODP Leg 170, seismic offshore data and regional geology of the Nicoya Peninsula, *Tectonics, 20,* 649-668, 2001.

Vannucchi, P., Ranero, C.R., Galeotti, S., Straub, S.M., Scholl, D.W., McDougall-Ried, K., Fast rates of subduction erosion along the Costa Rica Pacific margin: implications for non-steady rates of crustal recycling at subduction zones, *Journal of Geophysical Research* (in press.).

Vannucchi, P., Galeotti, S.; Clift, P. D.; Ranero, C.R.; von Huene, R. Long term subduction erosion along the Middle America Trench offshore Guatemala. *Geology* (submitted).

von Huene et al. Leg 67: The Deep Sea Drilling Project Mid-America Trench transect off Guatemala. *Geol. Soc. Am. Bulletin*, 91, 421-432, 1980.

von Huene R., J. Aubouin, et al., Site 565, in *Initial Report DSDP Leg 84*, edited by R. Von Huene and J. Aubouin, pp. 21-78, U.S. Goverment Printing Office, Washington, 1985.

von Huene, R., et al., Morphotectonics of the Pacific convergent margin of Costa Rica, in *Geologic and Tectonic Development of the Caribbean Plate Boundary in Southern Central America*, edited by P. Mann, *Spec. Pap. Geol. Soc. Am*., *295*, 291-308, 1995.

von Huene, R., and Flueh, E.R. A review of marine geophysical studies along the Middle American Trench off Costa Rica and the problematic seaward terminus of continental crust, *Profil 7*, Stuttgart, 143-159, 1994.

von Huene, R., Ranero C.R., Weinrebe W., and Hinz K., Quaternary convergent margin tectonics of Costa Rica, segmentation of the Cocos plate, and Central American Volcanism, *Tectonics, 19*, 314-334, 2000.

von Huene R., and Ranero, C.R., Subduction erosion and basal friction along the sediment starved convergent margin off Antofagasta, Chile, *Journal of Geophysical Research*, 2003.

von Huene, R., Ranero, C. R. and Watts, P. Tsunamigenic slope failure along the Middle America Trench in two tectonic settings. *Marine Geology* (in press).

Walther, C. The crustal structure of the Cocos ridge off Costa Rica. J. *Geophys. Res., 108*, doi:10.1029/2001JB000888, 2003.

Walther, C.H.E., E.R. Flueh, C.R. Ranero, and R. von Huene, Seismic investigations at the Pacific Margin of Nicaragua, *Geophys. J. Int*., 141, 759-777, 2000.

Watkins, J. S, et al., *Init. Repts. DSDP,* 66, Washington, D. C., U.S. Govt. Printing Office, 1982

Werner, R., K. Hoernle, P. van den Bogaard, C.R. Ranero, R. von Huene, and D. Korich, Drowned 14 m.y. old Galapagos archipelago off the coast of Costa Rica: Implications for tectonic and evolutionary models, *Geology, 27*, 499-502, 1999.

Wilson, D., 1996, fastest known spreading on the Miocene Cocos-Pacific plate boundary: *Geophysical Research letters,* v. 23, p. 3003-3006.

Ye, S., J. Bialas, E.R. Flueh, A. Stavenhagen, R. von Huene, G. Leandro, and K. Hinz, Crustal structure of the Middle American Trench off Costa Rica from wide-angle seismic data, *Tectonics, 15*, 1006-1021, 1996.

Appendix 1 – mapping profiles

profile	date	time	length	position	
number		UTC -6		latitude	longitude
HS #1	080803	2342		09-48.70N	84-46.00W
	100803	0206	240sm	11-27.19N	87-50.90W
HS #2	100803	0206		11-27.19N	87-50.90W
	100803	1533	148sm	11-59.17N	87-50.81W
HS #3	100803	2030		11-59.08N	88-06.91W
	120803	0907	369sm	13-42.40N	90-44.50W
HS #4	120803	1030		13-44.00N	90-44.00W
	130803	1200	216sm	13-39.62N	92-30.78W
HS #5	130803	1200		13-39.62N	92-30.78W
	140803	0246	77sm	12-31.77N	92-53.41W
HS #6	140803	0246		12-31.77N	92-53.41W
	140803	1042	80sm	13-45.06N	92-20.46W
HS #7	140803	1427		13-42.12N	92-14.71W
	140803	2230	82sm		
HS #8	140803	2300		12-26.14N	92-42.36W
	150803	0706	80sm		
HS #9	150803	0800		13-36.92N	92-02.02W
	150803	1312	50sm		
HS #10	150803	1720		12-46.93N	92-17.04W
	150803	2227	50sm		
HS #11	150803	2339		13-31.30N	91-49.70W
	160803	0442	51sm	12-44.05N	92-11.05W
HS #12	160803	0527		12-41.45N	92-04.82W
	160803	1030	51sm	13-28.78N	91-43.43W
HS #13	160803	1500		13-28.15N	91-36.08W
	160803	2100	56sm	12-35.62N	91-59.37W
HS #14	160803	2148		12-33.48N	91-33.43W
	170803	0315	54sm	13-23.00N	91-30.90W
HS #15	170803	0501		13-20.60N	91-24.04W
	170803	1029	55sm	12-30.23N	91-47.05W
HS #16	170803	1120		12-28.01N	91-41.17W
	170803	1656	55sm	13-19.00N	91-18.30W
HS #17	170803	1836		13-15.50N	91-12.20W
	180803	0245	81sm	12-00.53N	91-45.47W
HS #18	180803	0328		11-58.80N	91-39.49W
	180803	1125	81sm	13-12.96N	91-05.98W
HS #19	180803	1530		13-10.42N	90-59.51W
	180803	2335	82sm	11-56.17N	91-33.13W
HS #20	190803	0030		11-53.20N	91-27.15W
	190803	1200	115sm	13-39.06N	90-38.87W
HS #21	190803	1320		13-37.04N	90-33.03W
	200803	0100	117sm	11-51.24N	91-23.41W
HS #22	200803	0506		11-47.80N	91-14.61W
	200803	1826	116sm	13-29.50N	90-28.50W
HS #23	200803	2100		13-12.65N	90-28.40W
	210803	0407	74sm	12-10.00N	90-57.00W
HS #24	210803	0458		12-07.30N	90-51.00W
	210803	1046	58sm	13-01.00N	90-26.87W
HS #25	210803	1200		12-58.35N	90-20.23W
	210803	1523	32sm	12-29.31N	90-33.81W
HS #26	210803	1543		12-29.21N	90-33.60W
	220803	0733	153sm	13-22.40N	92-55.00W

profile	**date**	**time**	**length**	**position**	
number		UTC -6		latitude	longitude
HS #27	220803	1306		13-32.62N	92-55.00W
	220803	1702	41sm	13-50.70N	92-19.60W
HS #28	220803	1723		13-50.70N	92-19.60W
	230803	0114	67sm	13-18.95N	91-29.04W
HS #29	230803	0449		13-15.70N	91-23.03W
	230803	0900	40sm	13-16.36N	91-26.73W
HS #30	230803	1754		13-11.80N	91-10.20W
	230803	2345	56sm	12-51.57N	90-15.71W
HS #31	240803	0017		12-51.61N	90-15.81W
	240803	0255	25sm	12-28.43N	90-25.93W
HS #32	240803	0330		12-26.04N	90-19.43W
	240803	0628	29sm	12-52.45N	90-07.92W
HS #33	240803	0628		12-52.45N	90-07.92W
	240803	1200	59sm	13-14.08N	90-51.00W
HS #34	240803	1240		13-18.32N	90-44.88W
	240803	1354	34sm	13-30.42N	90-37.82W
HS #35	240803	1403		13-30.89N	90-38.30W
	240803	1418	3sm	13-28.76N	90-39.95W
HS #37	240803	1734		13-29.71N	90-41.58W
	240803	1824	8sm	13-22.00N	90-44.35W
HS #38	240803	1854		13-22.00N	90-43.40W
	240803	1935	7sm	13-28.30N	90-40.70W
HS #39	240803	2106		13-25.97N	90-36.21W
	240803	2303	19sm	13-07.98N	90-41.90W
HS #40	240803	2350		13-09.11N	90-39.78W
	250803	0413	44sm	12-48.35N	90-00.00W
HS #41	250803	0413		12-48.35N	90-00.00W
	250803	1526	114sm	11-59.02N	89-15.02W
HS #42	250803	2021		11-50.39N	88-12.10W
	260803	0851	125sm	12-44.61N	90-07.15W
HS #43	260803	0938		12-38.08N	90-09.60W
	260803	2155	122sm	11-45.25N	88-17.61W
HS #44	270803	0227		11-37.96N	88-18.54W
	270803	1445	124sm	12-31.72N	90-12.71W
HS #45	270803	1526		12-25.16N	90-14.38W
	280803	0336	122sm	11-31.69N	88-22.20W
HS #46	280803	0366		11-31.69N	88-22.20W
	280803	1900	113sm	10-04.40N	87-12.00W
HS #47	290803	0306		09-59.91N	87-14.62W
	300803	0258	113sm	11-25.08N	88-24.76W
HS #48	300803	0258		11-25.08N	88-24.76W
	300803	1642	138sm	12-24.63N	90-31.70W
HS #49	300803	1731		12-18.20N	90-34.48W
	310803	0703	137sm	11-18.50N	88-28.80W
HS #50	310803	0703		11-18.50N	88-28.80W
	010903	0628	279sm	09-43.35N	84-52.36W

Appendix 2 – magnetic profiles

DATE	TIME	COMMENT	LATITUDE	LONGITUDE	LENGTH
11.08.03	10:16 Uhr	begin	13-05.33N	90-26.40W	
12.08.03	09:07 Uhr	end	13-42.40N	90-44.50W	224sm
	14:16 Uhr	begin	13-07.50N	90-48.90W	
13.08.03	04:20 Uhr	begin	13-48.97N	92-25.95W	
	12:00 Uhr	end	13-39.62N	92-30.78W	165sm
	19:41 Uhr	begin	13-28.41N	92-32.31W	
14.08.03	02:46 Uhr	end	12-31.77N	92-53.41W	77sm
	02:46 Uhr	begin	12-31.77N	92-53.41W	
	10:42 Uhr	end	13-45.06N	92-20.46W	80sm
	14:27 Uhr	begin	13-42.12N	92-14.71W	
	22:30 Uhr	end			82sm
	23:00 Uhr	begin	12-26.14N	92-42.36W	
15.08.03	07:06 Uhr	end			80sm
	17:20 Uhr	begin	12-46.93N	92-17.04W	
	22:27 Uhr	end			50sm
	23:39 Uhr	begin	13-31.30N	91-49.70W	
16.08.03	04:42 Uhr	end	12-44.05N	92-11.05W	51sm
	05:27 Uhr	begin	12-41.45N	92-04.82W	
	10:30 Uhr	end	13-28.78N	91-43.43W	51sm
	15:00 Uhr	begin	13-28.15N	91-36.08W	
	21:00 Uhr	end	12-35.62N	91-59.37W	56sm
	21:48 Uhr	begin	12-33.48N	91-33.43W	
17.08.03	03:15 Uhr	end	13-23.00N	91-30.90W	54sm
	05:01 Uhr	begin	13-20.60N	91-24.04W	
	10:29 Uhr	end	12-30.23N	91-47.05W	55sm
	11:20 Uhr	begin	12-28.01N	91-41.17W	
	16:56 Uhr	end	13-19.00N	91-18.30W	55sm
18.08.03	03:28 Uhr	begin	11-58.80N	91-39.49W	
	11:25 Uhr	end	13-12.96N	91-05.98W	81sm
	15:30 Uhr	begin	13-10.42N	90-59.51W	
	23:35 Uhr	end	11-56.17N	91-33.13W	82sm
19.08.03	00:30 Uhr	begin	11-53.20N	91-27.15W	
	01:00 Uhr	end	11-51.24N	91-23.41W	115sm
	12:00 Uhr	begin	13-39.06N	90-38.87W	
	13:20 Uhr	end	13-37.04N	90-33.03W	115sm
	12:18 Uhr	continuation	12-34.16N	90-55.41W	
	18:26 Uhr	end	13-29.50N	90-28.50W	116sm
	21:00 Uhr	begin	13-12.65N	90-28.40W	
21.08.03	04:07 Uhr	end	12-10.00N	90-57.00W	74sm
	04:58 Uhr	begin	12-07.30N	90-51.00W	
	10:46 Uhr	end	13-01.00N	90-26.87W	58sm

DATE	TIME	COMMENT	LATITUDE	LONGITUDE	LENGTH
	12:00 Uhr	begin	12-58.35N	90-20.23W	
	15:23 Uhr	end	12-29.31N	90-33.81W	32sm
	15:43 Uhr	begin	12-29.21N	90-33.60W	
22.08.03	07:33 Uhr	end	13-22.40N	92-55.00W	153sm
	13:06 Uhr	begin	13-32.62N	92-55.00W	
	17:02 Uhr	end	13-50.70N	92-19.60W	41sm
	17:23 Uhr	begin	13-50.70N	92-19.60W	
23.08.03	01:14 Uhr	end	13-18.95N	91-29.04W	67sm
	17:54 Uhr	begin	13-11.80N	91-10.20W	
	23:45 Uhr	end	12-51.57N	90-15.71W	56sm
24.08.03	00:17 Uhr	begin	12-51.61N	90-15.81W	
	02:55 Uhr	end	12-28.43N	90-25.93W	25sm
	03:30 Uhr	begin	12-26.04N	90-19.43W	
	06:28 Uhr	end	12-52.45N	90-07.92W	29sm
	06:28 Uhr	begin	13-11.39N	90-51.72W	
	12:00 Uhr	end	13-14.08N	90-51.00W	51sm
	17:34 Uhr	begin	13-29.71N	90-41.58W	
	18:24 Uhr	end	13-22.00N	90-44.35W	8sm
	18:54Uhr	begin	13-22.00N	90-43.40W	
	19:35 Uhr	end	13-28.30N	90-40.70W	7sm
	21:06 Uhr	begin	13-25.97N	90-36.21W	
	23:03 Uhr	end	13-07.98N	90-41.90W	19sm
	23:50 Uhr	begin	13-09.11N	90-39.78W	
25.08.03	04:13 Uhr	end	12-48.35N	90-00.00W	44sm
	04:13 Uhr	begin	12-48.35N	90-00.00W	
	15:26 Uhr	end	11-59.02N	89-15.02W	114sm
	20:21 Uhr	begin	11-50.39N	88-12.10W	
26.08.03	08:51 Uhr	end	12-44.61N	90-07.15W	125sm
	09:38 Uhr	begin	12-38.08N	90-09.60W	
	21:55 Uhr	end	11-45.25N	88-17.61W	120sm
27.08.03	02:27 Uhr	begin	11-37.96N	88-18.54W	
	14:45 Uhr	end	12-31.72N	90-12.71W	124sm
	15:26 Uhr	begin	12-25.16N	90-14.38W	
28.08.03	03:36 Uhr	end	11-31.69N	88-22.20W	122sm
	08:56 Uhr	begin	11-21.60N	88-15.82W	
	19:00 Uhr	end	10-04.40N	87-12.00W	113sm
29.08.03	22:49 Uhr	begin			
30.08.03	02:58 Uhr	end	11-25.08N	88-24.76W	70sm
	02:58 Uhr	begin	11-25.08N	88-24.76W	
	16:42 Uhr	end	12-24.63N	90-31.70W	138sm
	17:31 Uhr	begin	12-18.20N	90-34.48W	
31.08.03	07:03 Uhr	end	11-18.50N	88-28.80W	137sm

Appendix 3 – dredge positions

Dredge 1:

23.08.2003-08-30 15:20 – 19:05 UTC
Start: 13°16.33' N – 91°26.79' W 2075 m
End: 13°17.14' N – 91°25.67' W 1168 m

Dredge_2:

23.08.2003 20:17 – 21:31 UTC
Start: 13°17.91' N – 91°25.09' W 1598 m
End: 13°17.19' N – 91°25.36' W 1126 m

Appendix 4 – OBH - positions

	LATITUDE	LONGITUDE	DEPTH
OBH 53	10°10.03 N	86°57.02 W	3398 m
OBH 54	10°04.00 N	86°50.56 W	3551 m
OBH 55	10°03.07 N	87° 03.53 W	3048 m
OBH 56	09°56.06 N	86° 58.52 W	3120 m

Appendix 5 – list of trawls: general comments

09.08. 03: trawl 01: RMT 8; net in water: 15.15h; wire out: 2,000m; begin of trawl: 16.30h; end of trawl: 17.30; trawl on deck: 19.00 (i.e. at darkness) (dusk between 18.15 and 18.45)
Result: very good catch; big eels; few hatchetfish; big melamphaeids; 1 mesopelagic grenadier; some unknowns; 1 Malacosteus; lots of transparent things for Alison; briefly:
something for everybody except Tammy;

10.08. 03: trawl 02: tucker trawl with CCE net in water: 16.45; wire out:1,900m; begin of trawl: 17.00; end of trawl: 18.55; trawl on deck: 19.45
estimated depth: 1,000m; seafloor at about 2,100m
cod end did not close
Result: many live fish: myctophids, Scopelarchus, Scopelogadus, lots of transparencies; not a single hatchetfish; no stomiids

13.08. 03 trawl 03: tucker trawl with CCE net in water: 0.00h; wire out: 400m begin of trawl: 0.15 end of trawl: 1.15h; trawl on deck: 1.30h
estimated depth: 200m seafloor at about 2,000m
Result: mainly epipelagic; few myctophids few crusties; many jellies no hatchetfish; stomatopods

13.08. 03 trawl 04: tucker trawl with CCE net in water: 1.45h wire out: 600m for first hour, 800m for last 45min; end of trawl: 3.40h; trawl on deck: 4.00h
estimated depth: 300 and 400m resp.; seafloor at about 2,100m
Result: right depth but almost no fish or crusties; few mytophids

13.08. 03 trawl 05 RMT8 net in water: 16.35; wire out: 1800m; begin trawl: 17.45; end trawl: 18.45h; net on deck: 19.45
estimated depth: 900-1,000m; seafloor at 5.600m; strong currents!
Result: melamphaeids, myctophids, angler, mesopelagic grenadier; crusties; no eels, not a single hatchetfish, no stomiids, no Chauliodus

14.08 03 trawl 06 RMT8 net in water: 11.10h wire out 1.600m for 45 min and 1.400m for another 45min; end of trawl 13.30; net on deck: 14.15h
estimated depth: 700-800m; depth of seafloor: 2,300m
Result: good catch: melamphaeids, myctophids, angler, eel, stomiid, no hatchetfish, no chauliodus or gonostoma; many bathylagus

15.08. 03 trawl 07 Tucker trawl with CCE net in water: 13.30h; start trawl: 13.15h; wire out 1,500 and 1,300m resp. for about 60 min each; net on deck: 17.00
estimated depth: 600-700m; seafloor at 4,000m
Result: (1 live myctophid; Cyclothone, jellies, heteropod, pyrosoma
Too shallow for high surface temperatures? very clear water!)
Wrong: Good catch! Big cephalopod was blocking the entrance/exit of the cod end: behind it: melamphaeids, myctophids, bathylagus, one stomiid and tiny hatchetfish

16.08. 03 trawl 08 Tucker trawl with CCE net in water: 10.55; start trawl: 11.50h wire out: 1,800m, for 50 min and 1,600m for another 50min; net on deck: 16.45
estimated depth: 900m resp. 800m; seafloor at 2,100m at the beginning of trawl, and at1,200m at the end
Result: rather good catch; 3 big anglers alive; myctophids; 6 bathylagus, many melamphaeids; big Serrivomer, Idiacanthus; tiny Chauliodus

18.08. 03 trawl 09 RMT8 net in water: 11.50h wire out 1.300m for 50 min and 1.100m for another 50 min; end of trawl 14.30; net on deck: 14.45h
estimated depth: 700-600m; depth of seafloor: 1,280m
Result: average catch; 4 Bathylagus; myctophids, melamphaeids, 6 heteropods; no anglers or hatchets or stomiids etc.

20.08. 03 trawl 10 RMT8	net in water: 1.05h; wire out: 1,400m for 50min and 800m for 40 min end of trawl: 3.40; net on deck: 4.05h estimated depth: 700m and 400m; seafloor at 3,500m Result: average catch; 1, big Serrivomer; 8 bathylagus, few myctophids, melamphaeids, 1rattail; very similar to daytime catch: mostly non-migrators
22.08. 03 trawl 11 Tucker trawl	net in water: 8.05h; wire out: 1,800m for 45min and 1,600m for 45 min begin of trawl: 9.00h, end of trawl: 11.05; net on deck: 11.50h estimated depth: 900m and 800m; seafloor at 5,100m Result: rather poor: only few melamphaeids and myctophids; no other fish; some crusties; some jellies
23.08. 03 trawl 12 Tucker trawl	net in water: 01.20h; wire out: 1,600m for 45min and 1,400m for 45 min; begin of trawl: 2.10h; end of trawl: 3.50h; net on deck: 4.30h estimated depth: 800m and 700m; seafloor at 1,950; then going over seamound at 1,500m Result: Rather good catch, but limited number of species; many live fish and crusties: Bathylagus, melamphaeids, myctophids, 1 Idiacanthus
25.08. 03 trawl 13 RMT8	net in water: 15.45h wire out: 1,800m for 45min; and 1,600m for another 45min; begin if trawl: 16.45h, end of trawl: 18.35h; net on deck: 19.15h; seafloor at:2,250mn Result: Good catch; higher number of species: many Bathylagus, different melamphaeids, some stomiids, many myctophids, no hatchetfish, Gonostoma, Chauliodus, Anoplogaster, Eurypharynx..
26.08. 03 trawl 14 Tucker trawl	net in water: 21.55 h; wire out: 1,600m for 45min; and 1,400m for another 45min; begin of trawl: 22.45, end of trawl: 0.40h; net on deck:1.15h; seafloor at 4,200m Result: Average catch; mostly melamphaeids; 2 anglers; 2 Idiacanthus; myctophids; no migrators like Bathylagus
28.08. 03 trawl 15 Tucker trawl	net in water: 5.15 h (dawn); wire out: 1,600m for 50min; 1,700m for 55min; begin of trawl: 6.10h; end of trawl: 8.00; net on deck: 8.45h; seafloor at 4,100m Result: cod end completely filled with small jellyfish; only four fish (Cyclothone)
29.08. 03 trawl 16 RMT8	net in water: 6.05h; wire out: 2,000m for 40min and 1,800 for 50 min; begin of trawl: 7.05h; end of trawl: 8.45h net on deck: 9.45h estimated depth: 900m; seafloor at: 3,200m Result: Excellent catch: eels, myctophids, hatchetfish (some); macrourids, melamphaeids; anglers; stomiids; Bathylagus (some), many diverse crustaceans (animals mostly dead due to high a speed when hieving the net)
29.08. 03 trawl 17 RMT8	net in water: 12.05h; wire out: 1,600m for 45min and 1,800 for 45 min; begin of trawl: 13.00h; end of trawl: 14.55h; net on deck: 15.45h estimated depth: 700-800m; seafloor at 3,000m Result: good catch: eels alive, melamphaeids, alive; hatchetfish; Bathylagus; anglers; stomiids; many diverse crustaceans
29.08. 03 trawl 18 RMT8	net in water: 18.00h; wire out: 1,800m for 45min and 800 for 45 min; begin of trawl: 18.55h; end of trawl: 20.50h; net on deck: 21.20h estimated depth: 900 and 400m; seafloor at 2,800m; seamount? Result: excellent catch: Migrators and non-migrators; Bathylagus and others in good shape, alive; anglers, rattails; Scopelengys; eels; different melamphaeids

Appendix 6 – summary table of lateral line results

Table1: List of species collected on Sonne and their associated neuromast types.

Photograph	Family	Species	number	Canal Organs	Papillate FS organs	Stitches
	Melamphaidae	*Melamphaes simus*	1	√	**?**	√
	Melamphaidae	*Melamphaes sp.*	13	√	√	√
	Melamphaidae	*Poromitra crassiceps*	1	√	**?**	√
	Melamphaidae	*Scopeloberyx opisthopterus*	1	√	√	√
	Melamphaidae	*Scopeloberyx sp.*	8	√	√	√
	Macrouridae	**Nezumia sp.**	1	√	**?**	**X**
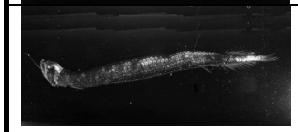	Stomidae	**Stomias boa**	3	√	**?**	**?**

Photograph	Family	Species	number	Canal Organs	Papillate FS organs	Stitches
	Idiacanthidae	*Idiacanthus fasciola*	9	**?**	√	**X**
	Neoscopelidae	*Scopelengys tristis*	7	√	**?**	**?**
	Oneirodidae	*Microlophichthys sp.* (not *M. microlophus)*	1	**X**	√	**X**
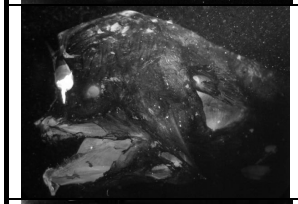	Oneirodidae	*Lophodolos acanthognathus*	1	**X**	√	**X**
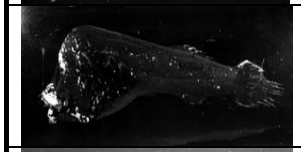	Centrophtynidae	*Centrophryne spinulosa*	1	**X**	√	**X**
	Melanocetidae	*Melanocetes johnsonii* female	6	**X**	√	**X**

Photograph	Family	Species	number	Canal Organs	Papillate FS organs	Stitches
	Melanocetidae	*Melanocetes johnsonii* juvenile male	1	**X**	**?**	**X**
	Nemichthyidae	*Avocettina infans*	7	√	**X**	√
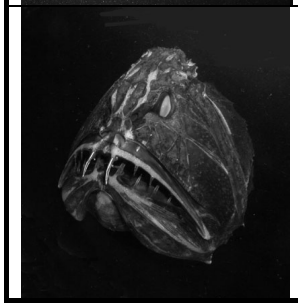	Anoplogasteridae	*Anoplogaster cornuta*	1	√	√	**X**

Total of 62 specimens collected.

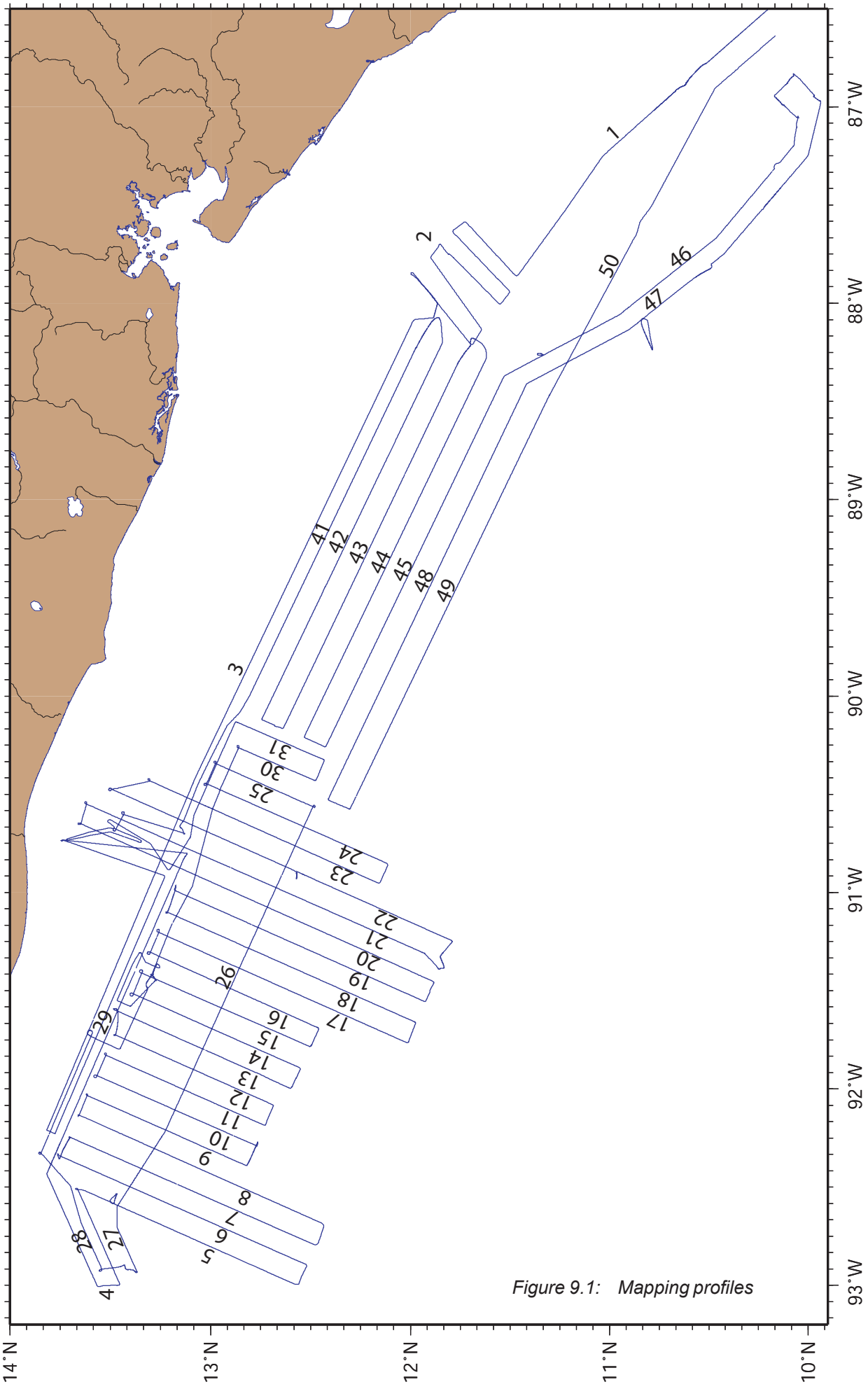

Figure 9.1: Mapping profiles

Appendix 7 – Captain's report

F.S. "S O N N E" Reise SO 173/2

Eingesetzte Geräte		Einsätze
RMT	Rectangle Midwater Trawl	: 11
TN	Tucker Netz	: 7
Sonde (Test)		: 1
DR	Kettensackdredge	: 2
OBH	Ocean Bottom Hydrograph (Aufnahme)	: 4

Vermessen wurden :

Mit HS	: 3769 sm
Mit MAG	: 2924 sm

Eingesetzte Winden :

Winde	*D/M .*	*Typ*	*RF-Nr*	*SO 173/2 Einsatz*	*Gesamt Einsatz*	*SO 173/2 S`länge*	*Gesamt S`länge*	*Zust.*
W 1	18,2	LWL	812001	0000 h	0000 h	000000 m	0000000 m	1
W 2	18,2	LWL	810001	0000	1659	000000	0966465	4/
W 4	11,0	NSW	818045	0000	0034	000000	0036663	2
W 5	11,2	NSW	812106	0000	0012	000000	0008455	4*
W 6	18,2	DRAKO	818238	0064	0807	033275	0763371	3

*sehr schlechtes Spulverhalten

Winde	*SO 173/2 gefierte max.Länge*	*jemals gefierte max.Länge*
W 1	0000 m	8022 m
W 2	0000	7603
W 4	0000	8ß81
W 5	0000	7000
W 6	2374	7609

Geräteverluste :
Keine

Abkürzungen im Stationsprotokoll:

z.W.	zu Wasser
a.D.	an Deck
Boko	Bodenkontakt
Bosi	Bodensicht
SL(max.)	(maximale)Seillänge
LT	Lottiefe nach Hydrosweep
W x	eingesetzte Winde
SM	Simrad- Multibeam-Lot
PS	Parasound
XPNDR	Transponder

Zeit : UTC – 06 Stunden
08.08.03

Profil HS #1

2342	Beginn Profil div. Kurse; V=8/11Kn		09-48.70N 84-46.00W

09.08.03

1502	Unterbrechen Profil		10-30.51N 86-46.53W

Station RMT #1 W6

1512	RMT z/W Kurs 310°. V=2.5Kn	LT = 3680 m	10-31.16N 86-46.91W
1632	Slmax 2000m	LT = 3702 m	10-33.92N 86-49.22W
1741	Beginn Hieven		10-35.98N 86-51.50W
1846	Ende Station, RMT a/D		
1905	Fortsetzung Profil HS #1		10-37.35N 86-54.50W

10.08.03

0206	Ende Profil 240sm		11-27.19N 87-50.90W

Profil HS #2

0206	Beginn Profil div. Kurse; V=11Kn		11-27.19N 87-50.90W
1533	Ende Profil 148sm		11-59.17N 87-50.81W

Station TN #2 W6

1646	TN z/W, Kurs 290°; V=2.5Kn	LT = 2138 m	11-51.84N 88-00.13W
1800	Slmax 2000m	LT = 2168 m	11-52.33N 85-01.81W
1853	Beginn Hieven		11-52.68N 88-03.15W
1945	Ende Station, TN a/D		

Profil HS #3

2030	Beginn Profil, div. Kurse, V=11/10Kn		11-59.08N 88-06.91W

11.08.03

1008	MAG z/W		13-05.15N 90-26.41W
1016	MAG ausgesteckt; L300m		13-05.33N 90-26.40W

12.08.03

0907	Ende Profil 369sm, MAG 224sm		13-42.40N 90-44.50W
	Beginn Hieven MAG		
0915	MAG a/D		13-42.78N 90-44.44W
	Anfahrt Rendevous Punkt Aufnahme 1 Beobachter Guatemala		

Profil HS #4

1030	Beginn Profil, div. Kurse, V=11/10Kn		13-44.00N 90-44.00W
1416	MAG ausgesteckt, L200m		13-07.50N 90-48.90W
2345	MAG a/D		

13.08.03

Station TN #3 W6

0006	TN z/W, Kurs 293°; V=2.0Kn		13-45.67N 92-18.06W
0020	Slmax 400m	LT = 1930 m	13-45.79N 92-18.43W
0114	Beginn Hieven		13-46.37N 92-19.89W
0127	Ende Station, TN a/D		

Station TN #4 W6

0135	TN z/W, Kurs 293°; V=2.0Kn		13-46.60N 92-20.37W

0257	Slmax 800m	LT = 1721 m	13-47.55N	92-22.57W
0344	Beginn Hieven		13-48.09N	92-23.90W
0406	Ende Station, TN a/D			
0420	MAG ausgesteckt L300m		13-48.97N	92-25.95W
1200	Ende Profil 216sm; MAG 165sm		13-39.62N	92-30.78W

Profil HS #5

1200	Beginn Profil, div. Kurse, V=10Kn		13-39.62N	92-30.78W
1315	MAG a/D		13-29.10N	92-35.02W

Test Sonde :

1325	Sonde z/W	LT = 5708 m	13-28.93N	92-34.90W
1443	Slmax 4000m	LT = 5700 m	13-28.91N	92-35.17W
1605	Sonde a/D, Ende Station			

Station RTM #5 W6

1638	RMT z/W, Kurs 106°, V=2.5Kn		13-28.90N	92-34.90W
1744	Slmax 1800m	LT = 5713 m	13-28.67N	92-33.93W
1845	Beginn Hieven		13-28.28N	92-32.75W
1932	Ende Station, RMT a/D			
1941	MAG z/W		13-28.41N	92-32.31W
2000	Fortsetzung Profil		13-30.03N	92-34.24W

14.08.03

0246	Ende Profl 77sm, MAG 77sm		12-31.77N	92-53.41W

Profil HS #6

0246	Beginn Profil, div. Kurse, V=10Kn		12-31.77N	92-53.41W
1042	Ende Profil 80sm, MAG 80sm		13-45.06N	92-20.46W
1102	MAG a/D		13-45.33N	92-21.28W

Station RMT #6 W6

1110	RMT z/W; Kurs 116°; V=2.5Kn		13-45.13N	92-21.25W
1200	Slmax 1600m	LT = 2134 m	13-44.50N	92-19.61W
1330	Beginn Hieven		13-42.74N	92-16.02W
1411	RMT a/D; Ende Station			

Profil HS #7

1427	Beginn Profil, MAG z/W		13-42.12N	92-14.71W
2230	Ende Profil 82sm; MAG 82sm			

Profil HS #8

2300	Beginn Profil		12-26.14N	92-42.36W

15.08.03

0706	Ende Profil 80sm; MAG 80sm			

Profil HS #9

0800	Beginn Profil		13-36.92N	92-02.02W
1312	Ende Profil 50sm; MAD 50sm			

1319	MAG a/D			12-48.67N 92-22.63W
Station #7 TN W6				
1326	TN z/W, Kurs 113°; V=2.5Kn	LT = 4046 m		12-48.67N 92-22.63W
1414	Slmax 1500m	LT = 4046 m		12-47.89N 92-20.94W
1620	Beginn Hieven			12-46.18N 92-17.00W
1658	TN a/D, Ende Station			
1711	MAG z/W			12-46.26N 92-17.43W
Profil HS #10				
1720	Beginn Profil			12-46.93N 92-17.04W
2227	Ende Profil	50sm; MAG 50sm		
Profil HS #11				
2339	Beginn Profil			13-31.30N 91-49.70W
16.08.03				
0442	Ende Profil	51sm; MAG 51sm		12-44.05N 92-11.05W
Profil HS #12				
0527	Beginn Profil			12-41.45N 92-04.82W
1030	Ende Profil	51sm; MAG 51sm		13-28.78N 91-43.43W
1040	MAG a/D			13-28.52N 91-43.30W
Station TN #8 W6				
1051	TN z/W, Kurs 113°; V=2.5Kn	LT = 1612 m		13-28.33N 91-43.21W
1153	Slmax 1800m	LT = 1541 m		13-27.89N 91-40.92W
1350	Beginn Hieven			13-27.82N 91-36.41W
1438	TN a/D, Ende Station			
Profil HS #13				
1500	Beginn Profil, MAG z/W			13-28.15N 91-36.08W
2100	Ende Profil	56sm; MAG 56sm		12-35.62N 91-59.37W
Profil HS #14				
2148	Beginn Profil			12-33.48N 91-33.43W
17.08.03				
0315	Ende Profil	54sm; MAG 54sm		13-23.00N 91-30.90W
Profil HS #15				
0501	Beginn Profil			13-20.60N 91-24.04W
1029	Ende Profil	55sm; MAG 55sm		12-30.23N 91-47.05W
Profil HS #16				
1120	Beginn Profil			12-28.01N 91-41.17W
1656	Ende Profil	55sm; MAG 55sm		13-19.00N 91-18.30W
Profil HS #17				
1836	Beginn Profil			13-15.50N 91-12.20W

18.08.09

0245	Ende Profil	81sm		12-00.53N	91-45.47W
Profil HS #18					
0328	Beginn Profil			11-58.80N	91-39.49W
1125	Ende Profil	81sm; MAG 81sm		13-12.96N	91-05.98W
1134	MAG a/D			13-13.36N	91-06.23W
Station RMT #8		W6			
1150	RMT z/W; Kurs 116°; V=2.5Kn		LT = 1287 m	13-12.82N	91-05.87W
1234	Slmax 1300m		LT = 1280 m	13-12.18N	91-04.19W
1400	Hieven			13-10.89N	91-00.25W
1506	RMT a/D; Ende Station				
Profil HS #19					
1530	Beginn Profil; MAG z/W			13-10.42N	90-59.51W
2335	Ende Profil	82sm; MAG 82sm		11-56.17N	91-33.13W
19.08.03					
Profil HS #20					
0030	Beginn Profil			11-53.20N	91-27.15W
1200	Ende Profil	115sm; MAG 115sm		13-39.06N	90-38.87W
Profil HS #21					
1320	Beginn Profil			13-37.04N	90-33.03W
0018	MAG a/D			11-55.94N	91-18.53W
0100	Ende Profil	117sm; MAG 115sm		11-51.24N	91-23.41W
Station RMT #10		W6			
0106	RMT z/W; Kurs 116°; V=2.5Kn		LT = 3680 m	11-51.24N	91-23.41W
0153	Slmax 1400m		LT = 3450 m	11-49.90N	91-22.92W
0400	Hieven			11-51.03N	91-19.75W
0408	RMT a/D, Ende Station				
Profil HS #22					
0506	Beginn Profil			11-47.80N	91-14.61W
1017	Unterbrechen Profil (Bootsmannöver; Test Notrudersteuerung;				
	Test ADP			12-34.04N	90-53.68W
1218	MAG z/W, Fortsetzung Profil			12-34.16N	90-55.41W
1826	Ende Profil	116sm; MAG 116sm		13-29.50N	90-28.50W
Profil HS #23					
2100	Beginn Profil			13-12.65N	90-28.40W
21.08.03					
0407	Ende Profil	74sm; MAG 74sm		12-10.00N	90-57.00W
Profil HS #24					
0458	Beginn Profil			12-07.30N	90-51.00W
1046	Ende Profil	58sm; MAG 58sn		13-01.00N	90-26.87W
Profil HS #25					
1200	Beginn Profil			12-58.35N	90-20.23W
1523	Ende Profil	32sm; MAG 32sm		12-29.31N	90-33.81W
Profil HS #26					

1543	Beginn Profil			12-29.21N 90-33.60W

22.08.03

0733	Ende Profil	153sm; MAG 153sm		13-22.40N 92-55.00W
0741	MAG a/D			13-22.05N 92-55.80W

Station RMT #11 W6

0804	RMT z/W, Kurs 85°; V=2.5Kn	LT = 4399 m	13-22.28N 92-56.04W
0900	Slmax 1800 m	LT = 4547 m	13-23.30N 92-55.31W
1107	Hieven		13-25.57N 92-54.92W
1146	RMT a/D, Ende Station		
1206	MAG z/W		13-26.92N 92-54.28W

Profil HS #27

1306	Beginn Profil		13-32.62N 92-55.00W
1702	Ende Profil	41sm, MAG 41sm	13-50.70N 92-19.60W

Profil HS #28

1723	Beginn Profil		13-50.70N 92-19.60W

23.08.03

0114	Ende Profil	67sm, MAG 67sm; MAG a/D		13-18.95N 91-29.04W

Station RMT #12 W6

0118	RMT z/W, Kurs 117°, V=2.5Kn	LT = 1948 m	13-19.06N 91-28.82W
0212	Slmax 1600m	LT = 1732 m	13-18.76N 91-24.86W
0303	Hieven		13-16.60N 91-22.90W
0432	RMT a/D, Ende Station		

Profil HS #29

0449	Beginn Profil		13-15.70N 91-23.03W
0900	Ende Profil	40sm	13-16.36N 91-26.73W

Station DR #1 W6

0922	DR z/W	LT = 2061 m	13-16.35N 91-26.76W
1007	Boko SL 2100m	LT = 2061 m	13-16.42N 91-26.68W
1020	Slmax 2374 m		13-16.43N 91-26.67W
1142	Hieven		13-17.11N 91-25.70W
1242	DR a/D, Ende Station		

Station DR #2 W6

1342	DR z/W	LT = 1601 m	13-17.91N 91-25.01W
1448	Boko, Slmax 2001 m	LT = 1416 m	13-17.67N 91-25.17W
1525	Hieven		13-17.18N 91-25.37W
1612	DR a/D; Ende Station		
1620	MAG z/W		13-14.14N 91-24.85W

Profil HS #30

1754	Beginn Profil		13-11.80N 91-10.20W
2345	Ende Profil	56sm; MAG 56	12-51.57N 90-15.71W

24.08.03

Profil HS #31

0017	Beginn Profil		12-51.61N	90-15.81W
0255	Ende Profil	25sm; MAG 25sm	12-28.43N	90-25.93W
Profil HS #32				
0330	Beginn Profil		12-26.04N	90-19.43W
0628	Ende Profil	29sm; MAG 29sm	12-52.45N	90-07.92W
Profil HS #33				
0628	Beginn Profil		12-52.45N	90-07.92W
1120	MAG a/D		13-11.39N	90-51.72W
1200	Ende Profil	59sm; MAG 51	13-14.08N	90-51.00W
Profil HS #34				
1240	Beginn Profil		13-18.32N	90-44.88W
1354	Ende Profil	34sm	13-30.42N	90-37.82W
Profil HS #35				
1403	Beginn Profil		13-30.89N	90-38.30W
1418	Ende 3sm		13-28.76N	90-39.95W
	Anfahrt Rendevous Punkt Abgabe 1 Beobachter Guatemala			
1614	MAG z/W		13-42.12N	90-43.89W
Profil HS #37				
1734	Beginn Profil		13-29.71N	90-41.58W
1824	Ende Profil	8sm; MAG 8sm	13-22.00N	90-44.35W
Profil HS #38				
1854	Beginn Profil		13-22.00N	90-43.40W
1935	Ende Profil	7sm; MAG 7sm	13-28.30N	90-40.70W
Profil HS #39				
2106	Beginn Profil		13-25.97N	90-36.21W
2303	Ende Profil	19sm; MAG 19sm	13-07.98N	90-41.90W
Profil HS #40				
2350	Beginn Profil		13-09.11N	90-39.78W
25.08.03				
0413	Ende Profil	44sm; MAG 44sm	12-48.35N	90-00.00W
Profil HS #41				
0413	Beginn Profil		12-48.35N	90-00.00W
1526	Ende Profil	114sm; MAG 114sm	11-59.02N	89-15.02W
1537	MAG a/D			
Station RMT #13		W6		
1547	RMT z/W, Kurs 109°, V=2.5Kn	LT = 2161 m	11-58.19N	88-13.49W
1700	Slmax 1800m	LT = 2108 m	11-55.49N	88-08.57W
1836	Hieven		11-53.54N	88-05.01W
1920	RMT a/D, Ende Station			
1934	MAG z/W		11-51.35N	88-04.38W
Profil HS #42				

2021	Beginn Profil			11-50.39N	88-12.10W
26.03.03					
0851	Ende Profil	125sm; MAG 125sm		12-44.61N	90-07.15W
Profil HS #43					
0938	Beginn Profil			12-38.08N	90-09.60W
2140	MAG a/D			11-45.69N	88-18.26W
2155	Ende Profil	122sm; MAG 120sm		11-45.25N	88-17.61W
Station TN #14		W6			
2155	TN z/W		LT = 4269 m	11-45.25N	88-17.61W
2248	Slmax 1600m		LT = 4424 m	11-43.17N	88-15.46W
2332	Hieven			11-42.63N	88-13.80W
27.08.03					
0116	TN a/D, Ende Station				
0124	MAG z/W			11-41.20N	88-10.67W
Profil HS #44					
0227	Beginn Profil			11-37.96N	88-18.54W
1445	Ende Profil	124sm; MAG 124sm		12-31.72N	90-12.71W
Profil HS #45					
1526	Beginn Profil			12-25.16N	90-14.38W
28.08.03					
0336	Ende Profil	122sm; MAG 122sm		11-31.69N	88-22.20W
Profil HS #46					
0366	Beginn Profil			11-31.69N	88-22.20W
0458	MAG a/D			11-20.27N	88-16.03W
0510	Unterbrechen Profil			11-19.93N	88-15.86W
0856	MAG z/W			11-21.60N	88-15.82W
0912	Fortsetzung Profil			11-19.72N	88-15.75W
1900	Ende Profil	113sm; MAG 113sm		10-04.40N	87-12.00W
1913	MAG a/D			10-04.22N	87-10.83W
Station TN #15		W6			
0510	TN z/W, Kurs 25°; V=2.5Kn		LT = 3785 m	11-19.93N	88-15.86W
0658	Slmax 1700m		LT = 3790 m	11-20.82N	88-15.34W
0800	Hieven			11-21.54N	88-15.33W
0847	TN a/D, Ende Station				
OBH #55					
1940	Hydrophon z/W		LT = 3080 m	10-03.40N	87-06.23W
1940	Release Command				
1942	Hydrophon a/D				
2023	OBH gesichtet				
2044	OBH a/D			10-03.39N	87-03.32W
OBH #53					

2125	Hydrophon z/W	LT = 3274 m	10-07.34N	86-59.41W
2130	Release Command			
2131	Hydrophon a/D			
2224	OBH gesichtete			
2235	OBH a/D		10-10.18N	86-56.76W
OBH #54				
2317	Hydrophon z/W	LT = 3701 m	10-06.20N	86-52.82W
2322	Release Command			
2322	Hydrophon a/D			
2358	OBH gesichtet			
29.08.03				
0036	OBH a/D		10-04.43N	86-50.03W
OBH #56				
0145	Hydrophon z/W	LT = 3211 m	09-58.07N	86-56.60W
0148	Release Command			
0150	Hydrophon a/D			
0237	OBH gesichtet			
0251	OBH a/D		09-56.32N	86-58.12W
Profil HS #47				
0306	Beginn Profil		09-59.91N	87-14.62W
Station RMT #16	W6			
0605	RMT z/W, Kurs 310°; V=2.5Kn	LT = 3026 m	10-08.24N	87-24.76W
0707	Slmax 2000m	LT = 3011 m	10-09.88N	87-26.88W
0847	Hieven		10-12.39N	87-29.64W
0935	RMT a/D, Ende Station			
Station RMT #17	W6			
1201	RMT z/W, Kurs 320°; V=2.5Kn	LT = 3029 m	10-29.23N	87-48.66W
1300	Slmax 1800m	LT = 3034 m	10-30.12N	87-49.73W
1500	Hieven		10-32.85N	87-51.25W
1548	RMT a/D; Ende Station			
Station RMT #18	W6			
1800	RMT z/W. Kurs 253°; V= 2.5Kn	LT = 2762 m	10-49.95N	88-04.74W
1856	Slmax 1800m	LT = 2337 m	10-50.25N	88-06.72W
2016	Hieven		10-47.73N	88-12.03W
2116	RMT a/D, Ende Station			
2249	MAG z/W			
30.08.03				
0258	Ende Profil 113sm; MAG 70sm		11-25.08N	88-24.76W
Profil HS #48				
0258	Beginn Profil		11-25.08N	88-24.76W
1642	Ende Profil 138sm; MAG 138sm		12-24.63N	90-31.70W
Profil HS #49				
1731	Beginn Profil		12-18.20N	90-34.48W

31.08.03

0703	Ende Profil	137; MAG 137sm	11-18.50N	88-28.80W
0714	MAG a/D		11-18.04N	88-27.93W

Profil HS #50

0703	Beginn Profil		11-18.50N	88-28.80W

01.09.03

0628	Ende Profil	279sm	09-43.35N	84-52.36W